DOE/NASA/0615-79/1
NASA CR-159465

DEVELOPMENT OF A PHASE-CHANGE THERMAL STORAGE SYSTEM USING MODIFIED ANHYDROUS SODIUM HYDROXIDE FOR SOLAR ELECTRIC POWER GENERATION

Barry M. Cohen
Richard E. Rice
Peter E. Rowny
Comstock & Wescott, Inc.

December 1978

Prepared for
NATIONAL AERONAUTICS AND SPACE ADMINISTRATION
Lewis Research Center
Under Contract NAS 3-20615

for
U.S. DEPARTMENT OF ENERGY
Office of Solar, Geothermal, Electric and Storage Systems
Division of Energy Storage Systems

TABLE OF CONTENTS

A P P E N D I X A

DYNATECH R/D COMPANY REPORT

"The Thermophysical Properties
of a Thermal Energy Storage Material"

A P P E N D I X B

A P P E N D I X C

A P P E N D I X D

LIST OF SYMBOLS FOR COMPUTER ANALYSIS

A P P E N D I X E

LIST OF SYMBOLS FOR SCALING PROCEDURE

A P P E N D I X F

REFERENCES

LIST OF TABLES

LIST OF FIGURES

SUMMARY

Anhydrous sodium hydroxide modified by addition of 8% sodium nitrate and 0.2% manganese dioxide has been under development as a phase-change heat storage medium for a number of years for application to electrically powered, low temperature space and water heating. This medium is low in cost, has a high heat storing capacity, and is compatible with steel containers and heat exchangers. Therefore, it is of interest for use in solar powered electricity generating systems.

The purpose of this program was to make an analytical and experimental study of a phase-change thermal storage system utilizing this medium, suitable for use in a solar total energy system, and to develop a preliminary design of such a storage system consistent with the following specifications:

> Storage capacity is 3.1×10^6 kJ operating over the range of 516 K to 584 K. The heat transfer fluid for charging and extracting heat is Therminol-66. The maximum charging rate is 1.8×10^6 kJ/hr with the Therminol-66 temperature at 584 K ± 2 K, and the maximum extraction rate is 1.0×10^6 kJ/hr with the Therminol-66 inlet temperature 516 K ± 11 K and outlet temperature 582 K ± 2 K.

The analysis showed that supplemental heat of about 10% of the heat extracted from storage, added to the Therminol-66 during discharge to help maintain the outlet temperature within the specified range, had a large beneficial effect on the size and cost of the storage system. Therefore such supplemental ("deficit") heating was employed in the design of the system.

A mathematical simulation of the system and computer program were available as a result of prior work. These were amended to facilitate use in the present work.

The program comprised the following tasks:

... Measurement of physical and thermophysical properties of the storage medium.

... Adaptation of the previously developed simulation and computer program to present requirements.

... Development of a reference design of a system meeting the operating requirements.

... Design and construction of an experimental model of 1/10 scale, and a test-bed in which to test it.

... Operation of the 1/10 scale model under test conditions consistent with the specifications, and collection of experimental data.

... Correlation of data with computer-predicted results.

... Modification of the simulation and computer program until correspondence was acceptable.

... Development of a preliminary design meeting the operating specifications and estimation of the system cost.

Satisfactory correspondence between experimental data and computer predicted results has been obtained, and the preliminary design developed. The storage unit consists of a cylindrical vessel, surrounded by thermal insulation, containing the storage medium in which is immersed a heat exchanger consisting of a number of helical coils of steel tubing, manifolded for parallel flow at the top and bottom, through which the Therminol-66 flows downward during charging and upward during heat extraction.

The preliminary design summary is as follows:

Vessel height and diameter	2.35 m (92.5")
Insulation thickness	0.61 m (24")
System height and diameter	3.6 m (142")
System weight	27300 kg (60,200 lb)
Amount of storage medium	18000 kg (39,700 lb)
Unit cost	$33,700
Heat exchanger	.00635 m (1/4") tubing; 280 coils, each 27.7 m (91 ft) long
Storage output	3.31×10^3 MJ
Specific cost	$11.2/MJ
Insulation loss	3.25% of total storage output per day
Deficit heating	10.2% of storage output

INTRODUCTION

In the generation of electric power from solar heat, by means of a heat engine, storage of heat is necessary in order to make the power generation system independent of the solar insolation. The heat storage element of such a system is one of the more costly elements of the system, and the cost goals for thermal storage have not yet been achieved.

One approach to thermal storage for solar-electric systems which offers a possibility for reducing the cost of storage is the use of thermal storage media which undergo phase changes between solid and liquid states, or between solid states, within the operating temperature range, making the latent heats of the phase changes, as well as sensible heat, available for heat storage and retrieval.

Objective

The objective of the work reported herein has been to study the dynamic performance of a phase change thermal storage unit employing a passive heat exchanger, suitable for use in a solar total energy system, operating in the mid-temperature range, to develop a preliminary design for such a unit, and to estimate its cost.

Concept for Phase-Change Thermal Storage

The concept for the use of the phase change medium, which has been studied in this work, comprises a vessel containing the medium in which is immersed a single fixed heat exchanger, through which a single heat transfer fluid is passed for charging heat into storage when heat is available from the solar collectors, and for retrieving heat from storage as required at other times.

The particular configuration studied consists of a cylindrical steel vessel, and a heat exchanger consisting of a number of helical coils of steel tubing which are manifolded together, inside the vessel, at the top, and at the bottom, forming parallel flow paths for the heat transfer fluid. When heat is being charged into storage,

the fluid flows downward through the heat exchanger, and upward when stored heat is being retrieved.

A thermal gradient exists within the medium (with the higher temperature in the upper part of the vessel) which moves vertically and changes shape during thermal cycling.

The medium undergoes an increase in volume as it melts, and to accommodate this a clearance space must be allowed at the top of the vessel. This space is open to the atmosphere through a "breather" tube which allows air to enter and leave during cycling, and which insures that the vessel operates unpressurized. The vessel is surrounded by thermal insulation, the outer surface of which is protected by a metallic shroud.

Heat Storing Medium

The heat storing medium used in the work reported herein is tradenamed Thermkeep* and has the following composition:

Anhydrous NaOH (commercial grade)	91.8% by wt.
Sodium nitrate	8.0%
Manganese dioxide	0.2%

The commercial grade of NaOH commonly contains 1-2% of sodium chloride, 1/2-1% of sodium carbonate, and smaller amounts of other salts and hydroxides.

Salt baths of similar composition sold under several tradenames have been used industrially for many years at temperatures of 750 K and higher for metal cleaning and descaling. These baths are contained in large steel tanks. When the advantages of anhydrous NaOH as a phase change heat storage medium were recognized, this composition was used because of this existing industrial experience with the containment and stability of the material.

As a heat storing medium, Thermkeep has the advantages of

... high heat storing capacity with latent heats of fusion and a solid state phase change in the temperature range 566 K to 507 K,

---

* Registered trademark Comstock & Wescott, Inc.

... chemical stability and insignificant vapor pressure at temperatures up to 750 K,

... stability in contact with air allowing the venting of containment vessels to the atmosphere,

... compatibility with steel for containment and heat exchangers up to 750 K,

... low cost and ready availability, and

... large scale industrial experience as a metal cleaning salt.

Background

The use of Thermkeep as a high temperature phase change thermal energy storage (TES) medium has been under development by Comstock & Wescott, Inc. since 1958. The initial proposed use for TES units was for domestic space heating in conjunction with heat pumps. Off-peak electric energy was to be used to charge the TES units which would assist the heat pumps during periods of high heating requirement. This development, sponsored by the Edison Electric Institute and the Philadelphia Electric Co. was carried through a successful field test from 1962-1964, but was then discontinued because the anticipated large scale use of heat pumps did not materialize.

Beginning in 1964, in cooperation with the Hooker Chemicals and Plastics Corp., Comstock & Wescott undertook further development of the heat storage material and development of equipment for several anticipated applications of thermal storage. Extensive studies were carried out on chemical formulations and the compatibility of Thermkeep with containment materials, which has resulted in nearly complete elimination of corrosion of containers and heat exchangers fabricated from ordinary mild steel at temperatures up to 755 K (900 F).

A result of the cooperative effort between Comstock & Wescott and Hooker Chemicals and Plastics Corp. has been the development of the Thermbank Electric Water Heater, which was designed to provide hot water for all-electric buildings. Five Thermbanks were successfully carried through a one-year field test in a cooperative program

with the Hydro Electric Power Commission of Ontario. A Thermbank Electric Water Heater of this type has been supplied to the NASA Lewis Research Center under Contract No. NAS3-20240 for in-house testing and evaluation.

The applications described above used electric energy to charge heat into storage, stored it at temperatures up to 755 K (900 F), and delivered it at approximately 340 K (150 F) for space and wate. heating. In these applications the temperature of the heat delivered from storage can be allowed to drop substantially below the maximum storage temperature as the thermal energy store is depleted without affecting the system efficiency.

When heat from solar collectors is stored and retrieved from storage for power generation, a drop in temperature of the heat supplied to the heat engine reduces the efficiency of the power generating cycle. Therefore, the heat from storage must be delivered to the heat engine at a temperature close as possible to that at which it is charged into storage. This requirement for delivery of stored heat at a nearly uniform temperature imposes a new set of conditions on the design of the heat exchangers, and experience with heat exchangers designed for the previously developed devices does not apply.

Scope of Work

The study has included both analysis and the design, construction, and testing of a sub-size thermal storage unit for the acquisition of experimental data for correlation with the analysis. The analysis was based in part upon the results of prior work by Comstock & Wescott under Purchase Order No. 87-5030 from Sandia Laboratories, Livermore, CA, to develop a mathematical model and write a computer program describing the dynamic behavior of a phase change thermal storage system using Thermkeep as the medium. In addition, the work has included the measurement of certain thermophysical properties of the medium.

Specifically, the program has included the following tasks:

1. Experimental determination of the effect of accidental contact between Therminol-66 (heat transfer fluid) and Thermkeep at temperatures up to 613 K.

2. Determination of physical properties of Therm-keep:

   a. Thermal conductivity of the solid phase from room temperature to the melting point, and of the liquid phase from the melting point to 750 K.

   b. Density of the solid from room temperature to the melting point, and of the liquid to 750 K.

   c. Heat capacity of the solid and liquid to 750 K, including the heat of transition from one phase to the other.

   d. Viscosity of the liquid from the melting point to 750 K.

3. The development of a Reference Design, based upon the previously developed Phase Change Computer Program (suitably modified for this purpose), for a phase change thermal energy storage (TES) unit suitable for use in a solar electric power generation system, utilizing Therminol-66 as the heat transfer fluid for charging and retrieving stored heat. The TES unit has the following operating requirements:

   Storage capacity is 3.1×10^6 kJ operating over the range of 516 K to 584 K. The heat transfer fluid for charging and extracting heat is Therminol-66. The maximum charge rate is 1.8×10^6 kJ/hr with the Therminol-66 temperature at 584 K ± 2 K, and the maximum extraction rate is 1.0×10^6 kJ/hr with the Therminol-66 outlet temperature at 582 K ± 2 K and inlet temperature at 516 K ± 11 K.

4. The design and construction of a subscale TES system, of one-tenth the scale of the Reference Design. The subscale system includes the TES unit and a test bed which permits testing under operating conditions consistent with the operating characteristics of the Reference Design.

5. The operation of the subscale TES system under a range of conditions and the collection of experimental data.

6. Comparison of the experimental data with results predicted by the analytical model via the computer program, and revision until satisfactory agreement was attained.

7. A Preliminary Design of a full scale TES unit and estimation of the cost of this unit.

TECHNICAL DISCUSSION

MATERIAL PROPERTY STUDIES

A subcontract was issued by Comstock & Wescott, Inc. to Dynatech R/D Company, Cambridge, Mass., to determine some relevant properties of the storage medium, Thermkeep. This was in conjunction with evaluating the feasibility of using Thermkeep in thermal storage devices for solar energy applications. Dynatech was selected because of the company's experience in measuring properties of inorganic heat-of-fusion heat storage materials (Ref. 1). A copy of Dynatech's final report, "The Thermophysical Properties of a Thermal Energy Storage Material," dated January, 1978, is included as Appendix A.

The work had two objectives:

1. To determine the consequences of contact between the heat transfer fluid, Therminol-66 (T-66), and Thermkeep, and

2. To measure specified thermophysical properties of Thermkeep.

Regarding the compatibility of Therminol-66 and Thermkeep, the Dynatech analysis showed that no detrimental reactions occur between the two materials. The major effect occurred in the Therminol-66. A gradual increase in its viscosity was observed when the Therminol-Thermkeep mixture was in contact with air at elevated temperatures (593 K; 320 C). Dynatech recommended the use of a cover gas, such as dry He, over the Thermkeep to remove any water or T-66 which may accumulate in the Thermkeep due to a leak in the heat exchanger. This is not necessary from an operational standpoint and neglects the fact that air breathing is required to maintain the proper balance of $NaNO_3$ which otherwise is slowly reduced to $NaNO_2$ while the unit operates.

The thermophysical property measurement phase required determination of the following properties of Thermkeep as a function of temperature:

1. The enthalpy (or specific heat).

2. The thermal conductivity of the solid and liquid phases.

3. The density in both phases.

4. The viscosity of the liquid.

Data are provided in the report on all but the enthalpy of the material. It was found that the Quantitative Thermal Analyzer (QTA) used for accurate calorimetric study of materials, owing to its design, would not provide accurate data in the temperature region of interest. Consequently, the data utilized for enthalpy vs. temperature in the course of this work was based upon the best information which Comstock & Wescott had prior to this project. It is felt that at some point this ought to be improved upon but correlation of analysis with experiment has shown that the present data are reasonably good.

REFERENCE DESIGN STUDY

Computer Model

A mathematical analysis and computer program were written to estimate the performance of a Thermkeep thermal energy storage device to meet the requirements of the Sandia Midtemperature Solar Test Facility and to design the one-tenth scale test model. It was expected to require modification for correlation with actual data obtained from tests on the model. It was formulated as a design tool which would properly account for the thermodynamics of the process, approximately account for the heat transfer between the T-66 and the Thermkeep, and allow for easy handling of a variety of operating modes, from solar daily cycles to laboratory test modes.

It is an analytical program rather than a design program in the sense that it requires a specific unit design as input, and outputs the calculated performance of that unit. This program is used for design by analysis of a large matrix of design options and separate parametric evaluation of the output by the engineer.

The physical processes associated with the heat storage medium are quite complex and would be difficult, if at all possible, to model even given a large dedicated effort. The medium undergoes a solid-liquid phase change with a volume contraction associated with solidification. It is a non-eutectic multi-component material so that solidification, in part, probably occurs by precipitation of NaOH from the melt when the solubility is below the actual concentration. A solid-solid phase transformation occurs in the NaOH with a corresponding latent heat.

Note: All symbols are defined in the Computer Analysis Symbol List presented as a fold-out in Appendix D.

Another computer analysis was formulated earlier in a prior program to attempt to account for some of these effects. It is a considerably more costly program to use; it is less flexible, and it would not as easily lend itself to the incorporation of empirical modifications. It is also based, in large part, upon a published phase diagram for the system $NaOH-NaNO_3$. It is not known, however, whether or not this is truly characteristic of Thermkeep which is composed of commercial grade chemicals containing impurities as well as the basic two components above.

Consequently, it was decided that a simpler analysis, of the type to be described herein, would be more desirable. This earlier analysis is described in Appendix C.

General Description

The computer analysis is formulated around the design concept of the proposed thermal storage unit. The design concept consists of a vertical cylinder containing the heat storage medium. A heat exchanger is immersed in the Thermkeep. The heat transfer fluid, T-66, flows through the heat exchanger tubing. (Any fluid which does not undergo vaporization can be modeled using its particular thermophysical properties.) The heat exchanger consists of a number of parallel heat exchanger tubes which are identical geometrically and assumed to pass equal flows of T-66. The tubes are manifolded at the top and bottom of the unit, the hot end being at the top. During charging, T-66 enters at the top and exits from the bottom, and vice versa during discharging.

It is desired to know how the unit will respond to particular stimuli, e.g., flow rate, temperature, and flow direction of T-66, both internally and as a "black box" characterized by what the outside world sees. The analysis has been constructed with two major sections. One contains the analysis of the heat transfer between the T-66 and medium within the unit. The other characterizes the stimulus and determines the status of the T-66 delivered to the unit as a function of the operating time. This latter section is modified at will to allow modeling of various modes of operation. The mode described herein is the solar daily cycle which was used in developing the approximate Reference Design described in a subsequent section.

Figure 1 describes the solar daily cycle which was taken to be typical of the mode of operation of the Sandia Test Facility. The solar collectors generate heated T-66 which is supplied to the boiler of a toluene based Rankine power cycle. The boiler demands 250 kw for twelve hours a day. During the other twelve hours the system is shut down. The solar collectors produce a varying heat output over nine hours, peaking at 500 kw, starting at zero in the morning and dropping to zero in the late afternoon. The excess heat is stored to allow operation when the collector output is deficient.

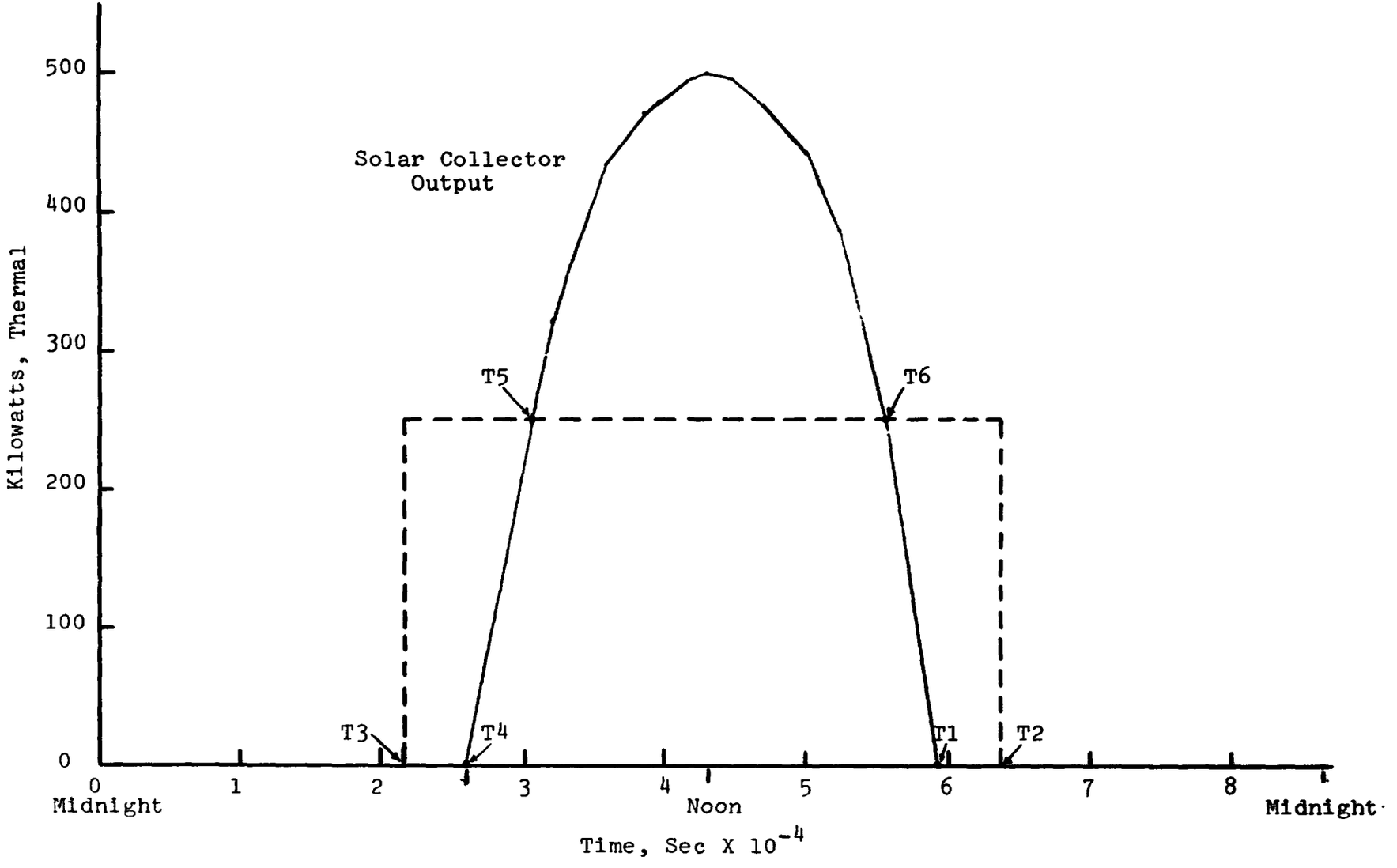

Figure 1. Typical solar daily cycle at Sandia Total Energy Test Facility.

During charging of the unit, the flow rate to the storage unit is determined by the available excess solar heating, and the temperature change of the T-66 as it passes through the unit:

$$w_f = \frac{q_{ex}}{c_f (T_H - T_o)} ,$$

where w_f is the T-66 flow rate to the storage unit, q_{ex} is the excess thermal power from the collectors (i.e., above boiler demand), c_f is the T-66 specific heat, and T_H and T_o are the T-66 inlet and outlet temperatures, respectively, of the TES unit. w_f is limited to some realistic value of pump capacity.

During discharge of the unit, the flow rate is held constant as if the fluid were heated over the full temperature range. It will, in fact, exit somewhat cooler than the charging temperature. In this case, a boost heater is assumed and the amount of this heating required is calculated.

The unit begins at a fully charged condition and is perturbed by the solar daily cycle. The calculation proceeds until a repetitive cyclic operation is achieved and the unit is characterized by its steady static cyclic performance under this mode of operation. Cumulative heat balances over the cycle are made to define the performance. The important factors are the daily heat absorption by the unit, the daily heat delivery, the daily heat loss to the environment, and the daily make-up heating (boost heating) requirement.

Based upon the best knowledge available at the time, a method was devised for estimating cost of materials and fabrication for a given design. These costs are computed at the beginning of each analysis for the particular design configuration. The costs are printed out in an itemized fashion for each part of the assembled unit and lead to a total unit cost.

Further details of the computer model used to develop the Reference Design are given in Appendix B.

Reference Design Analysis

The computer analysis which was described above and in Appendix B was used to produce a "reference design" for a Thermkeep thermal energy storage unit. This unit was specified as being subjected to the solar daily cycle as described on Figure 1. The unit was designed to provide a reasonable compromise between cost and efficiency as will be explained later. Aside from the heat flow specifications, the fluid utilized was Therminol-66. It was assumed that during charging the fluid would enter storage from the solar collector field at 584 K (311 C) and that during discharge it would enter storage from the boiler at 516 K (243 C).

The design selected was to become the basis for the design of a laboratory model of one-tenth scale in size, heat flows, fluid flows, etc., but with equivalent performance in terms of outlet temperatures, losses, and other factors. Eventually, after adjustments to the computer analysis had been made based upon empirical correlations, a new final reference design would be composed which would more accurately represent how a unit for Sandia Laboratories STETF would appear.

Note: At the point in the project when the reference design was composed, the available specific energy over the operating range was thought to be 450 kJ/kg. Subsequent investigation showed this to be closer to 410 kJ/kg. However, the results to be discussed herein were based upon the larger value. They are shown to describe the method and trends but a roughly 10% addition to cost and size would be expected. The study was not rerun since the model was already in fabrication when the correction was discovered. The later analyses utilize the correct enthalpy vs. temperature relationship. Any graphs and tables presenting results using the lower value are so noted.

The procedure for design was as follows. Preliminary screening of some of the parameters had shown that the primary variables are the quantity of storage medium and the total heat exchanger surface area. Thus, data were generated for a specific tube size and a preliminary reference design was produced. The secondary variables were

then tested to determine where improvements could be made to arrive at a reference design.

The unit is presumed to be a shell and tube device with helically coiled parallel tubes with a specified tube size, number and length. The variable parameter was the total inside surface area of the tubes. Heat exchangers were sized to produce about 703 g/cm^2 (10 psi) peak pressure drop as a starting point. The reference tube size was 6.35 mm (1/4") o.d. steel tubing, with 4.57 mm (0.180") i.d. The ratio of vessel (shell) height to diameter, i.e., the "aspect ratio" was fixed at 1 for screening. During cooling, flow enters the bottom end or element 1, and vice versa during heating.

For computational purposes, the solar collector and boiler demand characteristic as described was input. A sufficient number of points were input and straight lines were assumed between them. This characteristic was adapted from the "winter cycle" of the Sandia Laboratories and provides peak collector output of 500 kW, steady boiler demand of 250 kW and more excess heating available during charging than required during discharging. When steady state cyclic operation is achieved, the excess is simply wasted. The total storage demand is 3.45 x 10^6 kJ by this cycle, not 3.1 x 10^6 as specified in the contract, but a simple scaling could reduce this to the proper value.

A 12-hour idle period is specified which is consistent with Sandia Laboratories' mode of operation. This creates an unusual situation where the capacity is low but the end rate is high since it occurs for a short period of time. It is expected that a unit sized to operate throughout the idle period would perform better over the complete cycle.

The computer analysis was run over enough cycles to stabilize the unit performance. A criterion was found acceptable whereby the unit cycles until the storage cyclic input minus the storage cyclic output is close to the nominal stand-by or surface loss. This condition is approached by starting with the unit fully charged to peak fluid temperature and then cycled until the stable full charge gradient is reached.

Flow rate modulation during charging was provided based upon fluid outlet temperature to attempt to maintain heat balance around the solar collectors. A maximum

total flow of 5 kg/sec was specified to collectors and boiler. In a thermocline system, 2.95 kg/sec would be required at 500 kW output so that an increase of 70% is allowed -- a value which is adjustable.

Figures 2 and 3 describe the results of analysis plotted in two different ways, Figure 2 being constant surface area lines with amount of Thermkeep as the coordinate axis, Figure 3 being the opposite. Overall efficiency is defined as

$$\eta_o = \frac{Q_o}{Q_o + Q_s + Q_a}$$

where Q_o = storage daily output

Q_s = storage daily surface loss

Q_a = fluid auxiliary heating

Q_a is computed as the cyclic amount of heat required to bring the fluid up to 584 K (311 C), the peak temperature. In fact, the specification allows as low as 580 K (307 C) so that the overall efficiency is somewhat pessimistic as will be discussed later. Q_s is based upon 45.7 cm (18") of rock wool insulation. In application, Q_s and Q_a would be weighted differently depending upon their effect on total system economics. Without knowledge of how to weight them accurately, the above definition of efficiency was used. It is not a pure thermodynamic efficiency but was felt to be adequate when comparing designs subjected to the same duty cycle.

Surface areas ranged from 37.16 sq m (400 sq ft) to 185.8 sq m (2000 sq ft) in parallel tubes sized for 69 kPa (10 psi) peak pressure drop as discussed. Thermkeep quantities were varied from 6000 kg to 50000 kg. Figure 3 shows the normal improvement expected with increasing surface area with no significant increase in performance beyond 148.6 sq m (1600 sq ft). Figure 2 shows an unexpected decrease in performance with large amounts of storage medium. This is believed to be due to the formation of permanent solid throughout the unit with inadequate surface to extract heat from it. The calculation

is believed to be pessimistic for solid heat transfer and real performance may be somewhat better.

Cost factors were developed whereby materials costs were estimated at market values and fabrication costs were scaled from the Mod I Thermbank costs according to the normal "six-tenths" factor whereby fabrication costs increase as the 0.6 power of the size ratio. This unit is the accepted rule for process industry equipment such as heat exchangers, vessels, etc.

Figures 4 and 5 show the costs of storage in dollars per thousand kilojoule based upon the resultant storage output which is taken to be the unit capacity. The important criterion, however, is not simply cost of storage but cost at an acceptable efficiency. Figure 6 is cross plotted from Figures 2 through 5 taking cost of storage for constant overall efficiency. From these curves and from some interpolation, a preliminary reference design was selected which uses 15000 kg of Thermkeep and 83.6 sq m (900 sq ft) of surface area. The cost was estimated at \$27,880 with a total storage output of 3.225×10^6 kJ for \$8.64/MJ. A total efficiency of 0.911 was predicted.

All data were obtained with only 10 numerical elements. It was determined that the grid size, beyond 10 or so, had a small effect on the computed performance. Figure 7 shows the stable temperature swings for a 10 element grid and Figure 8 shows these for a 25 element grid. Using a finer grid improves the computed performance slightly to a total output of 3.237×10^6 kJ for \$8.61/MJ and an overall efficiency of .914. Overlaying the two temperature maps shows them to be similar except that the 25 element grid has more definition (high frequency resolution) as expected. T1 through T6 are key times as described on Figure 9.

The major effect of the 12-hour stand-by period (T2 to T3) is a loss of high temperature heat through the top of the unit. This heat is mainly sensible heat of the liquid phase above the melting range of the NaOH-8% $NaNO_3$ mixture (see Figure B1). This aspect of performance (and others) might be improved by decreasing the $NaNO_3$ content and thereby raising the melting range of the mixture, so that the high temperature heat loss would come principally from latent rather than sensible heat.

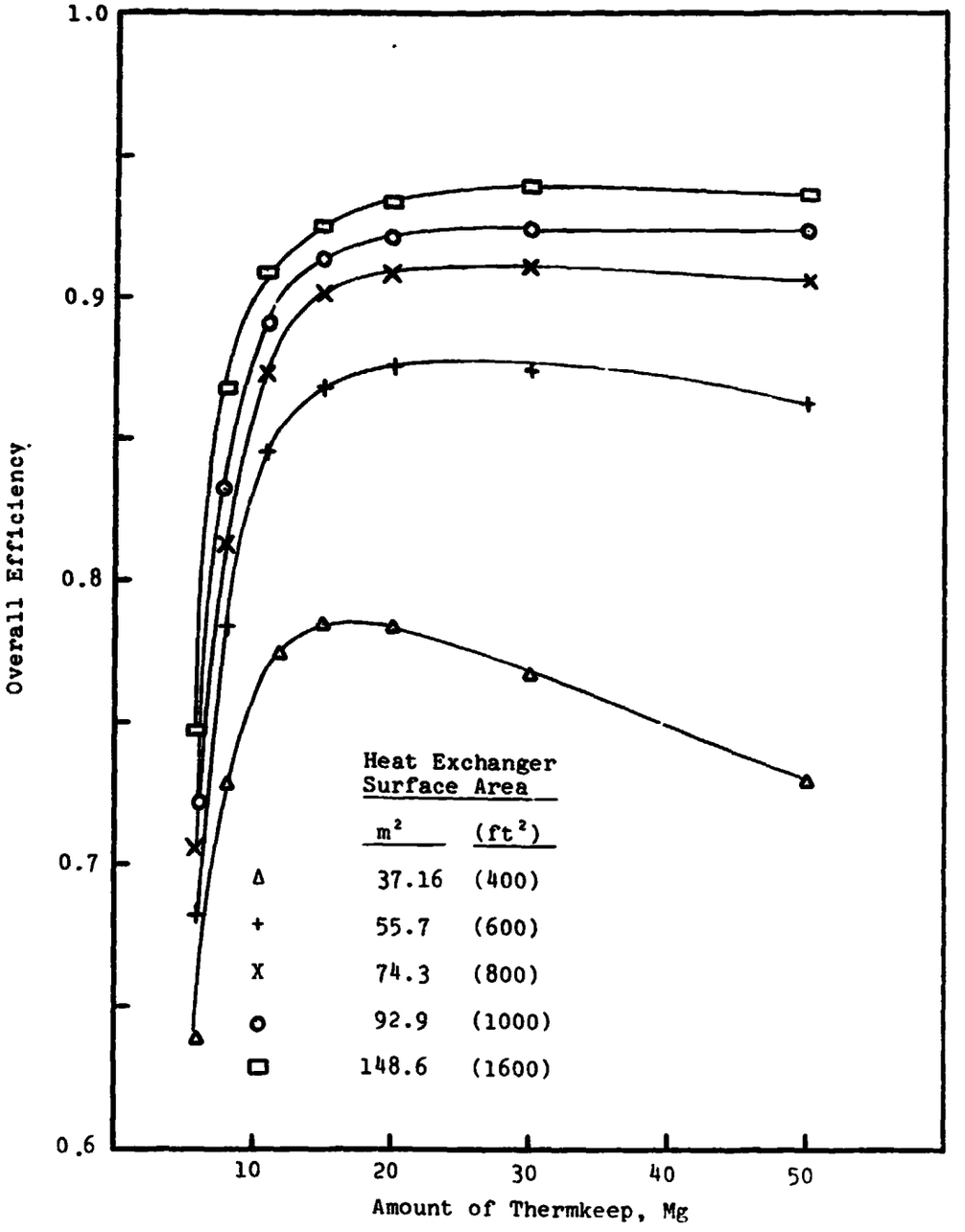

Figure 2. Overall efficiency as a function of Thermkeep mass, showing effect of heat exchanger surface area.

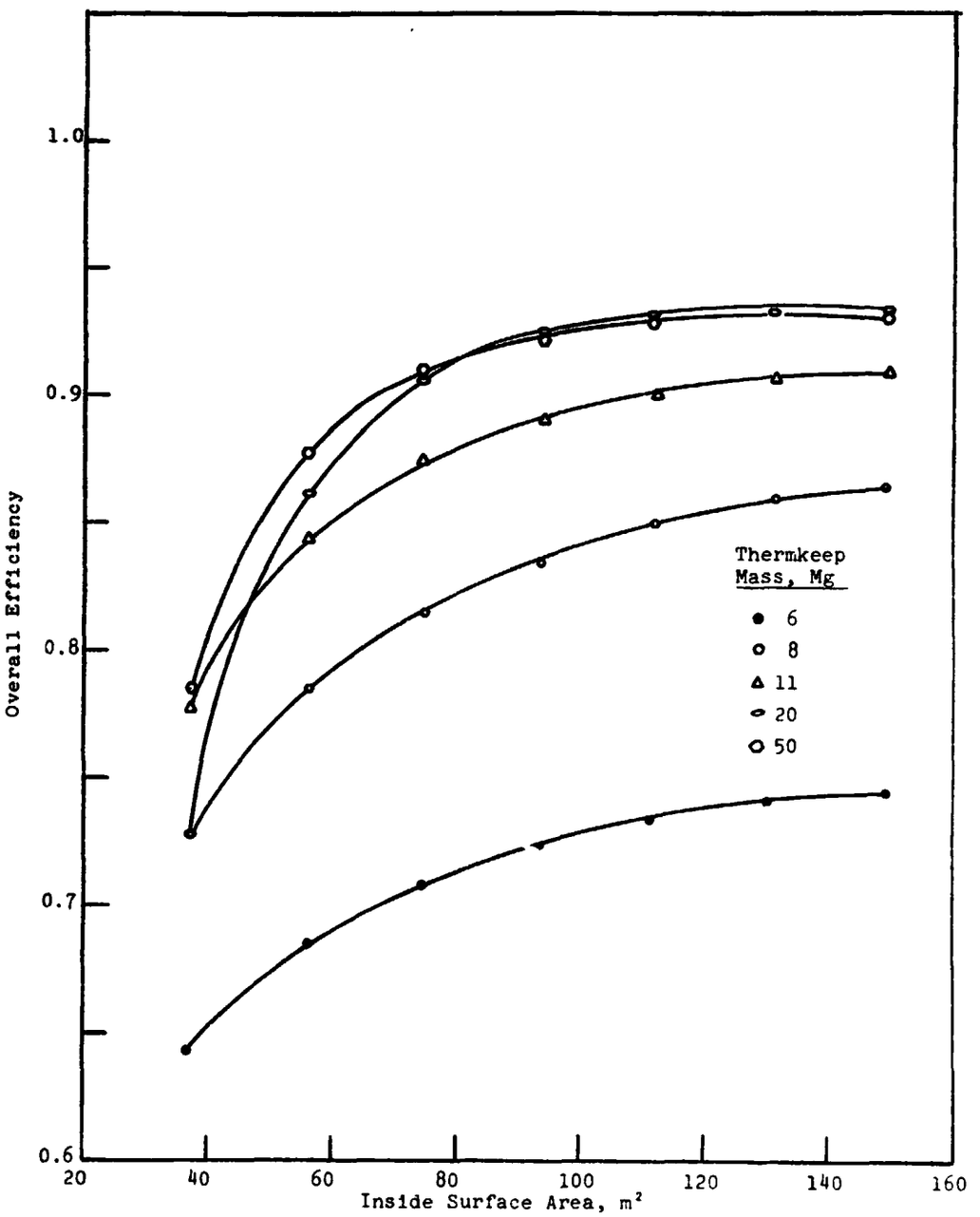

Figure 3. Overall efficiency for constant Thermkeep mass at various heat exchanger surface areas.

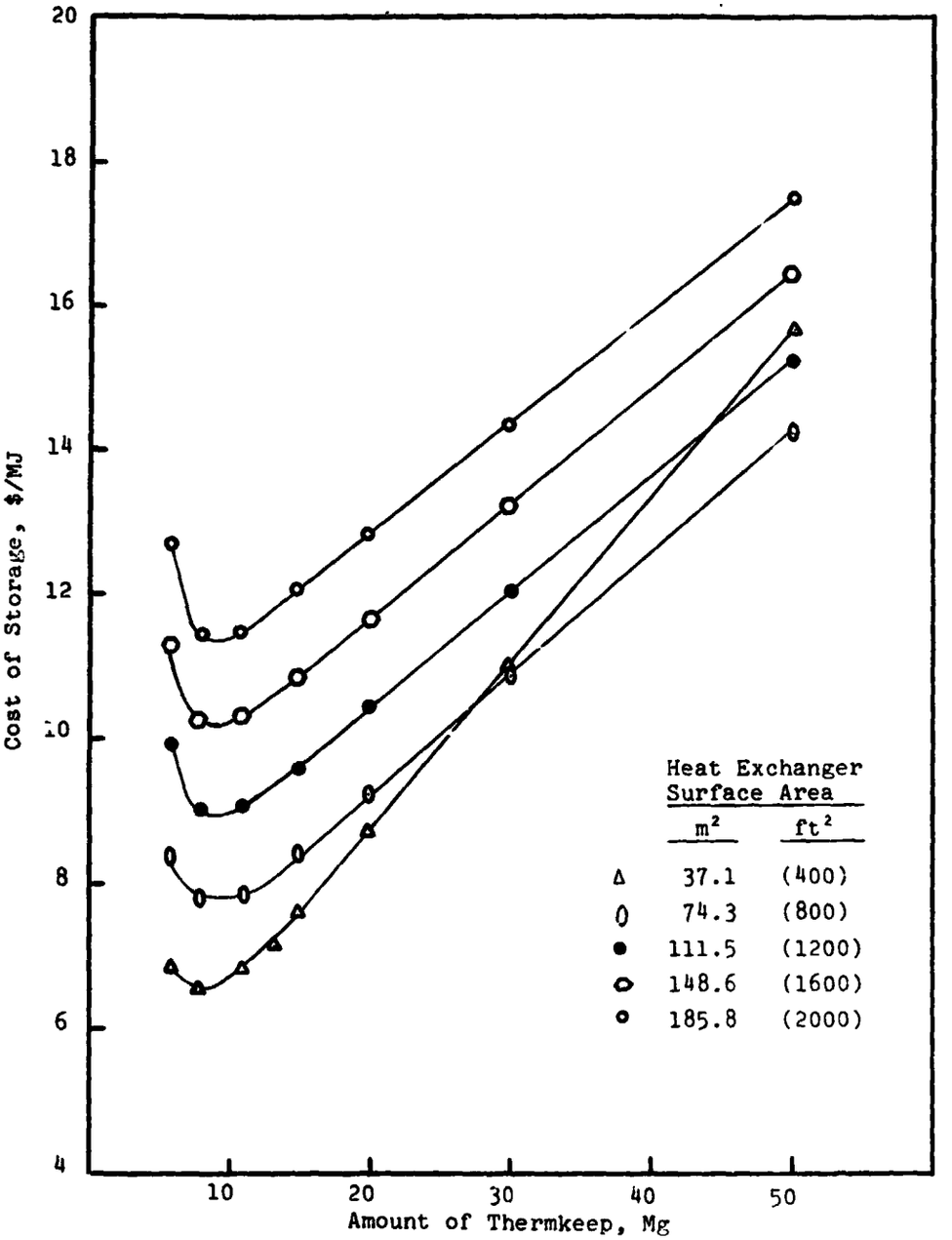

Figure 4. Cost of storage for constant heat exchanger surface area at various Thermkeep masses.

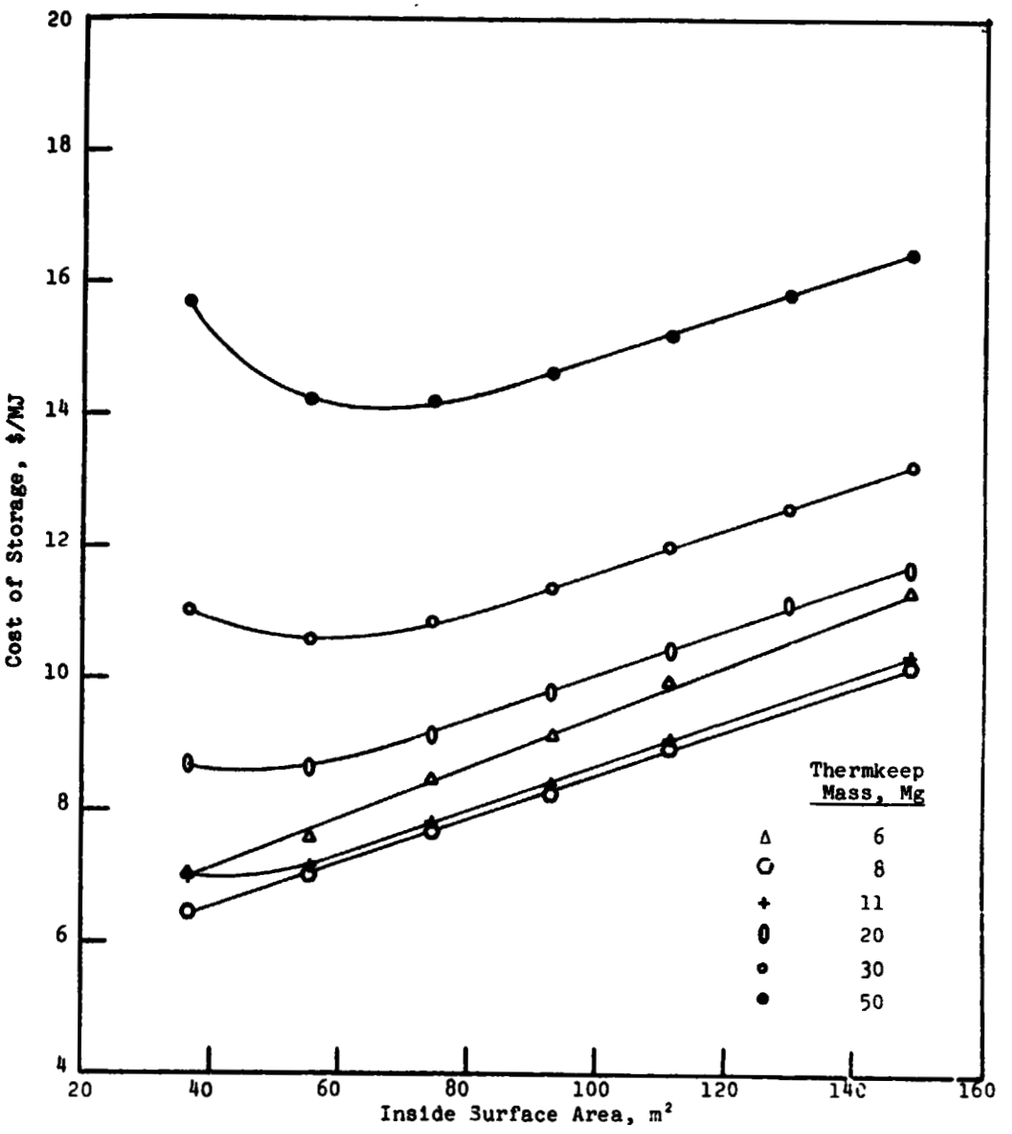

Figure 5. Cost of storage for constant Thermkeep mass at various heat exchanger surface areas.

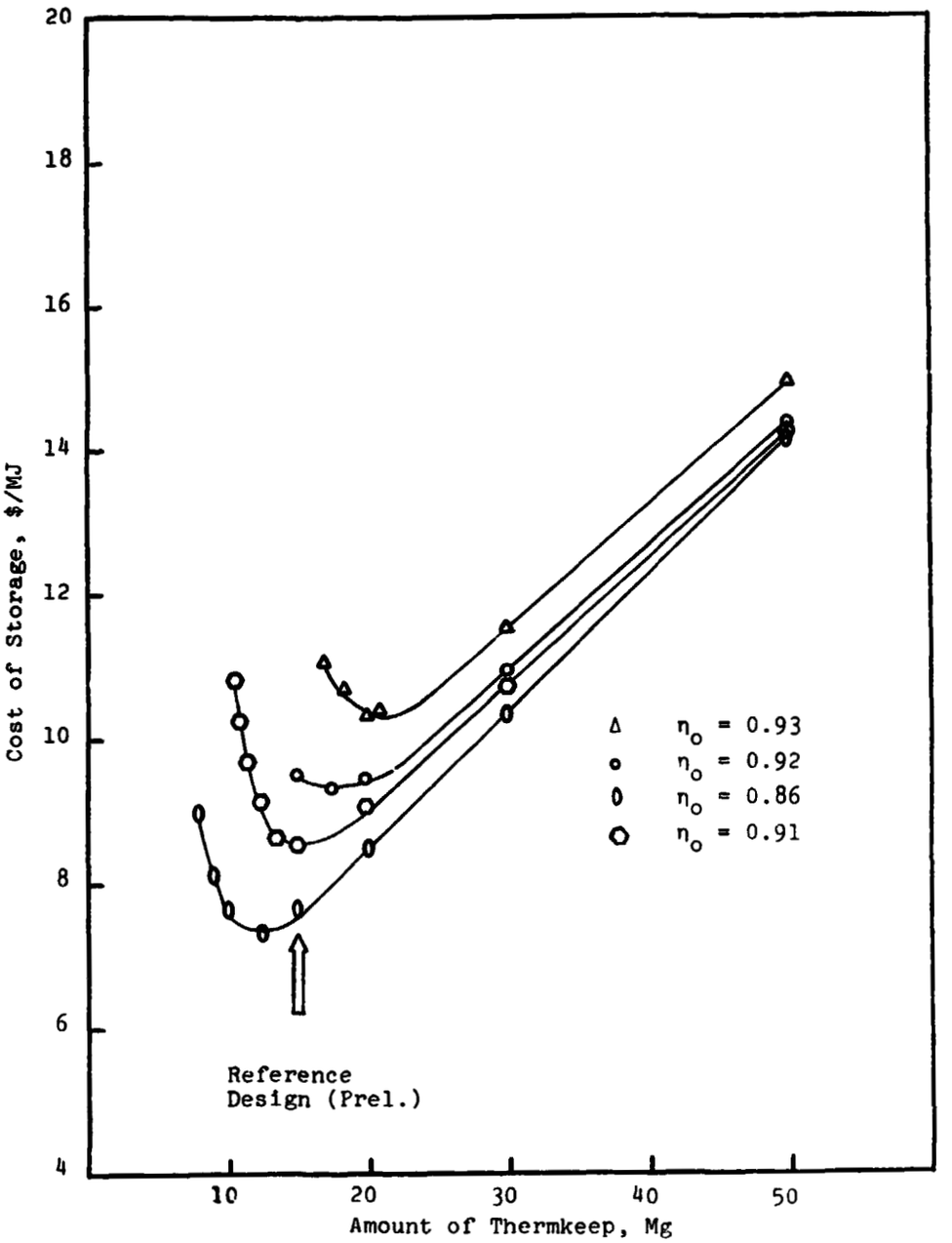

Figure 6. Specific cost of storage for various TES designs at fixed overall efficiencies.

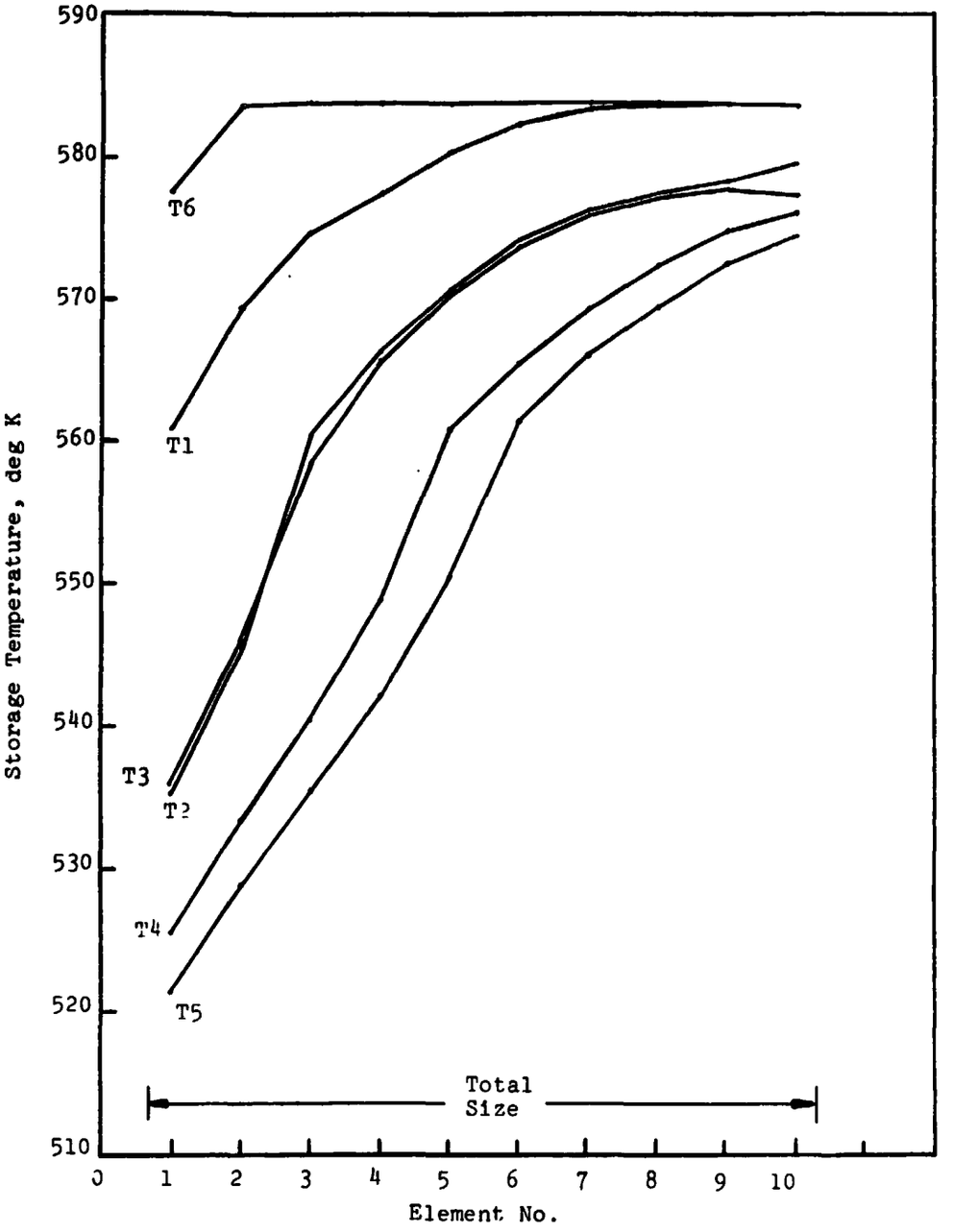

Figure 7. Reference design with 10 element grid (preliminary).

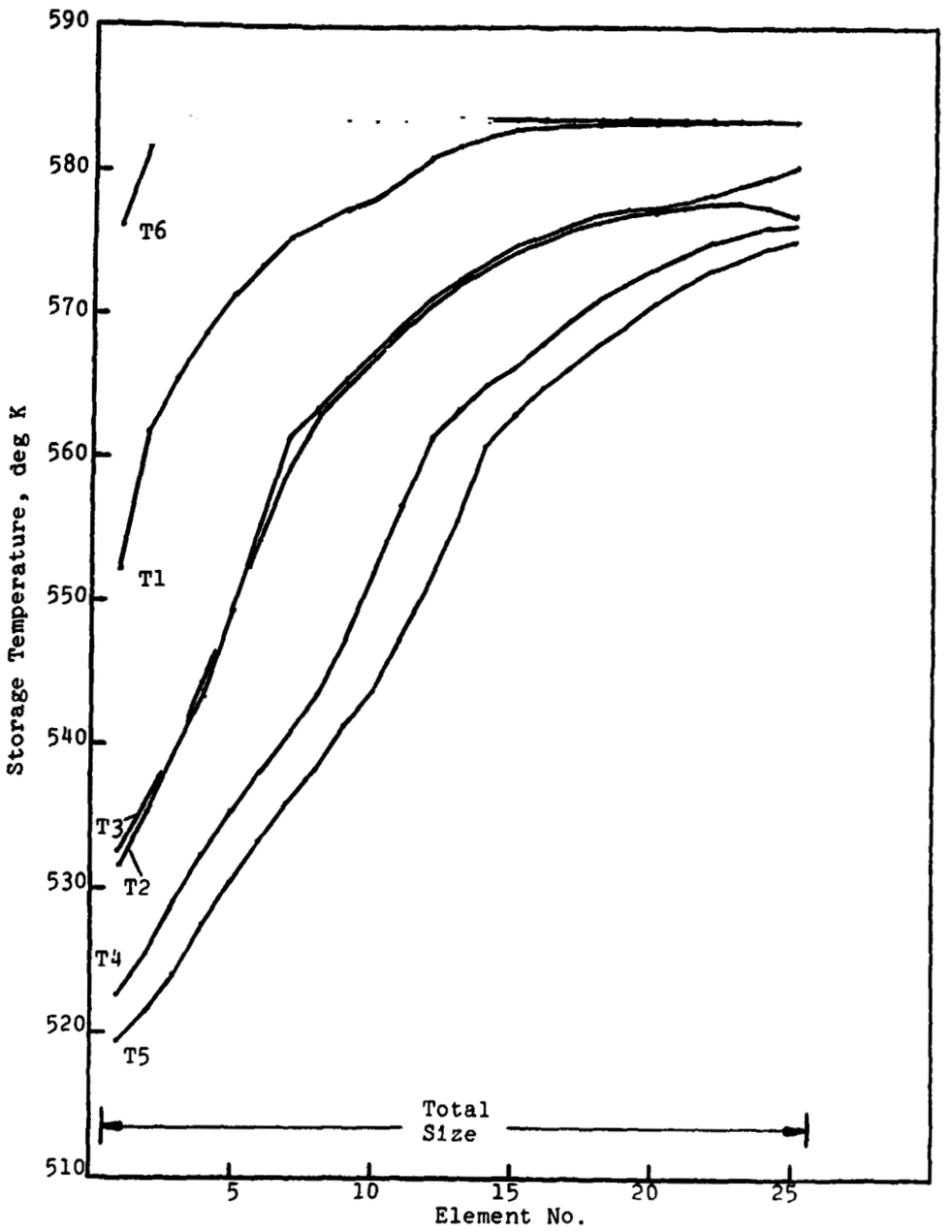

Figure 8. Reference design with 25 element grid (preliminary).

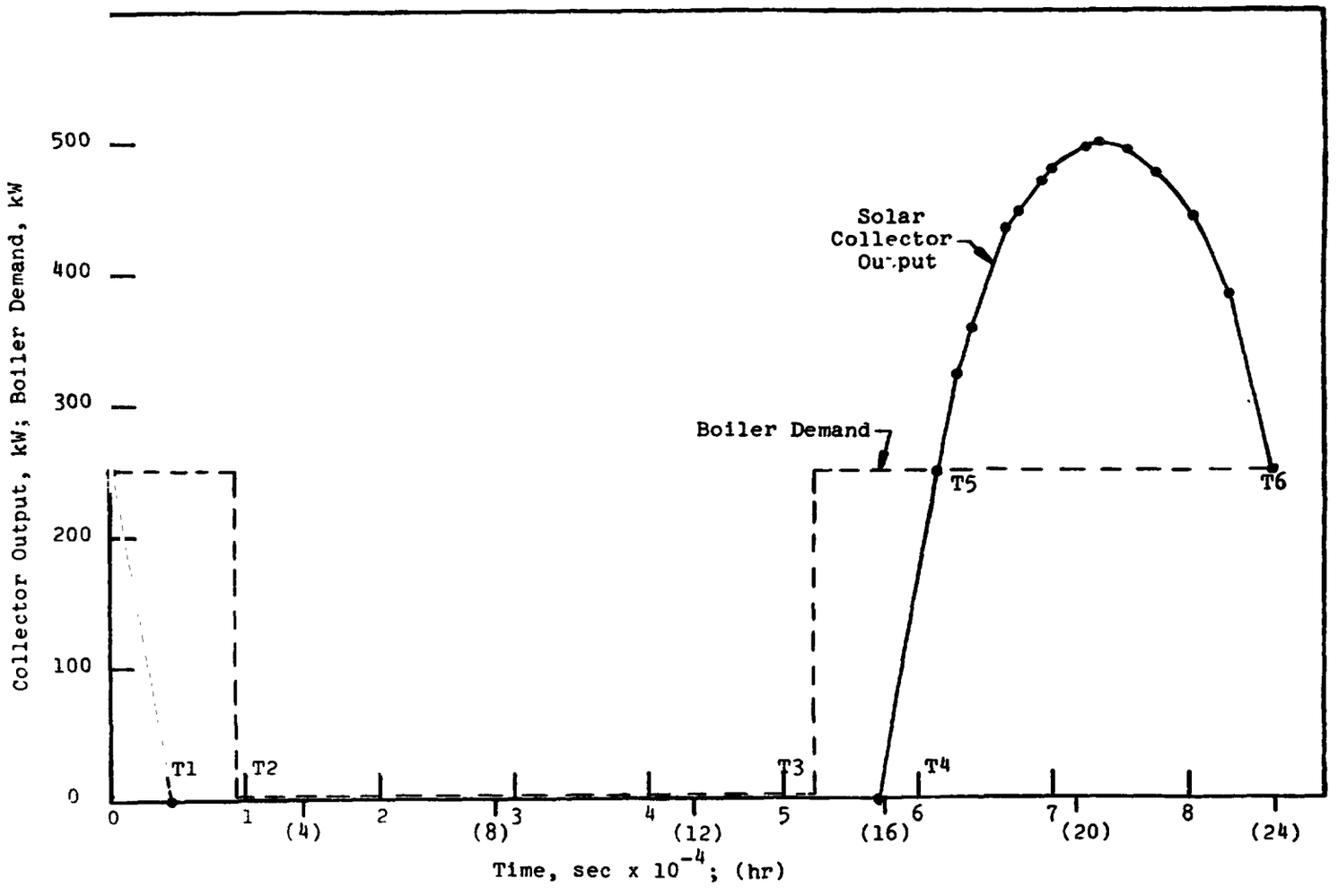

Figure 9. Reference duty cycle.

The fact that pure liquid with low specific heat exists above 578 K (305 C) is a contributing factor for the high temperature drops in this region during extraction of heat and during idle. In a unit design, it may be possible to use higher quality insulation only at the top and stainless steel outlet tubes to reduce loss.

The preliminary reference design consists of 15000 kg of Thermkeep; 252 parallel coiled tubes, 0.635 cm o.d. x 0.457 cm i.d. x 23.1 m long (0.25" o.d. x 0.180" i.d. x 75.8 ft long); a vessel whose inside dimensions are 2.23 m (7.31 ft) diameter by 2.23 m (7.31 ft) height. Total outside dimensions are 3.17 m (10.4 ft diameter by 3.19 m (10.5 ft) height. Total outlet capacity is 3.237×10^6 kJ at 91.44% overall efficiency. Of the 8.56% inefficiency, about 2.5% is due to surface losses which could be improved with high quality but expensive insulation.

The next step was to evaluate the effects of minor parameters. The preliminary reference design was used as a basis for all these parametric evaluations. Figure 10 shows the effect of increasing tube size. It can be shown from the cylindrical conduction equation that for equal surface areas and equal deposition of solid that small diameter tubes provide less conduction resistance so that the results were not unexpected. Clearly, the cost of storage increases and the overall efficiency decreases with increasing tube size. 0.635 cm (1/4") o.d. tubes are considered to be the smallest practical for fabricating the unit so that this size would be retained. A 25-element grid was used here but 10 elements were used for the rest of the studies.

Figure 11 shows the effect of variation in aspect ratio (vessel height/vessel diameter). As aspect ratio increases for the same volume, surface losses increase and axial conduction decreases. The results show decreasing performance with aspect ratio, suggesting that surface losses are more significant than axial conduction. In fact the decrease in efficiency can be attributed almost solely to increased insulation loss. From a pure surface loss standpoint, it can be shown a priori that an aspect ratio of 1 is an optimal configuration. The aspect ratio of 1 is therefore retained.

Figure 12 shows the effect of increased fluid velocity, i.e., changing tube lengths and number to achieve the same surface area with higher velocities and consequently higher pressure drops and pumping powers. While there is

an expected performance improvement with increased velocity, this must be weighed against increased pump power. If we assume that mechanical power in a total energy system is obtained at 10% efficiency, then in the extremes, viz., 76 kPa and 710 kPa (11 psi and 103 psi), the following is true. It takes 57600 kilojoules-thermal to produce the 5760 kilojoules-mechanical required to pump fluid for a day at 76 kPa (11 psi) and 551160 kilojoules-thermal to produce the 55116 kilojoules-mechanical at 710 kPa (103 psi), a net increase of 493560 kilojoules-thermal. The additional 1% overall efficiency at 3.2×10^6 kilojoules-storage per day yields 32000 kilojoules-thermal which is not justified. Even from 76 kPa to 145 kPa (11 psi to 21 psi), an additional 52560 kilojoules-thermal is required to obtain 0.35% of 3.2×10^6 kilojoules or 9600 kilojoules-thermal. Thus, the 70 kPa (11 psi) specification was accepted. The peak pump power is now 0.33 kW-ideal vs. 3.12 kW at 711 kPa (103 psi) and 0.64 kW at 145 kPa (21 psi). Peak power may be reduced by reducing peak allowable flow which may be worth considering.

Figure 13 shows the effect of insulation thickness on the preliminary reference design. Performance improves with insulation thickness but with diminishing returns due largely to the cylindrical geometry. The increase in cost from 0.305 m (12") to 0.457 m (18") is $450 which affords about 1%; the increase in cost from 0.457 m (18") to 0.61 m (24") is $520 which affords 0.5%; the increase in cost from 0.61 m (24") to 0.76 m (30") is $600 which affords 0.2%. The decision was made to go to 0.76 m (24") of insulation but in reality a cost-effectiveness study for all parameters ought to be done which assesses the impact on the whole Total Energy System.

Figure 14 shows the effect of peak allowable storage flow due to flow modulation during charging. Beyond a certain point, the excess flow doesn't provide any gain since the unit can do no more than come to a full charge. Below that point inadequate flow modulation prevents insufficient unit recharge. It would appear that something a bit smaller than the 5 kg/second total flow or 3.5 kg/second storage flow would be tolerable but a rapid deterioration of performance eventually results. For now, the 5 kg/sec (3.5 kg/sec storage flow) will be retained.

The final reference design is now essentially the preliminary reference design with 0.61 m (24") of rock wool insulation. The estimated unit cost is $28,399 with a capacity of 3.24×10^6 kilojoules output, for $8,765 per thousand kilojoules. The total efficiency from a 25-element grid analysis is 0.919 and the insulation loss is 2.2% of the total storage capacity.

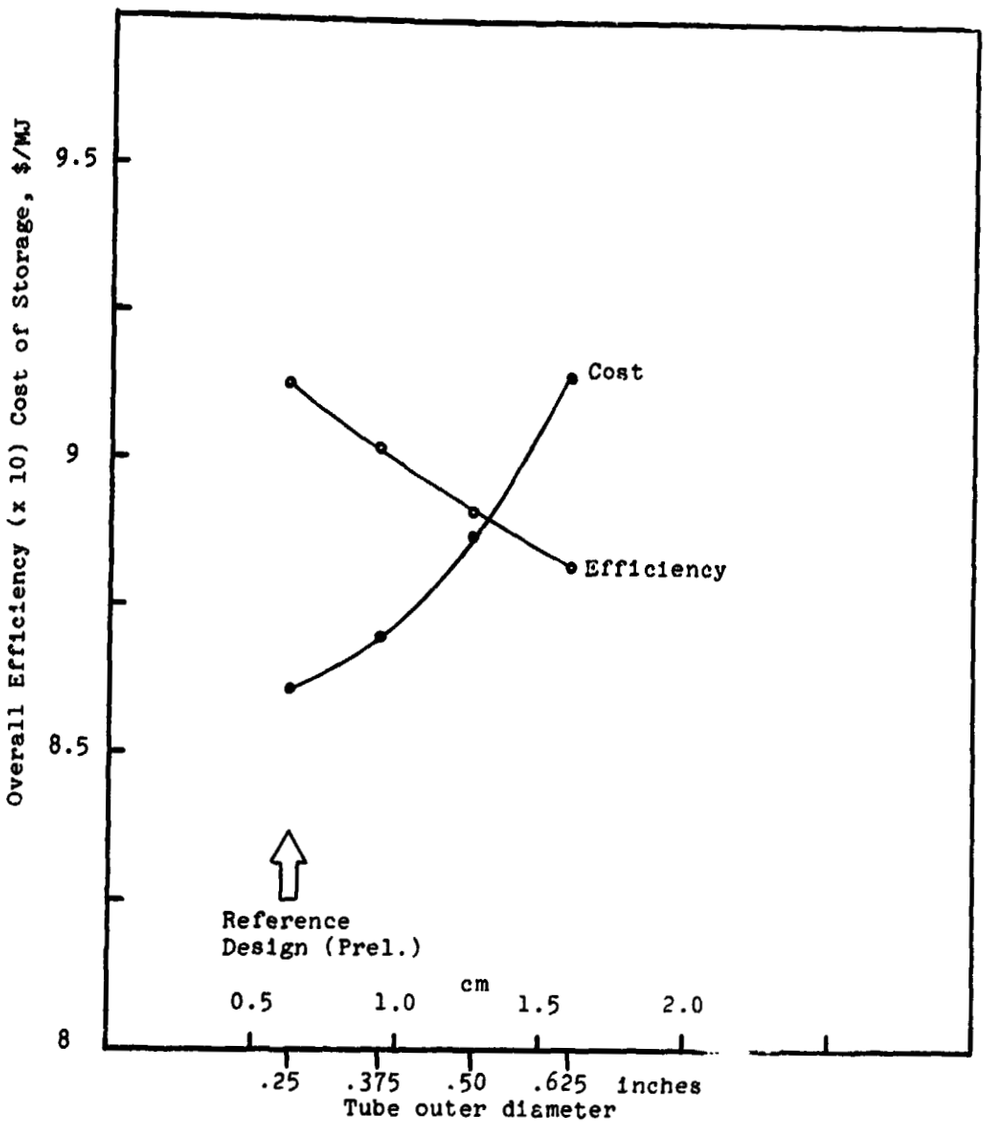

Figure 10. Effect of tube size on cost and performance (25 element grid).

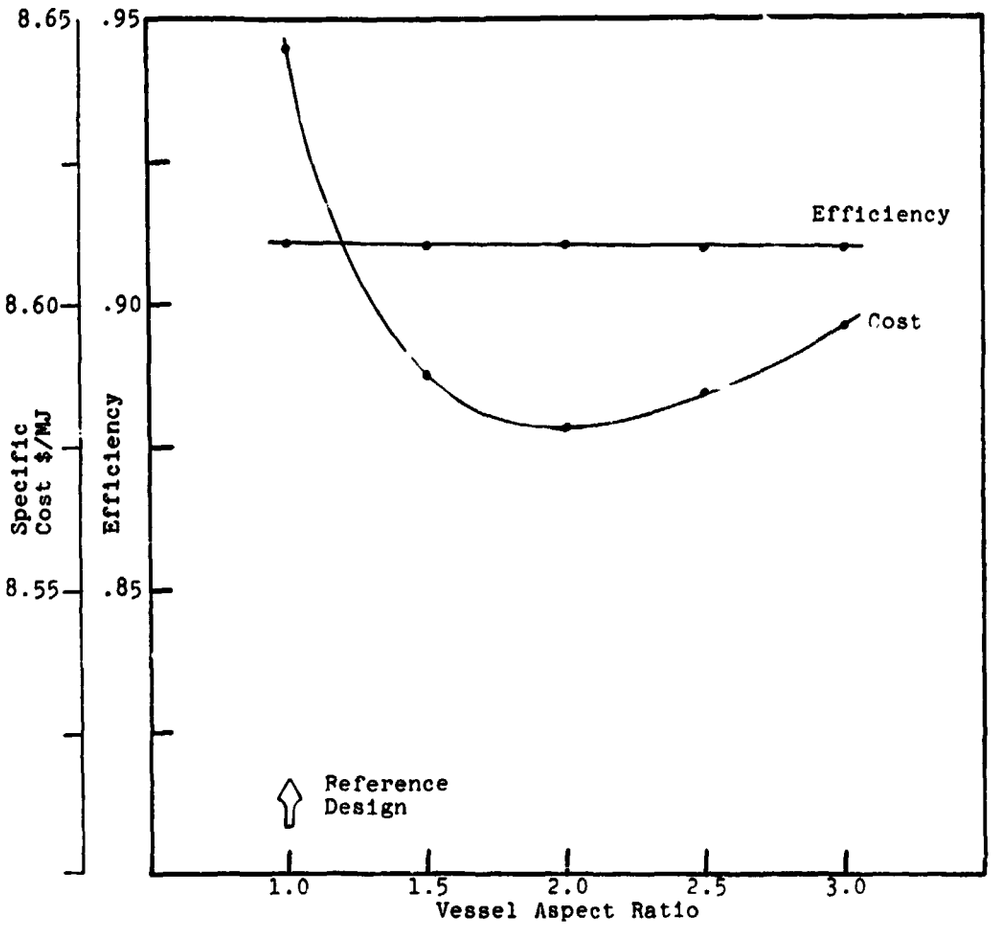

Figure 11. Effect of vessel aspect ratio on cost and performance.

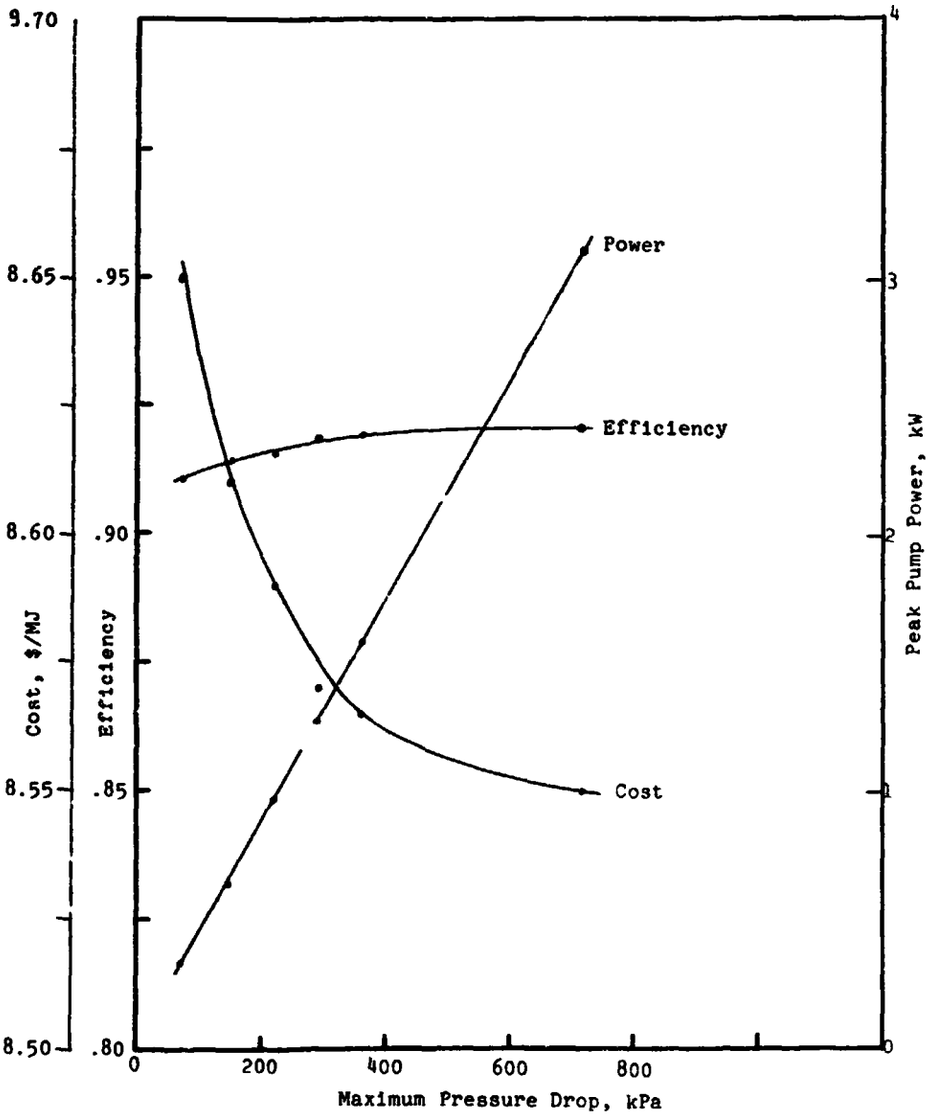

Figure 12. Effect of fluid velocity on cost and performance (10 element grid)

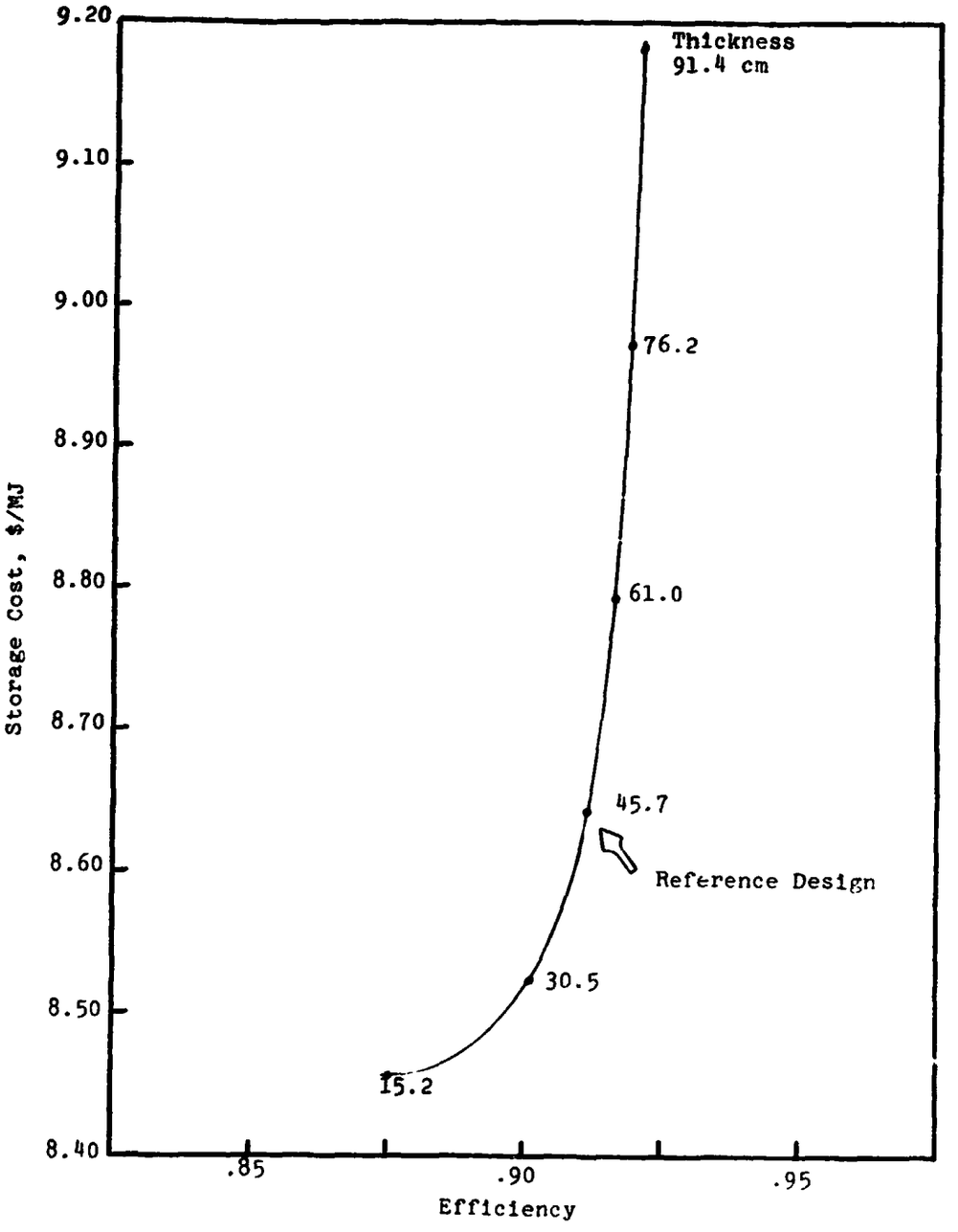

Figure 13. Effect of insulation thickness on cost and performance (10 element grid).

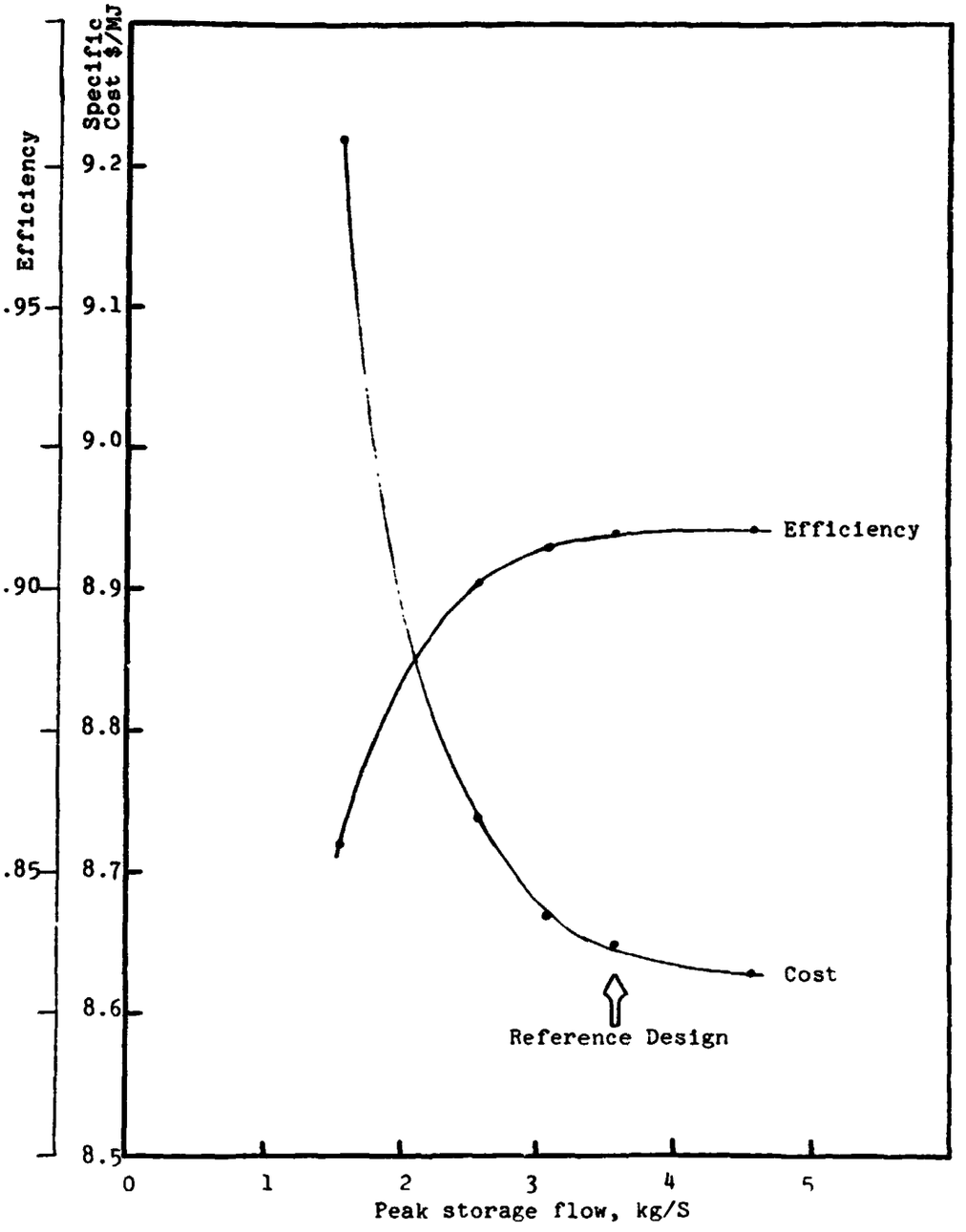

Figure 14. Effect of peak allowable storage flow on cost and performance.

Figure 15 is a map of the movement of the thermal gradient during stable cyclic operation, for a 25-element grid.

The overall efficiency is based upon the insulation loss of 72,000 kilojoules and 213,500 auxiliary input to bring the fluid to 584 K (311 C). A modified efficiency can be utilized which involves bringing the fluid to 580 K (307 C), the specified minimum temperature, when it drops below this value. Then the modified auxiliary input becomes 87,270 kilojoules and the modified overall efficiency becomes 0.953. Figure 16 is a graph of the fluid outlet temperature vs. cycle time during discharge.

The configuration is now a vessel which is 2.23 m diameter by 2.23 m height (7'4" diameter by 7'4" height), containing 252 tubes, 0.635 cm o.d. x 0.4572 cm i.d. (0.25" o.d. x 0.180" i.d.), and 15,000 kg (33,000 lb) of Thermkeep. The total overall dimensions including insulation are 3.474 m diameter by 3.50 m height (11'5" diameter x 11'6" height). The tubes would be constructed as individual identical helical spring-like coils, all parallel to each other along the vertical axis of the unit.

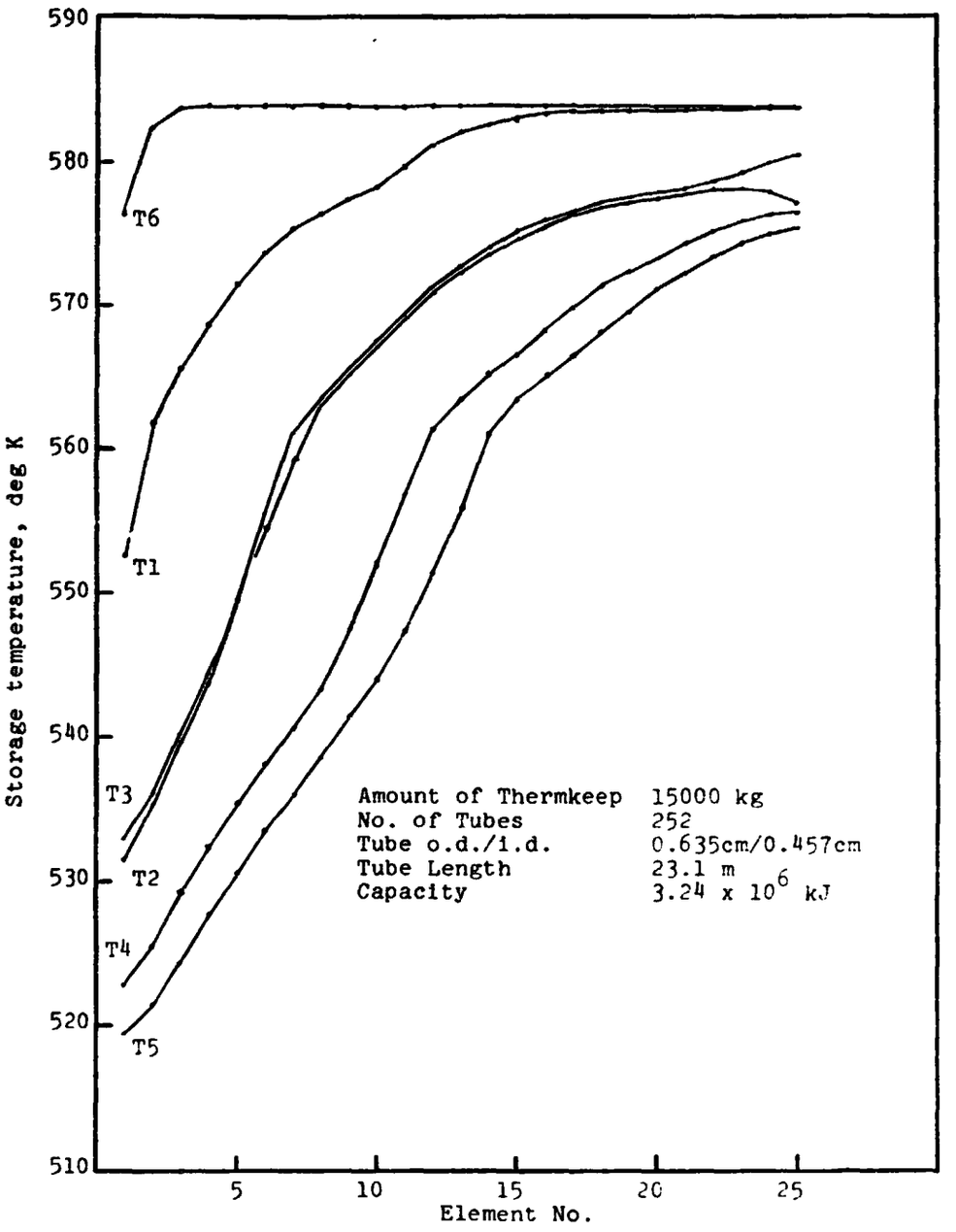

Figure 15. Final full-scale reference design -- movement of thermal gradient.

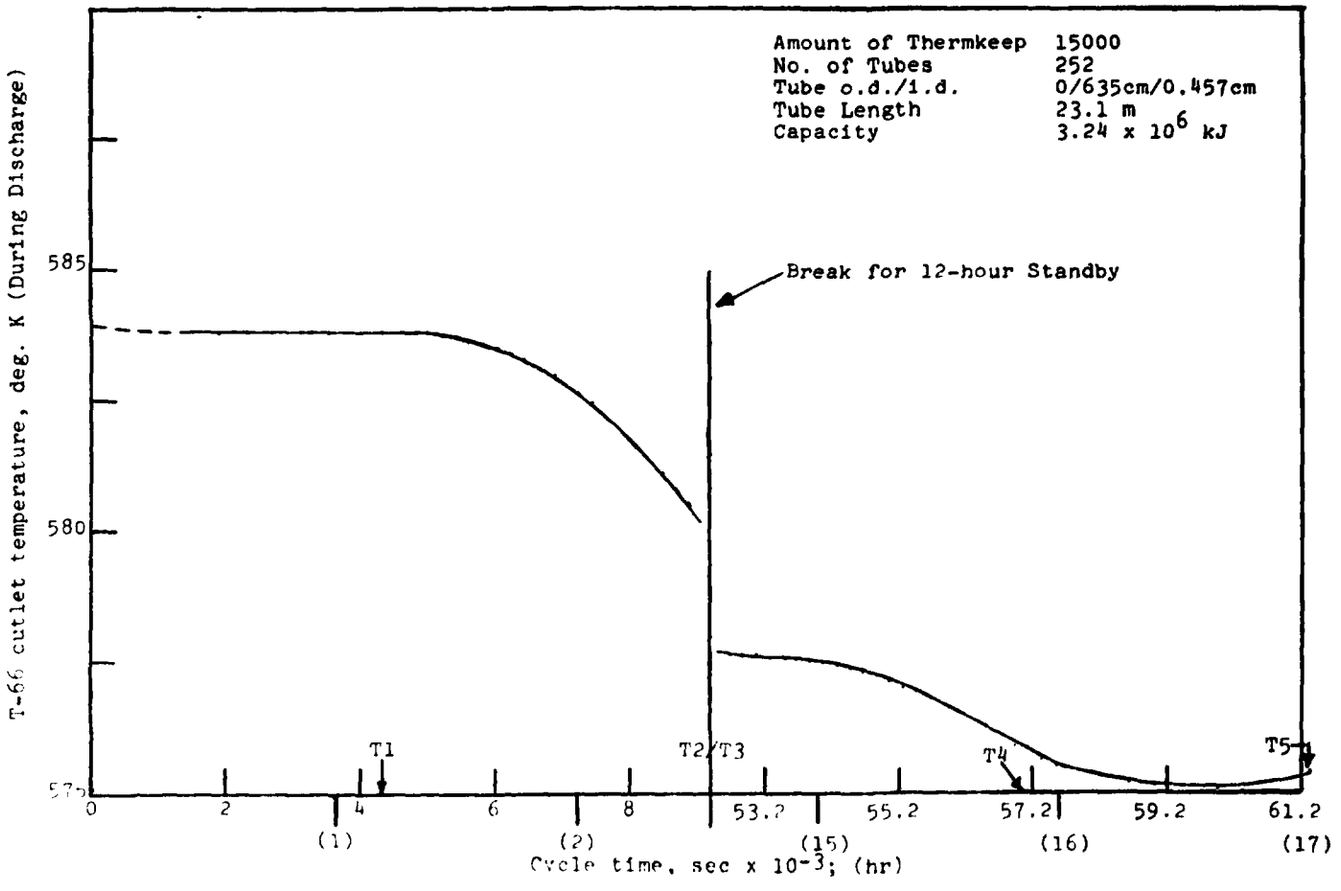

Figure 16. Final full-scale reference design -- variation of Therminol-66 outlet temperature during discharge.

SUBSCALE TES UNIT

Following the completion of the reference design for the full scale unit, it was necessary to design a model thermal storage unit of about one-tenth scale. This would be a realistic engineering model whose test data would provide confidence that a full scale unit would perform as expected, i.e., that a unit scaled up from the model would essentially perform like the model. If the original computer analysis were completely correct, then the model, if directly scaled, would become the full size design. However, since incorrect data were used in the reference design and model design, as previously discussed, and since some analytical modification would be expected, then a direct scaleup was not expected to truly provide a full size design.

The subscale unit analytical design consisted of two parts. The first part was the examination of the theoretical criteria for scaling and the second part was the computer analysis of model designs resulting in a choice whose output characteristics were in some direct relationship to those of the full scale unit. These tasks are described below.

Scaling Procedure

There are a number of methods for analyzing engineering processes and designing scale models. The best of these appears to be to write the differential equations describing the process, non-dimensionalize the variables, extract coefficients which are dimensionless groups and set these groups equal to each other.

Using the same assumptions in writing these equations as in writing the computer analysis, one can write the differential equations for infinitesimal elements in the height direction. An energy balance is made around the element of storage medium which includes axial conduction, surface losses, and heat transfer from (or to) the heat transfer fluid. An energy balance around the fluid then accounts for only transfer to (or from) the storage element.

The differential energy balance around an element is written as

$$c_s M_L \frac{\partial t}{\partial \tau} dx = k_t a_t \frac{\partial^2 t}{\partial s^2} ds + (\Sigma ka) \frac{\partial^2 t}{\partial x^2} dx - UA_L(t_f - t)dx$$

$$- \frac{2\pi k_i (t-t_s)}{\ell n \left(\frac{d_{sh}}{d_v} \right)} dx$$

while the energy balance around the fluid is written as

$$c\rho V_L \frac{\partial t_f}{\partial \tau} dx = \dot{m}c \frac{\partial t_f}{\partial x} dx + UA_L(t - t_f)dx.$$

Note: All symbols are defined in the Scaling Procedure Symbol List presented as a fold-out in Appendix E.

Note that the conduction down the tubes is taken along the tube locus since it is coiled. The derivatives along ds, a tube incremental length, may be transferred to the dx direction by

$$ds = \frac{L_t}{h_v} dx$$

so that

$$\frac{\partial^2 t}{\partial s^2} ds = \left(\frac{h_v}{L_t} \right) \frac{\partial^2 t}{\partial x^2} dx$$

Moreover, making the substitutions

$$\mu = \frac{\tau}{P}$$

$$\nu = \frac{x}{h_v}$$

$$\theta = \frac{t}{t_L}$$

results in the energy balances being

$$\frac{\partial \theta}{\partial \mu} = \left(\frac{k_t a_t P}{c_s M L_t} + \frac{(\Sigma ka)\ P}{c_s M h_V} \right) \frac{\partial^2 \theta}{\partial \nu^2} - \frac{UAP}{c_s M} \ (\theta_f - \theta)$$

$$- \frac{2\ k_i h_v}{\ell n \left(\frac{d_{sh}}{d_v} \right)} \ \frac{P}{c_s M} \ (\theta - \theta_s)$$

$$\frac{\partial \theta_f}{\partial \mu} = \frac{\dot{m} P}{V} \frac{\partial \theta_f}{\partial_\nu} + \frac{UAP}{\rho c V} \ (\theta - \theta_f)$$

The terms which now want to remain constant, i.e., the coefficients which are dimensionless groups are

$$\frac{k_t a_t P}{c_s M L_t} \qquad \frac{(\Sigma ka) P}{c_s M h_V}$$

$$\frac{UAP}{c_s M} \qquad \frac{2\pi k_i h_v P}{\ell n \frac{d_{sh}}{d_v} \; c_s M}$$

$$\frac{mP}{\rho V} \qquad \frac{UAP}{\rho c V}$$

and the $\theta(\mu,\nu)$ and $\theta_f(\mu,\nu)$ will behave exactly the same in the model and in the full size unit. In fact, due to the temperature dependence of many of the properties, it is desirable to have $t(\mu,\nu)$ and $t_f(\mu,\nu)$ behave the same and then the properties at any point μ,ν will be identical. Were it not for this dependence, the experiment could be carried out over a different temperature range by selecting a different t_L.

While it is possible to manipulate the coefficients in a variety of ways and probably arrive at a reduced scale version which in some way represents the real process, consider the most important term in the process, the heat transfer between the T-66 and the Thermkeep. This is described by the overall heat transfer coefficient, U, which is composed of the fluid-to-wall resistance, the tube wall itself, the solid build up on the tube, and the solid to liquid phase resistance.

This term is quite complex and it may be concluded that the best, if not the only, way to assure similitude would be to retain the cycle period, P, the tube configuration, the amount of Thermkeep per tube, and the flow per tube. Then the tubes in the model act essentially identically to the tubes in the full scale unit. This implies that the model should be a full height version of cross-sectional area reduced by the scaling factor as well as the number of tubes, total flow, and implicitly the mass of storage medium. The duty cycle is, of course, the same with respect to time but with heat flows reduced by the scaling factor.

Consider what a scaling like this does to each of the dimensionless groups defined above.

(1) $$\frac{k_t a_t P}{c_s M L_t}$$

This term has the same values of k_t, P, c_s, and L_t for the model and the full scale unit. The total tube conduction area is reduced by the scaling factor since the total number of tubes is reduced accordingly and the total mass of storage medium is reduced also by the scaling factor. Thus, this term is unchanged.

(2) $$\frac{(\Sigma\ ka)P}{c_s M\ h_v}$$

The values of the thermal conductivities, k, P, c_s, and h_v are identical for the model and the full size unit. If the thickness of the vessel is reduced by the square root of the scaling factor and since the circumference of the vessel drops by the square root of the scaling factor, then a term due to the vessel wall goes down by this factor. The medium axial conduction area also automatically drops by the scaling factor. In the denominator, M drops by the scaling factor so that the group remains unchanged from model to full scale.

(3) $$\frac{UAP}{c_s M}$$

The values of U, P, and c_s are identical in both the model and the full size unit, the rationale for equal U having been already explained. The tube surface area is scaled down because of the reduced number of tubes and the Therm-keep total mass is also scaled by the same factor so that the ratio of A/M is unchanged, and the group remains unchanged.

(4) $$\frac{\dot{m}P}{\rho V}$$

P and ρ are the same while the total flow m is scaled and the total volume of T-66 in the tubes is scaled so that the group remains unchanged.

(5) $$\frac{UAP}{\rho c V}$$

The term U, P, ρ, and c are identical for both the model and the full scale unit while the tube surface area and the total volume of T-66 in the tubes are scaled identically. Thus the group remains unchanged.

(6) $$\frac{2\pi k_i \, h_v P}{\ell n \left(\frac{d_{sh}}{d_v}\right) c_s M}$$

The values of k_i, h_v, P, and c_s are identical for the model and the full scale unit. Retaining the equality of the groups requires setting

$$\left[\frac{1}{M\ell n \left(\frac{d_{sh}}{d_v}\right)}\right]_{model} = \left[\frac{1}{M\ell n \left(\frac{d_{sh}}{d_v}\right)}\right]_{F.S.}$$

Noting that the storage medium masses are in the ratio of the scaling factor, R, this requires that

$$\ell n \left(\frac{d_{sh}}{d_v}\right)_{model} = R\ell n \left(\frac{d_{sh}}{d_v}\right)_{F.S.}$$

or

$$\left(\frac{d_{sh}}{d_v}\right)_{model} = \left(\frac{d_{sh}}{d_v}\right)^{R}_{F.S.}$$

Referring to the reference design discussions

$$\left(\frac{d_{sh}}{d_v}\right)_{F.S.} = \frac{3.47}{2.23} = 1.56$$

which is to say that

$$\left(\frac{d_{sh}}{d_v}\right)_{model} = (1.56)^{10} = 85.4.$$

The model shroud would be 60 m (197') in diameter! This is caused by the cylindrical conduction geometry and the fact that the vessel surface decreases only as the square root of the scaling factor.

The solution to this problem was to reduce the surface losses in a different way. Rather than increase the insulation thickness, we can use a reasonable insulation thickness and reduce the temperature difference between the model vessel and the model shroud. This involves the heating of the shroud to an adequately high temperature. Consequently, for safety reasons and to conserve the amount of shroud heating required to maintain a desired temperature, another layer of insulation and an outer unheated shroud are used.

The use of the differential equations to scale the full size unit neglects the heat transfer at the top and bottom ends of the unit. However, it should be clear that since the cross-sectional area of the unit has been reduced by the scaling factor, and since the number of tubes has also been reduced accordingly, the end losses approximately go down by the scaling factor as well.

Subscale Unit Design

As was discussed in the previous section, the scaling guidelines are straightforward and the model was designed as a full height cylindrical section of the full scale unit. The cross-sectional area is one-tenth of that of the full scale so that the diameter is $\frac{1}{\sqrt{10}}$ or .316 of that of the full scale unit. The number of tubes was reduced from 252 to 25 but the length was identical.

The major analytical design task with respect to the model was that of selecting a temperature to which to bring the heated inner shroud in order to sufficiently reduce the surface losses from the vessel. The result of this was that the model would contain 45.7 cm (18") of mineral wool insulation between the vessel and the heated shroud and the shroud temperature would be maintained at 498 K (225 C). The unit would then have another 15.2 cm (6") of insulation contained by an outer shroud.

The criterion was used that the surface losses be the same fraction of the total capacity in both the model and the full size unit. While this criterion was met, there is a difference between the model and the full size unit. Since the effective ambient temperature has been increased and since there exists a gradient from the bottom to the top of the vessel, the distribution of temperature difference between the vessel and ambient is distorted.

In the full scale unit, with an ambient temperature of, say, 296 K (23 C), a top end temperature of 584 K (311 C) and a bottom end temperature of 516 K (243 C), the ratio of ΔT's comparing the top to the bottom is (584-296)/(516-296) = 1.31. In the model, with an effective ambient temperature of 498 K (225 C) and the same top and bottom end temperature, the ratio of ΔT's is (584-498)/(516-498) = 4.78. Consequently, while the total surface loss is in the right proportion, the top end of the unit is penalized

somewhat in that it loses relatively more heat than it does in the full size unit. Since overall the surface losses are only a couple of percent of the total capacity per day, the redistribution should be unimportant.

Figure 17 shows the storage response to solar cycle dynamics for the 1/10 scale model. This may be compared with Figure 15 (page 69), the response for the full scale unit. It is substantially identical. Figure 18 shows the fluid outlet temperature at the hot end (during discharge) vs. cycle time for the model. This may be compared with Figure 16 (page 71) for the full-scale unit. Again, the two are substantially the same. Note, however, that these results were obtained with the incorrect enthalpy as was the reference design. They are shown to demonstrate similarity between the two designs.

The model is basically an insulated vertical cylinder. The storage vessel is 0.70 m (27.5") diameter by 2.23 m (87.8") tall. Since it has 0.152 m (6") of insulation between the heated shroud and the outside shroud, the overall size is 1.93 m (6'4") diameter by 3.45 m (11'4") tall. This is somewhat large for the Comstock & Wescott building so it was installed in an area where a three foot deep pit had been previously constructed for a similar project.

Provision was made to remove the heat exchanger (should a T-66 leak develop). The cold side inlet comes into the unit from the top (or hot side) via an insulated duct so that heat is not transferred to the T-66 passing through it (due to contact with hot end Thermkeep). Heating elements were installed to keep the Thermkeep liquid or bring it back to the liquid state to facilitate replacement of the heat exchanger after repair.

The vessel contains 1500 kg of Thermkeep and 25 tubes, 0.635 cm (1/4") o.d. by 23.1 m (75'9") long, through which the T-66 passes. Measurements of temperature were made on the vessel surface and via horizontal wells extending into the vessel. These gave a measure of the Thermkeep thermal gradient. Their meaning and positioning will be discussed under data analysis.

Construction of Subscale TES Unit

The storage unit is comprised of:

- ... a steel vessel
- ... a heat exchanger which does not penetrate the bottom and is hung from the lid of the vessel
- ... a number of thermocouples set into wells which penetrate the vessel
- ... a number of thermocouples bonded to the surface of the vessel
- ... strip heaters attached to the outside surface of the vessel
- ... 45.7 cm (18") of mineral wool insulation
- ... a light gage sheet metal inner shroud to which are fastened flexible insulated heating wires
- ... 15.2 cm (6") of mineral wool insulation
- ... an outer shroud
- ... support legs
- ... support struts

The vessel was purchased from an outside shop. It stands 2.44 m (96") tall, has an o.d. of .718 m (28"); the side wall is .63 cm (1/4") thick, and the base plate is 1.27 cm (1/2") thick. Twenty holes are drilled into the vessel for insertion of the thermocouples. Figure 19 is a photograph of the vessel lying on its side with the thermocouple wells partially inserted.

Figure 20 shows how the thermocouple wells are formed. Type J (iron-constantan) thermocouple wire was stripped near the end and inserted into the steel well. The end of the well was pinched to clamp the ends of the wires and the flattened end was welded to seal it. The wells were inserted from inside the vessel to the proper depth and welded from the outside to the vessel wall.

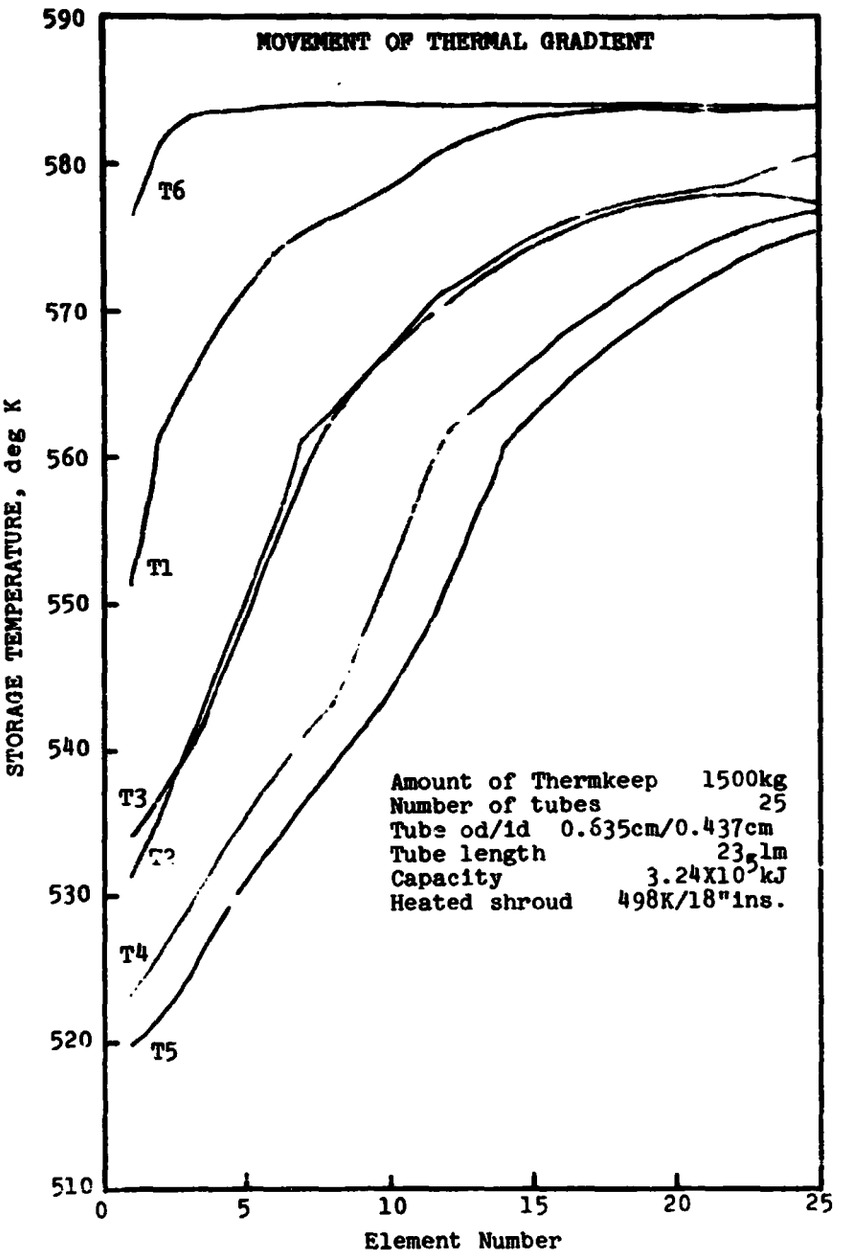

Figure 17. 1/10 model design Thermkeep thermal energy storage unit.

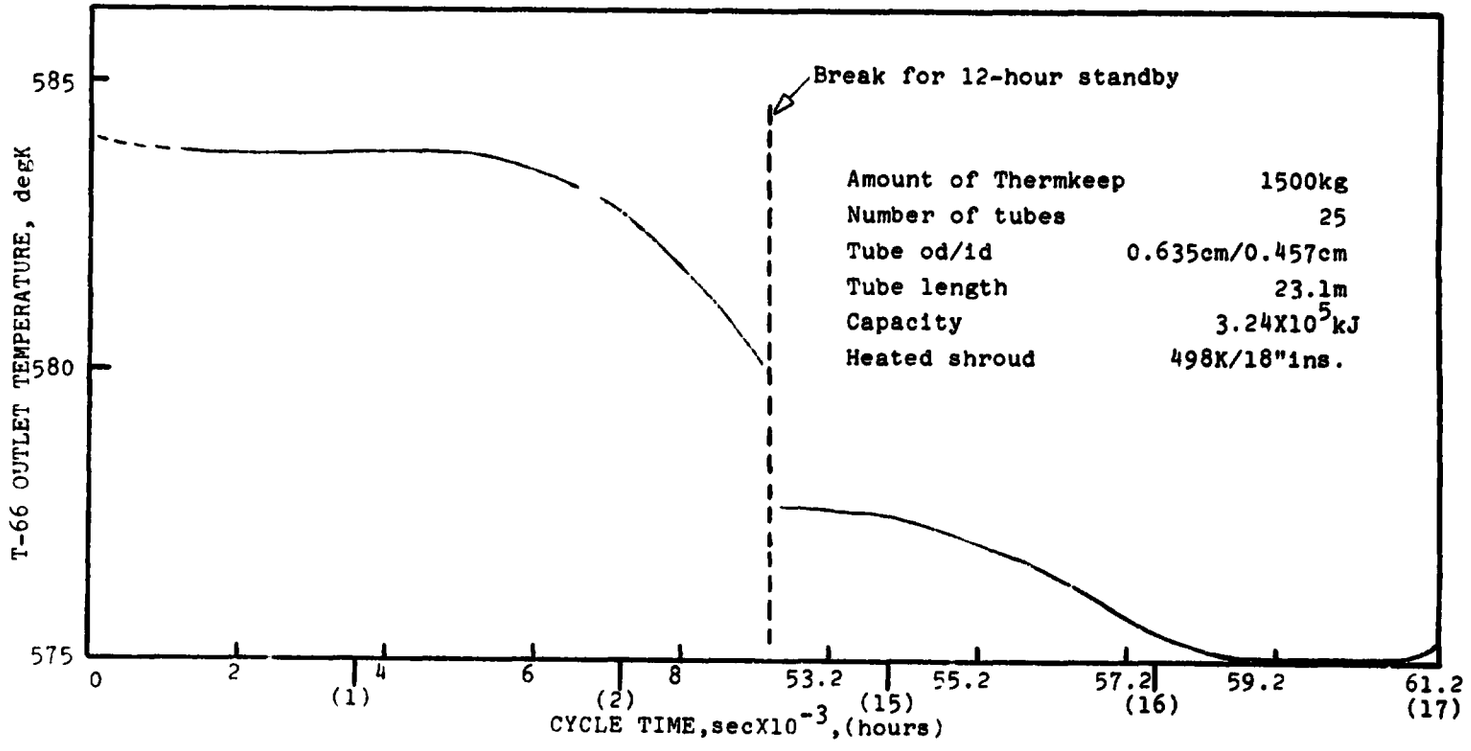

Figure 18. 1/10 model design -- Thermkeep Thermal Energy Storage Unit. Variation of Therminol-66 outlet temperature during discharge.

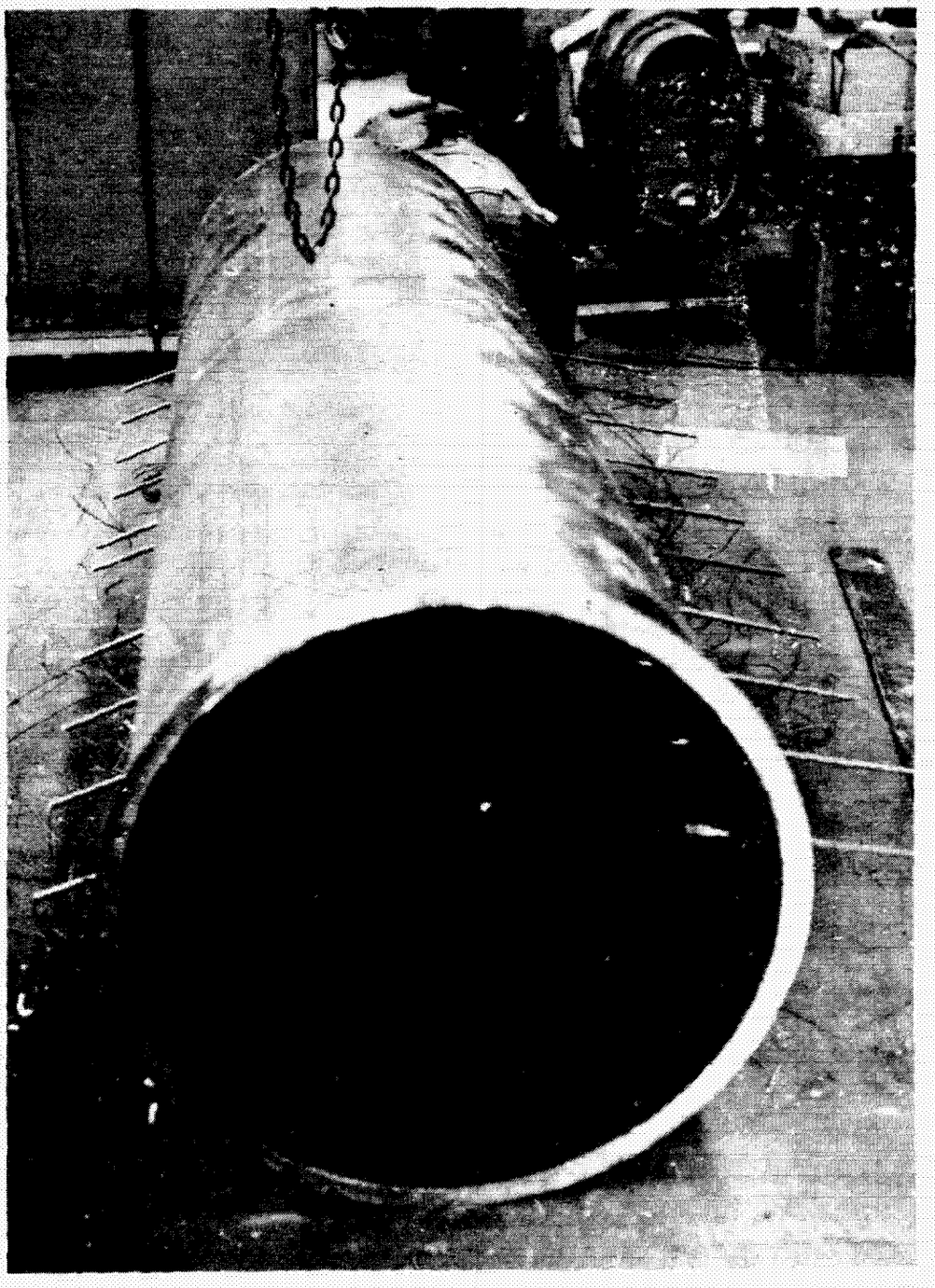

Figure 19. Subscale vessel and partially inserted thermocouple wells.

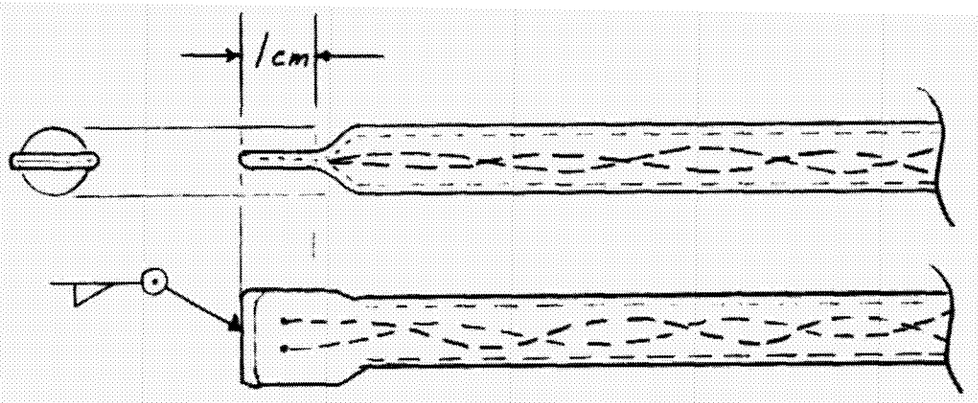

Thermocouple leads are stripped 1cm, laid side by side in a tube, and fixed in place by crimping. The tube end is then welded shut and helium leak-tested.

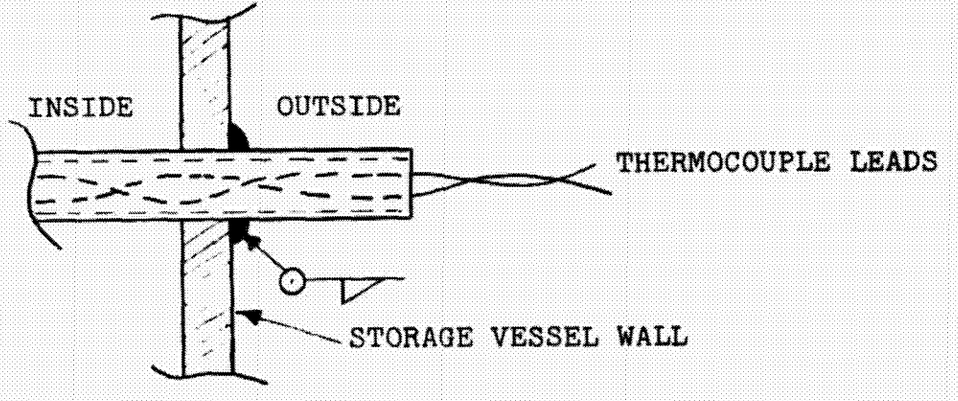

Figure 20. Probe thermocouple.

This design was selected to insure maximum contact between the thermocouples and the surface to be measured. If thermocouples were merely inserted, there was a possibility of poor thermal contact. On the other hand, removal is difficult and would require replacement by simply inserting thermocouples if a failure were to occur, but, due to the double shroud construction and the large quantity of insulation, the wells are not easily accessible anyway.

There are 20 thermocouple wells, arranged in two rows of 10 each, 154^{o} apart from each other and at different depths plus 52 on the surface of the vessel at other positions. The heat exchanger was designed to allow the tube coils to clear the rows of thermocouples should removal of the heat exchanger be necessary. As it turned out, at one point, the heat exchanger had to be removed due to a leak which was discovered before adding the Thermkeep and a couple of wells did not clear the coils and had to be broken to allow removal. These were replaced and the heat exchanger was additionally constrained to prevent this from occurring again.

The heat exchanger consists of twenty-five 23.1 m (76') long steel tubes, .635 cm (1/4") outside diameter by .7 mm (.03") wall thickness. They were coiled on a 10 cm (4") i.d. with a 3 cm (1.2") pitch, for total coil height of 2.2 m (87"). They were arranged inside the cylindrical vessel to be as evenly distributed as possible allowing for thermocouple well and lower manifold inlet tube clearance. The coils were provided with wires between turns to prevent sagging due to solid weight so that the pitch would be maintained. Wire lashing was provided between tubes to hold the lateral spacing between them since they are springlike otherwise and due to flexing would have uncontrolled separation.

Upper and lower manifolds were fabricated from two steel tubes each of 1.7 cm (.67") outside diameter and 2.3 mm (.09") wall thickness rolled into circles of 58.3 cm (23") and 35.8 cm (14"), then cross-connected by a straight length of 2.7 cm (1.05") o.d. steel pipe. The lower manifold was split in two spots to allow for clearing the thermocouple wells for removal. Tubes were welded both to the circular and the straight parts of the manifolds. The two manifolds were spaced in the height direction by a steel bar welded to the top manifold and threaded to a fixture on the bottom manifold.

Figure 21 is a photograph of the two manifolds connected by the bar. Figure 22 is a photograph of the nearly completed heat exchanger being welded. Figure 23 is a photograph of the heat exchanger looking from the bottom end which shows the split lower manifold and the clearance spaces.

The heat exchanger was inserted into the vessel from the open (top) end, three struts were welded across the top of the vessel and the heat exchanger was hung by hooks from these struts. The thermocouple wells were inserted to their approximate depths and welded to the vessel wall. Figure 24 is a photograph of the assembled heat exchanger inside the vessel looking into the top.

The bottom ends of the two shrouds were assembled onto the supporting feet for the vessel in the pit. The vessel was then set on top of its feet. Marinite insulating blocks were used to support the vessel and prevent a direct steel conduction path from the bottom of the vessel to the outside. Figure 25 is a photograph of the vessel standing on the above-described assembly showing the heating cable already fastened to the inner shroud.

The thermocouples were then bonded to the vessel surface and nine strip heaters of .75 kilowatts each were also attached to the vessel surface. Insulation was packed into the bottom of the shrouds and the sidewalls of the heated shroud were attached save for a section allowing space to walk inside to continue the insulating task. Figure 26 shows the completed vessel with part of the sidewall of the heated shroud in place. The inner insulation and the completed heated shroud was assembled. Figure 27 shows this completed assembly sitting in the pit.

The connections for the transfer of T-66 from the test rig to the storage unit were then made and the outer shroud and its insulation were then completed. Figure 28 shows a portion of the completed storage unit. Once the test rig was completed and checked out and it was possible to flow hot T-66 through the heat exchanger, the Thermkeep was added to the vessel. Thermkeep comes in the form of solid flakes and filling was done in steps with partial loads melted down to fill in the void spaces before adding more. Finally, the top of the unit was assembled and insulated.

Figure 21. Upper (left) and lower (right) heat exchanger manifolds.

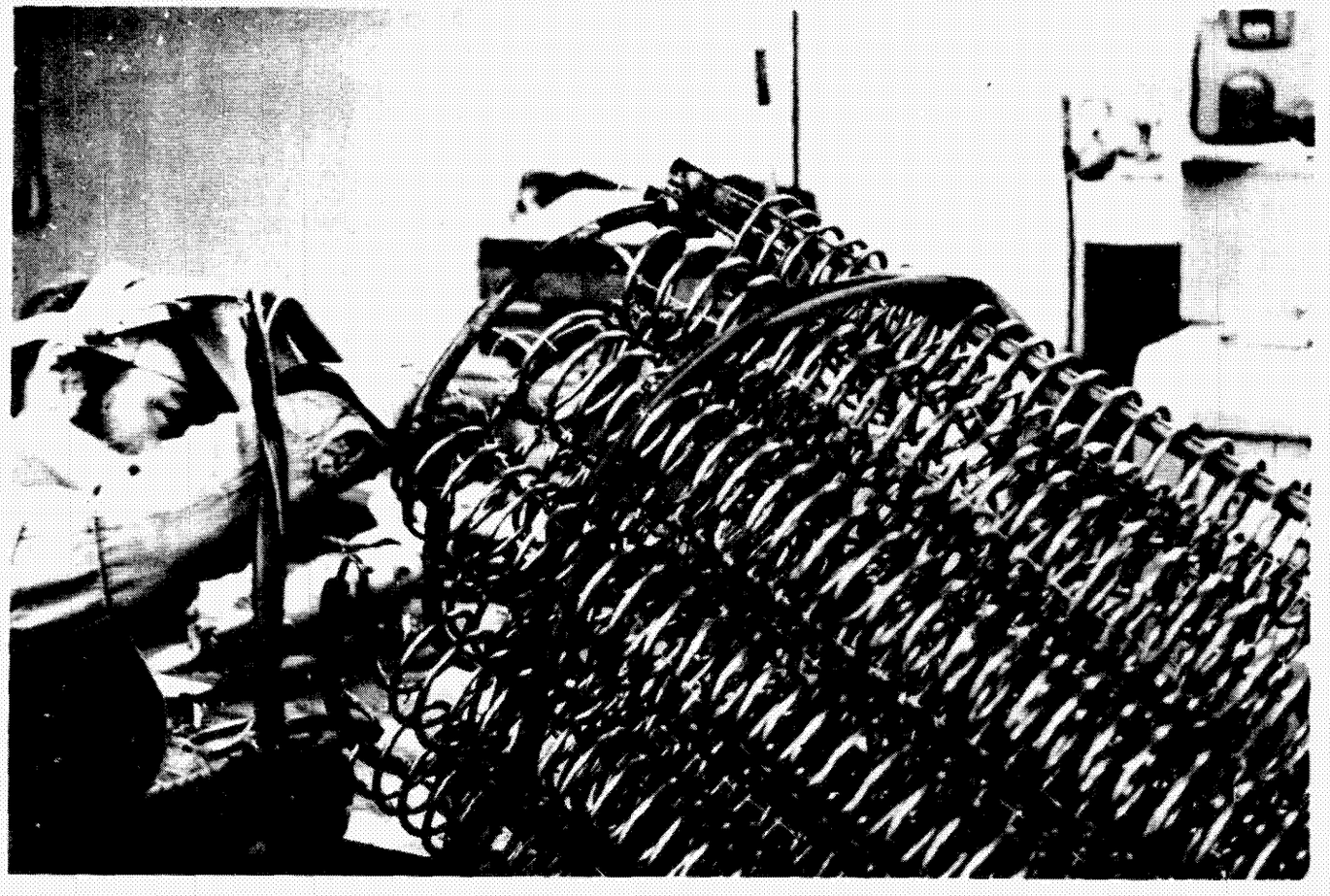

Figure 22. Welding of heat exchanger coils to lower manifold.

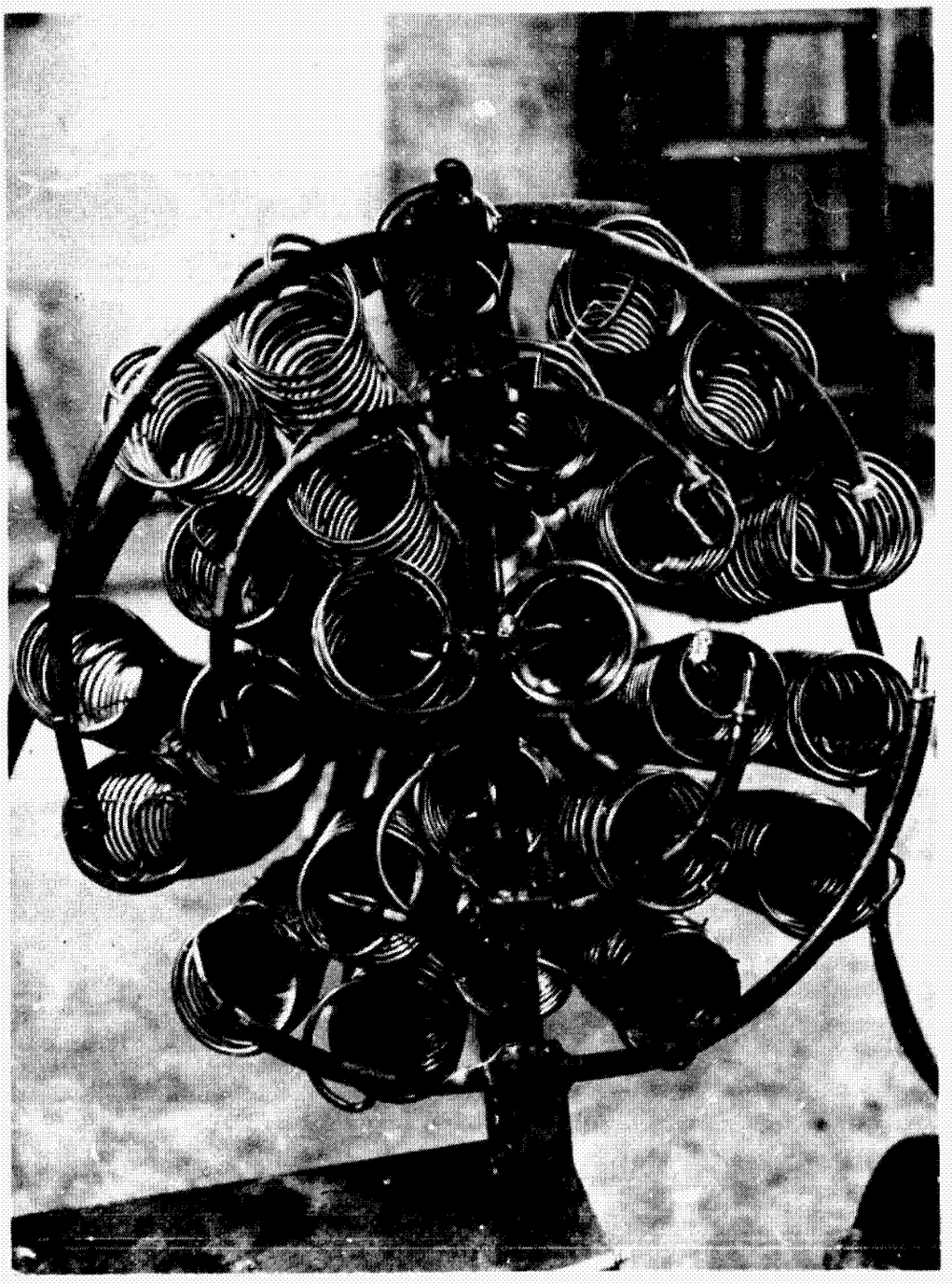

Figure 23. Bottom view of heat exchanger.

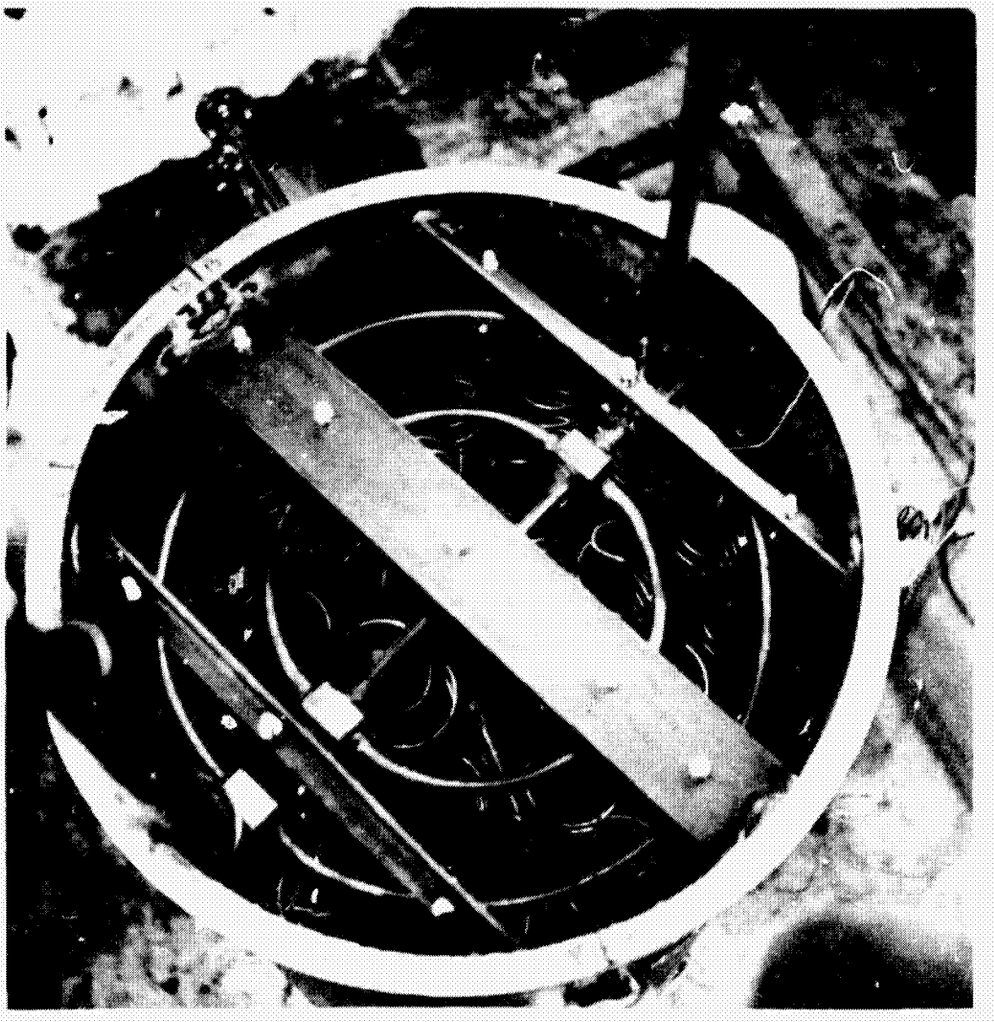

Figure 24. Heat exchanger positioned in vessel (top view).

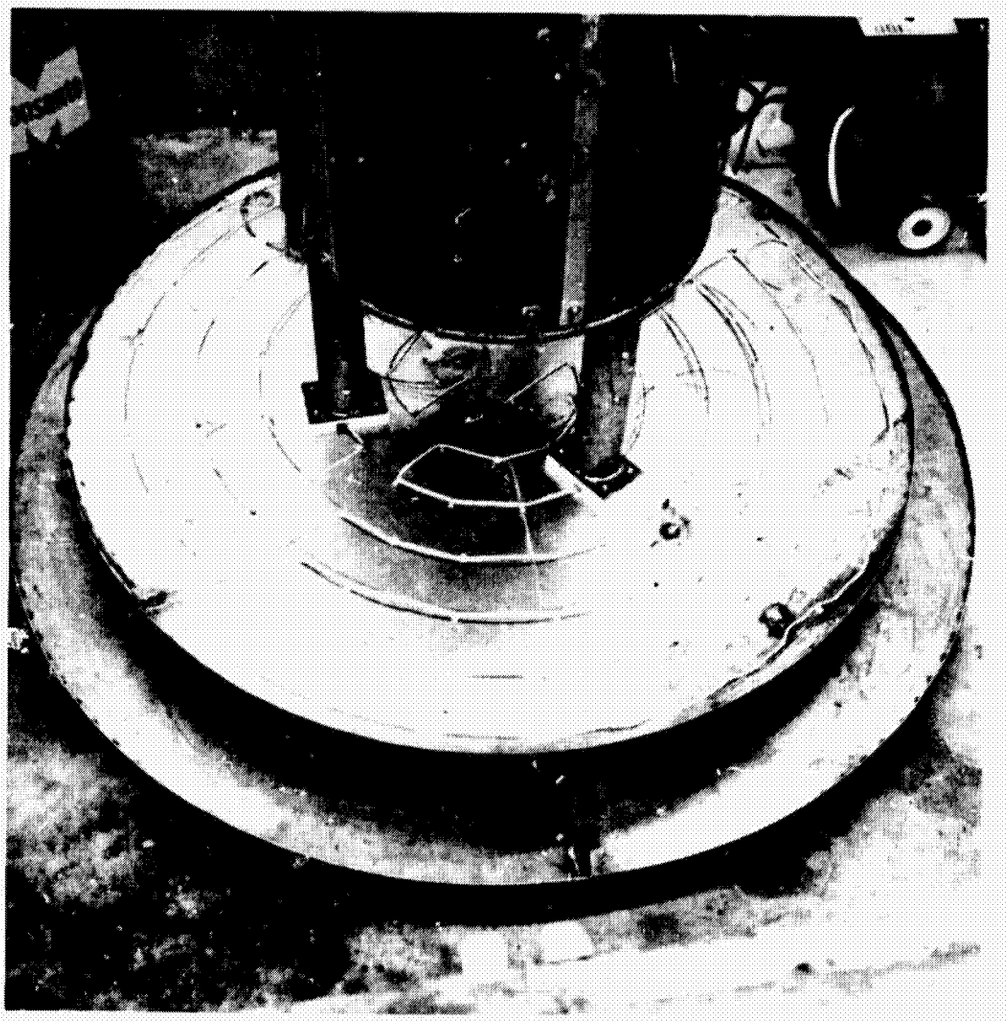

Figure 25. Vessel positioned on shroud assembly.

Figure 26. Vessel (with side heaters attached) showing insulation and vertical heater shroud partially complete.

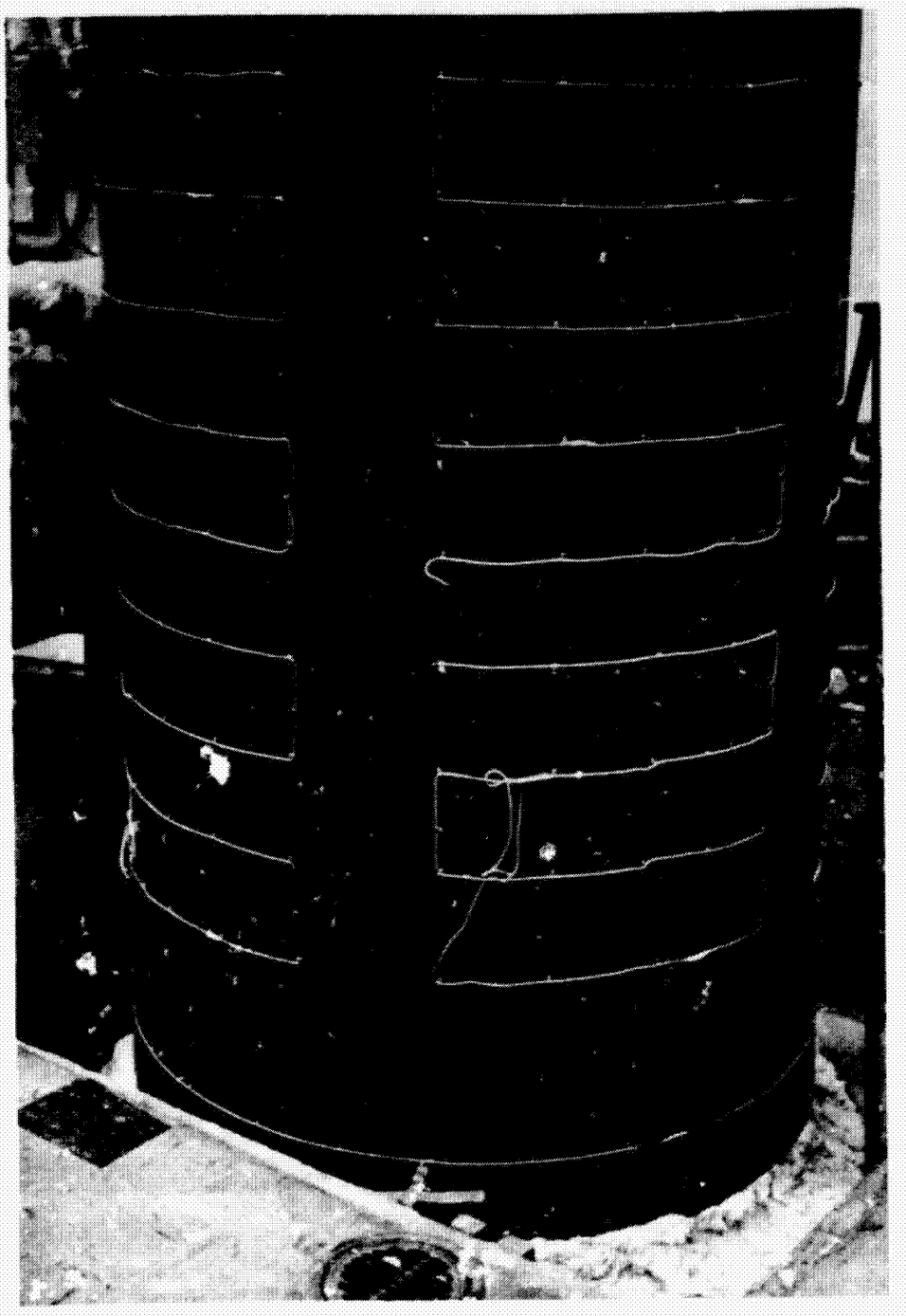

Figure 27. Subscale unit enclosed in inner (heated) shroud.

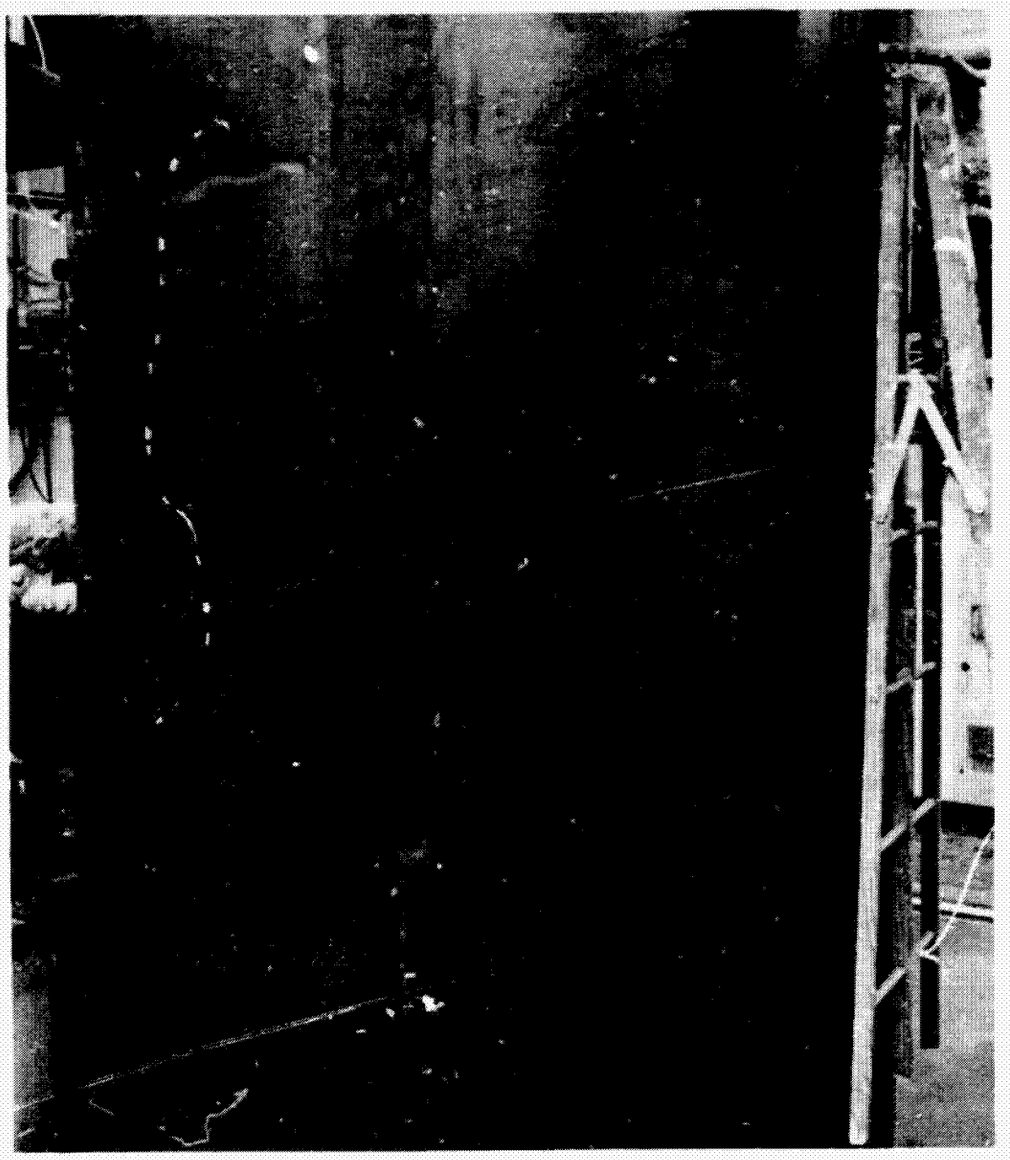

Figure 28. Subscale unit enclosed in outer shroud.

SUBSCALE TEST SYSTEM

A facility has been built which was used to test the performance of the model storage unit. This facility is required to deliver hot T-66 to the unit during charging with provision made to reheat the outlet T-66 as would be done by the solar collectors in the full-scale installation. On the other hand, it is required to deliver cool T-66 to the unit during discharging with provision made to recool the outlet T-66 as would be done by the toluene boiler in the full scale installation.

The test modes, including the solar daily cycle simulation, were to be characterized by constant inlet temperature of the T-66 both during charging and discharging, but, mainly in solar cycle testing, by variable flow rate. The operation of the collector field in the Sandia Laboratories' system maintains a fixed collector outlet temperature of 584 K (311 C) by variation of T-66 flow rate or dumping of excess heat if flow control cannot keep the temperature down due either to intense heating or lack of available storage capacity.

Consequently, T-66 is supplied to the model storage unit from a high capacity, well mixed reservoir controlled to the appropriate delivery temperature. Figure 29 is a schematic diagram of the test apparatus. It does not show incidental details, such as safety relief valves, over-temperature safety shutoffs and low liquid level safety shutoffs, pressure gauges, and temperature sensors installed in the actual system.

The reservoir is a 66 gallon horizontal cylindrical steel vessel. It is contained in a rectangular sheet steel box insulated by mineral wool. Set point temperature is maintained by three 10-kilowatt, 480 V tubular electric immersion heaters. This allows supply of the rated 25 kW of heating to the T-66 plus a margin to compensate for losses.

Control for the heaters to maintain set point is provided by a proportional plus reset plus rate type of driver and a solid state zero-crossover-firing power controller rated at 41 kVA. The rate function provides fast response while the reset feature provides long term accuracy on set point. A high temperature water cooled centrifugal circulating pump is used to mix the T-66 in the reservoir to prevent thermal stratification and the consequent poor temperature control which was experienced before installation of the pump.

When the mode of operation of the storage unit is that of charging, the T-66 exits from the bottom manifold cooler than it entered. Then the heaters are all that are required to maintain delivery temperature. On the other hand, during the discharging mode, the T-66 exits from the top manifold hotter than delivery temperature. Here the cooling which the toluene boiler would cause must be provided.

This cooling is done in a heat exchanger immersed in water in a 55-gallon drum. The heat exchanger is formed by two helical coils of 2.54 cm (1") copper tubing manifolded in parallel. Facility water flows into the drum at the bottom and exits hotter from a drain on the side of the drum near the top. The heat exchanger and water flow rate were chosen to inhibit boiling of the water (assuming a 584 K (311 C) T-66 inlet temperature), so that energy balances could be made from measured water temperature and flow rates.

The performance of the heat exchanger was calculated so that, without having to adjust the flow of water, the T-66 would be at least cooled below set-point delivery temperature. Moreover, it should never overcool so much that the 30 kW of heating capacity would be insufficient to return the T-66 temperature to set point. Therefore, no cooling control is required, the cooler is completely passive, and the heating control, which is quite dependable, is used both for charging and discharging tests to hold a constant delivery temperature.

The expansion tank, which compensates for the change in density of the T-66 with temperature changes, was fashioned after the guidelines described by Monsanto Company brochure, "Therminol Heat Transfer Fluids, a Design, Operating, and Maintenance Guide for Low-Cost, Low-Pressure Heat Transfer Systems." The capacity of the tank is such that the level of the T-66 stays within the tank regardless of the temperature. It has a side-mounted sight glass to observe the T-66 level. A slight pressure of dry nitrogen gas is maintained above the T-66 to prevent oxidation if air were present. A low level safety switch which shuts off the reservoir heaters was installed.

The T-66 is pumped to the storage unit by a high temperature rotary pump with graphite asbestos packing. Maximum flow is 7.5 gpm. The pump is driven by a shunt wound d.c. motor controlled by a motor controller which can be operated either manually or by command from an analog control system. The latter option was required to allow scheduling of the T-66 flow rate for solar cycle simulation.

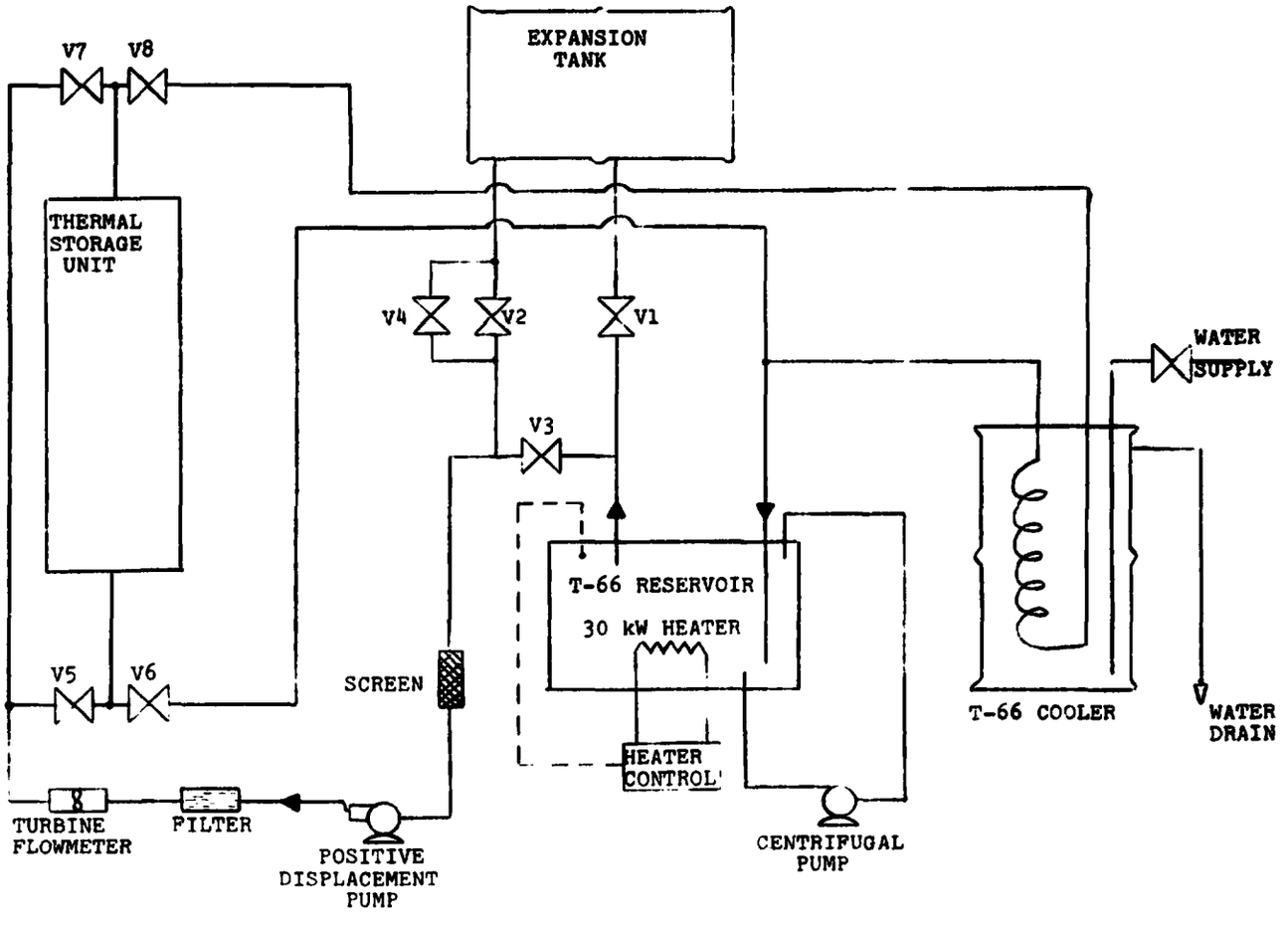

Figure 29. Test circuit schematic.

A high temperature turbine flowmeter is used in conjunction with a flow rate monitor (D/A converter) to generate a flow signal. The flow signal is used as a measure of the T-66 flow rate and also as a feedback signal for an analog flow control circuit commanding the motor controller for the delivery pump.

Two groups of valves can be seen on the schematic diagram (Figure 29). One group (V1-V4) is for regulation of function of the expansion tank. During startup, V1 and V2 are open, V3 and V4 are closed. This allows T-66 to pass through the expansion tank for deaeration. After a short period of time, V3 is opened, V1 and V2 are closed, and V4 which is smaller and on a smaller diameter pipe is open. This valve and pipe are sized smaller so that the expansion is allowed but thermal syphoning of the T-66 is inhibited.

The second group of four valves (V5-V8) controls the flow direction to the thermal storage unit. During a charging test (heating the storage medium), T-66 flows from the reservoir through valve V7 (V8 is closed), into the top manifold of the unit, through the heat exchanger, out of the bottom manifold, through valve V6 (V5 is closed) and back to the reservoir for reheating. During a discharge test (cooling of the storage medium and heating of the T-66), T-66 flows from the reservoir through valve V5 (V6 is closed), into the botton manifold, through the heat exchanger, out of the top manifold, through valve V8 (V7 is closed), through a heat exchanger which cools the T-66 with facility water to below the reservoir control temperature and back to the reservoir for reheating.

Figure 30 is a photograph of all of the aforementioned components of the test facility except for the expansion tank which is elevated beyond the upper edge of the photograph. The drum, containing the heat exchanger for cooling the T-66, is in the left foreground with the drain to the left side. The rectangular box to the rear contains the T-66 heated reservoir. Connections to the upper and lower manifolds of the storage unit are in the right foreground with the edge of the pit containing the unit also visible. This photograph was taken before the pipes were insulated with Fiberglas.

Pressure measurements using standard Bourdon-tube gauges were made at various points in the circuit: upstream of the high temperature rotary pump; between the pump and filter; between the filter and the flowmeter; upper heat exchanger manifold; and lower heat exchanger manifold.

Figure 30. Major components and piping for test system.

In addition to the temperature measurements inside the storage unit, certain temperatures were measured in the external circuit: water supply temperature, water drain temperature; T-66 temperatures into and out of the cooler heat exchanger; upper and lower manifolds of the storage heat exchanger; and two points inside the heated reservoir plus the control point which is near the delivery tube. All temperature sensors are type J (iron-constantan) thermocouples.

Figure 31 is a block diagram schematic of the circuit logic for the analog flow control circuit. The feedback loop compares the measured flow rate from the output of the flowmeter with a desired flow rate and causes the motor controller to adjust pump speed until the error is effectively zero. For steady flow rate testing, a fixed value of desired flow is input to the comparator. The rest of the circuitry is used to program the flow using the cam program controller.

The block function q(t) represents the cam program controller. To use it, one takes a circular disk, which rotates at a predetermined rate in the controller, and forms the desired function by cutting the disk accordingly. A cam follower displaces an amount determined by the disk pattern and generates a 0 to 8 VDC analog signal. Normally this is coupled to an appropriate temperature controller which then could, for example, regulate a furnace temperature to achieve a certain controlled process.

In this case the controller output is taken to be a rate of heat flow, either the excess heat from the solar collectors which one is attempting to put into storage, or the heat deficiency of the solar collectors which one is attempting to extract from storage. As was discussed in the section on analysis, the flow rate to the storage unit is determined differently for charging than for discharging.

The storage unit is, in essence, a large thermal regenerator. It is characteristic of such a device that, as heating or cooling proceeds, the outlet temperature of the fluid changes. During discharge, the delivery temperature to the boiler will drop and during charging, the delivery temperature to the solar collectors will rise. In the former case, the temperature deficiency is accepted and it is assumed that, possibly, a means of boosting the temperature, e.g., a fuel-fired burner would be provided.

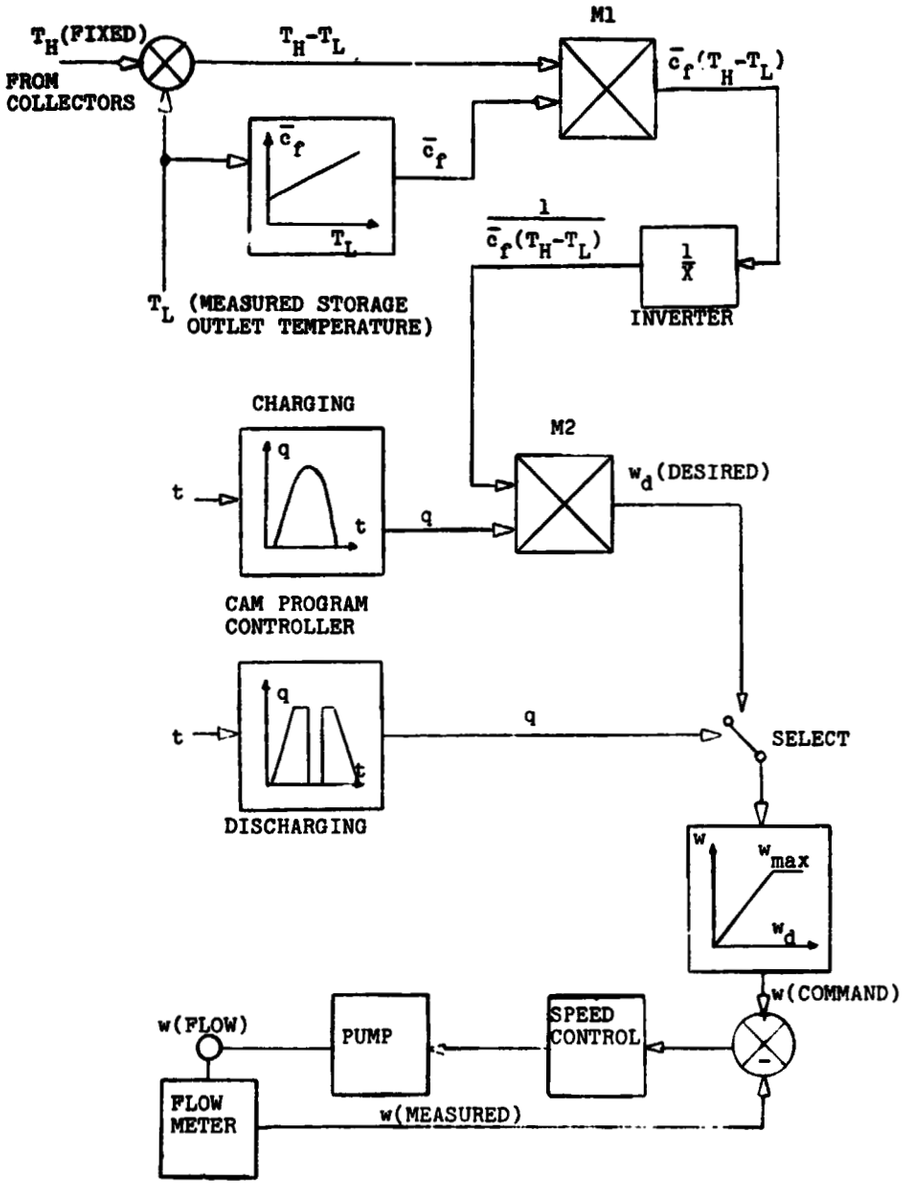

Figure 31. Main T-66 pump control circuit schematic.

In the latter case, it is assumed that the flow rate through the collectors would be increased to attempt to absorb all the heat collected in the face of a diminishing temperature rise. The additional circuitry shown accomplishes this additional flow rate adjustment.

For discharging, a cam is cut which outputs the difference between the fixed flow rate demanded by the boiler and the flow rate which is expected from the solar collectors as described by the characteristic curve. The multiplier (M2) shown on the block diagram would be bypassed and the flow demanded would be in direct proportion to the output of the program controller. The shape of the flow demand is such that flow begins at zero in the late afternoon when the collector output becomes equal to the boiler demand. Thereafter, the storage flow increases until the collector output ceases and all the boiler flow passes through storage. The flow rate is constant until the beginning of the nighttime idle period at which point it becomes zero. In the early morning, after the idle, storage flow begins at full boiler flow, stays constant until collector output begins and decreases steadily to zero flow which occurs when the collector output rises to the value of the boiler demand.

During charging, one would like to absorb all the output of the solar collectors. If this occurred, one could write the equation

$$q_{ex} = w_f \bar{c}_f (T_H - T_L)$$

where T_H is the fixed delivery temperature from the collectors (584 K; 311 C), T_L is the variable outlet temperature from storage, $\bar{c}_f$ is the average T-66 specific heat over the range T_L to T_H, w_f is the required flow and q_{ex} is the heat available to go into storage. The flow rate function becomes

$$w_f = \frac{q_{ex}}{\bar{c}_f (T_H - T_L)}$$

The control circuit takes the value of T_L, as measured at the lower manifold, and uses it first to form the difference, $T_H - T_L$, in the summer shown, and second to form the average specific heat in the function block $\bar{c}_f\ (T_L)$ where this can be described as a function of T_L only with T_H fixed. The outputs of both of these operations are input to the multiplier to form the product $\bar{c}_f(T_H - T_L)$ which is then inverted to form $1/\bar{c}_f(T_H - T_L)$. This value together with q(t) is input into the multiplier to form the demanded flow according to the aforementioned equation. Lastly, it is expected that the pump would be limited to some realistic flow rate, at least to limit the pressure loss through the system so that the function $w(w_d)$ is essentially a limiter whereby $w \equiv w_d$ up to w_{max} at which point it no longer increases. Moreover, the flowmeter cannot function below a minimum of about 0.75 gpm so that the solar characteristic cams were modified to demand no less than this.

Debugging the facility involved the usual problems associated with such a system. Erratic behaviour of the turbine flowmeter was traced to two problems, First, the wrong sensor head was provided. Rather, one rated for only 355 K (180 F) was received and had to be replaced by the factory. Second, problems were traced to the D/A converter and certain factory recommended adjustments had to be done.

It was expected that the test flow rate would be adequate to agitate the T-66 in the reservoir. However, the T-66 formed a thermocline (thermal stratification) and a centrifugal circulating pump had to be ordered. T-66 leaks developed in the plumbing, a problem which is known to be quite prevalent with this fluid, and these had to be repaired. Other minor problems were also rectified.

Overall, it is felt that a very useful test facility now exists. It can be used to model any test duty cycle which requires fixed temperatures and variable flow rates. The next section discusses the performance testing which was done on the model storage unit using this facility.

SUBSCALE TEST RESULTS AND EVALUATION

Preliminary Discussion

The steps which led to the final form of the analysis will be briefly discussed. Then all the data and the computer predictions will be presented and compared, the computer predictions being those from the final form of the analysis.

A number of changes were made to go from the design analysis used in the reference design tc the test analysis. Some relate to simulation of test conditions and will not affect the analysis to be used for design of a full scale unit. These modifications involve the ability to input the proper starting conditions of the unit (i.e., temperature distribution), to input a variable T-66 inlet temperature for runs where this temperature had not yet stabilized by the start of the test, to input the proper constant flow rate, and to override the solar cycle schedule normally in the program. Three decks of computer cards were produced from the original program. One simulates a single-pass heatup, one simulates a single-pass drawdown, and one simulates the square-wave cycling.

Other changes relate to updated knowledge of material properties. Since the reference design was produced, new information was received from the Monsanto Company on the properties of T-66 and new information was provided by Dynatech R/D Company on the properties of Thermkeep. These changes were incorporated into the program.

New tables of the enthalpy and solid fraction of Thermkeep as a function of temperature were input. These were composed on a rational basis but are not based upon laboratory measurements. As mentioned, the h(T) data expected from the subcontractor were never properly produced and C&W used the best information previously available.

The enthalpy vs. temperature curve was adapted from a temperature vs. time cooling curve done in the C&W laboratory (see Figure 32). The use of this has produced reasonably good results, as will be seen, but it is believed that some of the lack of agreement between test

and analysis can be attributed to the lack of accuracy in the enthalpy-temperature correlation. The solid fraction, $\phi(T)$, was adapted from a phase diagram for the binary system $NaOH-NaNO_3$ (Ref. 3). This also is not considered to be highly accurate, but it is not considered as significant a factor as the inaccuracy in the h(T) curve in contributing areas of lack of agreement.

The only important change made in the calculation procedure was the inclusion of a correction to the fluid side heat transfer coefficient caused by the winding of the tubes in a springlike helix (Ref. 4). The original computations were based upon straight tube correlations. The new correlation says that the critical Reynolds number for transition from laminar to turbulent flow is increased according to

$$Re_{crit} = 2100 \left[1 + 12 \left(\frac{d_t}{d_h} \right)^{0.5} \right]$$

where d_t is the tube diameter and d_h is the helix diameter.

Moreover, the heat transfer coefficient in laminar flow is increased as follows. Define

$$D = Re \left(\frac{d_t}{d_h} \right)^{0.5}$$

and

$$Q = \left(D^2 \, Pr \right)^{\frac{1}{4}}$$

Where Pr is the fluid Prandtl number, then

$$\frac{Nu_c}{Nu_s} = 0.181Q \left(1 - 0.839Q^{-1} + 35.4Q^{-2} - 207Q^{-3} + 419Q^{-4} \right)$$

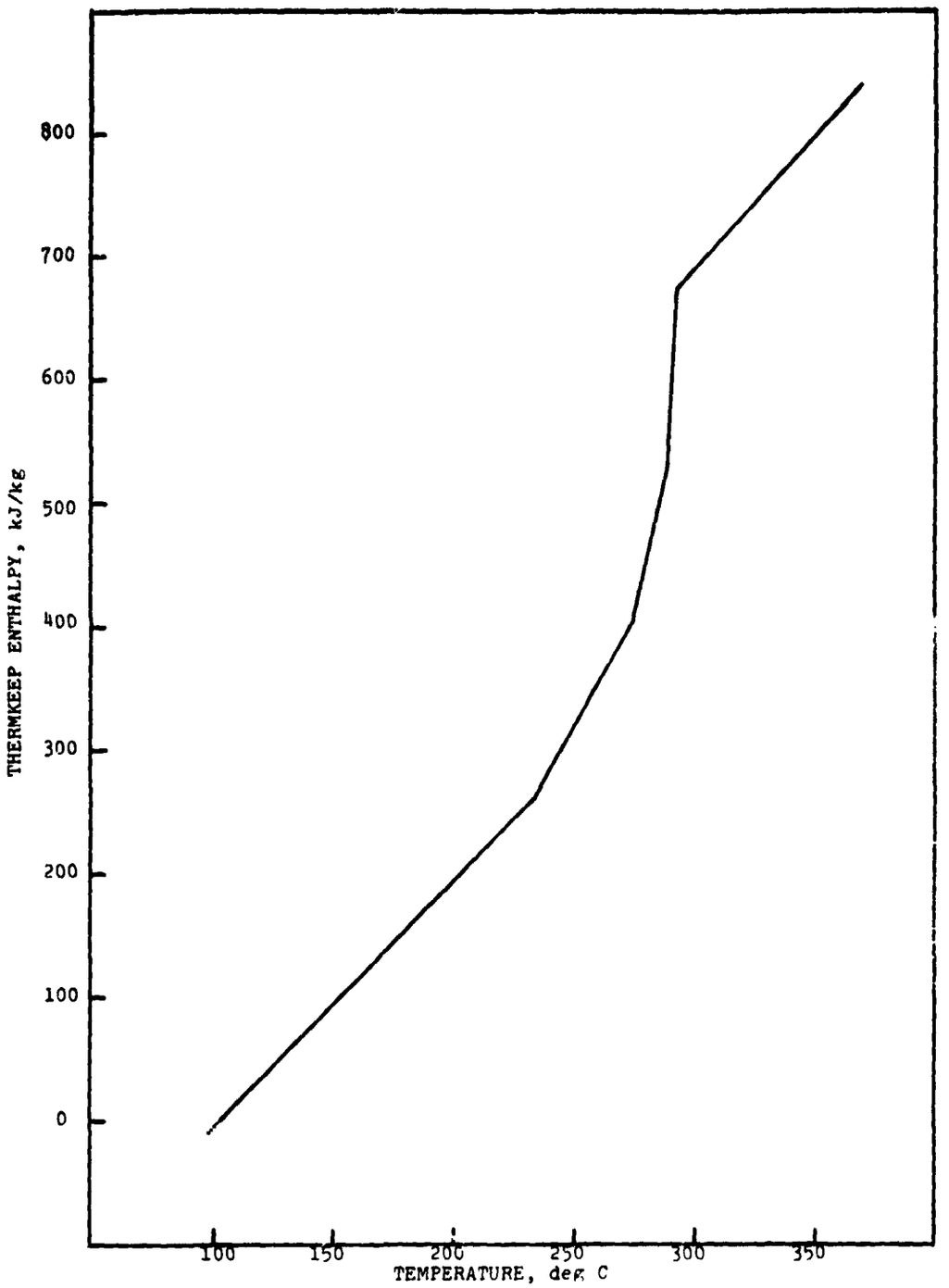

Figure 32. Thermkeep enthalpy from C&W cooldown data.

where Nu_c is the Nusselt number for curved tubes and Nu_s is the Nusselt number for straight tubes. Using this correction for the low flow rate tests brought the agreement from poor to good and this verifies its usefulness. Other than this change, the method of the computer analysis stands essentially as it was for the reference design analysis.

Description of Test Procedures

The model TES unit was installed into the test facility and then subjected to a variety of tests to determine its ability to accept heat from and deliver heat to the heat transfer fluid. These tests fell into four basic categories, each with its own objective.

1. One-Pass Charge/Discharge Testing

In this type of test, which was the basic source of data for tuning the computer analysis, the unit is brought to either a typical charged or a typical discharged condition and then either discharged or charged at a constant flow rate. The change of the internal condition of the unit was observed as a function of time as well as the change in delivery temperature of the T-66. A number of different flow rates were checked ranging from 0.05 kg/sec (1 gpm) to 0.29 kg/sec (6.3 gpm).

2. Idle Tests

In this type of test, the unit was brought to a hot or charged condition, flow was stopped, and the change in internal condition was recorded as a function of time. The purpose of this test is to eliminate the effect of heat transfer with the fluid and observe only the effects of axial conduction and losses to the environment.

3. Square-Wave Cyclic Testing

In this type of test, the unit is brought to a typical charged condition and then alternately discharged and charged at constant T-66 flow rates with minimal changeover times. The purpose of this test is to verify that the unit approaches a stable condition under cyclic operation and that, without specifying the starting condition for each segment of the test, except for the initial starting condition, the analysis could predict the performance after a number of repetitive cycles.

4. Solar Daily Cycle Testing

These tests were run to describe how the unit would function under solar cycle conditions where flows would vary according to a prescribed schedule and a control mode. This continual variation would create difficulty in using this type of test for tuning the analysis but would be a proof test of the unit under realistic conditions.

The test conditions were selected to be 1/10 scale of the typical full scale conditions. T-66 temperature during a charge was held at around 584 K (311 C) while during a discharge, it was held at around 516 K (243 C); however, these changed somewhat from test to test.

With a 25 kW heat load and a 68 K available overall ΔT, a T-66 flow of about 0.14 kg/sec (3 gpm) is required. The test flows ranged from 0.05 kg/sec (1 gpm) to 0.29 kg/sec (6.3 gpm) but most tests were run in the 0.09 to 0.16 kg/sec (2 to 3.5 gpm) range. A range of flows is desired since in an operational system, the flows would vary as the available collector output changes.

The primary objective of testing was to determine if the computer analysis to be used for the design of large scale TES units is accurate in its description of how the unit would respond to a given stimulus. If reasonable accuracy can be obtained, then the analysis can be used for determination of efficiencies, delivery temperatures, pressure drops, and any other factors considered important in designing a full-scale storage unit.

Comparison of Computed and Experimental System Response

One-Pass Charge/Discharge Test Results

For a steady flow discharge test, the unit is brought to a reasonable charged condition and a flow of T-66 (at low cycle temperature) is introduced into the bottom manifold. The hot-end outlet temperature of the T-66 as a function of time is the critical characteristic in that temperature deficiency here impacts directly on the turbine performance and must be compensated. Figures 33 through 40 plot the T-66 outlet temperature during drawdown tests for flow rates increasing from 0.05 kg/sec (1 gpm) to 0.29 kg/sec (6.3 gpm).

Except for test No. 007, which started at quite a low state of charge, the computer predictions agree reasonably well with the measurements. The only observation that seems at least somewhat consistent is that between 577 K and 566 K, the unit delivers more heat than predicted and vice versa below 566 K. This suggests that the h(T) curve used should be reshaped to have less of a plateau at 566 K with slightly more energy available above 566 K and a more rounded shape below 566 K.

Figures 41 through 49 are comparisons of measured thermal distribution with computed distribution. The computer technique assigns one value of temperature to any depth and ignores lateral gradients. As may be seen by some of the figures, especially in the lower temperature regions, the measured values do not necessarily fall on a single line. There are two axial rows of thermocouples, each row at a different radial position in the unit. Thus, the existence of radial (lateral) gradients would cause disagreement between each set. Radial gradients tend to occur in lower temperature regions because more of the Thermkeep is solid. Circulation in the liquid phase prevents this from occurring.

Note that the computed axial temperature profiles do not extend to the top of the vessel. The initial height of the Thermkeep depends on the initial temperature of the Thermkeep, and actually varies in some cases over a range of roughly 20cm during operation of the system. The computed points are associated with the estimated total height of Thermkeep defined by the initial measured temperature profile. The estimated distance of the Thermkeep surface from the top of the vessel is indicated on the figures. Thus, measured points above this estimated

Thermkeep surfaces are interpreted as being in the air space above the surface and are not computed by the analytical model.

Again, except for test No. 007, the data and analysis agree quite well. The analysis predicts a longer dwell at 566 K than actually seems to occur, suggesting that the plateau on the h(T) curve may be too strongly defined.

For a constant flow charging test, the unit is brought to a low state of charge and a flow of T-66 (at high cycle temperature) is introduced into the top manifold. The cold-end outlet temperature of the T-66 as a function of time is the critical characteristic in that rising outlet temperature requires additional flow to absorb the collector output without exceeding a specified upper temperature limit. Figures 50 through 54 plot the T-66 outlet temperature during charging tests for flow rates varying from 0.05 to 0.3 kg/sec (1 to 3.5 gpm).

Overall, the agreement is reasonably good. The computer prediction of the outlet temperature is higher than measured outlet temperature. This is possibly due to over-estimating the resistance of the solid Thermkeep layer. The rate of rise of the temperature is consistently good which could be indicative of a fair agreement in h(T) in the low temperature regions.

Figures 55 through 59 are comparisons of measured thermal distributions with computed distributions. Again, the computer seems to predict a stronger than measured plateau at 566 K which also may be due to incorrect shaping of h(T) in the vicinity of this temperature. Otherwise, the agreement is reasonably good. The fact that both the cold-end outlet and cold-end distribution are off in the same way, i.e., that the computer predicts higher temperatures than the data, could indicate an error in h(T) rather than in the resistance of the solid layer.

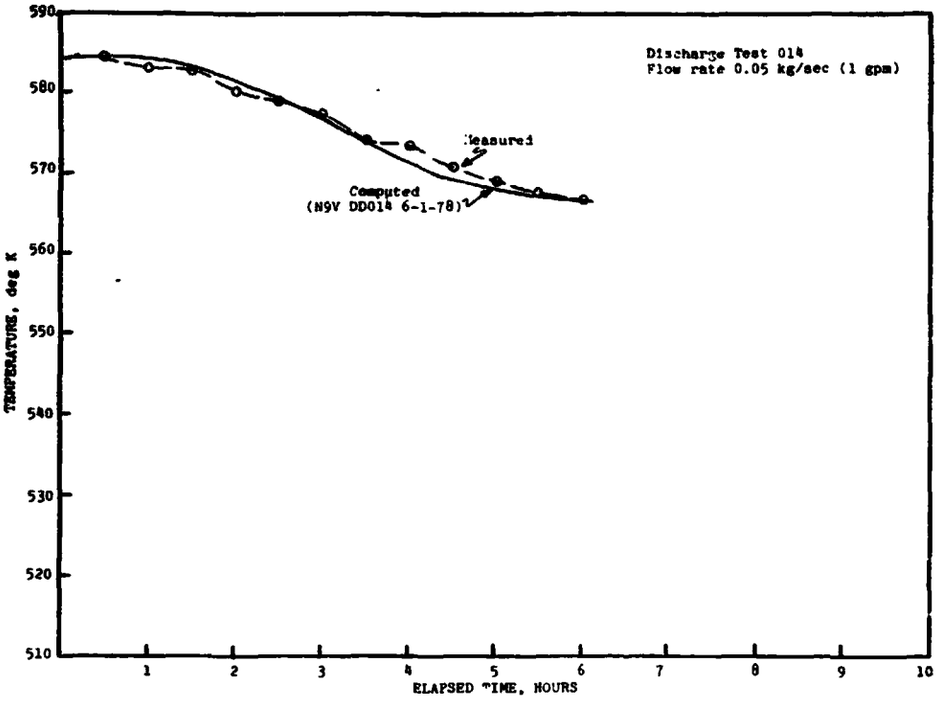

Figure 33. T-66 outlet temperature discharge test 014 (1 gpm).

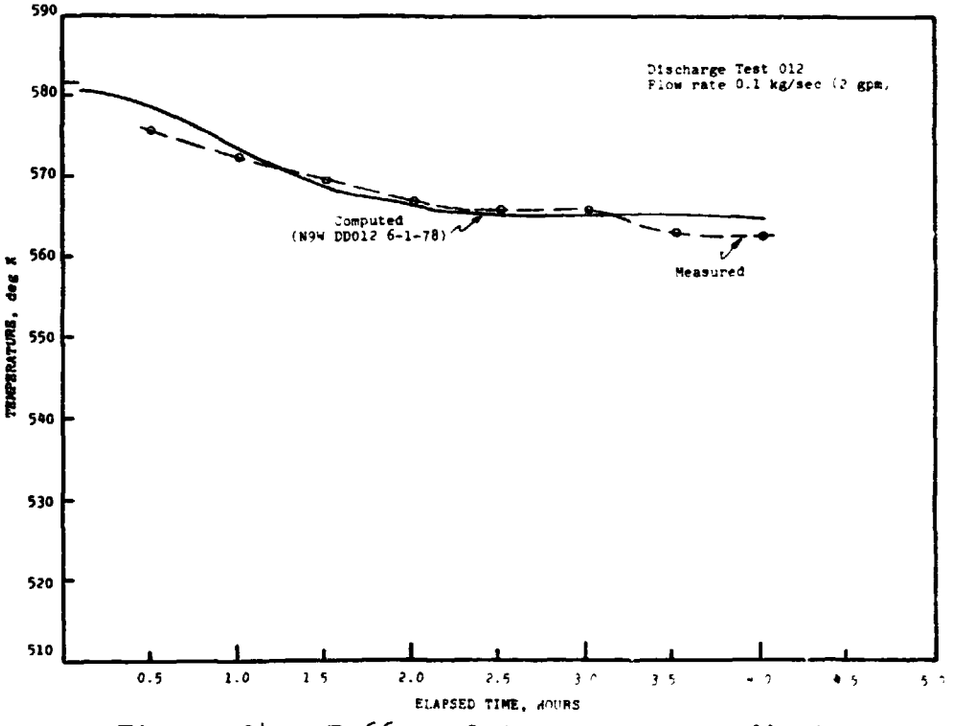

Figure 34. T-66 outlet temperature discharge test 012 (2 gpm).

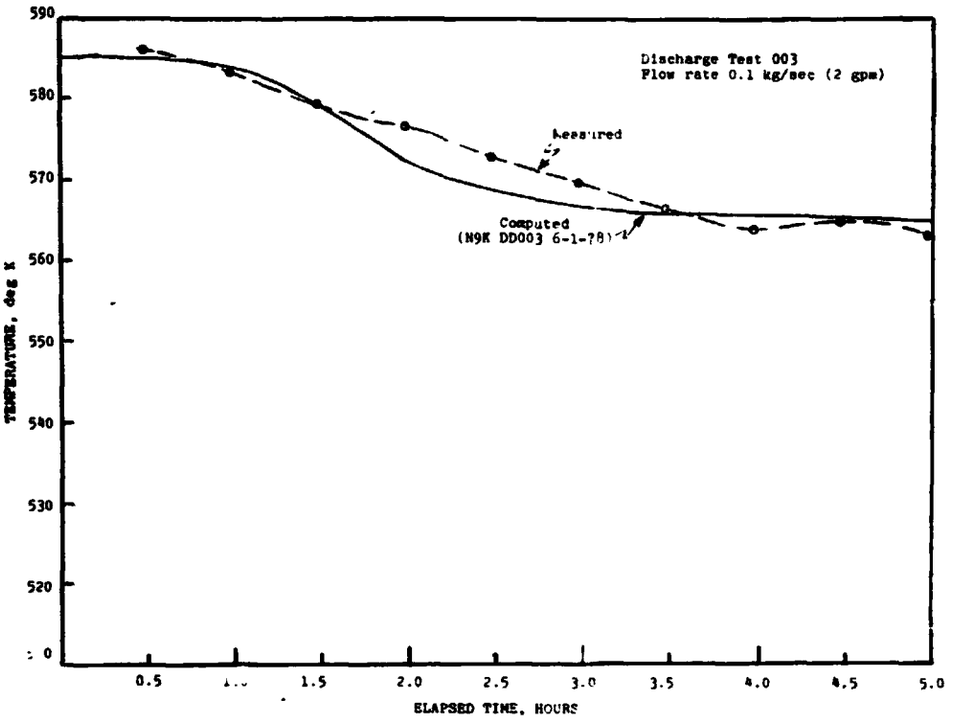

Figure 35. T-66 outlet temperature discharge test 003 (2 gpm).

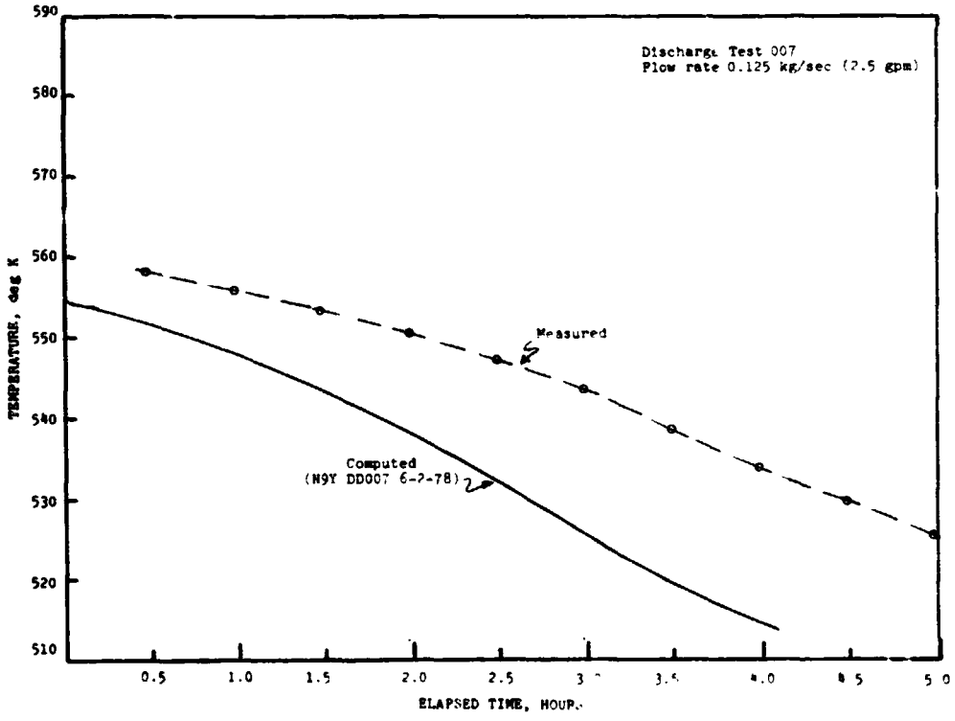

Figure 36. T-66 outlet temperature discharge test 007 (2.5 gpm).

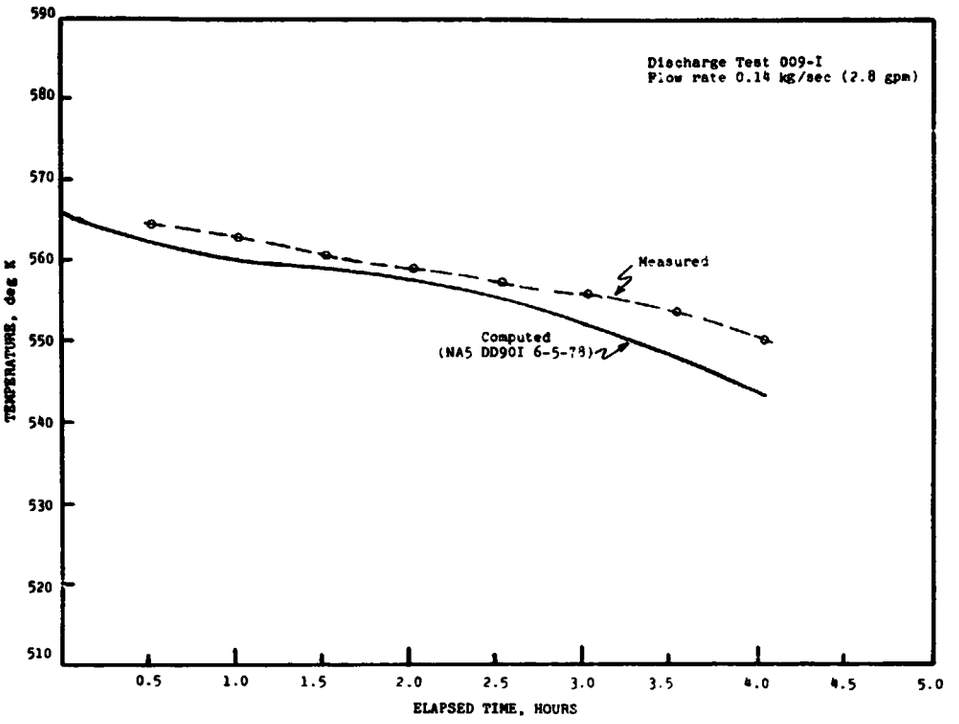

Figure 37. T-66 outlet temperature discharge test 009-I (2.8 gpm).

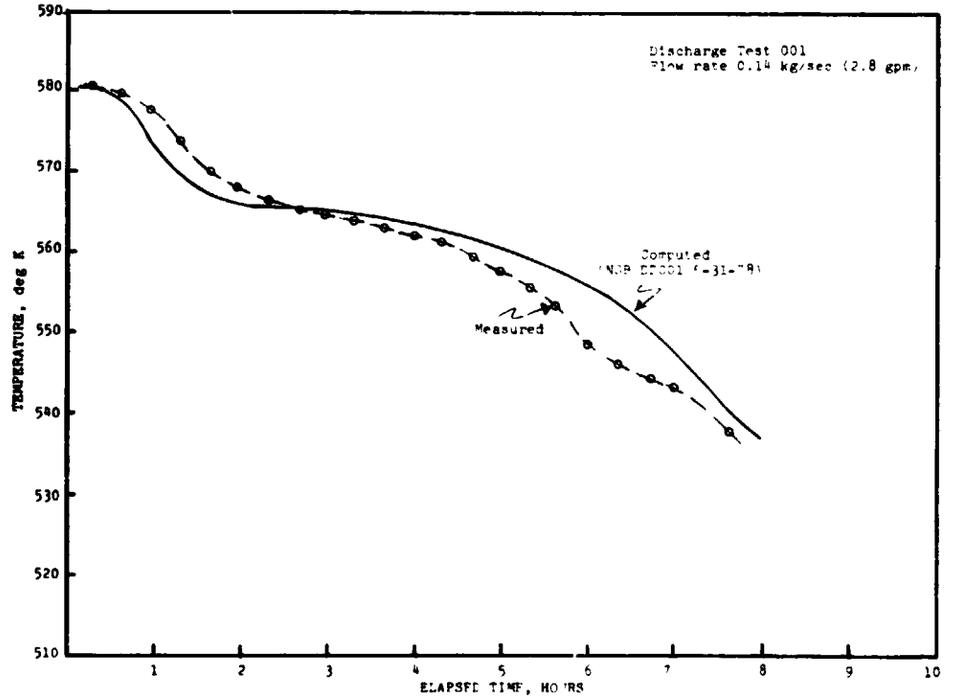

Figure 38. T-66 outlet temperature discharge test 001 (2.83 gpm).

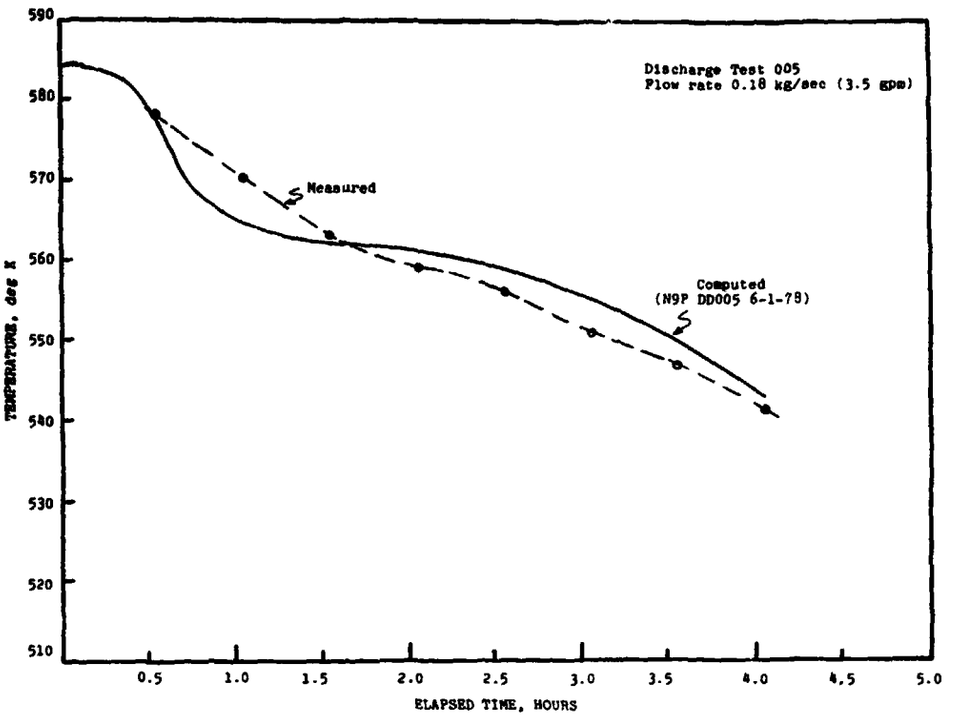

Figure 39. T-66 outlet temperature discharge test 005 (3.5 gpm).

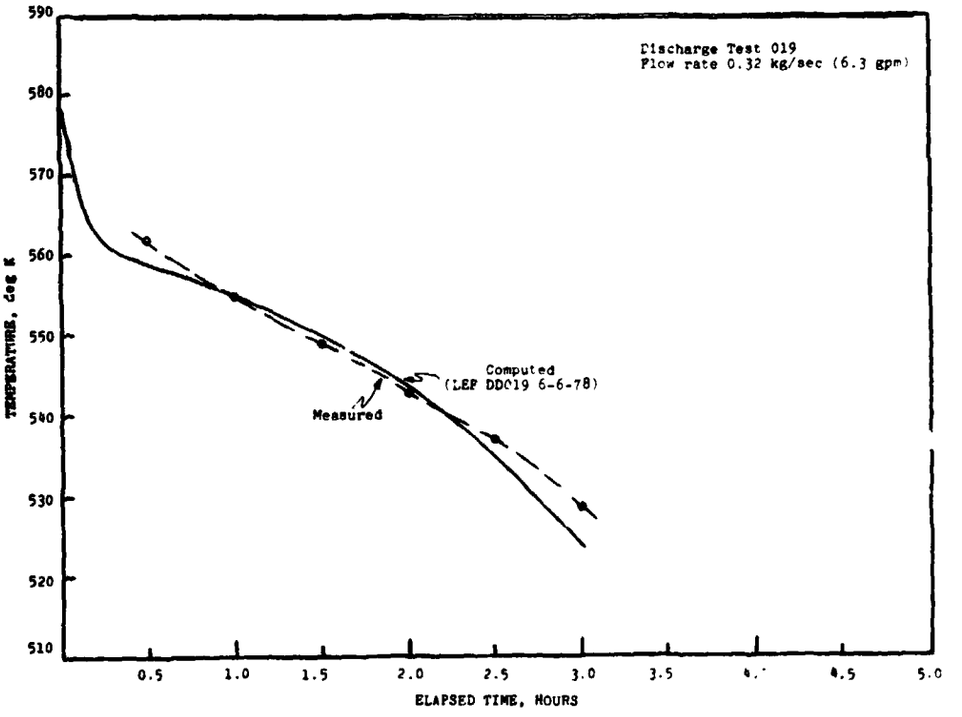

Figure 40. T-66 outlet temperature discharge test 019 (6.3 gpm).

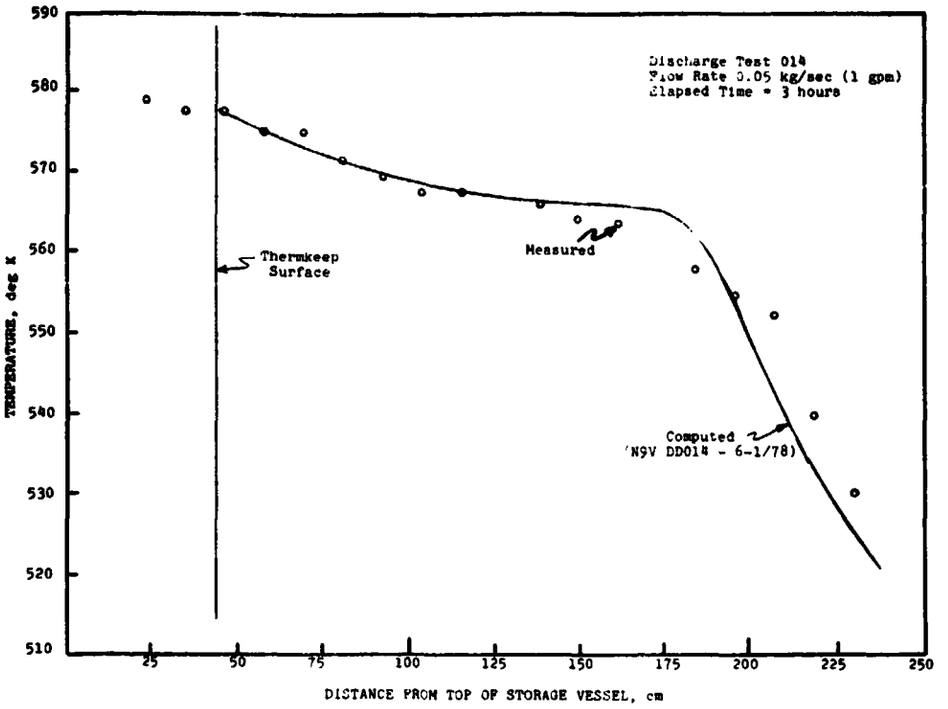

Figure 41. Thermkeep temperature profile, discharge test 014 (1 gpm), at 3 hrs.

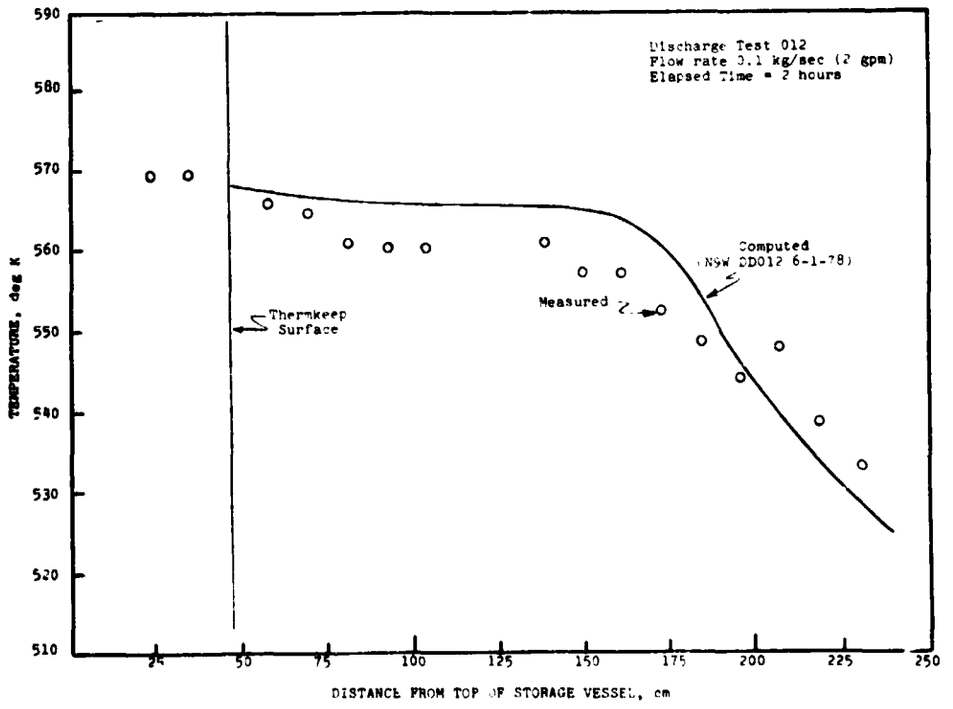

Figure 42. Thermkeep temperature profile, discharge test 012 (2 gpm), at 2 hrs.

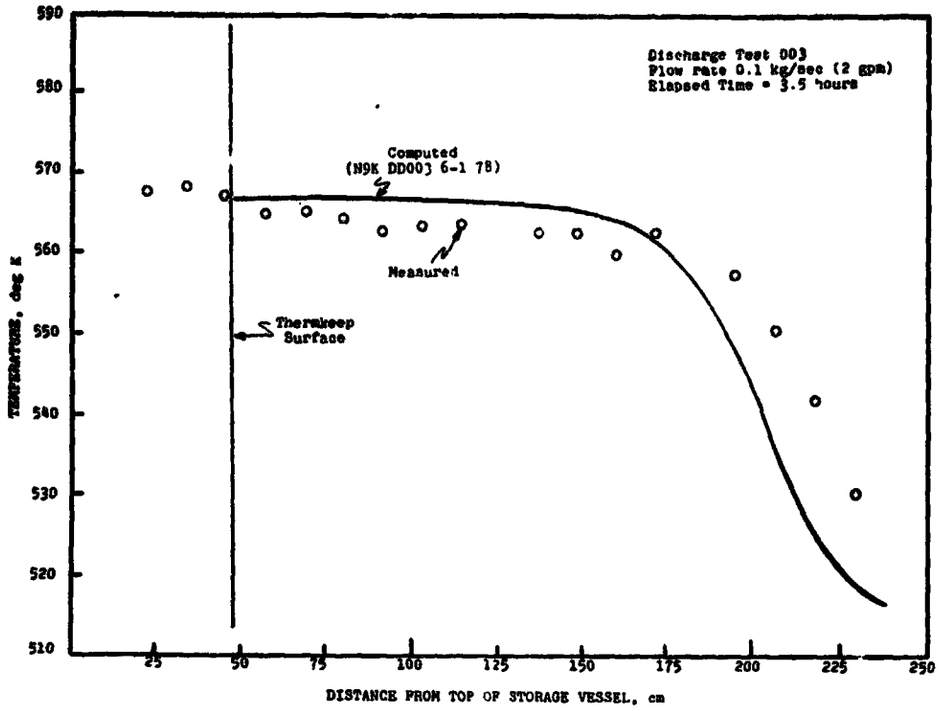

Figure 43. Thermkeep temperature profile, discharge test 003 (2.0 gpm), at 3.5 hrs.

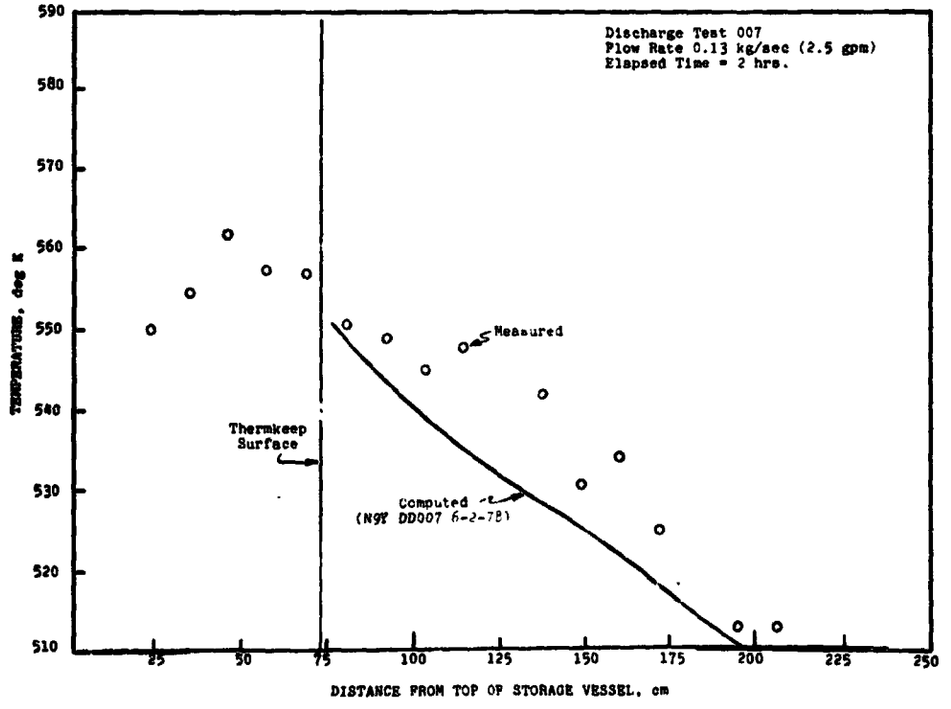

Figure 44. Thermkeep temperature profile, discharge test 007 (2.5 gpm), at 2 hrs.

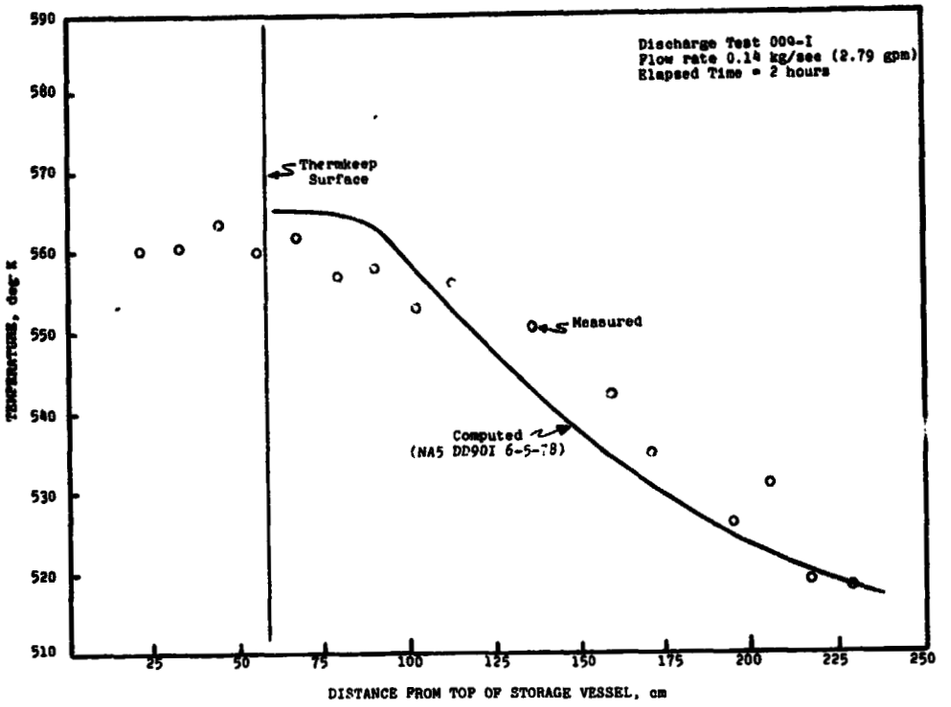

Figure 45. Thermkeep temperature profile, discharge test 009-I (2.79 gpm), at 2 hrs.

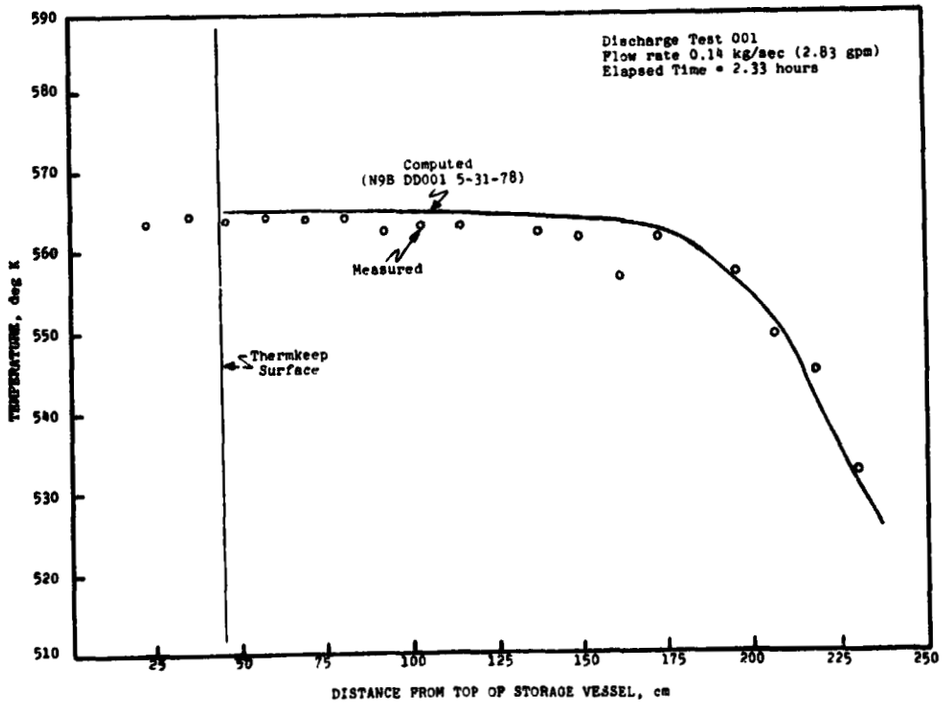

Figure 46. Thermkeep temperature profile, discharge test 001 (2.83 gpm), at 2.33 hrs.

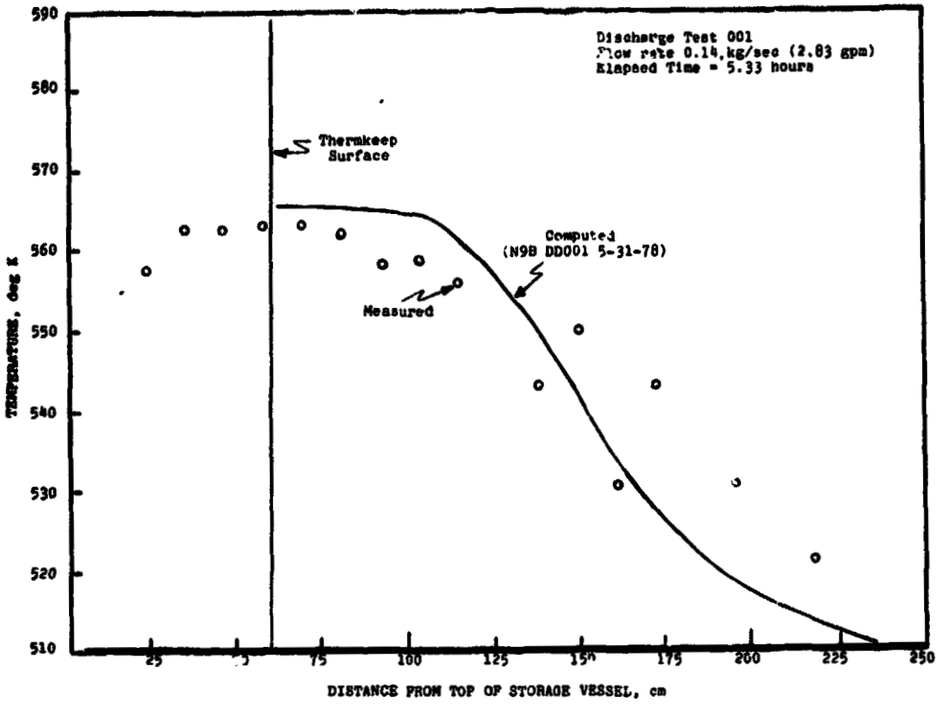

Figure 47. Thermkeep temperature profile, discharge test 001 (2.83 gpm) at 5.33 hrs.

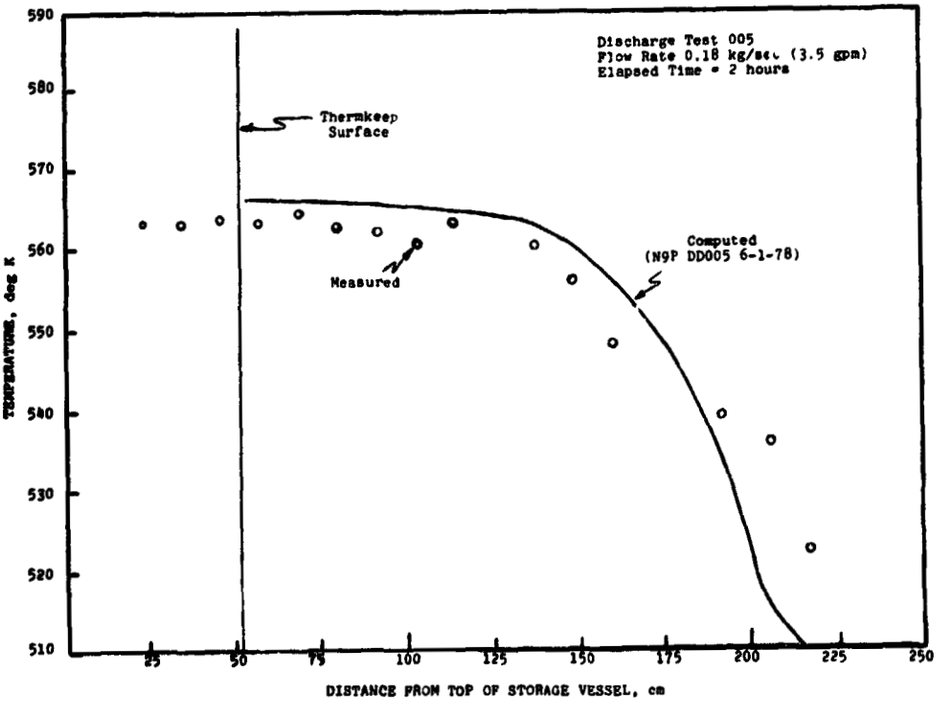

Figure 48. Thermkeep temperature profile, discharge test 005 (3.5 gpm), at 2 hrs.

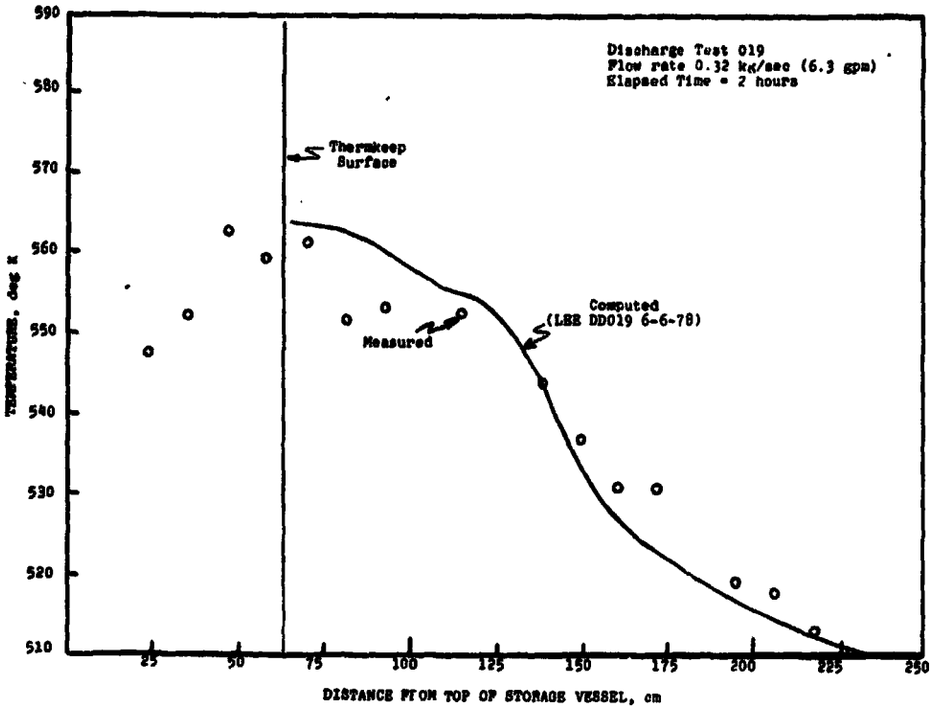

Figure 49. Thermkeep temperature profile, discharge test 019 (6.3 gpm), at 2 hrs.

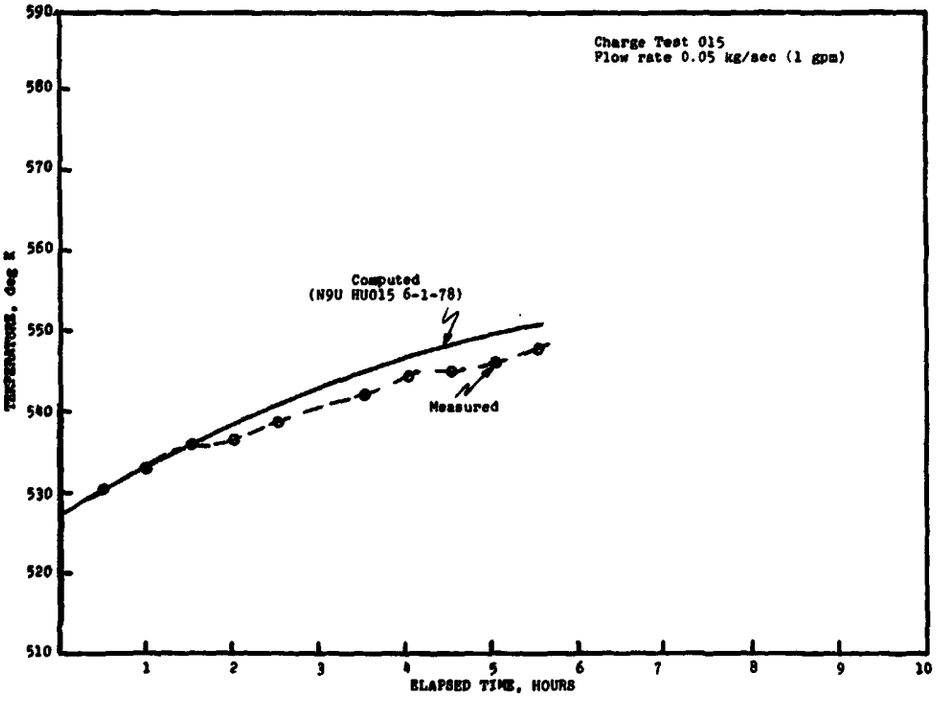

Figure 50. T-66 outlet temperature, charge test 015 (1 gpm).

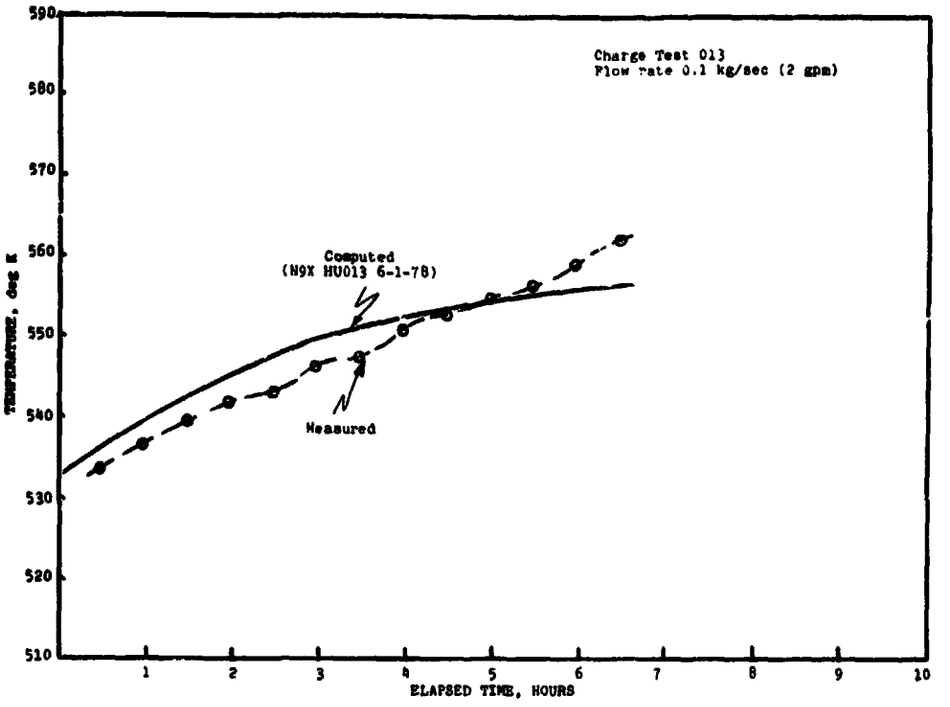

Figure 51. T-66 outlet temperature, charge test 013 (2 gpm).

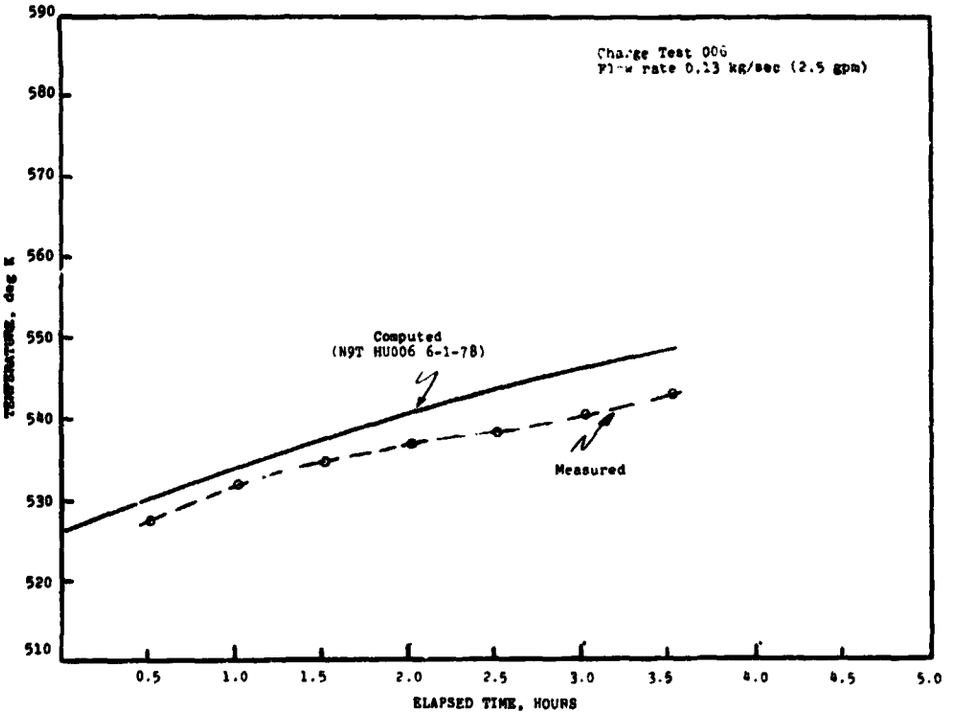

Figure 52. T-66 outlet temperature, charge test 006 (2.5 gpm).

C-2

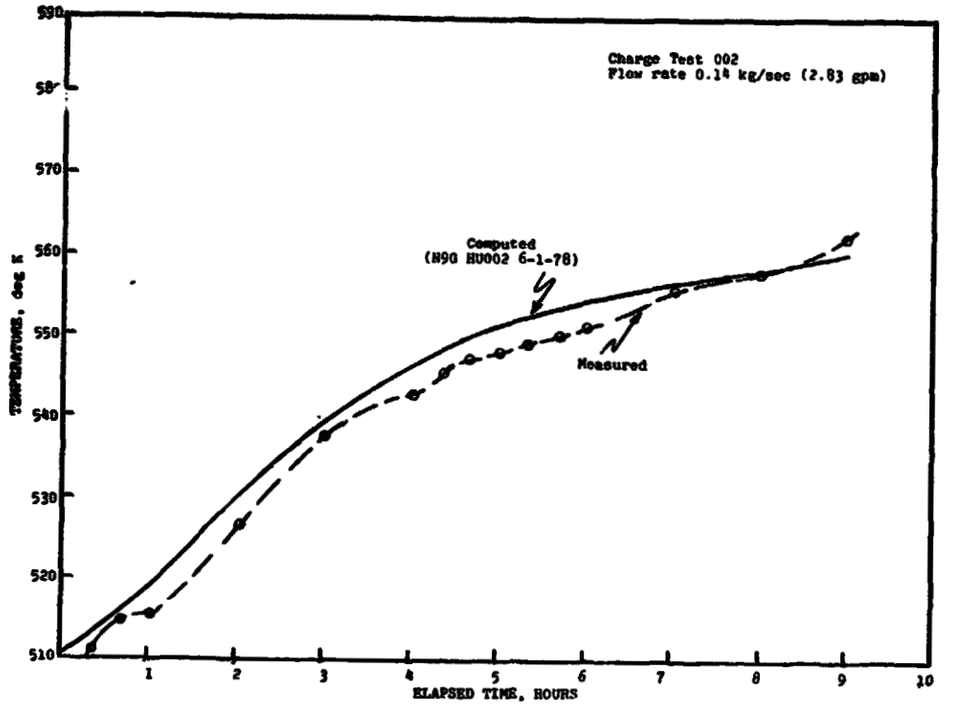

Figure 53. T-66 outlet temperature, charge test 002 (2.83 gpm).

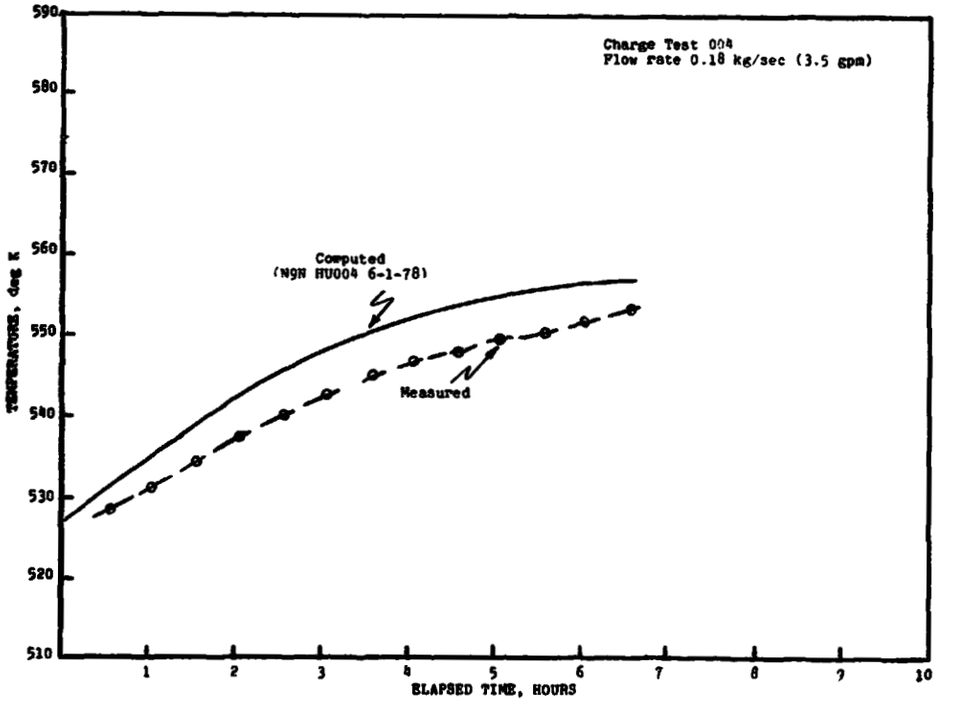

Figure 54. T-66 outlet temperature, charge test 004 (3.5 gpm).

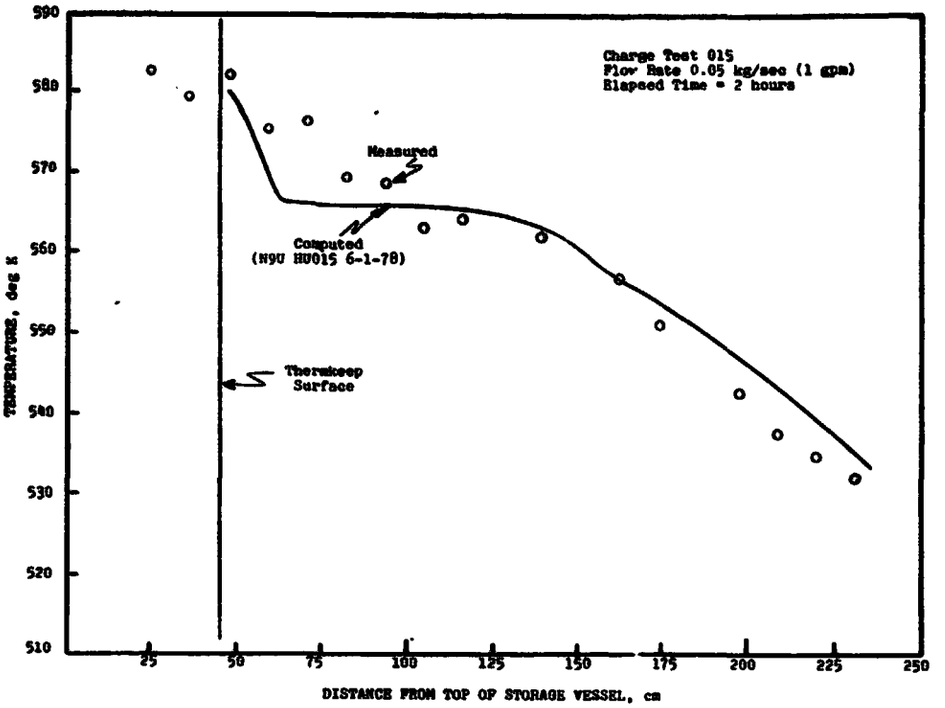

Figure 55. Thermkeep temperature profile, charge test 015 (1 gpm), at 2 hrs.

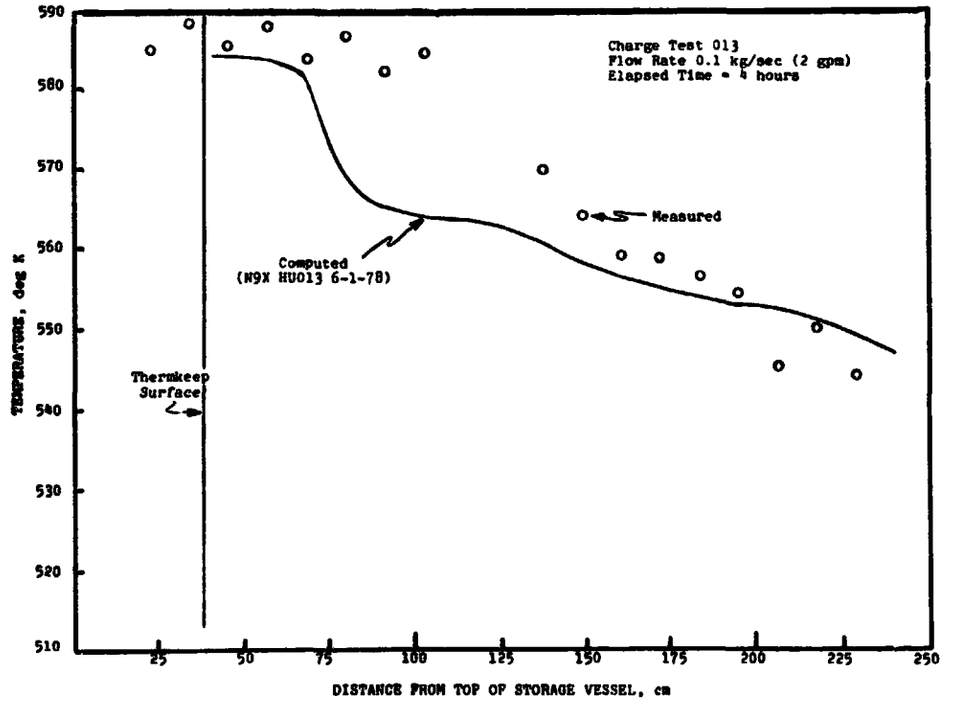

Figure 56. Thermkeep temperature profile, charge test 013 (2 gpm) at 4 hrs.

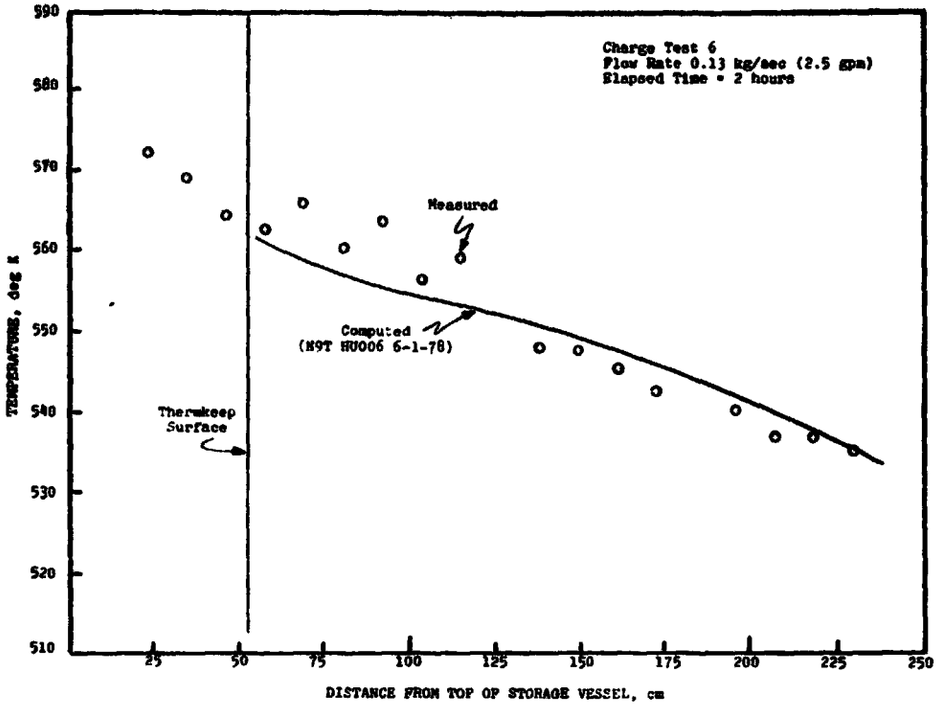

Figure 57. Thermkeep temperature profile, charge test 6 (2.5 gpm) at 2 hrs.

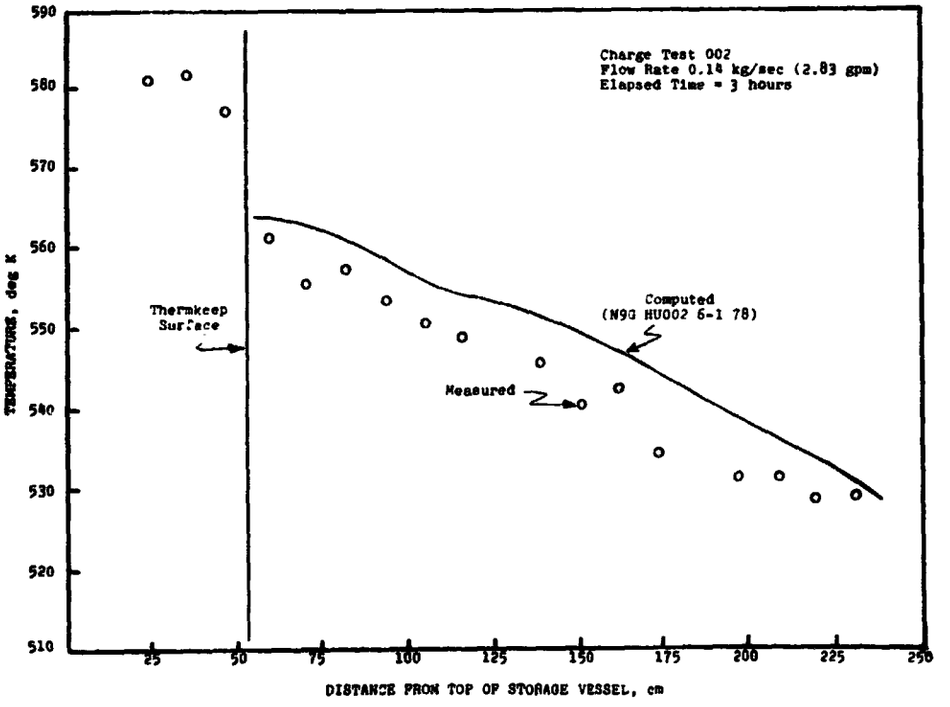

Figure 58. Thermkeep temperature profile, charge test 002 (2.83 gpm) at 3 hrs.

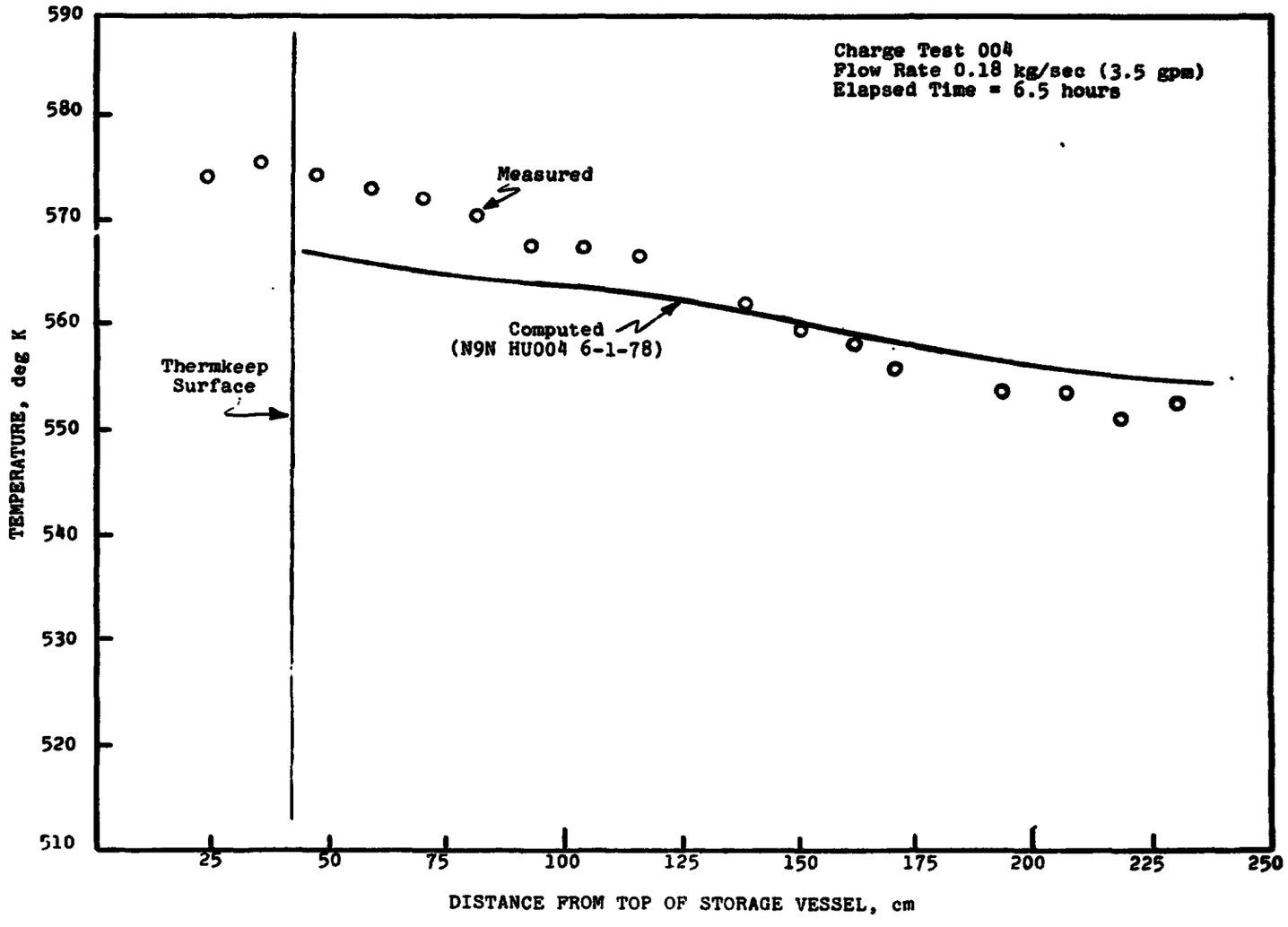

Figure 59. Thermkeep temperature profile, charge test 004 (3.5 gpm), at 6.5 hrs.

Idle Tests

For Test No. 010, the unit was charged and allowed to stand for 115 hours, during which time the thermal distribution was recorded. Figures 60 through 64 describe the computed and measured thermal distributions at the start of the test and after 25, 45, 65, and 115 hours.

Two characteristics are evident. First, the real temperature drop is greater than the computed. This may be due to the fact that the losses are actually higher than computed or due to the possible error in the h(T) curve which has already been suggested. In general, stand-by loss should be predictable although there are aspects of the model design which are not taken into account in the analysis and which could increase the stand-by losses.

First of all, the vessel has an internal height which is 15% greater than that occupied by the storage medium and causes more surface losses. Second, there are shroud support struts and support legs which cause heat loss but are not described by the program. Third, there is air circulation which can have a cooling effect on the exposed part of the heat exchanger in the open space at the top of the vessel and on the top surface of the Thermkeep. Moreover, values for insulation conductivity are not precise. There is also a capacitive effect associated with the insulation. When the vessel is heated, the insulation, which has a low thermal diffusivity, lags behind in temperature rise. During a standby, the insulation absorbs heat from the vessel in an attempt to come to equilibrium with it.

Overall, there seems to be no single reason for the more rapid temperature drop in the data than in the computer predictions. Rather, a combination of effects all of which move the results in the same direction, seem to be involved.

Square Wave Cyclic Testing

Two tests were run with repetitive cycling and minimal changeover time, thereby minimizing the effect of erroneous prediction of stand-by heat loss, as described above. During a flow test, the heat exchange between the fluid and the storage medium far exceeds the effect of stand-by losses and errors in stand-by loss are insignificant in terms of correlation.

The two tests were run at flows of 0.1 kg/sec (2 gpm) for 4 hours discharging, 4 hours charging, with one-hour periods for changeover. Test 017 ran two cycles, and test 018 ran three cycles. Four cycles were desired each time but operational problems prevented completion of the full four cycles.

Figures 65 and 66 describe the T-66 outlet temperatures during the first and second cycles of the two-cycle test (No. 017). The computed results are based on the initial measured temperature profile at the beginning of the first cycles, i.e., only at the start of the test sequence.

Figures 67 through 70 are the computed and measured thermal distribution at the end of each of the four segments. Agreement appears acceptable.

Figures 71 through 73 describe the T-66 outlet temperatures during each of the three cycles of test No. 018. Figures 74 through 79 describe the measured and computed thermal distributions at the end of each of the six segments. Again, agreement is acceptable.

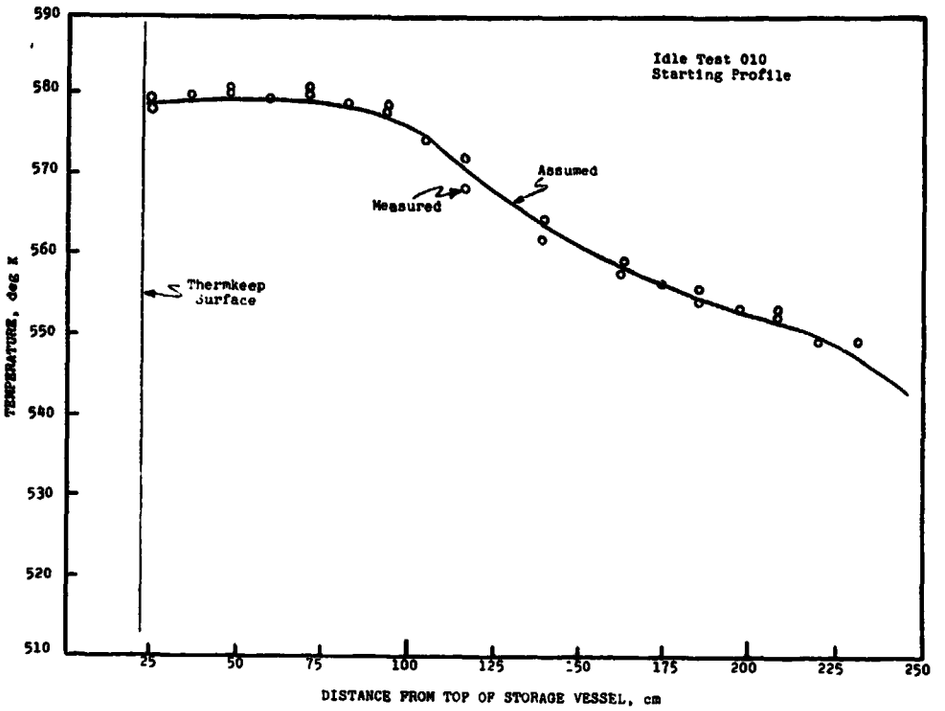

Figure 60. Initial Thermkeep temperature profile, idle test 010.

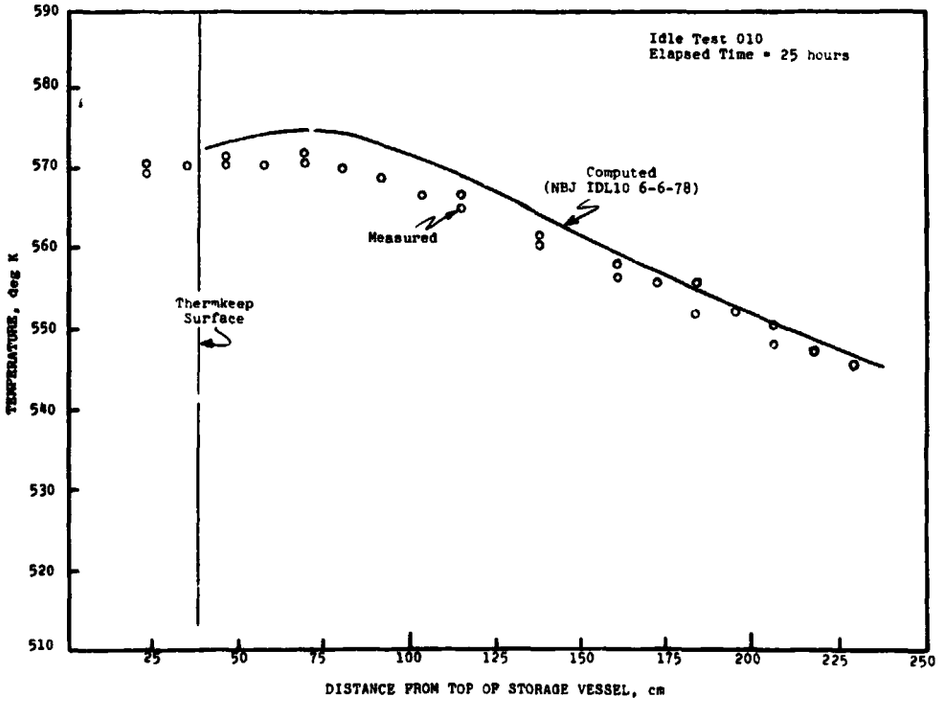

Figure 61. Thermkeep temperature profile, idle test 010, at 25 hrs.

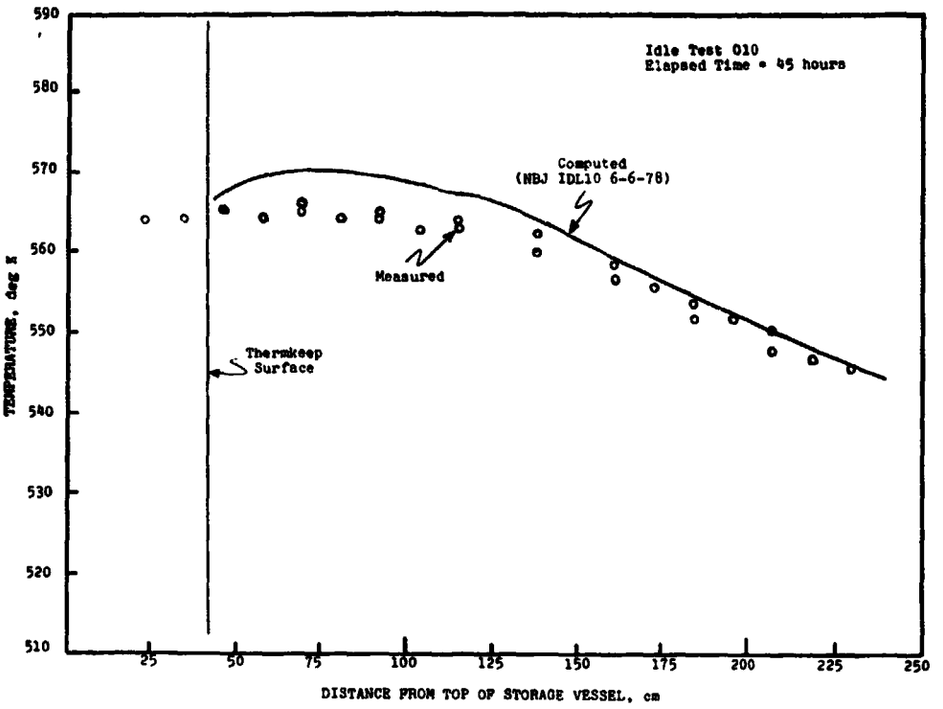

Figure 62. Thermkeep temperature profile, idle test 010, at 45 hours.

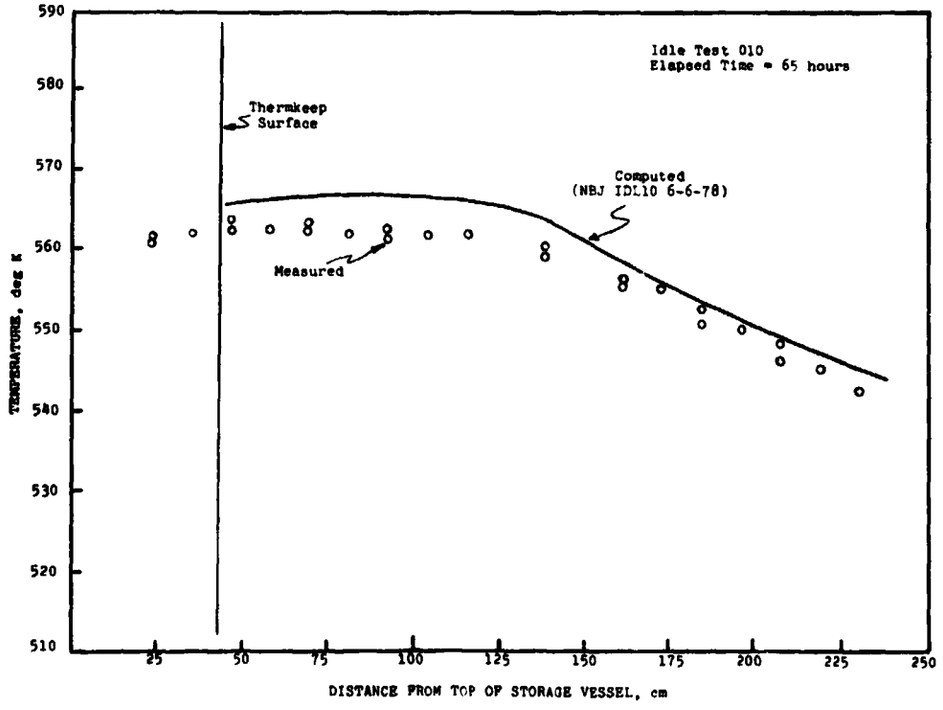

Figure 63. Thermkeep temperature profile, idle test 010, at 65 hours.

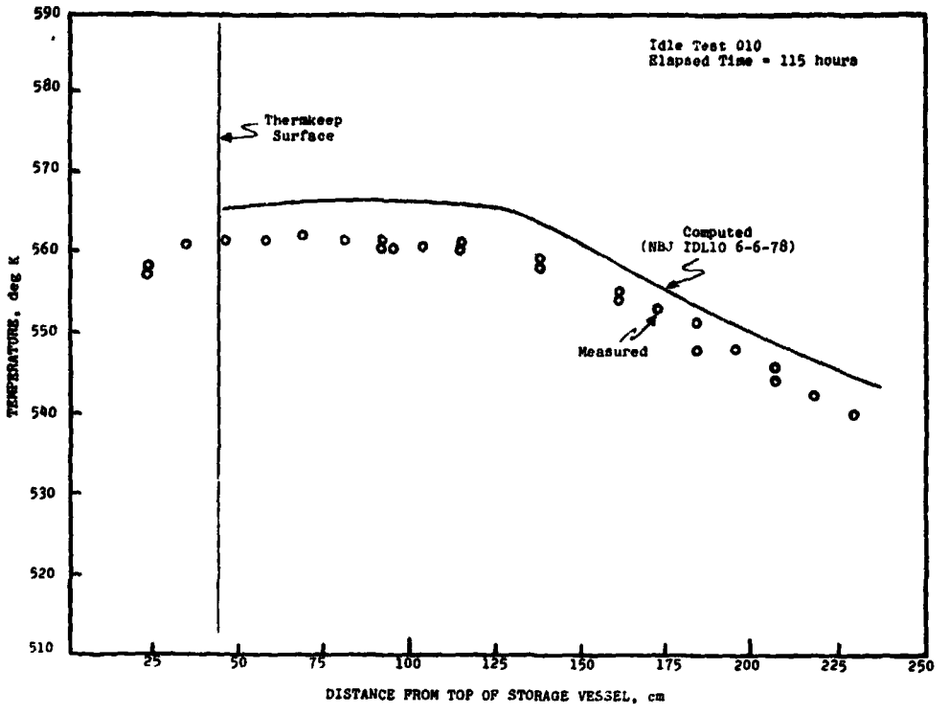

Figure 64. Thermkeep temperature profile, idle test 010, at 115 hours.

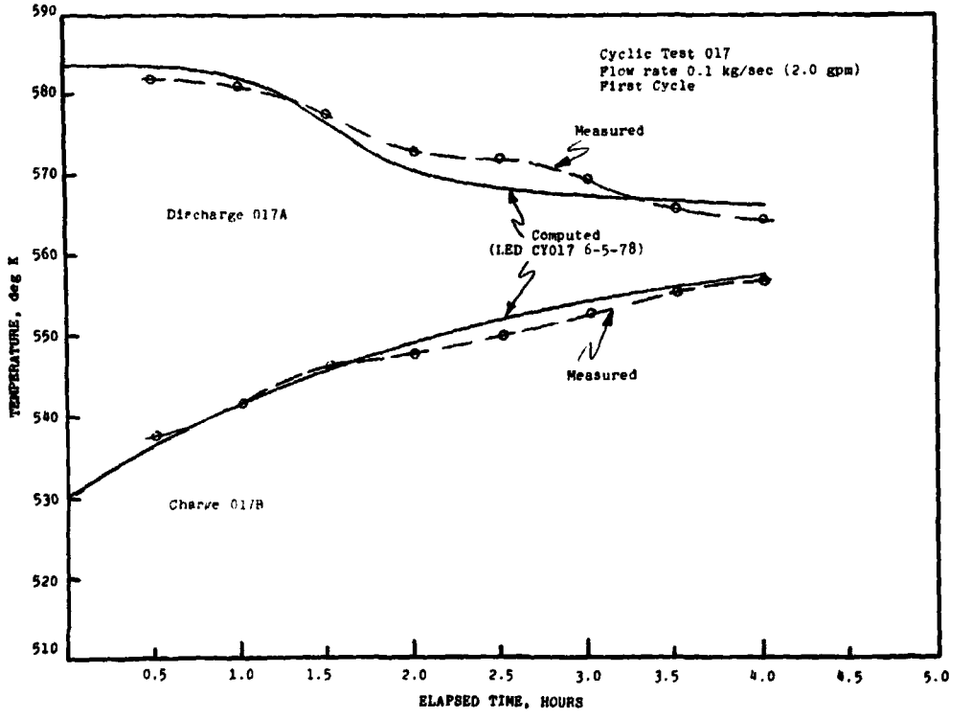

Figure 65. T-66 outlet temperature, cyclic test 017 (2 gpm), cycle 1.

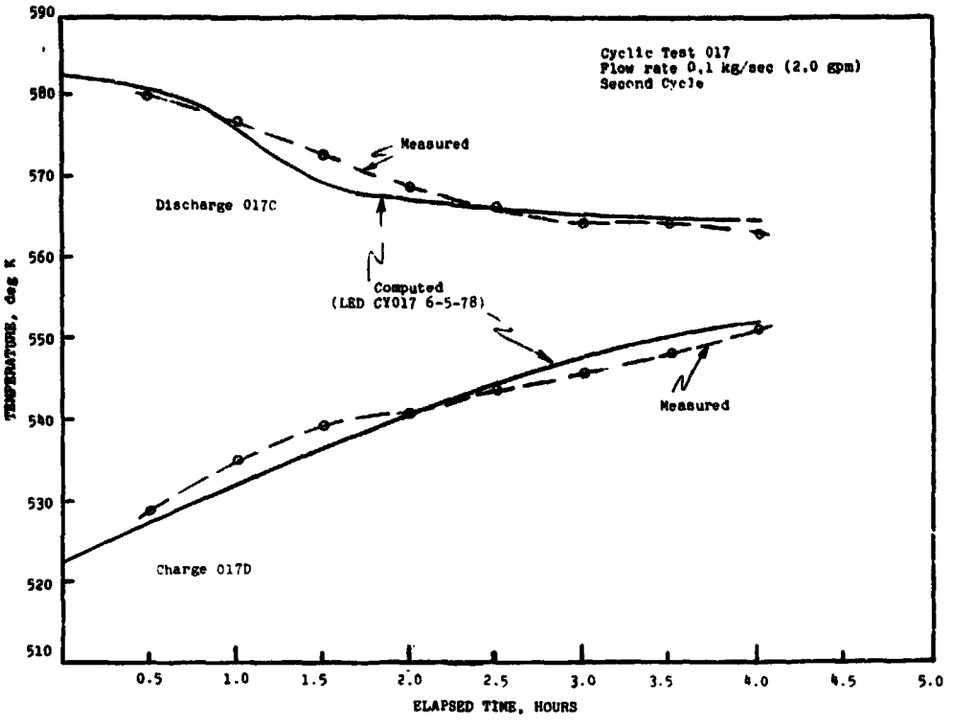

Figure 66. T-66 outlet temperature, cyclic test 017 (2 gpm), cycle 2.

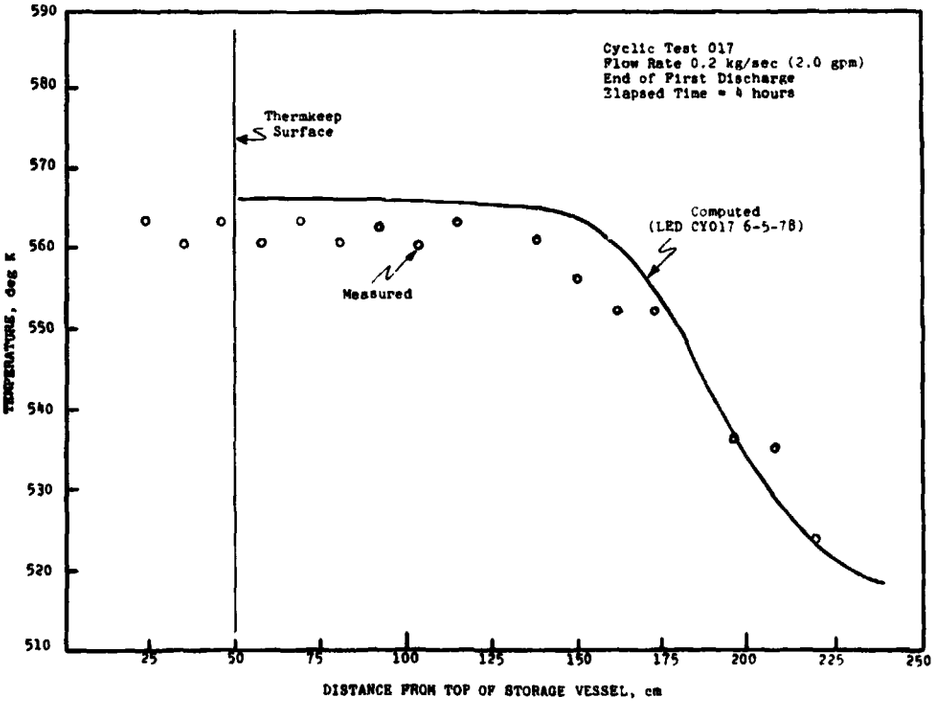

Figure 67. Thermkeep temperature profile, cyclic test 017 (2 gpm), at end of first discharge phase.

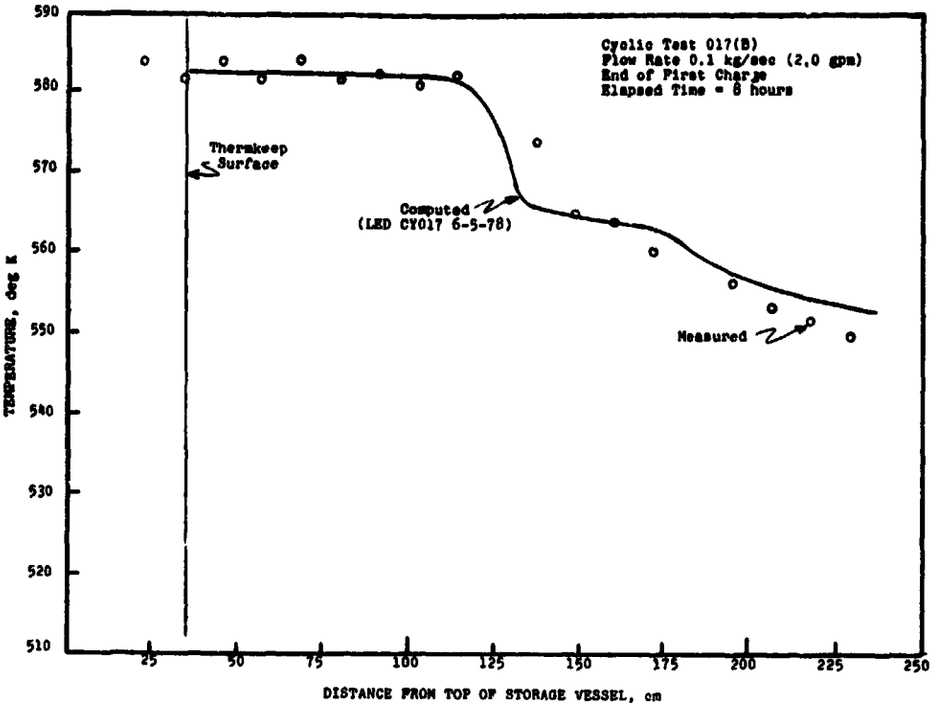

Figure 68. Thermkeep temperature profile, cyclic test 017 (2 gpm), at end of first charge phase.

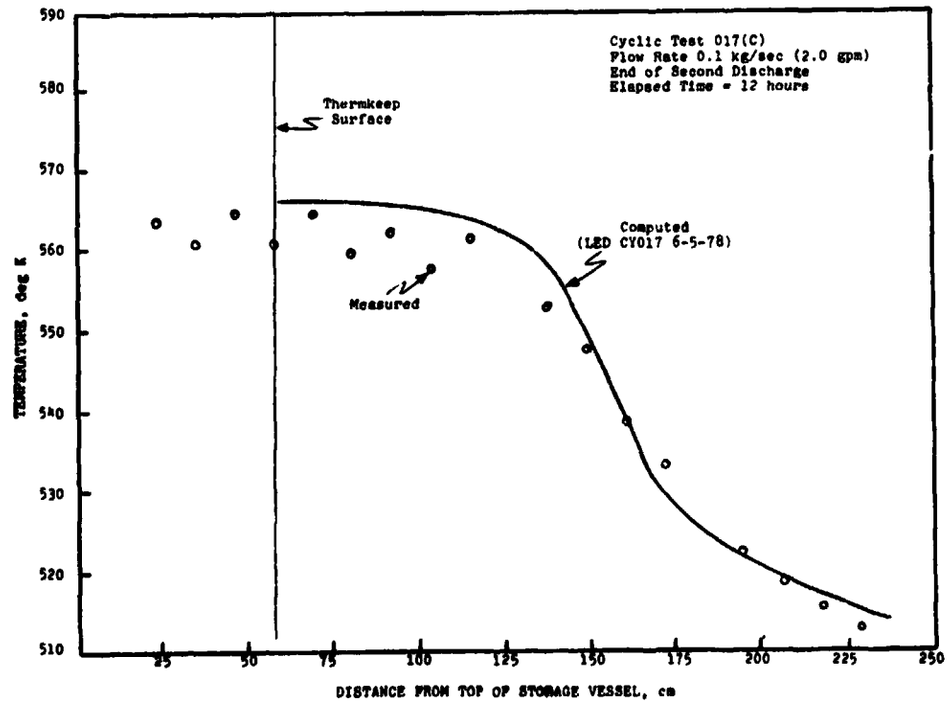

Figure 69. Thermkeep temperature profile, cyclic test 017 (2 gpm), at end of second discharge phase.

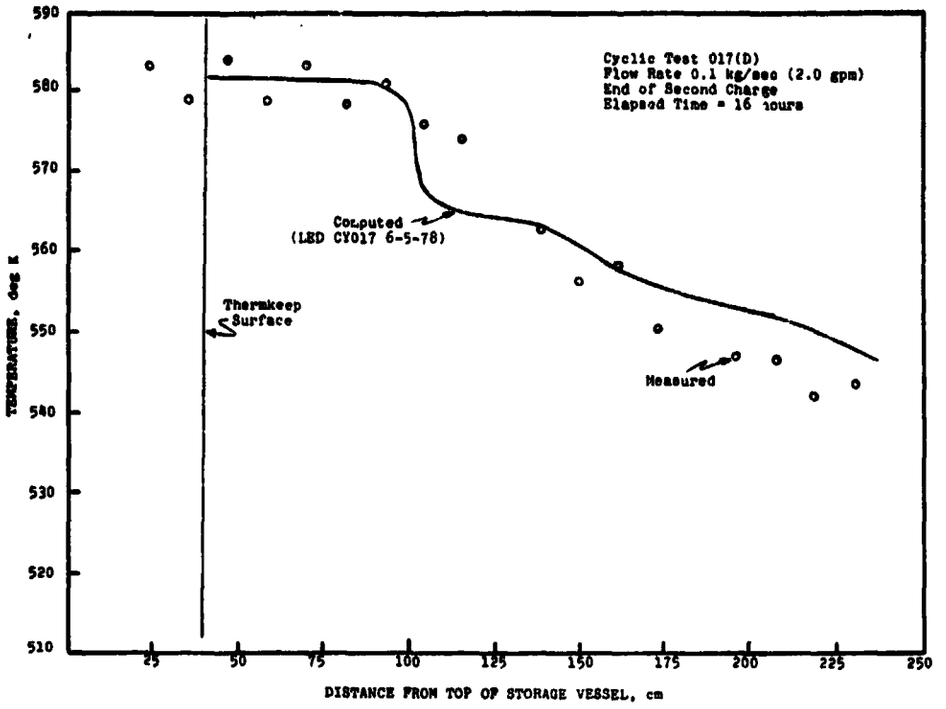

Figure 70. Thermkeep temperature profile, cyclic test 017 (2 gpm), at end of second charge phase.

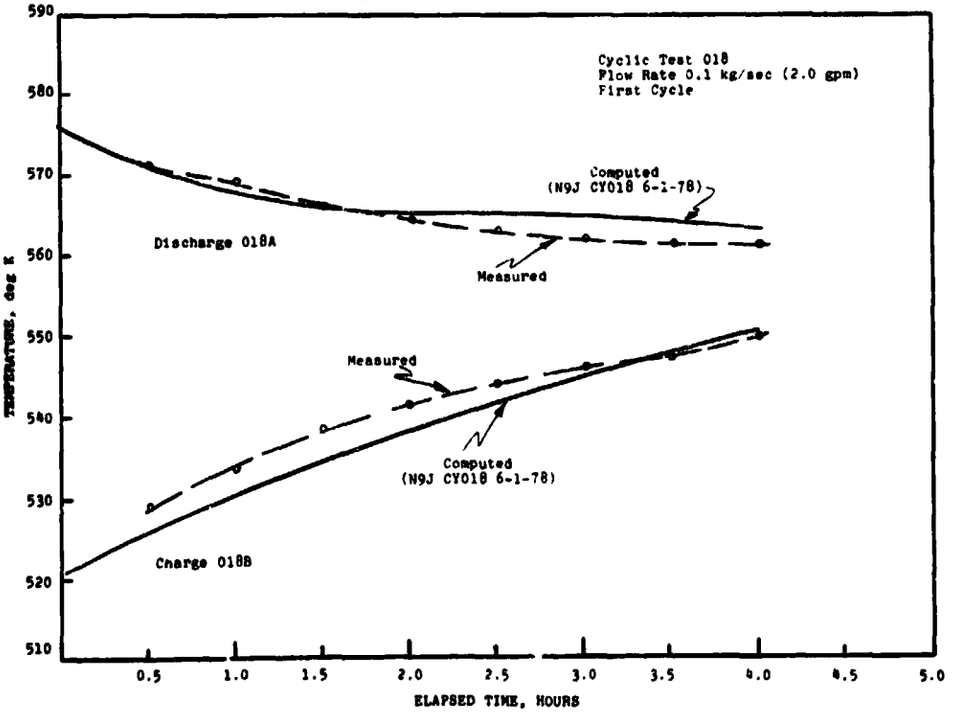

Figure 71. T-66 outlet temperature, cyclic test 018 (2 gpm), cycle 1.

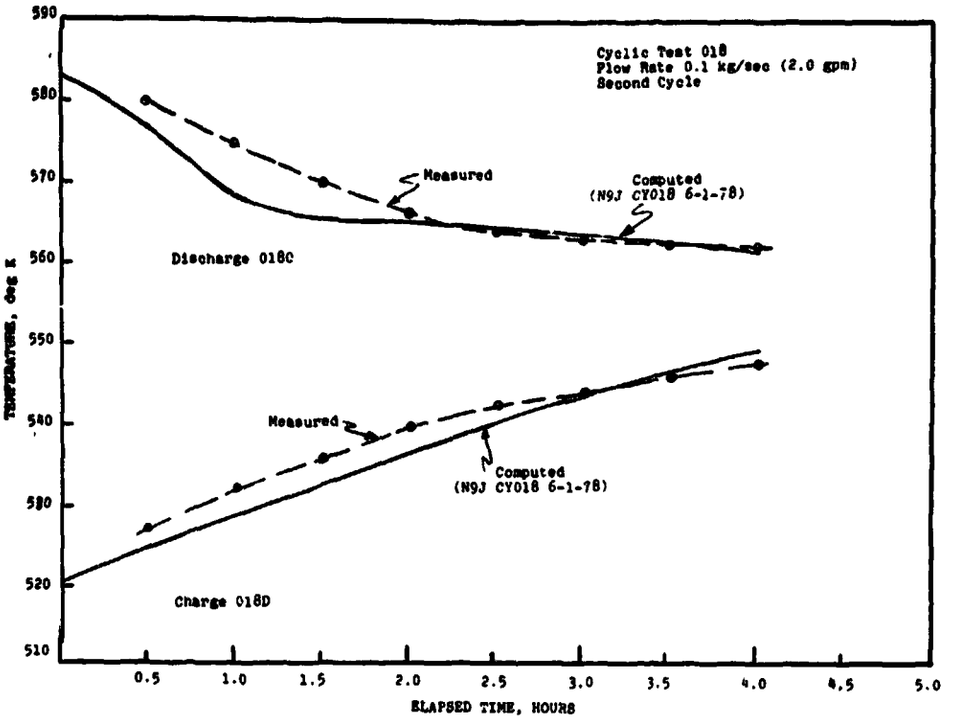

Figure 72. T-66 outlet temperature, cyclic test 018 (2 gpm), cycle 2.

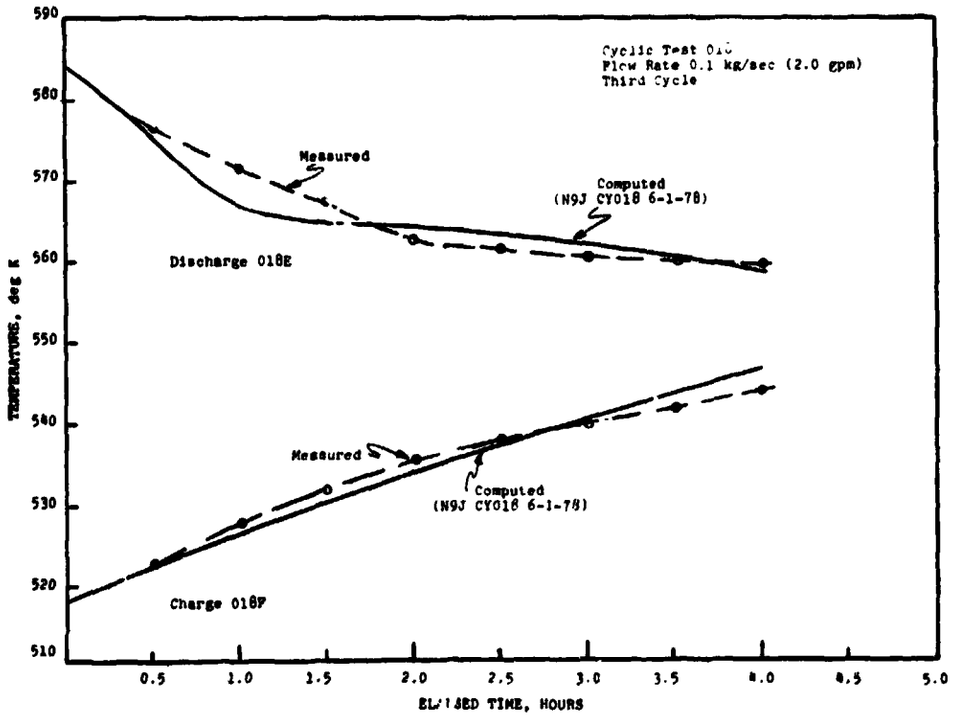

Figure 73. T-66 outlet temperature, cyclic test 018 (2 gpm), cycle 3.

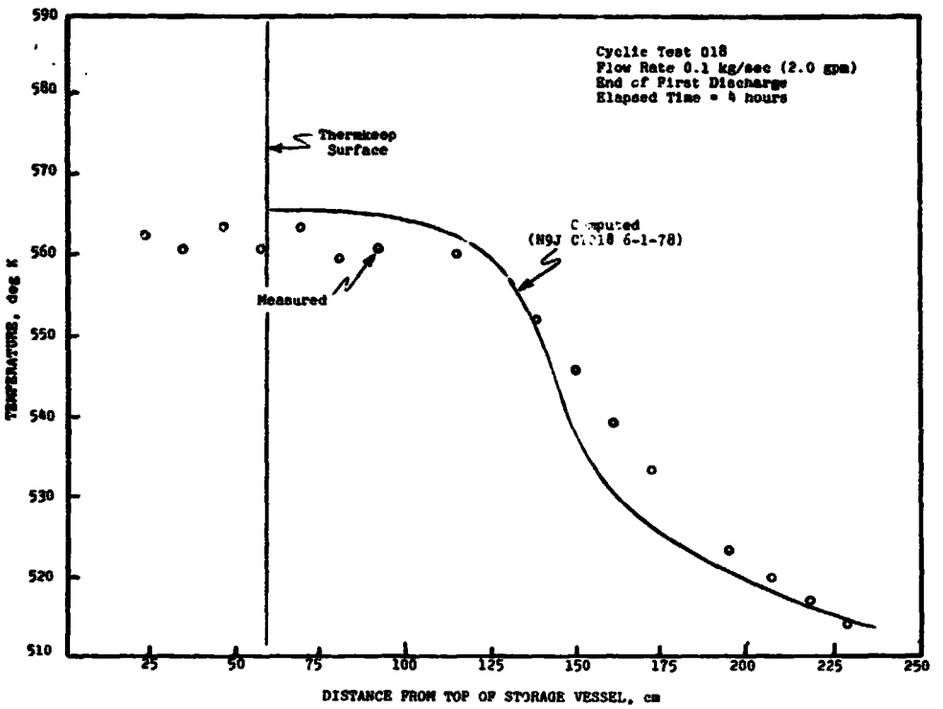

Figure 74. Thermkeep temperature profile, cyclic test 018 (2 gpm), at end of first discharge phase.

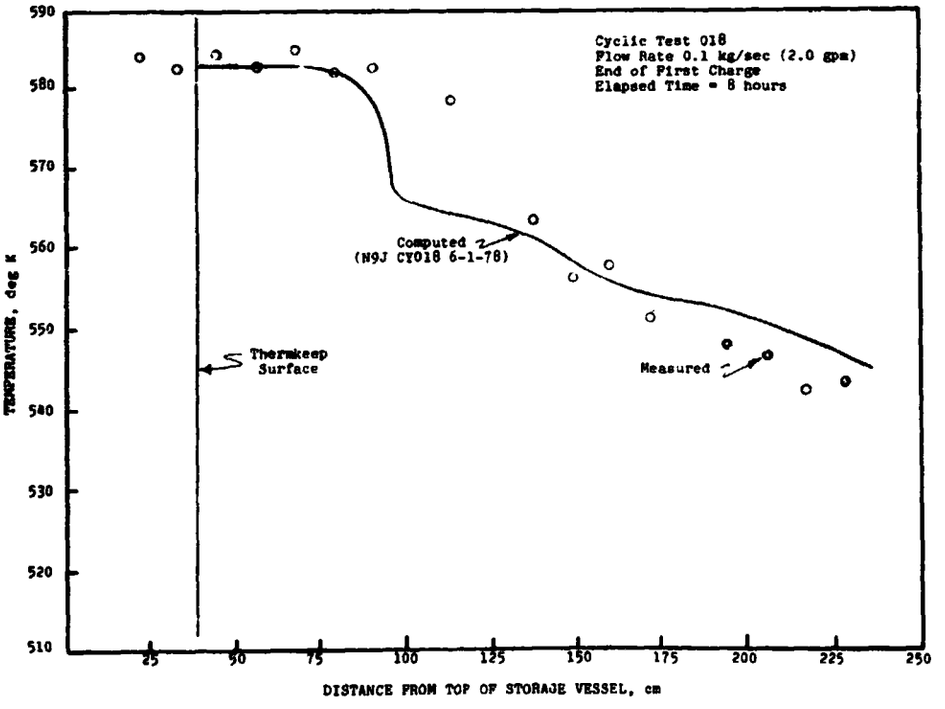

Figure 75. Thermkeep temperature profile, cyclic test 018 (2 gpm), at end of first charge phase.

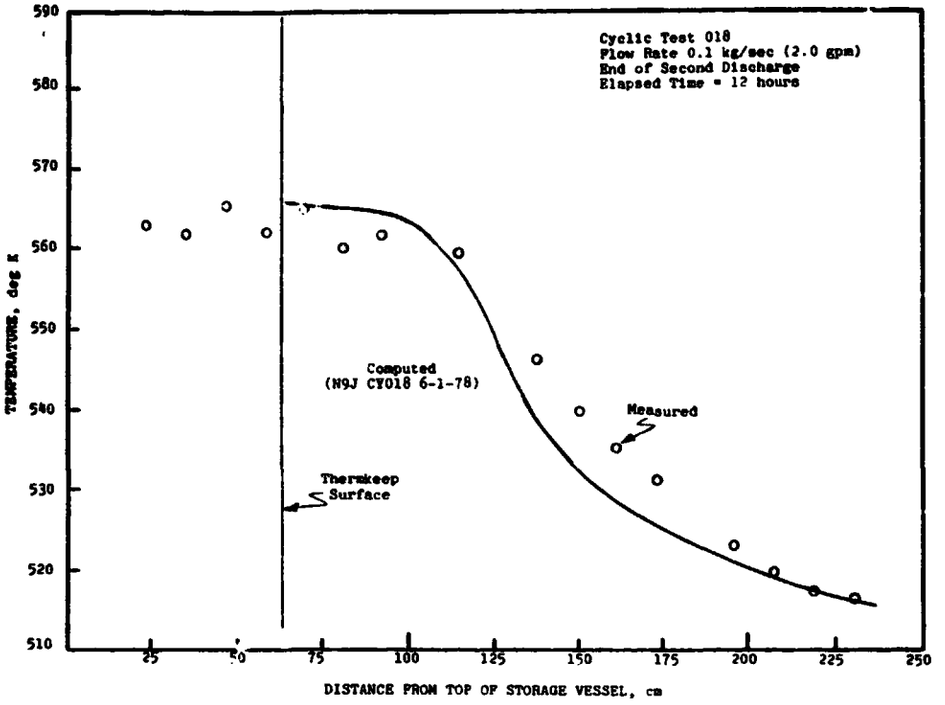

Figure 76. Thermkeep temperature profile, cyclic test 018 (2 gpm), at end of second discharge phase.

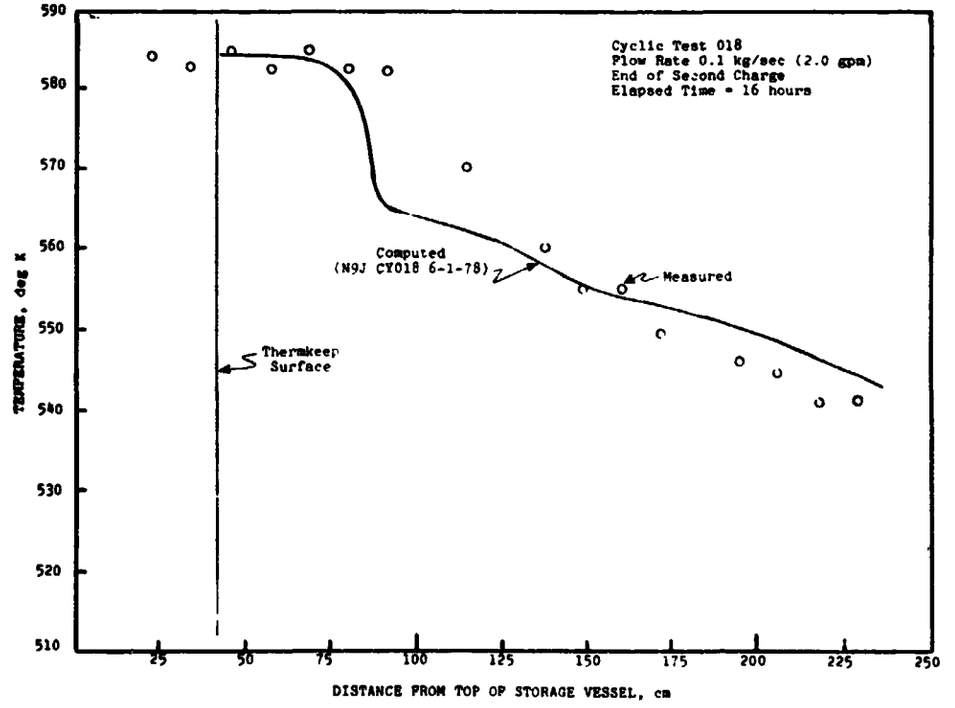

Figure 77. Thermkeep temperature profile, cyclic test 018 (2 gpm), at end of second charge phase.

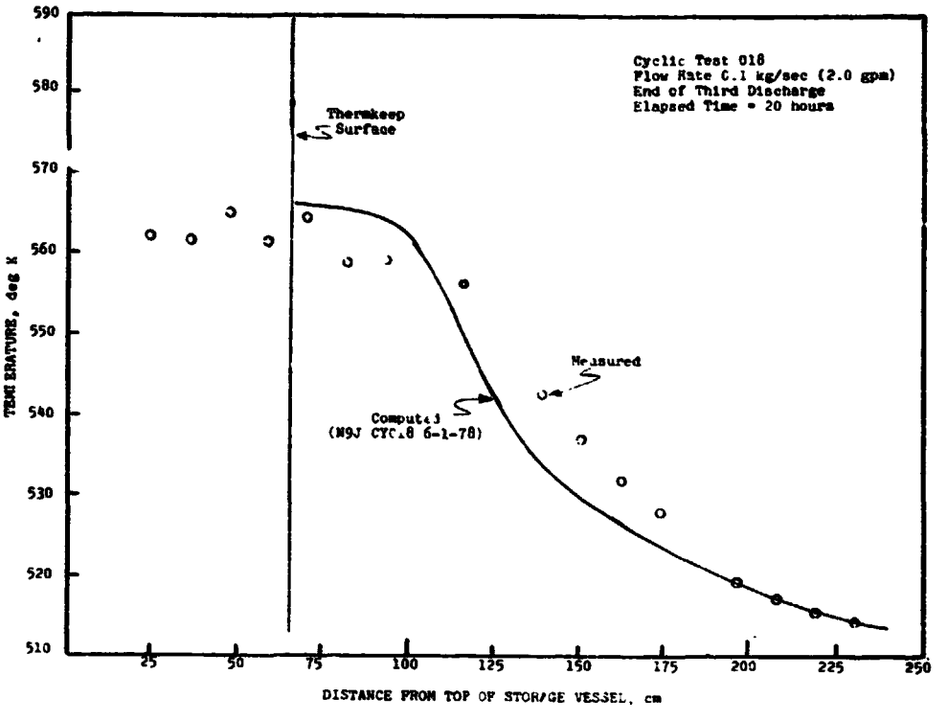

Figure 78. Thermkeep temperature profile, cyclic test 018 (2 gpm), at end of third discharge phase.

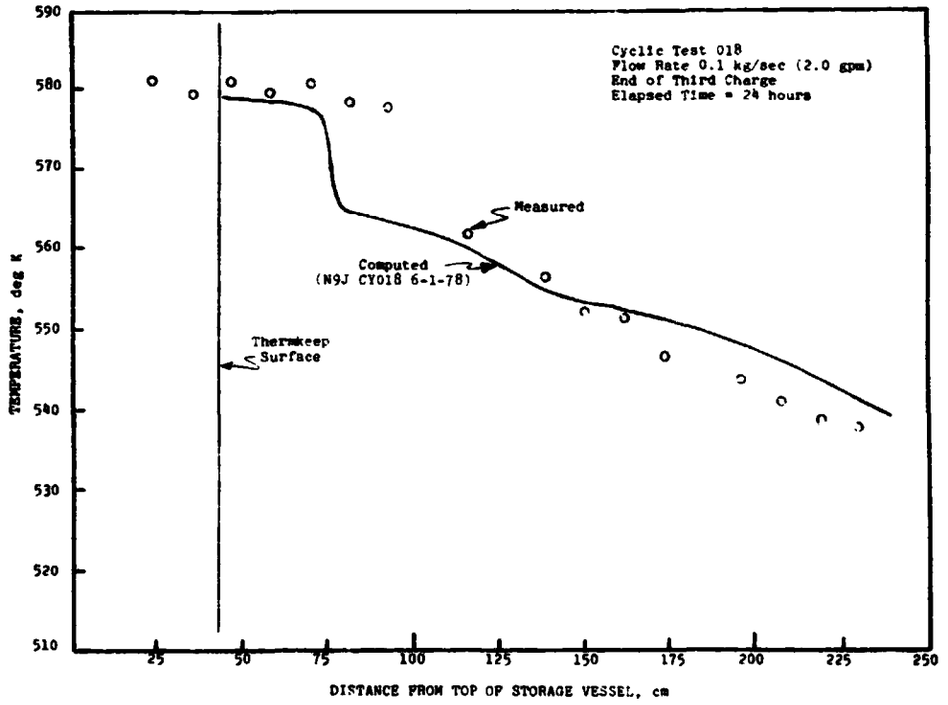

Figure 79. Thermkeep temperature profile, cyclic test 018 (2 gpm), at end of third charge phase.

Solar Cycle Simulation Tests

Two solar cycle tests were run with data being measured every 30 minutes. The first (test 020) was run as a system shakedown with the charging and discharging schedules compressed to 6/10 of normal, so that the twelve hours of boiler demand were decreased to 7.2 hours. This allowed the test to be run in the course of two normal workdays, and as there were no system malfunctions, the data are being presented. The second test (test 023) was run with the insolation and boiler demand just as described in Figure 1 (page 13).

The order of events in the computer program was modified so that a starting profile was input and computations began at the predawn start of boiler demand (time T3), and a cycle runs from then through the end of the overnight idle period. Next, the program used an input table of actual flow rates rather than calculating flow on the basis of the solar characteristic and the inlet and outlet temperatures. This modification removed any discrepancy between the actual flow as determined by the test bed electronics and the computed flow. Lastly, a change was made to allow for the fact that the test bed has a minimum flow rate of .75 gpm (about .04 kg/sec). Below this rate, the flowmeter is not accurate and the load on the pump causes it to pulsate. Therefore, the flow rate will stay at the minimum rate in response to any signal to pump at .75 gpm or lower. The computer analysis allowed an idle period between charging and discharging phases, because during the tests the flow was cut off early at the end of a phase or started late at the beginning of a phase. The times of cutoff or startup were calculated so that the total desired amount of heat was still transferred. With these modifications, the computer analysis duplicates the actual events.

The morning discharge period in which flow starts before dawn and later decreases as the sun rises is referred to in the data as the Phase 1 discharge to distinguish it from the afternoon, or Phase 2 discharge during which the sun sets and the unit continues to supply heat to the boiler unassisted.

During each phase the T-66 inlet temperature was maintained constant within limits -- near 516 K during discharge and 584 K during charging. The actual inlet temperatures were input into the computer to eliminate variations due to external effects on the control system.

Figure 80 shows the computer correlation to T-66 outlet temperature for Test 020 and Figures 81-84 compare the computed and actual Thermkeep temperature profiles for the first daily cycle. Figure 85 shows the varying rate of T-66 flow during the charge cycle. Note that the highest rate attained was 0.31 kg/sec, whereas the maximum possible rate is about 0.38 kg/sec. This is because the flow rate is electronically adjusted to account for the insolation characteristic and the return temperature, just as the computer analysis did previously. In a relatively low state of charge, the return temperature will be low and maintain a large ΔT which requires less flow.

Figures 86-90 show the computer correlations for the second cycle of Test 020. Agreement has improved for both charging and discharging phases and is very close at the end of the test (Figure 89). Figure 90 shows that the maximum flow rate was momentarily reached, and although the return temperature was high, the flow rate dropped off as the collector output dropped.

Solar Cycle Test 023 (Figures 91-101) was a full-scale simulation of two solar daily cycles. This test closely approximates the actual performance conditions of a full-scale storage unit in the field.

Figure 91 shows the correlation between computed and actual fluid delivery temperatures for both cycles. Agreement is very good, with two exceptions: during both charge phases, when the T-66 temperature approaches 560 K, computed and actual data begin to diverge. Similarly, the Phase 1 discharge of the second cycle (from 24 to 26.5 hours) is slightly divergent in the 560 K range.

The reason for this deviation has not been determined. Some factors which may be contributing are a misshapen enthalpy curve, some hysteresis which raises the latent heat plateau on heating and/or depresses the latent heat on cooling, possible segregation of the Thermkeep components which changes the specific heat and melting point of the bottom most elements, and expansion and circulation of hot liquid Thermkeep which shifts energies and volumes of the elements in ways unaccounted for by the computer.

Although the predicted return temperature was lower than actual during charging, which might suggest that less energy was absorbed by the unit, the profiles at the end of the charge phases (Figures 94 and 99) show that

temperatures are slightly higher than predicted inside the unit. In particular, Figure 99 shows an abrupt dip in the computed temperature at about 150 cm from the top of the vessel. This again is a reflection of the strong plateau in the enthalpy curve, which experimental data suggests are not as strong as we assumed Below the level of the dip, the discrepancy is roughly 15 K, or the same discrepancy which appears in the return fluid temperature during charging (see Figure 91) at about 32 hours elapsed time.

The final discharge phase showed good agreement between computed and actual data on the T-66 delivery temperature, and the test ended with the temperature profile also agreeing closely (Figure 100).

Figure 101 shows the variation in flow rate during the final charge phase. Although peak insolation occurred at about 30 hours elapsed time, the flow rate continued to rise and held near maximum (.35 kg/sec) for about an hour, while the collector output continued to drop.

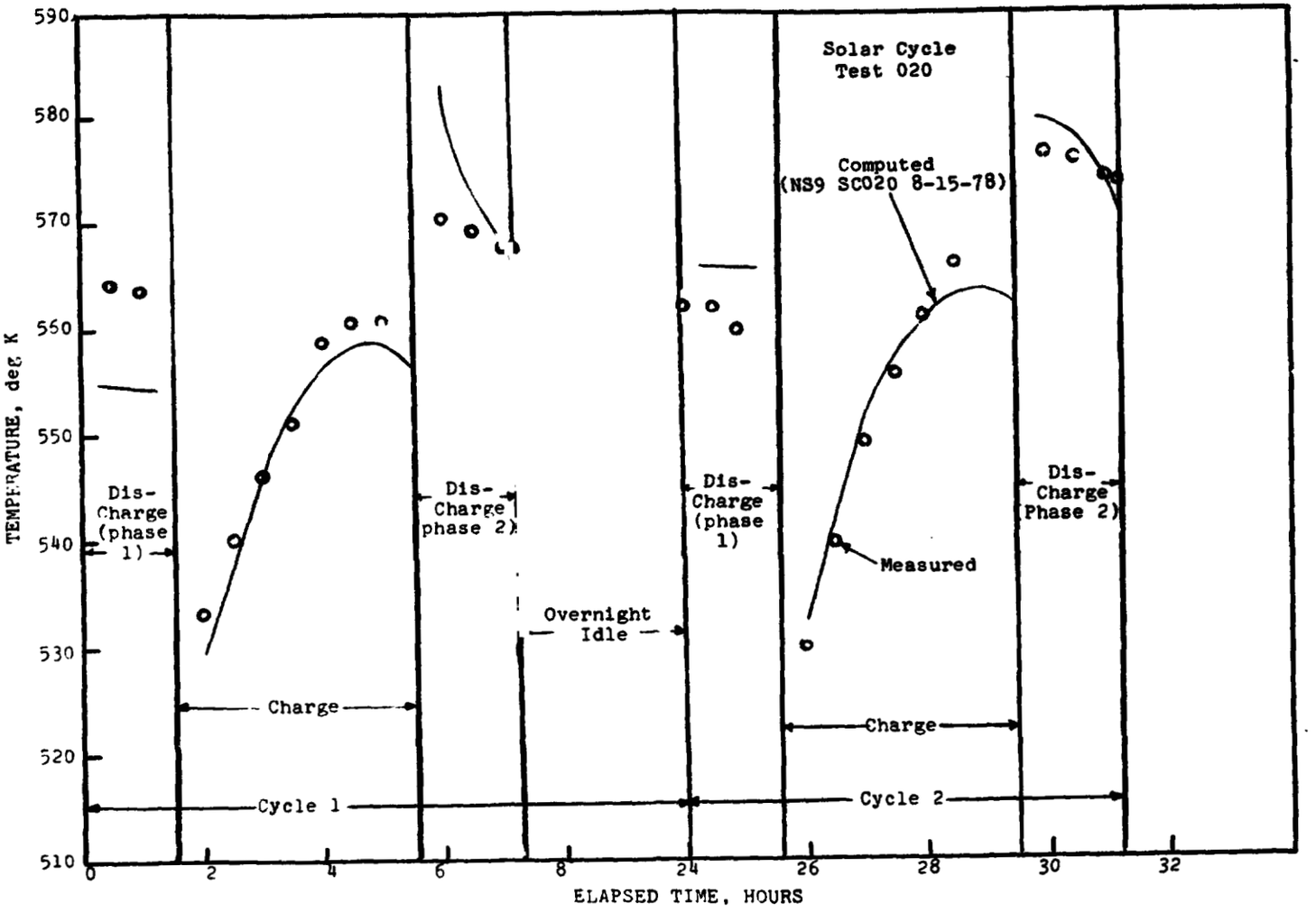

Figure 80. T-66 outlet temperature for 6/10 scale solar cycle simulation test.

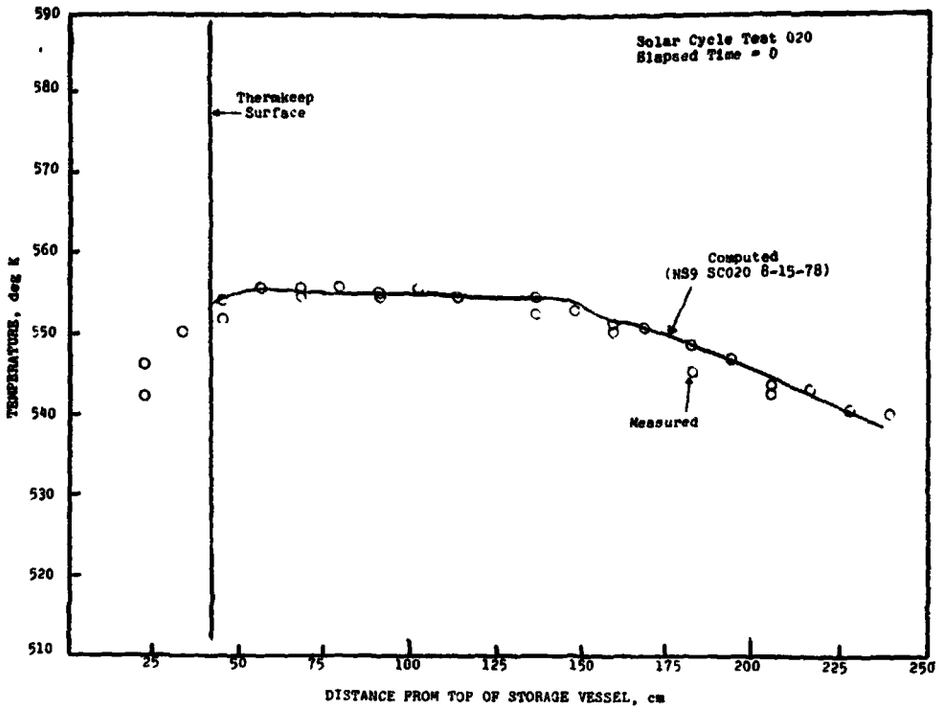

Figure 81. Thermkeep starting temperature, cycle 1.

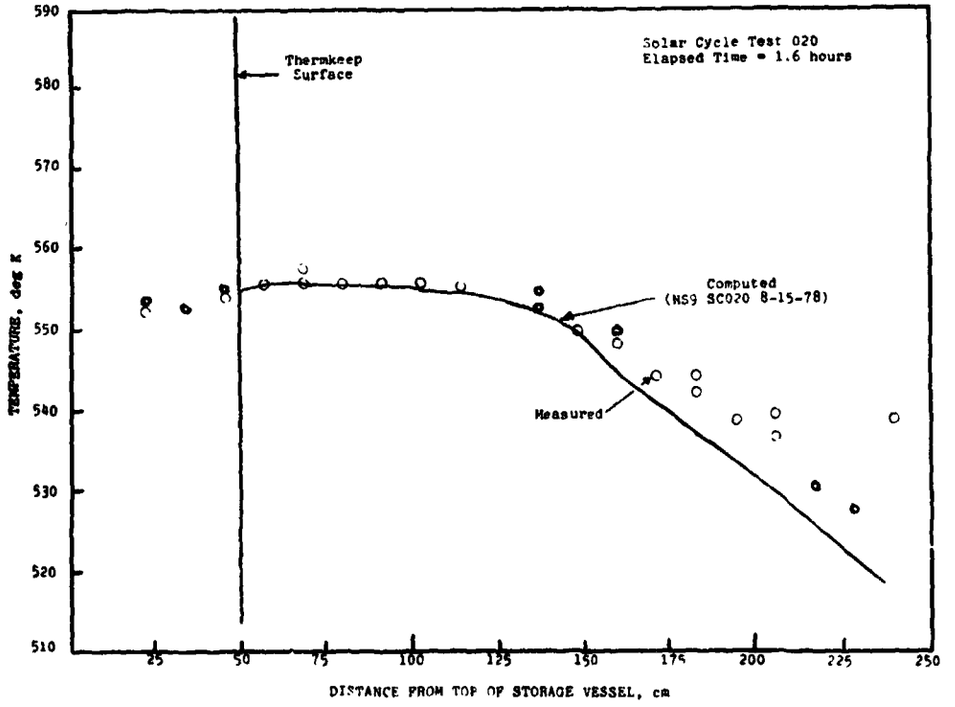

Figure 82. Thermkeep temperature at end of Phase 1 discharge, cycle 1.

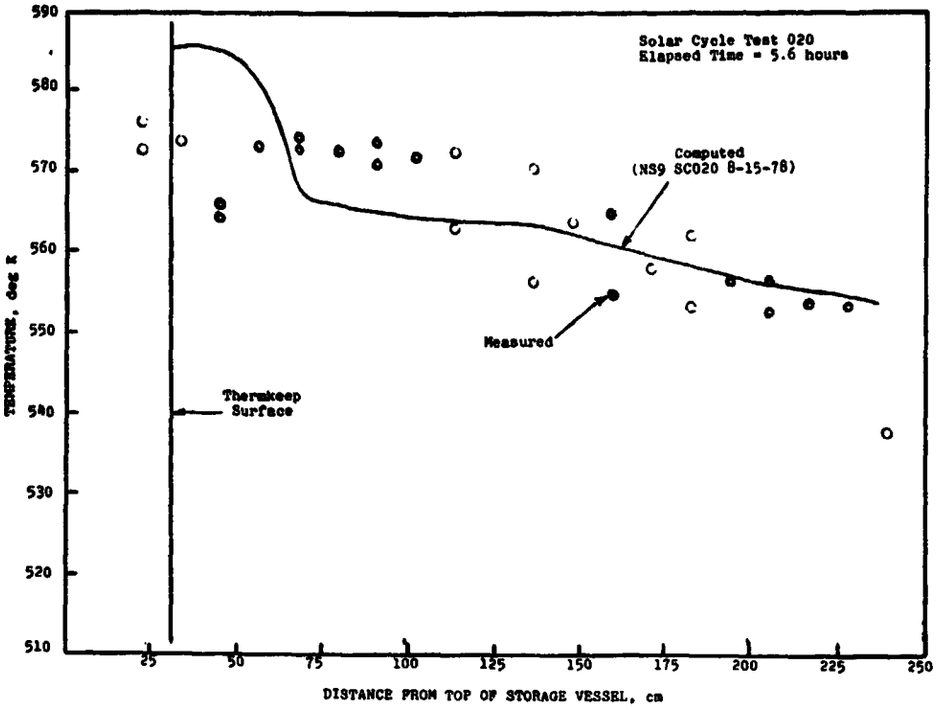

Figure 83. Thermkeep temperature at end of charge, cycle 1.

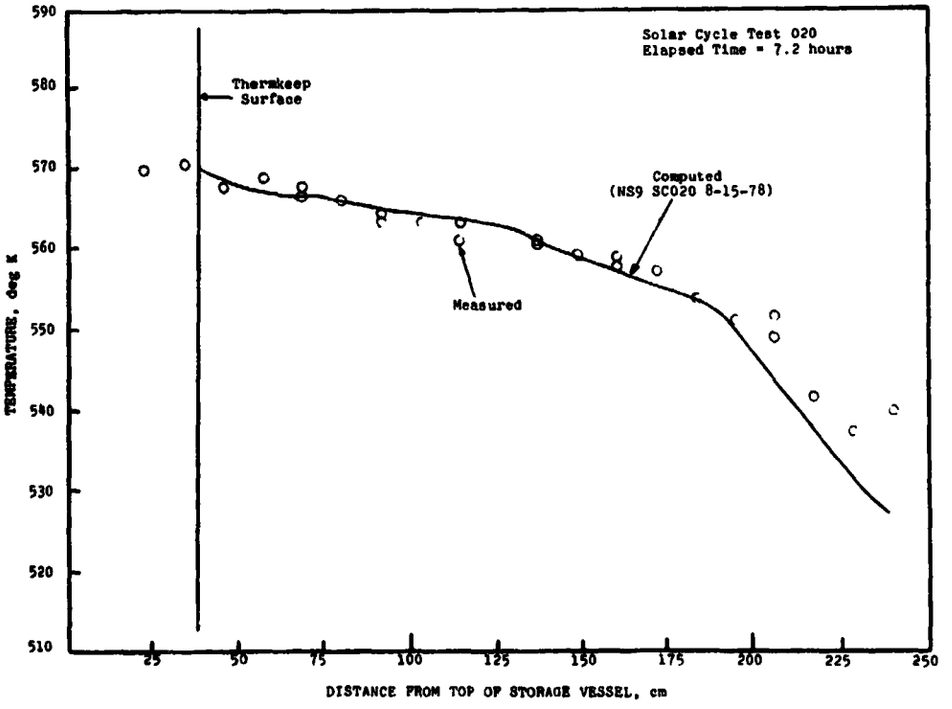

Figure 84. Thermkeep temperature at end of phase 2 discharge, cycle 1.

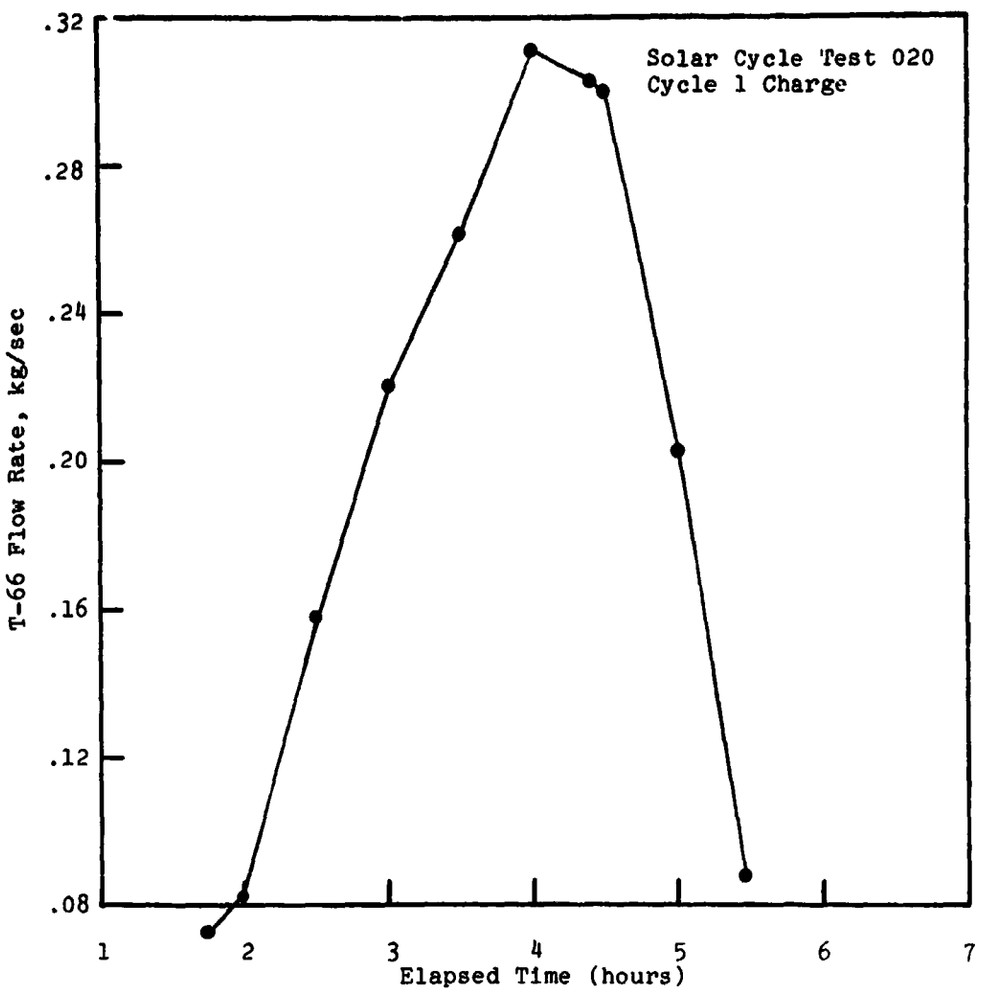

Figure 85. T-66 flow rate during charge.

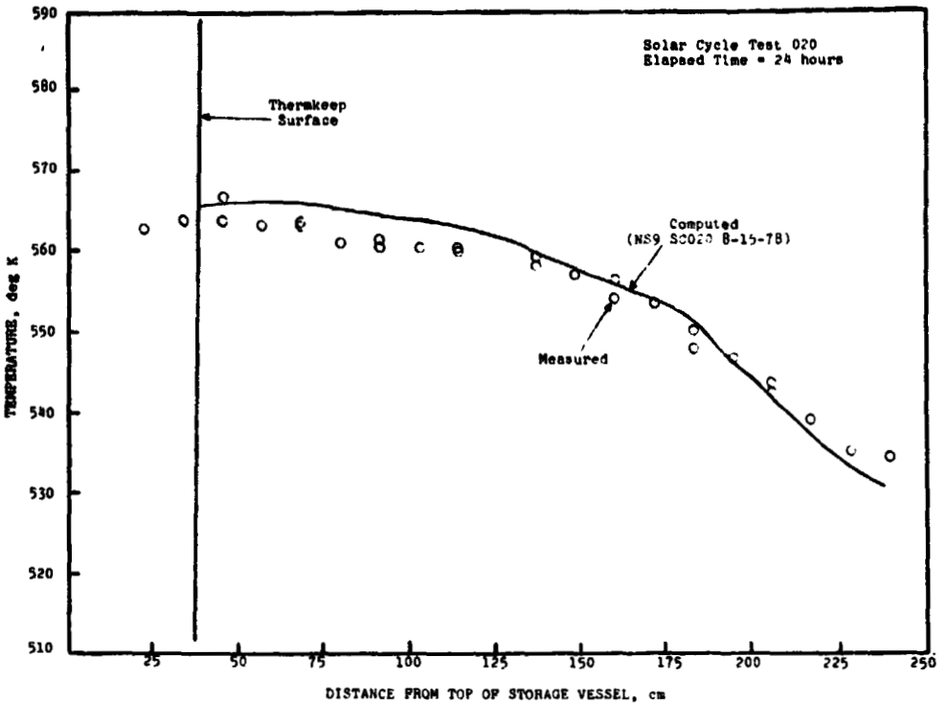

Figure 86. Thermkeep temperature at starting profile, cycle 2.

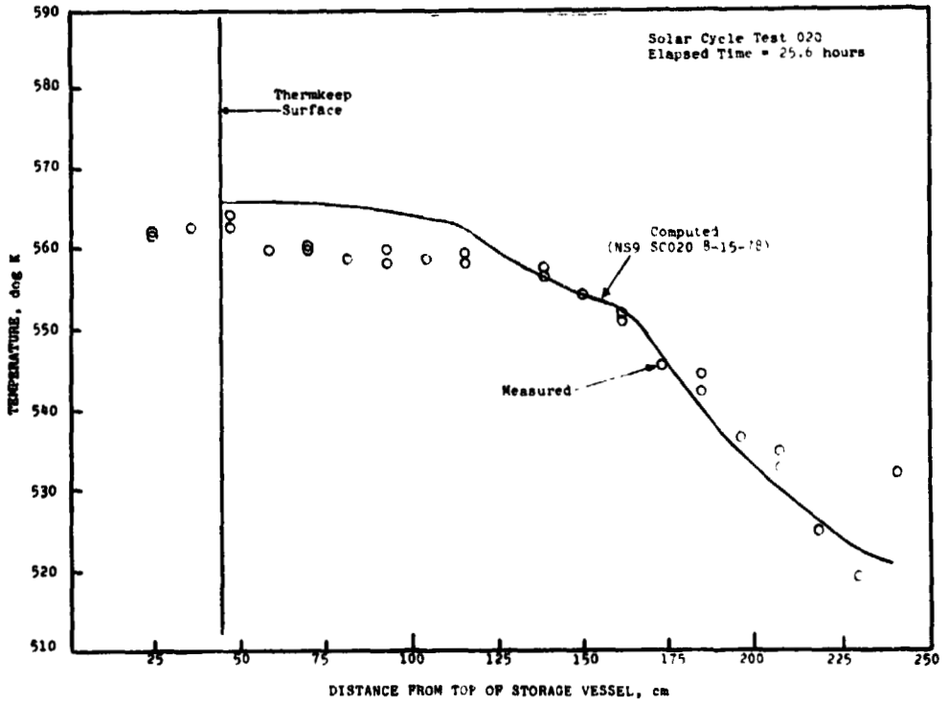

Figure 87. Thermkeep temperature at end of phase 1 discharge, cycle 2.

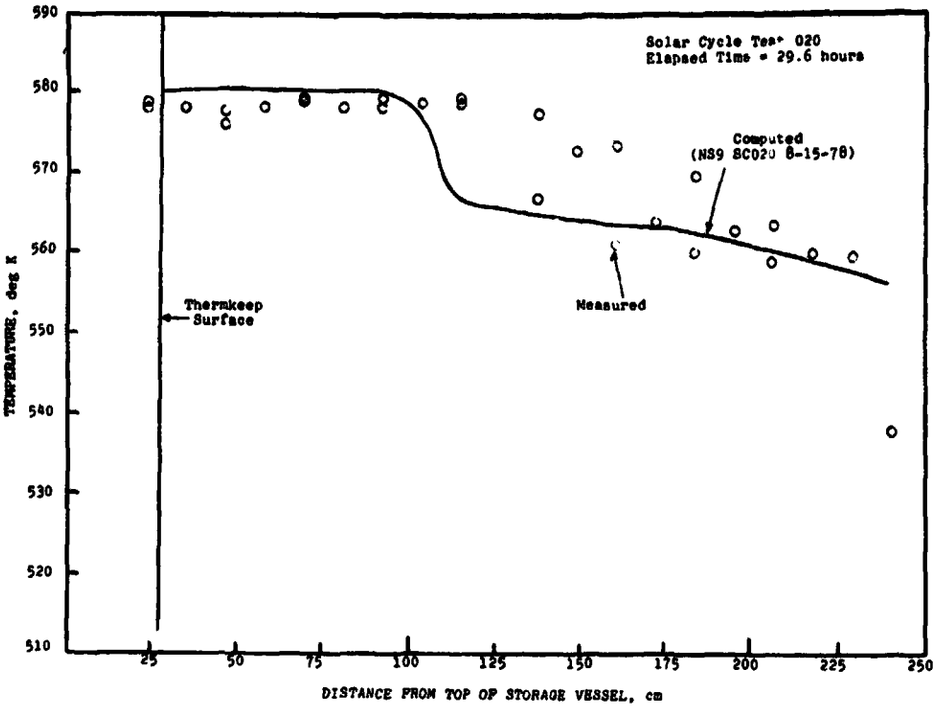

Figure 88. Thermkeep temperature at end of charge, cycle 2.

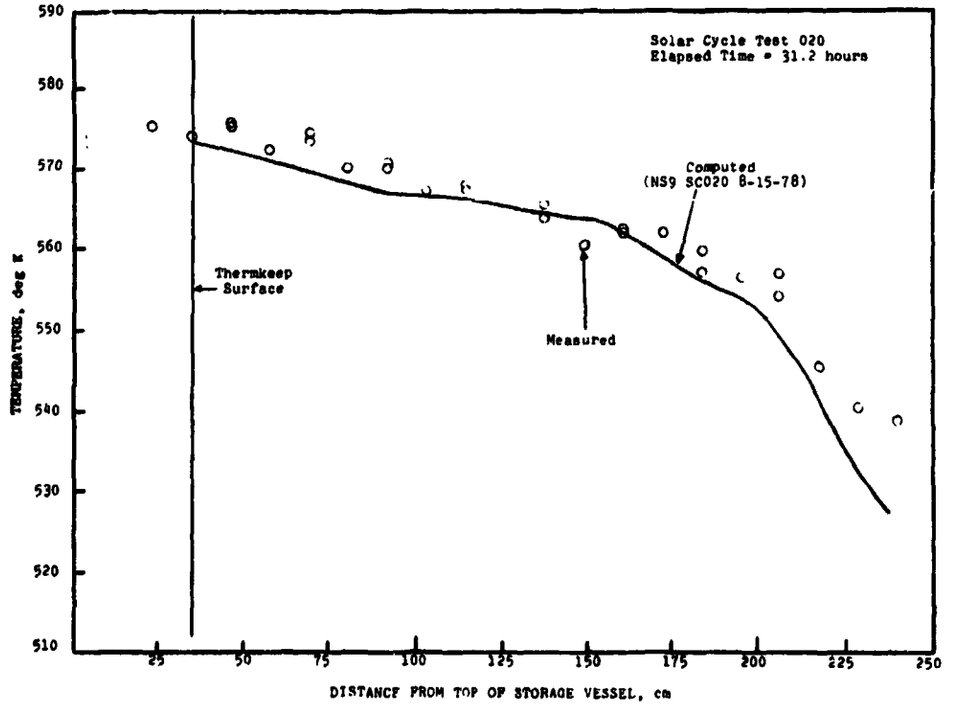

Figure 89. Thermkeep temperature at end of phase 2 discharge, cycle 2.

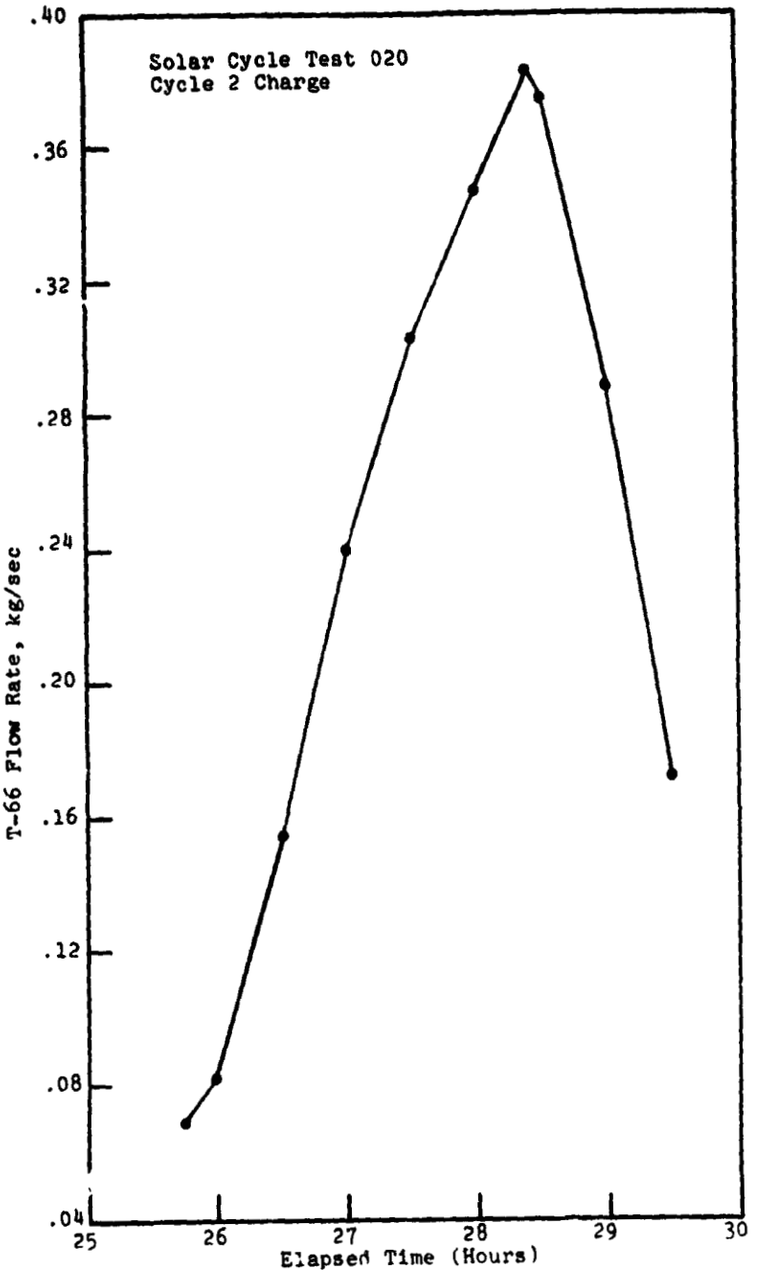

Figure 90. T-66 flow rate variation during second charge cycle.

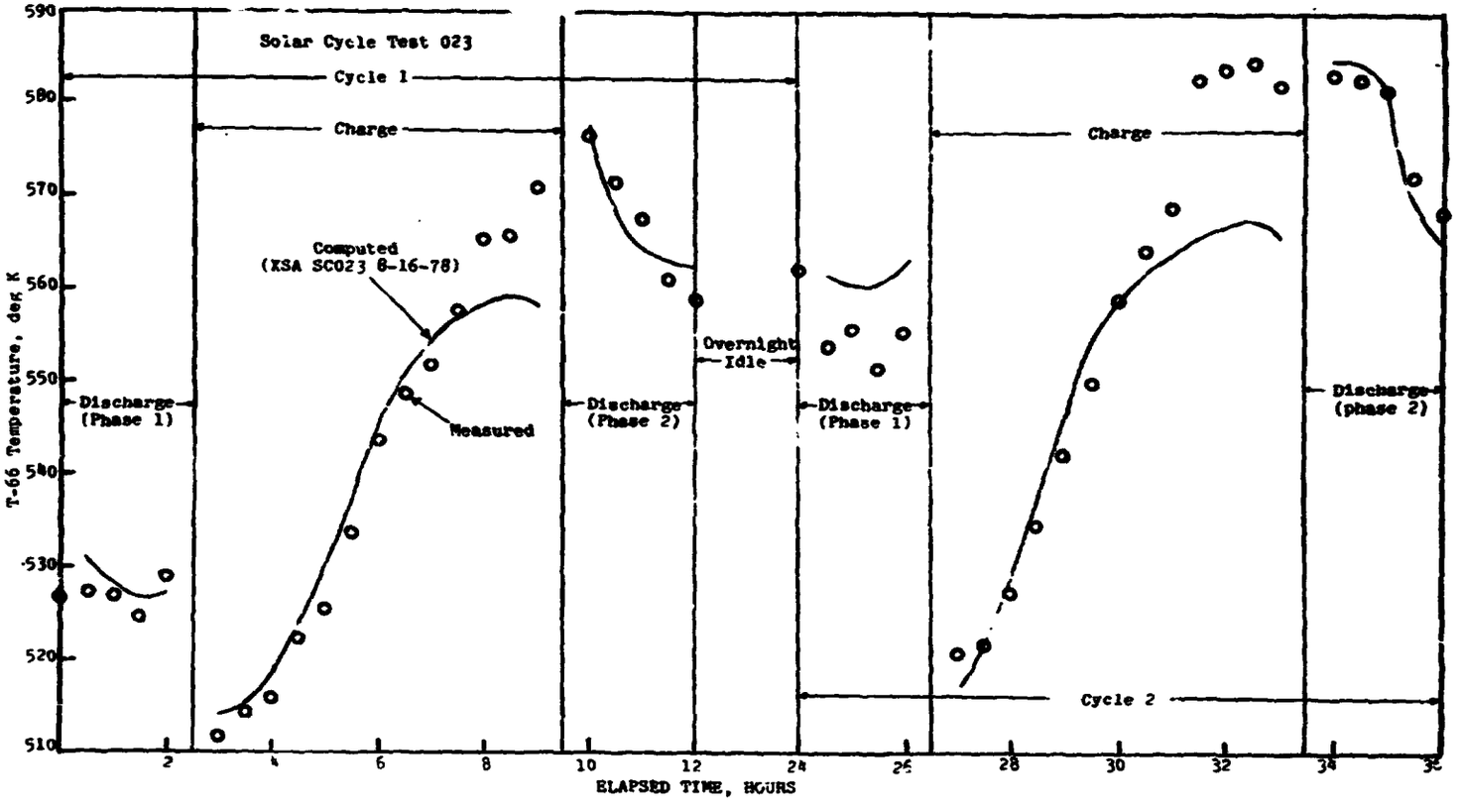

Figure 91. T-66 outlet temperature for full-scale solar cycle simulation test.

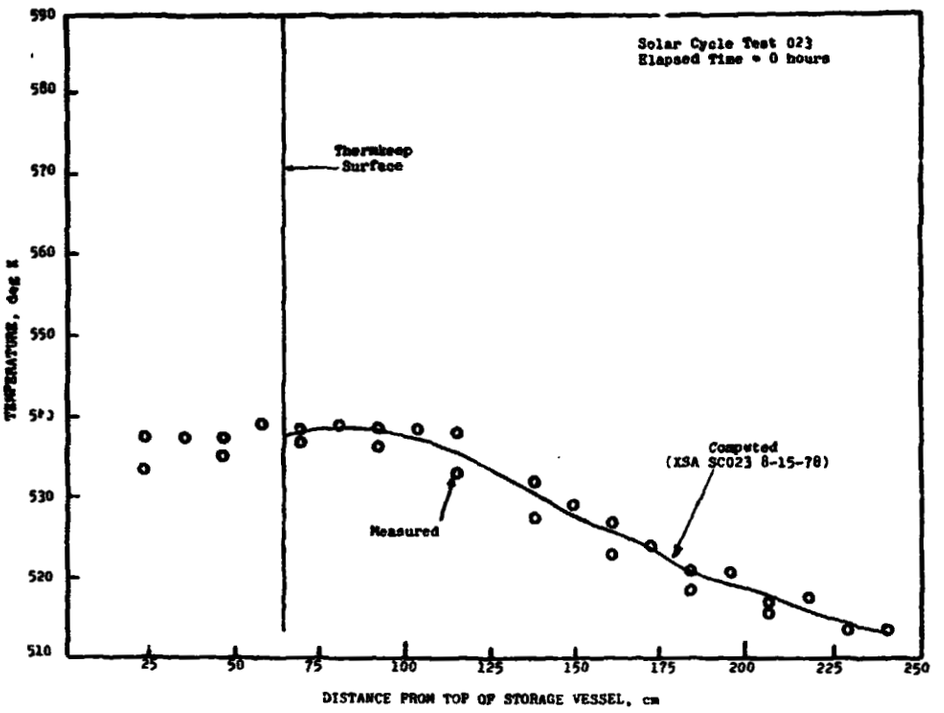

Figure 92. Thermkeep temperature, Test 023 starting profile, cycle 1.

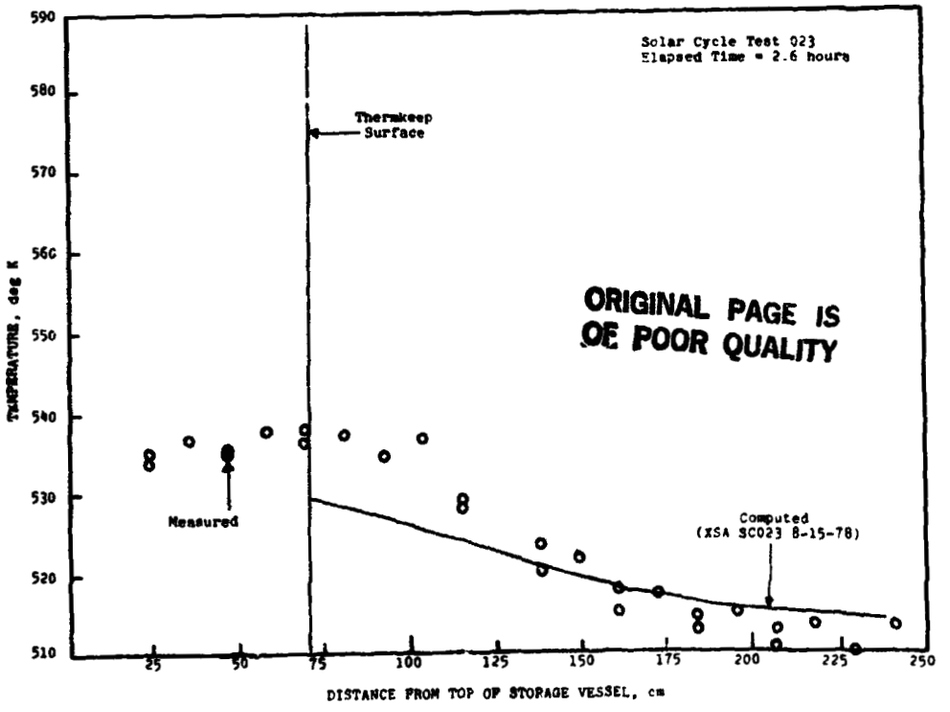

Figure 93. Thermkeep temperature at end of phase 1 discharge, cycle 1.

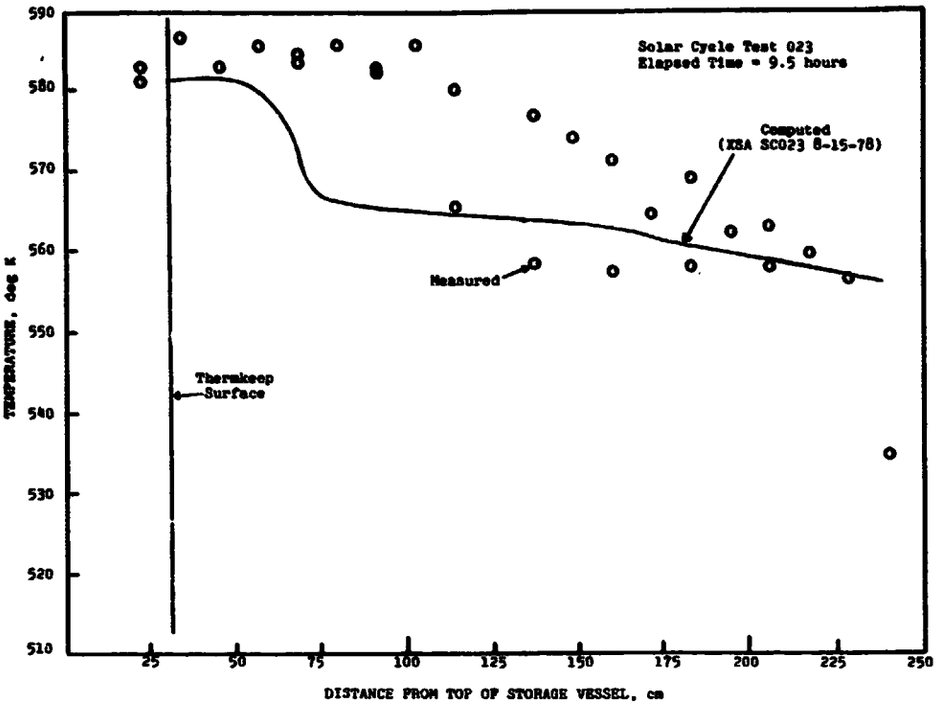

Figure 94. Thermkeep temperature at end of charge, cycle 1.

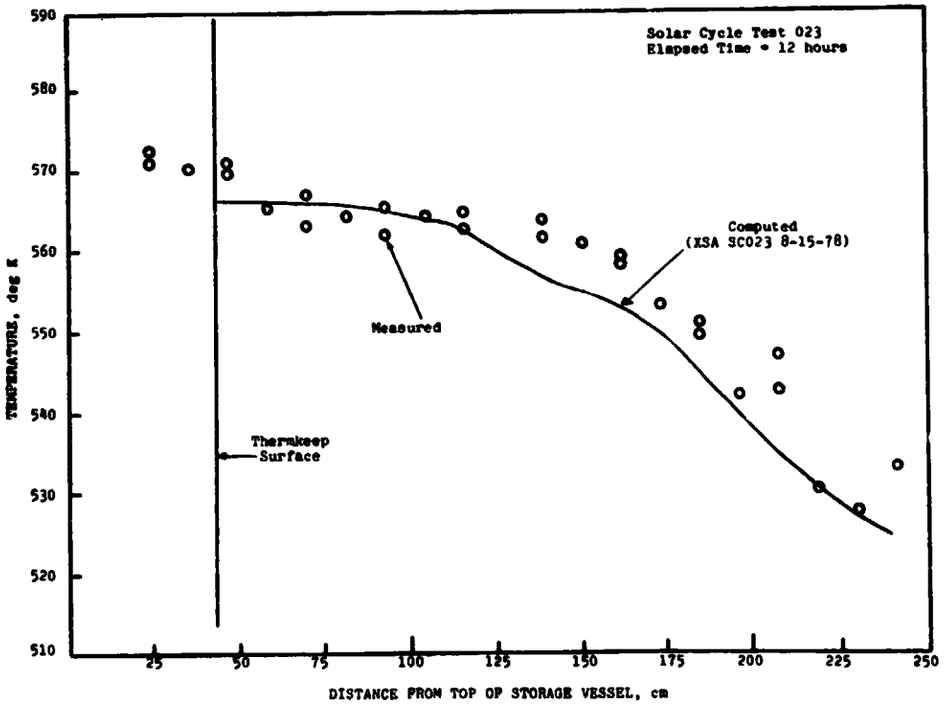

Figure 95. Thermkeep temperature at end of phase 2 discharge, cycle 1.

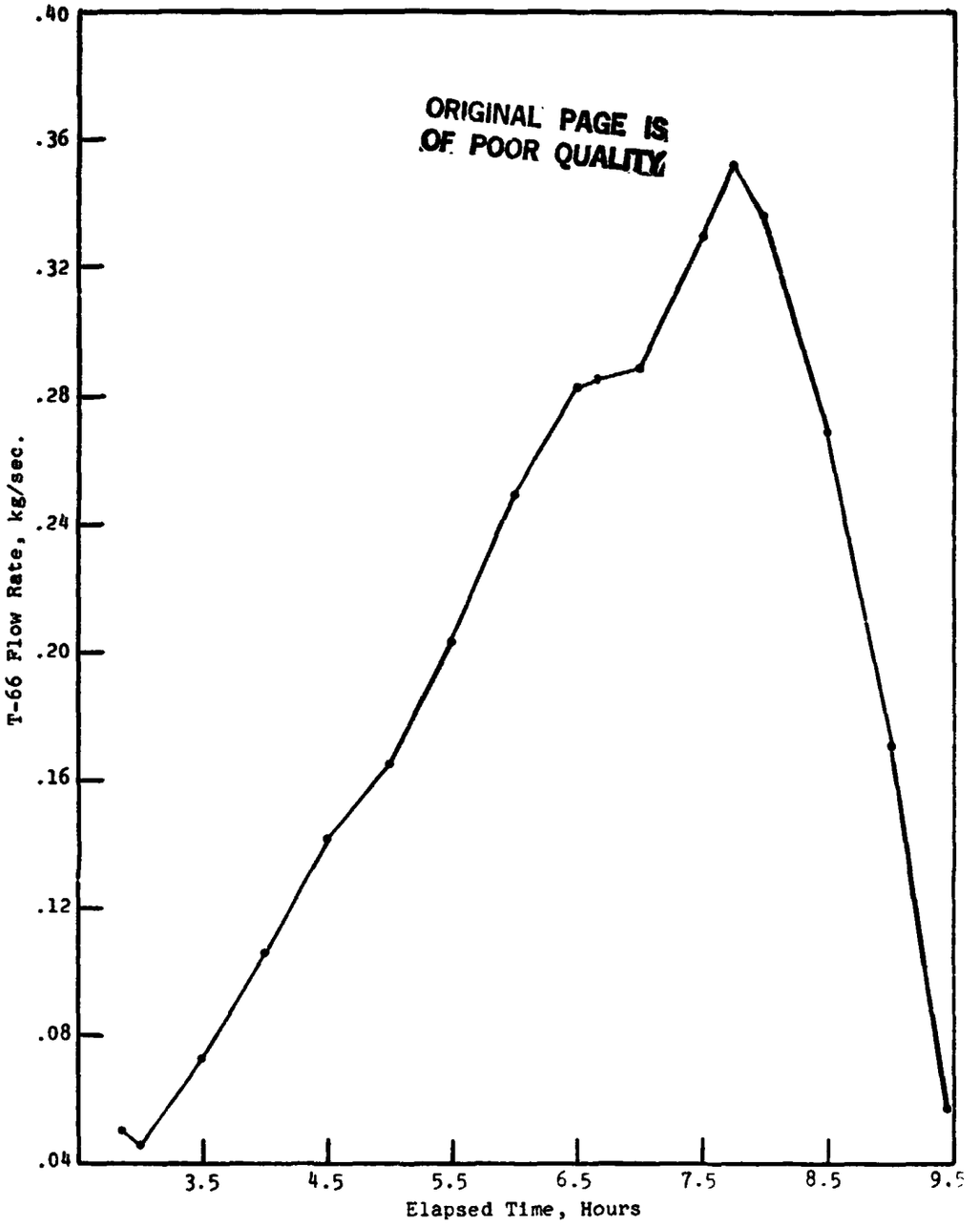

Figure 96. T-66 flow rate variation during first charge cycle.

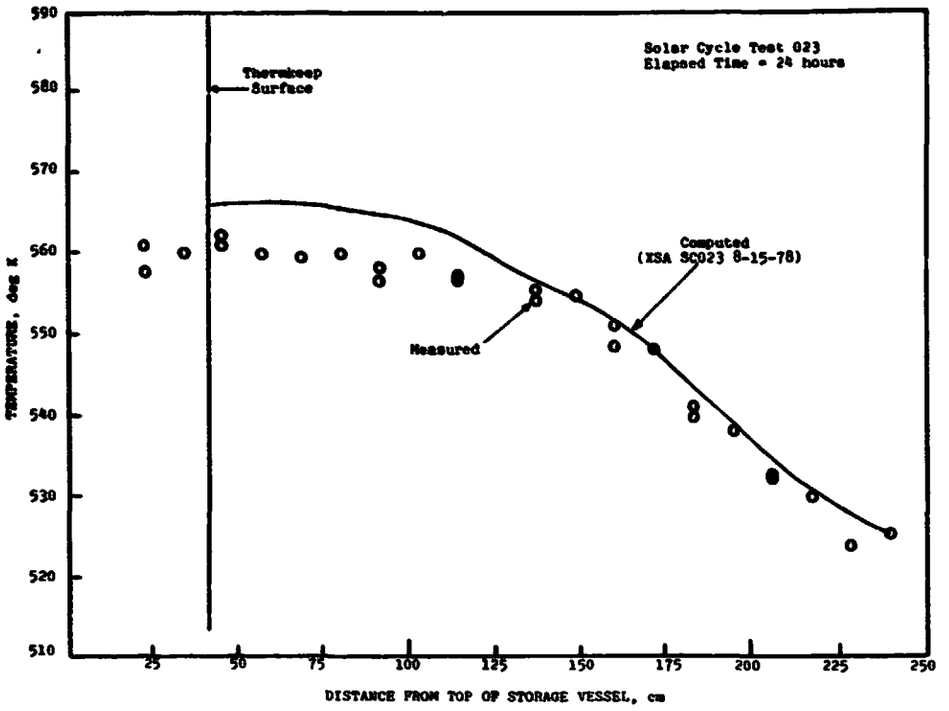

Figure 97. Thermkeep temperature at starting profile, cycle 2.

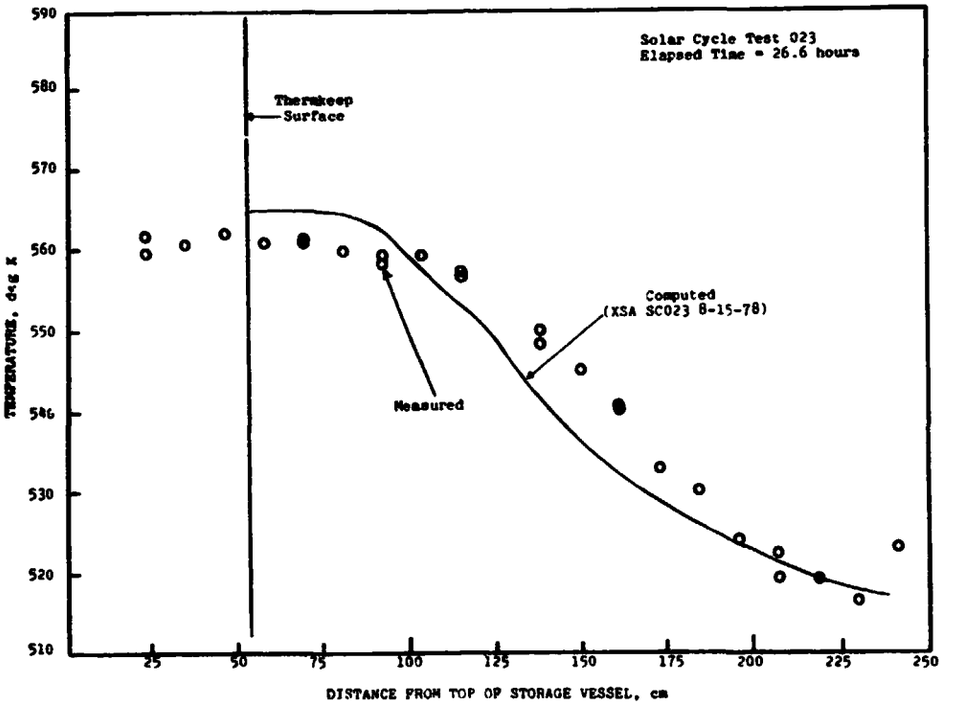

Figure 98. Thermkeep temperature at end of phase 1 discharge, cycle 2.

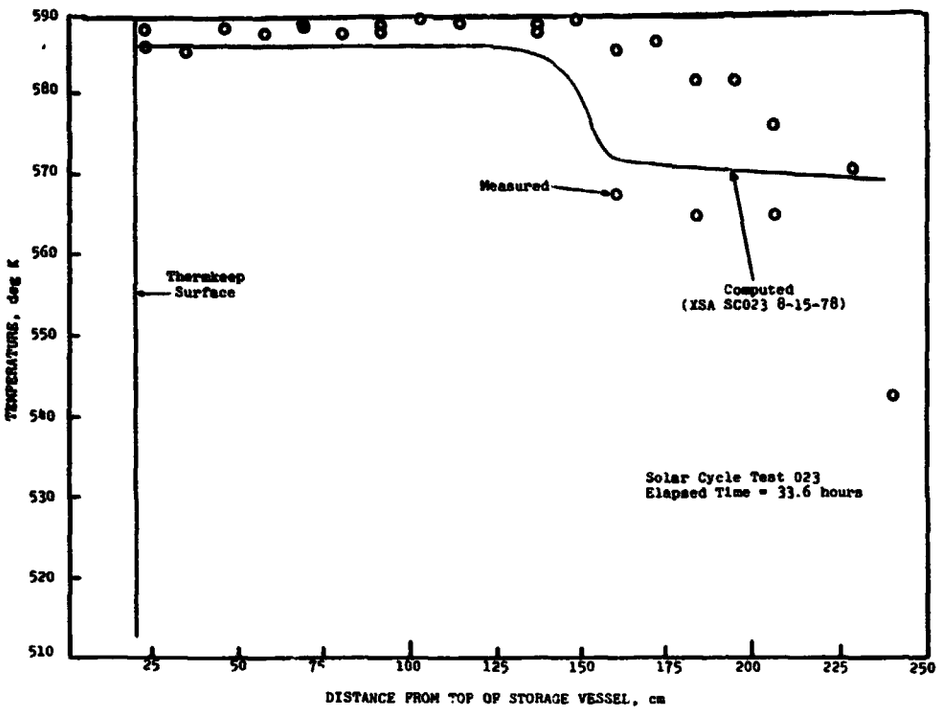

Figure 99. Thermkeep temperature at end of charge, cycle 2.

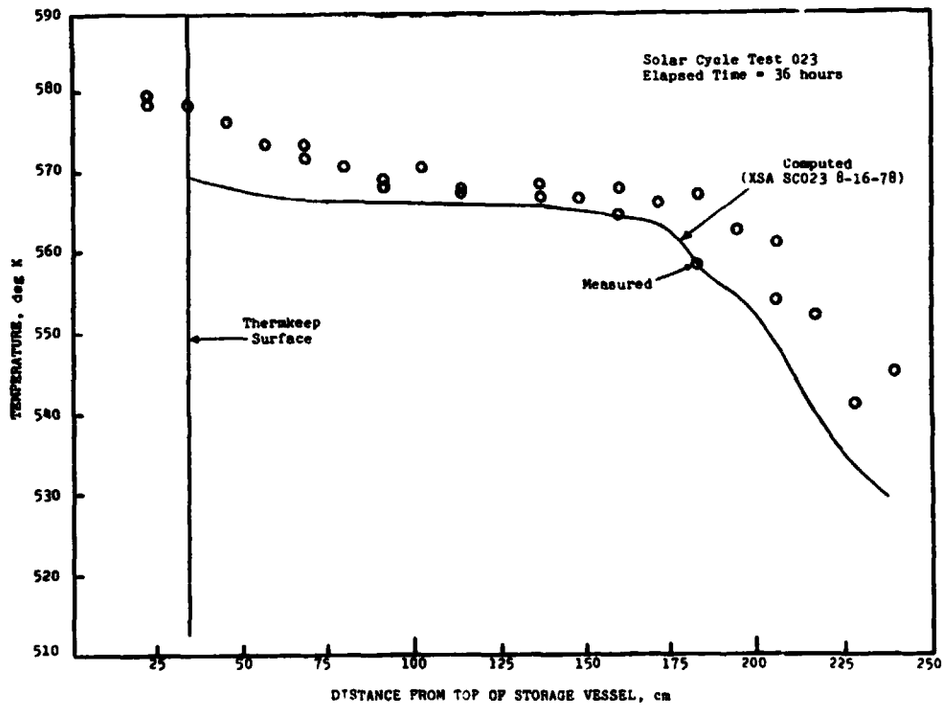

Figure 100. Thermkeep temperature at end of phase 2 discharge, cycle 2.

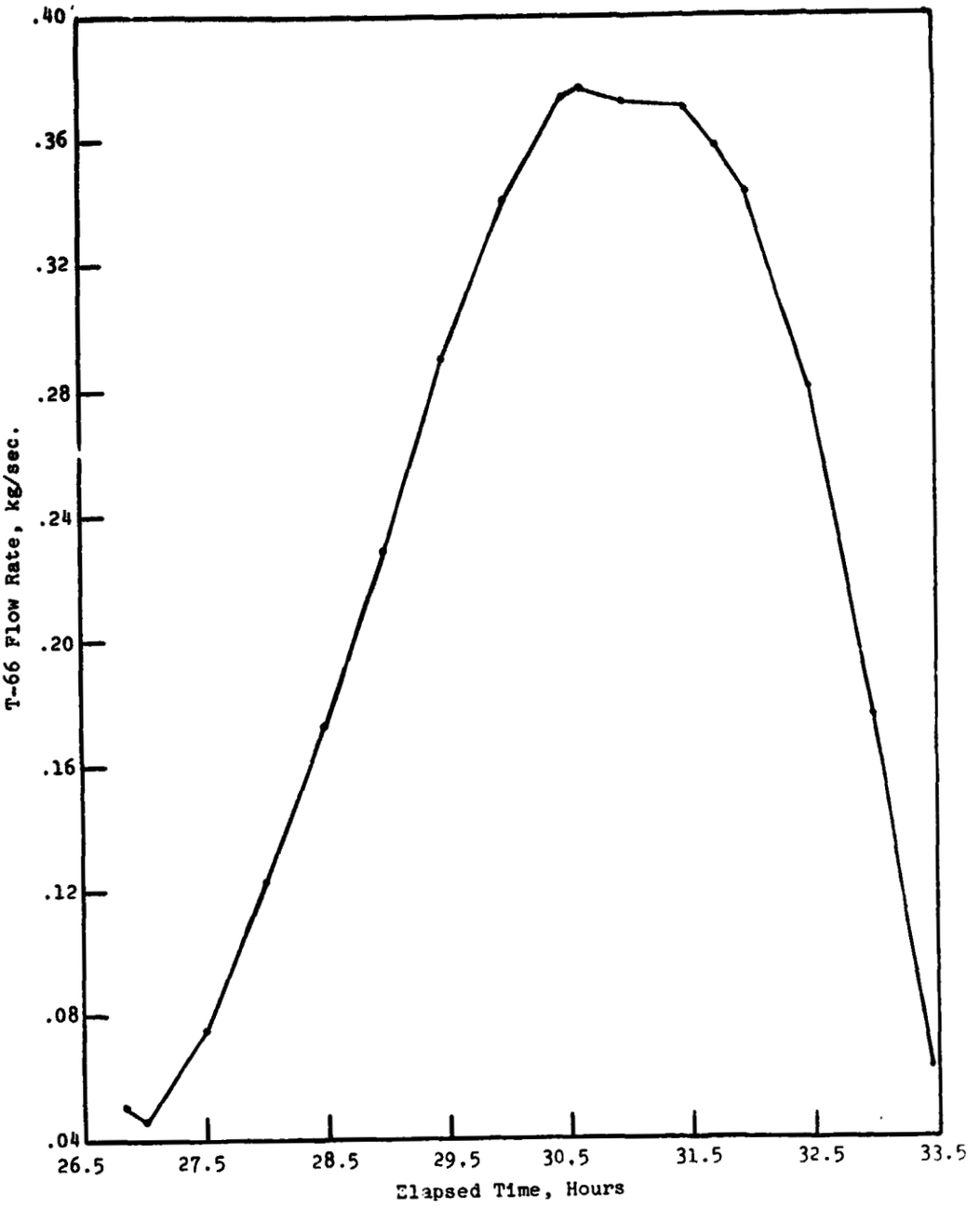

Figure 101. T-66 flow rate variation during second charge cycle.

PRELIMINARY DESIGN

With the computer model now reliably predicting experimental results, it was used to produce an updated design for a unit meeting the performance specifications as listed under Task 3, Page 7.

The primary variables affecting system performance are the quantity of storage medium and the total heat exchanger surface area. These two parameters were used to produce a first optimization. A figure of merit (F.O.M.) which is an efficiency based upon the deficit requirements of the unit (the amount of heat required to maintain the outlet temperature at a minimum of 580 K (307 C) during discharge) was used to describe the performance of each design.

$$F.O.M. = \frac{Q_o}{Q_o + Q_s + Q_D}$$

where Q_o = storage daily output

Q_s = storage daily surface loss

Q_D = fluid deficit heating

Surface areas from 55.7 m^2 (600 ft^2) to 167 m^2 (1800 ft^2) were run in units ranging from 10,000 to 50,000 kg of Thermkeep. All were run with the optimum aspect ratio of 1 (vessel height to vessel diameter) and standard 0.635 cm (1/4") tubing of a given length and number to produce about 69 kPa (10 psi) of pressure drop in the heat exchanger with a flow of 5 kg/sec of Therminol-66.

Figures 102 through 105 show the heat exchanger surface area and amounts of Thermkeep plotted against the figure of merit and the specific cost of storage in dollars per MJ. With some interpolation, the amount of Thermkeep was then cross plotted against specific cost at constant figures of merit (Fig. 106).

At this point, a first optimization is selected with one additional arbitrary limit -- reasonable size. A vessel with an aspect ratio of 1 tends to exceed 12 feet in diameter at about 20,000 kg, above which the unit would probably have to be fabricated and shipped in more than one piece. The highest F.O.M. at lowest specific cost for a reasonably sized unit falls at an F.O.M. of .88, as specific cost of $11.20/MJ and uses 18,000 kg of Therm-keep. The heat exchanger has 111.5 m^2 (1200 ft^2) of surface area.

This design was obtained using 10 numerical elements for computer analysis; a finer grid of 25 elements improves the computed performance slightly and brings the cost down to $11.17/MJ.

Next the design was tested to evaluate the effect of five minor parameters: tube size, fluid velocity, aspect ratio, insulation thickness, and peak flow through storage.

Figure 107 shows the effect of increasing tube size both against efficiency and cost. 0.635 cm (1/4") is believed to be the smallest practical size to work with; and as tubes get larger, the cost increases while efficiency decreases. The 0.635 cm (1/4") tubes are therefore retained.

Figure 108 shows the effect of increasing fluid velocity by increasing the length of the tubes and decreasing their number, retaining the same surface area. Performance does increase with velocity as expected; however, if we assume a 10% thermal-to-mechanical efficiency for driving the pump, any increase over 11 psi cannot be justified. To go to 145 kPa (21 psi), for example, the pump would use an additional 54,000 kJ output. Therefore, the 76 kPa (11 psi) speicification was accepted.

The effect of the vessel aspect ratio (height/diameter) on the specific cost and on the figure of merit is shown on Figure 109. Although the figure of merit is highest at the ratio 1.0, and the specific cost has a minimum at the ratio 2.0, the aspect ratio has so little effect on these parameters that it can be chosen on the basis of other factors. The aspect ratio 1.0 is used in the Preliminary Design.

Figure 110 shows the effect on the Figure of Merit and on specific cost of increasing insulation thickness. Performance does increase but with diminishing returns. The increase in total cost of the TES unit by increasing the

insulation thickness from 0.457 m (18") to 0.61 m (24") is $470 which affords about 1.5% increased performance.

The increase from 0.457 m (18") to 0.61 m (24") costs $560 and affords about 0.7% increased performance. From 0.61 m (24") to 0.76 m (30") costs $630 and affords less than 0.5%. Meanwhile, the loss from 0.457 m (18") of insulation is 3.9% of the daily storage, and from 0.61 m (24"), it is 3.3%. 0.76 m (30") makes the loss 2.9%. Thus, the 0.61 m (24") thickness was selected as the point at which returns begin to diminish most sharply.

The effect of varying the peak allowable storage flow is shown in Figure 111. 5 kg/sec seems to be the point below which efficiency begins to deteriorate rapidly and cost begins to escalate markedly. Therefore, 5 kg/sec is retained in the design.

The quantity of Thermkeep and the size of the heat exchanger, and consequently the size and cost of the TES unit are strong functions of Q_D, the deficit heating.

Figure 112 shows the relation between the specific cost of the TES unit and the deficit heating as percent of the daily output from storage when the unit is performing according to the solar cycle. The points on the curve correspond to a range of quantities of Thermkeep from 12,000 kg to 27,000 kg. Throughout, the aspect ratio of the vessel is 1.0, and the total inside surface of the heat exchanger tubes is in the same proportion to the mass of Thermkeep as in the Preliminary Design, namely, 0.00619 m^2/kg.

Preliminary Design

Vessel height and diameter	2.35 m (92.5")
Insulation thickness	0.609 m (24")
System height and diameter	3.6 m (142")
System weight	27290 kg (60,200 lb)
Amount of storage material	18000 kg (39,700 lb)
Unit cost	$33,700
Heat exchanger	.00635 m (1/4") tubing; 280 coils, each 27.73 m (91 ft) long
Figure of Merit based upon a 25-element grid	.882
Storage output	3.01 x 10^6 kJ
Specific cost	$11.2/MJ
Insulation loss	3.25% of storage output
Deficit heating	10.2% of storage output

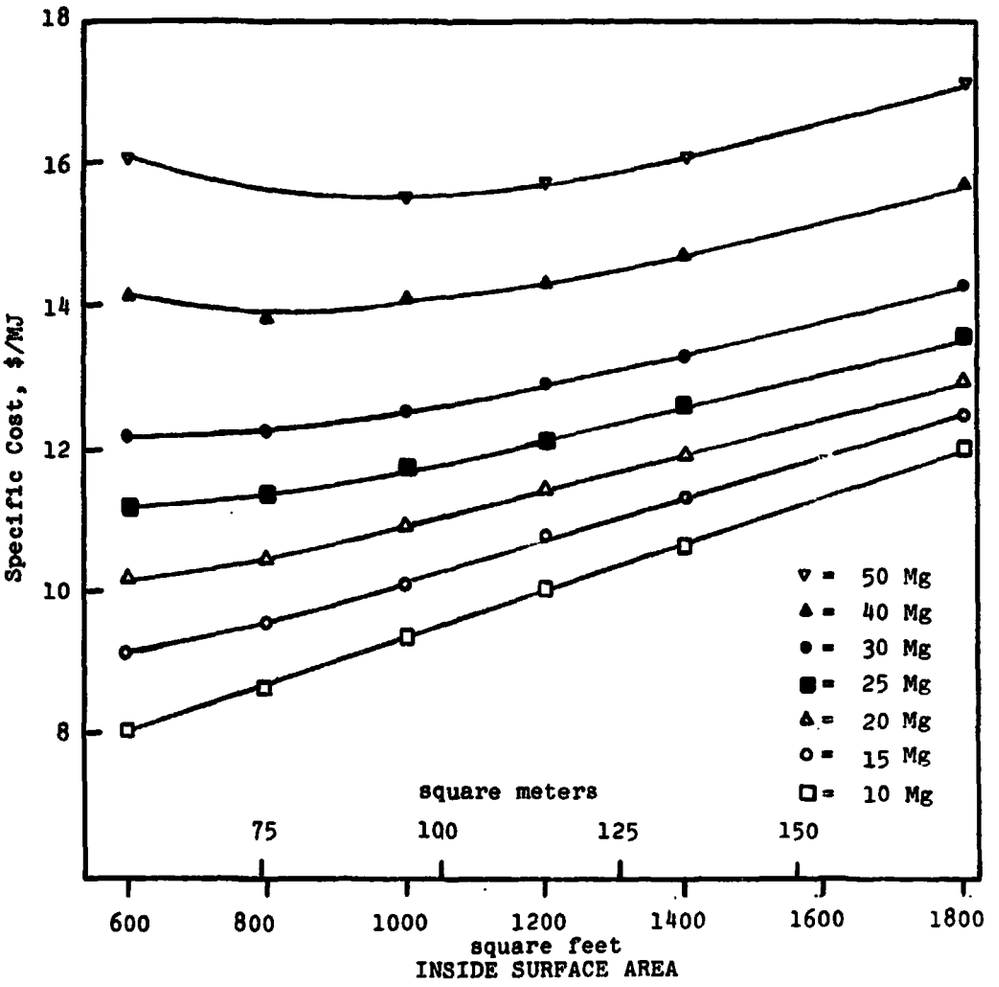

Figure 102. Specific cost of storage for various heat exchanger surface areas at constant Thermkeep masses.

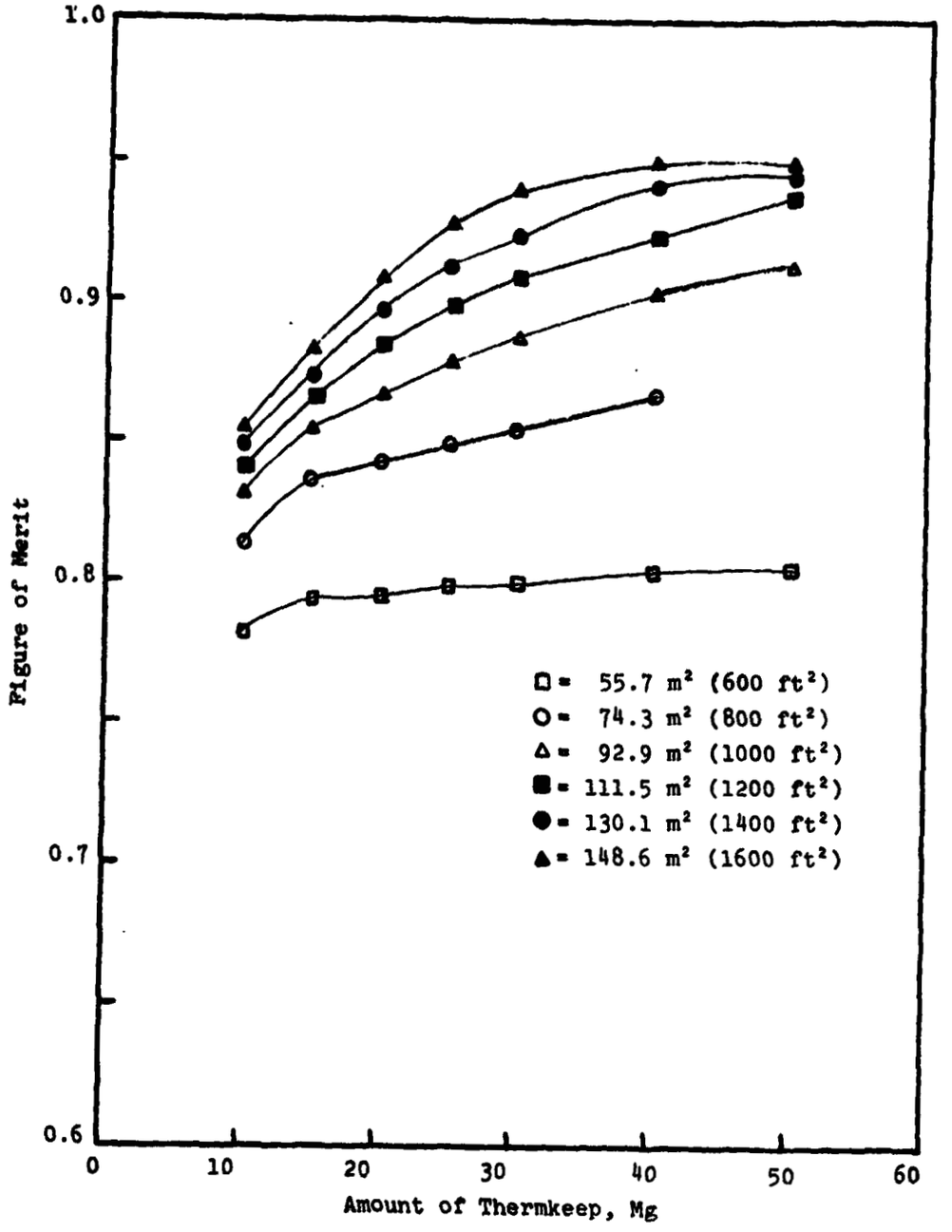

Figure 103. Figures of merit for various Thermkeep masses at constant heat exchanger surface areas.

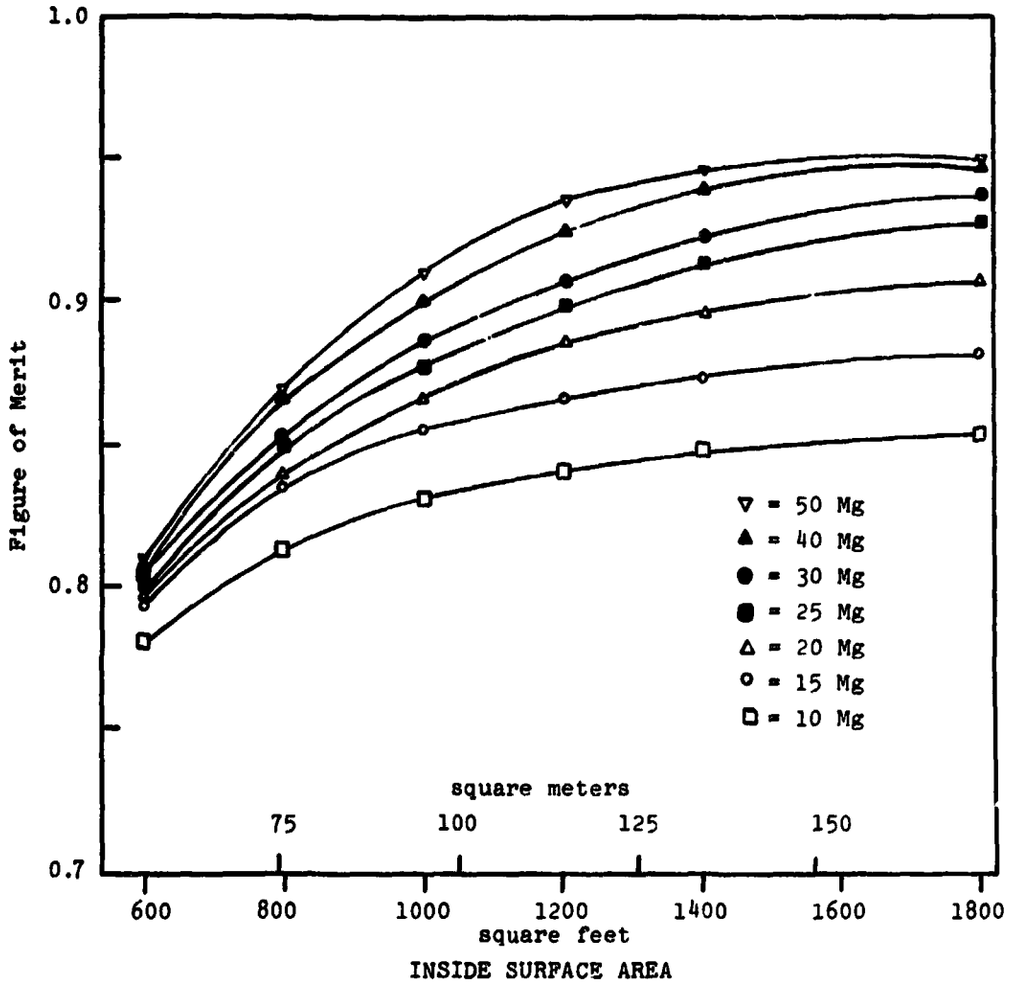

Figure 104. Figures of merit for various heat exchanger surfaces at constant Thermkeep masses.

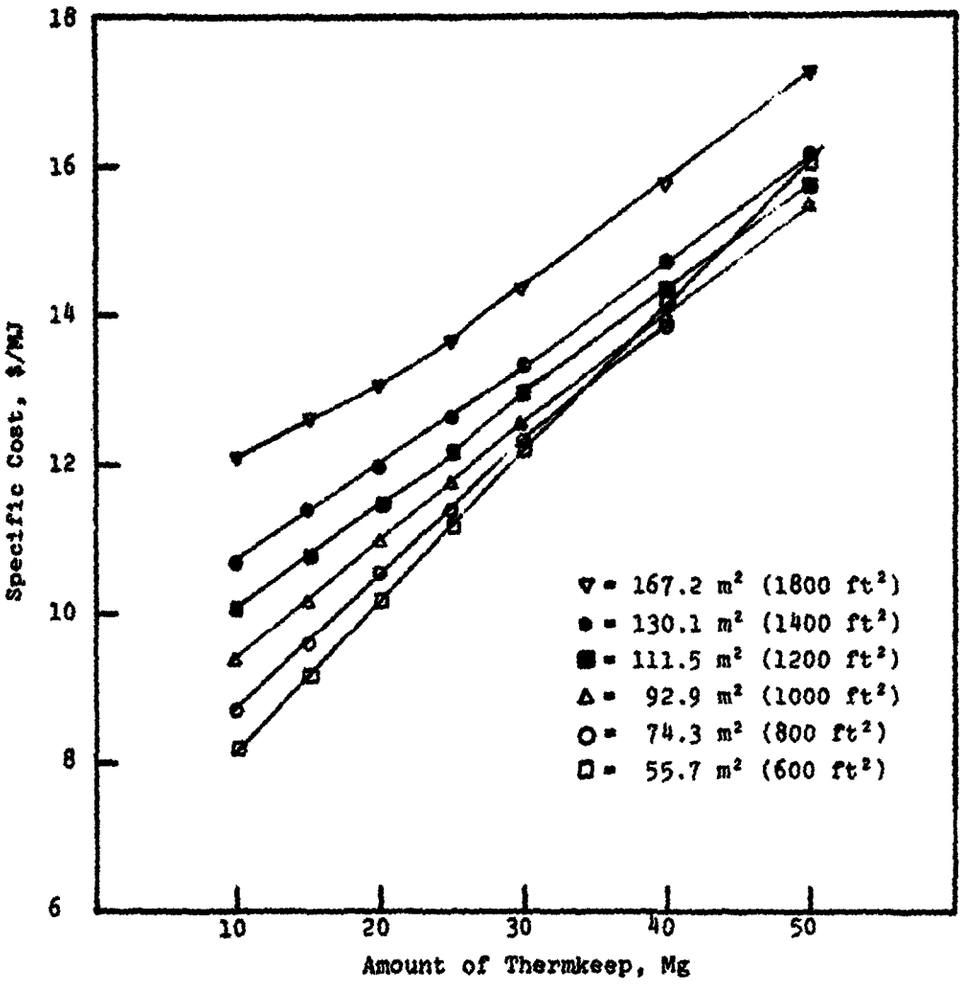

Figure 105. Specific cost of storage for various Thermkeep masses at constant heat exchanger surfaces.

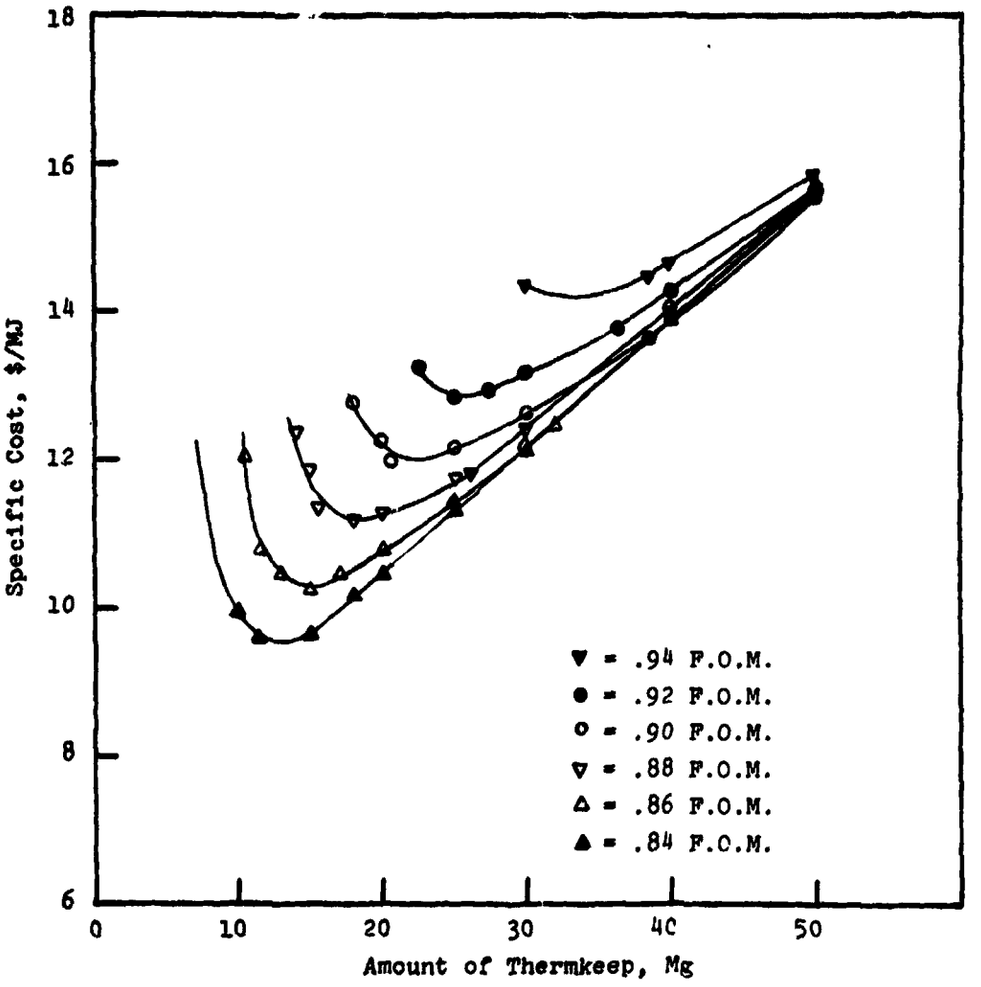

Figure 106. Specific cost of storage for various Thermkeep masses at constant figures of merit.

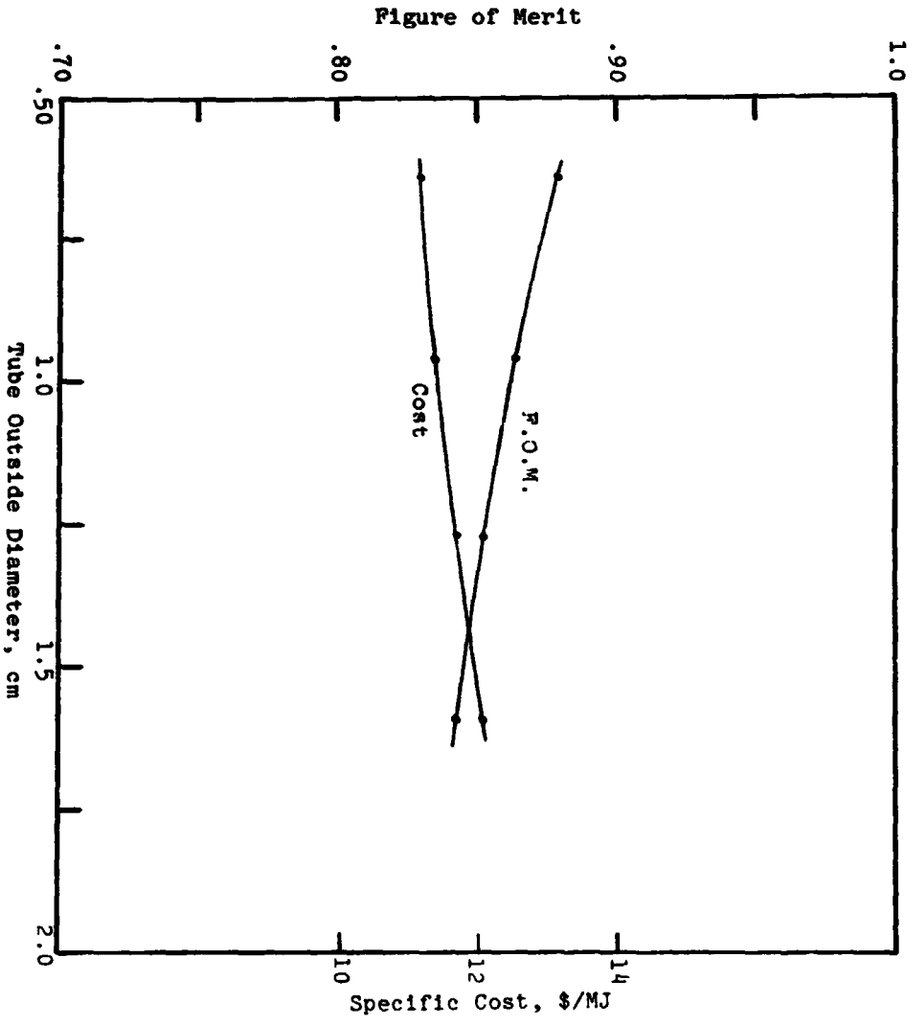

Figure 107. Specific cost of storage and figures of merit vs. tube diameters.

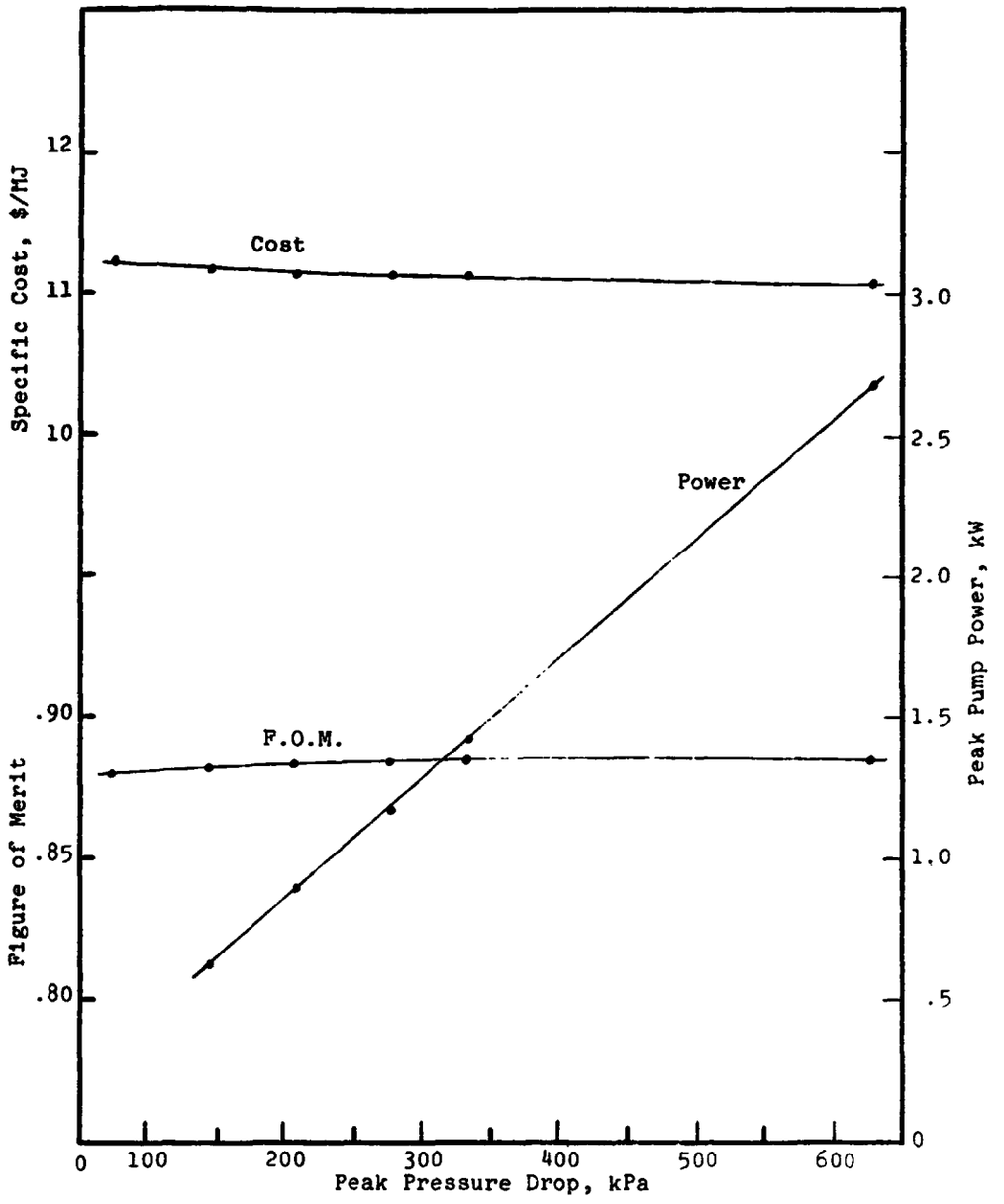

Figure 108. Specific cost of storage, peak pump power, and figures of merit at various heat exchanger pressure drops.

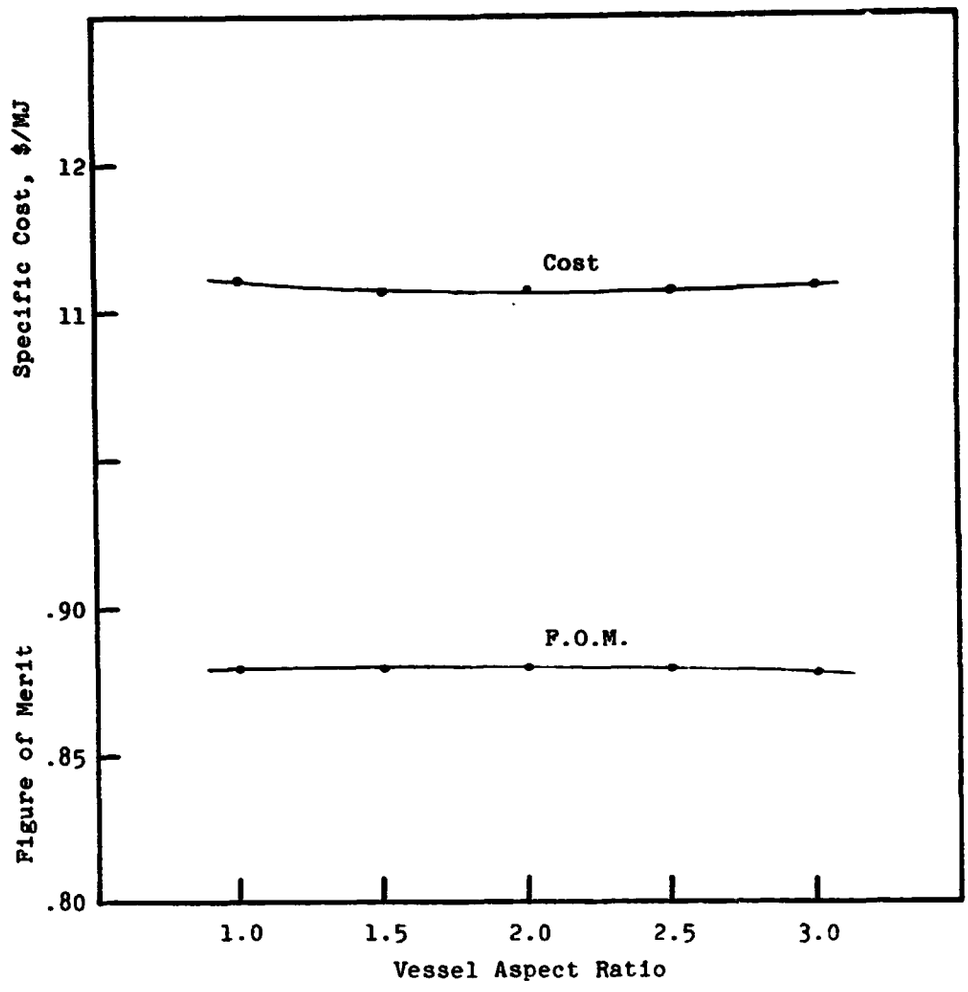

Figure 109. Specific cost of storage and figures of merit vs. aspect ratio.

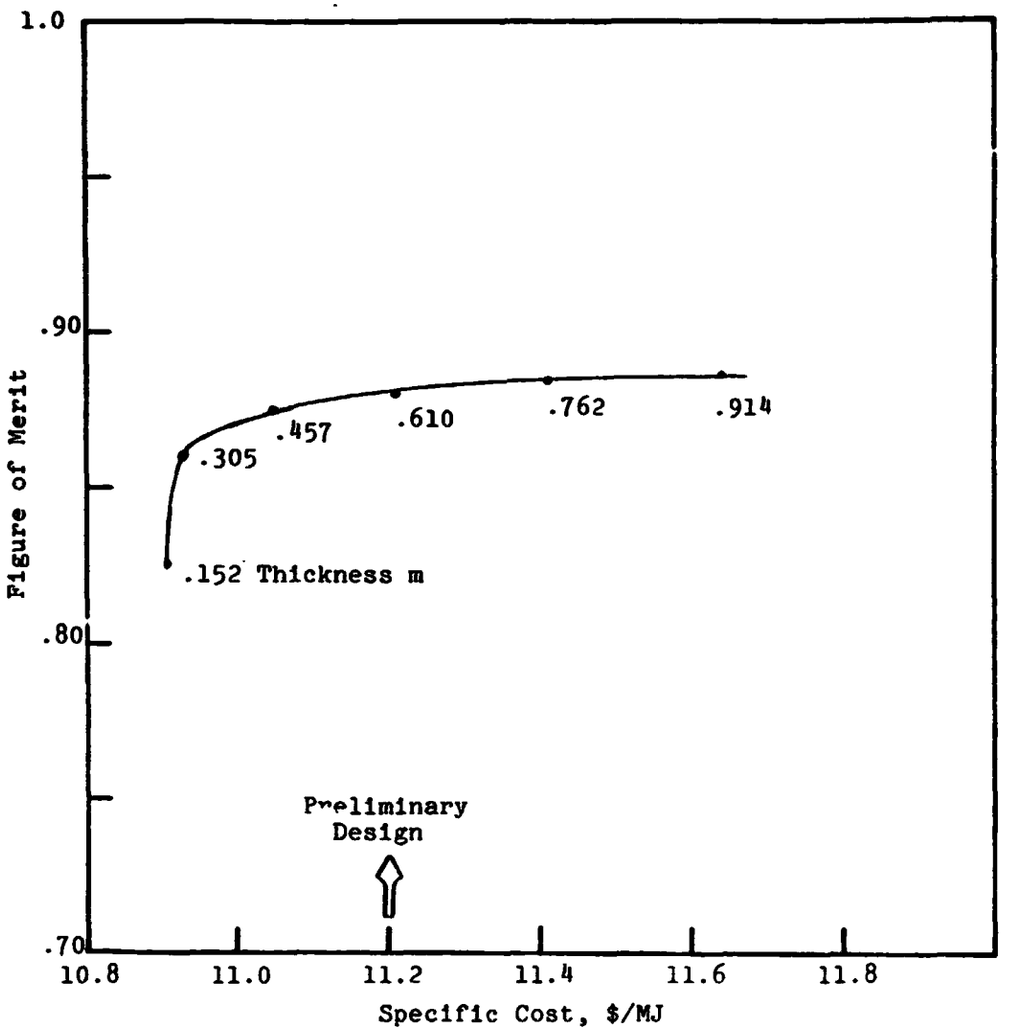

Figure 110. Effect of various insulation thicknesses on cost and performances.

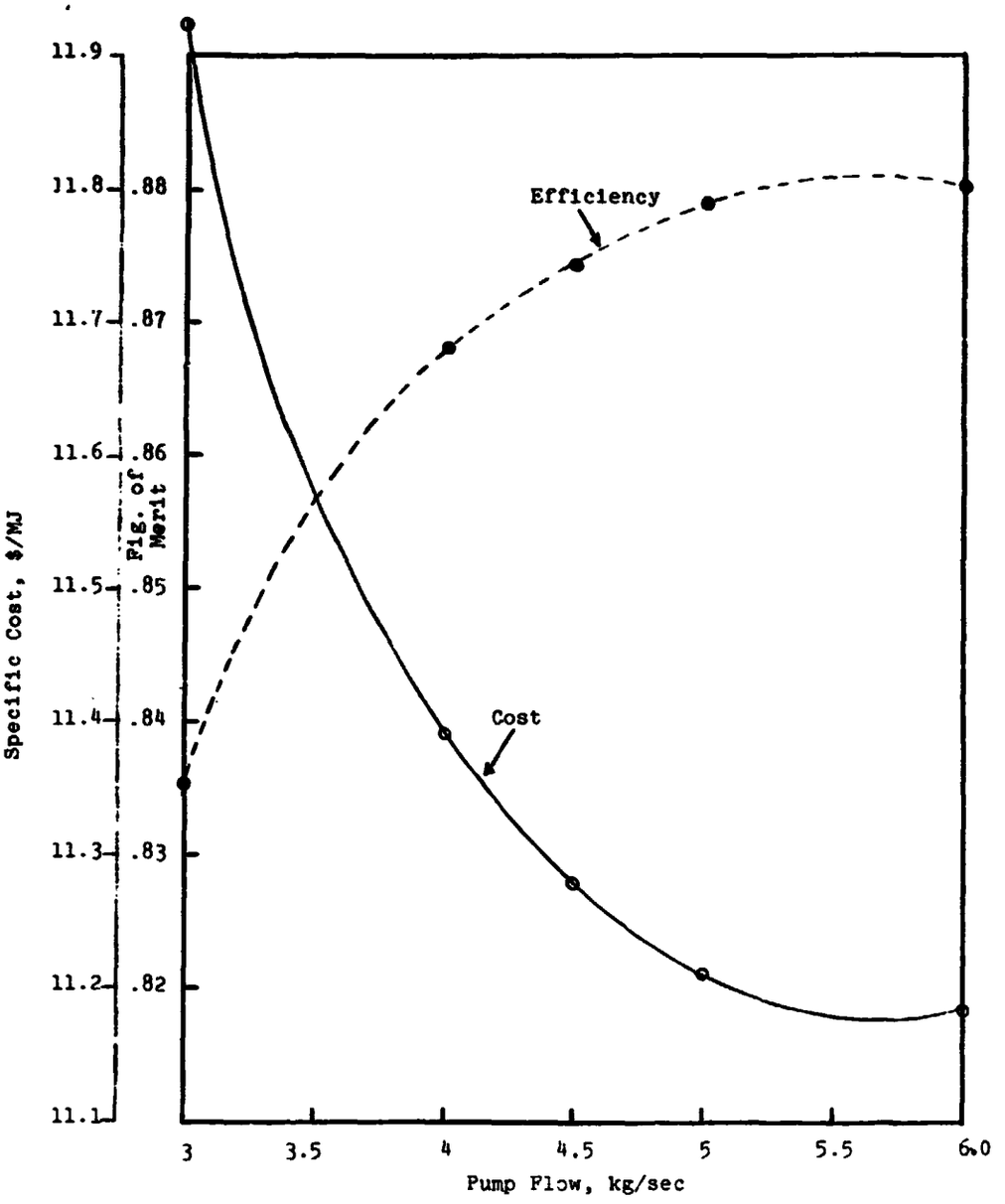

Figure 111. Specific cost of storage and figures of merit at various peak pump flows.

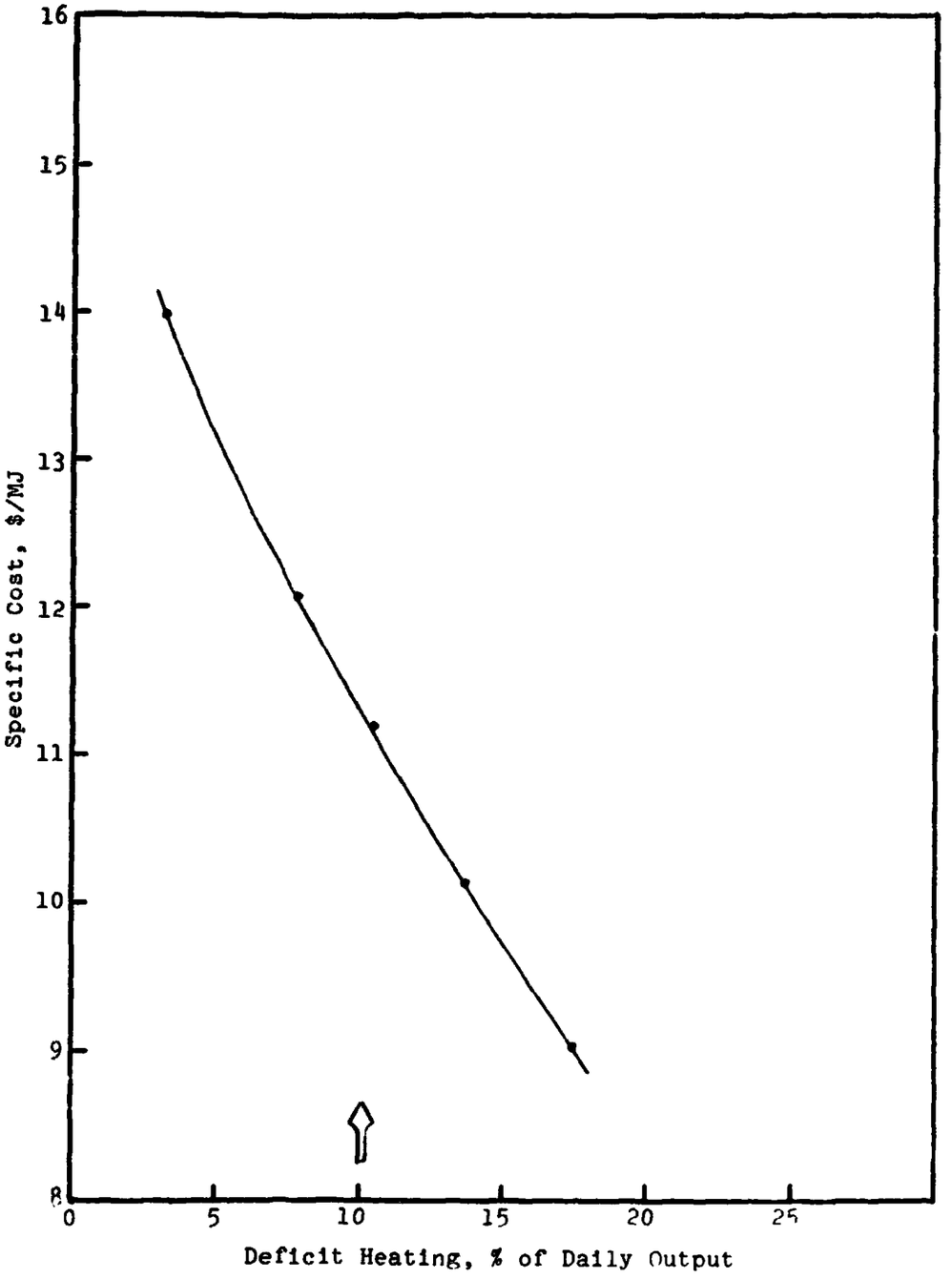

Figure 112. Specific cost versus deficit heating.

Cost Estimates

The estimated cost of the TES unit is calculated by the computer program by methods described in the preceding section titled Reference Design Study. Input data consists of the cost of material for each component, and a fabrication cost for each component which differs from part to part depending on the type of fabrication required. The input data for cost calculations are given in Table I. The detailed results of the cost calculation for the Reference Design are shown in Table II.

The materials costs were those obtained at the time of the construction of the subscale unit, i.e., 1977. The fabrication costs are based upon the actual manufacturing costs of two Thermbank electric water heaters of the type described in the Background section of the Introduction.

The estimated cost of the Preliminary Design TES unit is therefore representative of the cost to be expected if a very small number of units were to be fabricated. The fabrication component of the cost can be expected to decrease substantially if units are manufactured in large enough numbers so that the cost advantages of quantity production can be realized.

TABLE I

COST CALCULATION INPUT DATA

Shroud material cost, $/kg	0.509
Shroud side fabrication cost, $/sq m	10.1
Shroud side fabrication cost, $/kg	1.04
Shroud top fabrication cost, $/sq m	77.4
Shroud top fabrication cost, $/kg	7.92
Shroud bottom fabrication cost, $/sq m	99.8
Shroud bottom fabrication cost, $/kg	7.67
Shroud top thickness, m	0.00152
Shroud side thickness, m	0.00122
Shroud bottom thickness, m	0.00340
Vessel wall material cost, $/kg	0.472
Vessel end material cost, $/kg	0.481
Vessel fabrication cost, $/cu m	615.
Vessel fabrication cost, $/kg	2.45
Tube material cost coefficient	0.0280
Tube material cost, $/kg	4.41
Tube fabrication cost, $/kg	11.9
Tube fabrication cost, $/sq m	964.
Storage material cost, $/kg	0.441
Insulation cost, $/kg	0.287

TABLE II

COST CALCULATION OUTPUT DATA

Tube material cost, $	4100
Total tube cost, $	19200
Storage material cost, $	7940
Insulation cost, $	1180
Shroud side material cost, $	199
Shroud side total cost, $	377
Shroud bottom material cost, $	138
Shroud bottom total cost, $	641
Shroud top material cost, $	62
Shroud top total cost, $	346
Shroud total material cost, $	400
Shroud total cost, $	1360
Vessel material cost, $	1650
Vessel total cost, $	3940
Total materials cost for TES, $	15300
Total fabrication cost for TES, $	18400
TES total cost, $	33700

CONCLUDING REMARKS

The use of a phase change thermal storage media for the storage of heat from solar collectors for use in electric power generation may have economic advantages over other types of heat storage media. Previous experience with phase change thermal storage has been limited to electrically heated applications in which the stored heat is used for low temperature water and space heating. Developments of this kind have only been carried to point of small scale field testing of water heaters and space heaters.

The work reported herein has been undertaken to provide an assessment of the characteristics of a phase change thermal storage unit meeting the requirements of a mid-temperature range solar powered electricity generating system.

An analytical model and computer program have been developed for predicting the performance and estimating the cost of a phase-change TES unit using a passive heat exchanger. These have been applied to a phase change TES medium having the composition

NaOH (Commercial grade)	91.8% (wt)
$NaNO_3$	8.0
MnO_2	0.2

The heat transfer fluid for charging and extracting heat is Therminol-66.

By relatively simple modifications, the model and computer program can be applied to any phase change medium for which temperature-enthalpy data are available.

The computer-predicted performance has been correlated with experimental data obtained from tests on a TES unit and test bed which have a thermal storage capacity (input and output per cycle) of 0.3×10^6 kJ at a maximum input rate of 0.18×10^6 kJ/hr, and a maximum extraction rate of 0.10×10^6 kJ/hr, and contains 1800 kg of the TES medium.

Satisfactory agreement has been obtained between the computer predictions and the experimental data.

The program is now believed to be a reasonably reliable tool for predicting the effect on the operation of phase-change TES units of this type, of variations in the operating parameters, and variation in size and storage capacity.

The program has been used to predict the characteristics of a TES unit which has the following performance specifications:

> Heat storage capacity of 3.1×10^6 kJ, operating over the range of 516 K to 584 K. The heat transfer fluid for charging and discharging heat is Therminol-66. The maximum charge rate is 1.8×10^6 kJ/hr with the Therminol-66 temperature at 584 K ± 2 K. The maximum discharge rate is 1.0×10^6 kJ/hr with the Therminol-66 outlet temperature at 582 K ± 2 K and inlet temperature at 516 K ± 11 K.

The analysis showed that supplemental heat of about 10% of the heat extracted from storage, added to the Therminol-66 during discharge to help maintain the outlet temperature within the specified range, had a large beneficial effect on the size and cost of the storage system. Therefore, such supplemental ("deficit") heating was employed in the design of the system.

The characteristics of a TES unit employing the $NaOH-NaNO_3$ heat storing medium predicted by the analysis and computer program are as follows:

Preliminary Design

Vessel height and diameter	2.35 m (92.5")
Insulation thickness	0.609 m (24")
System height and diameter	3.6 m (142")
System weight	27290 kg (60,200 lb)
Amount of storage material	18000 kg (39,700 lb)
Unit cost	$33,700
Heat exchanger	.00635 m (1/4") tubing; 280 coils, each 27.73 m (91 ft) long
Figure of merit based upon a 25-element grid	.882
Storage output	3.01×10^6 kJ
Specific cost	$11.2/MJ
Insulation loss	3.25% of storage output
Deficit heating	10.2% of storage output

A P P E N D I X A

THE THERMOPHYSICAL PROPERTIES OF A THERMAL ENERGY STORAGE MATERIAL

Prepared for:

Comstock and Wescott, Inc.
765 Concord Avenue
Cambridge, Massachusetts 02138

Dynatech Report No.CAW-1

Work carried out under P.O. #23385

January, 1978

DYNATECH R/D COMPANY
A Division of Dynatech Corporation
99 Erie Street
Cambridge, Massachusetts 02139
Telephone: (617) 868-8050

TABLE OF CONTENTS

Report on

THE THERMOPHYSICAL PROPERTIES OF A THERMAL STORAGE MATERIAL

For: Comstock and Wescott, Inc.
765 Concord Avenue
Cambridge, Massachusetts 02139

Section 1

Introduction

The work described in this report was carried out at Dynatech R/D Company for Comstock and Wescott, Inc. under Contract No. 23385.

The purpose of this investigation was twofold. The first task was to experimentally determine the effect of accidental contact between Therminol-66, a heat transfer fluid, and Thermkeep, a potential thermal energy storage material over the approximate temperature range of 20 to 480C (70 to 900F). Once a compatible material was chosen, measurements of various properties using standard equipment and techniques available or developed especially for energy storage materials were utilized to generate baseline data on Thermkeep. The properties analyzed were differential thermal analysis, thermal conductivity in the solid and molten phases, density in the solid and molten phases, specific heat and heats of transformation, and viscosity. The temperature range of interest was 20 to 480C (70 to 900F).

Task 1

Section 2

PROPOSED PROGRAM FOR THE COMPATIBILITY OF THERMINOL-66 AND THERMKEEP

Dynatech proposed the following study for determining the compatibility of Therminol-66 (Monsanto Chemical Co.) with Thermkeep. Design and fabricate a special mild steel closed container vented to the outside, fabricated to contain the salt and Therminol-66. The Therminol-66 sample will be analyzed using a gas chromatograph prior to being heated in contact with the Thermkeep. The container will be heated at a fixed rate to one of three or four successive increasing temperatures up to the order of 300C. During the heating and at each temperature condition any vapors given off will be collected and analyzed. After the heating the salt sample will again be analyzed. Infra red spectra of the Therminol-66 will be obtained before and after heating with the Thermkeep. IR spectra of the condensed vapors will also be obtained. Following this the container will be heated once more to the next higher temperature and the procedure repeated.

Therminol-66 is stated to be a hydrogenated terphenyl with a boiling range of 340°C to 396°C. Thermkeep is stated by Comstock and Wescott to be largely anhydrous caustic soda (technical grade) containing variable amounts of sodium carbonate, 8% by weight of sodium nitrate, and 0.2% of Manganese dioxide. It is said to melt from 282°C to 292°C.

Section 3
EXPERIMENTAL PROCEDURE

A container was made from a 2-1/2" long nipple cut from standard 2-1/2" NPT iron pipe, threaded into a 2-1/2" NPT iron pipe cap with a 3" x 3" x 1/8" mild steel plate welded to the top of the nipple. A 3/8" - 3/4' reducing bushing was welded to the center of this plate and adapted from 3/8" NPT to 3/8" OD stainless steel tubing with Swagelock fittings. The resulting vessel is 4-3/4" high as measured from the top of the steel plate to the bottom of the 2-1/2" IPS pipe cap. The stainless steel tube passes into a 500 ml Erlenmeyer flask submerged in a trichloroethylene-dry ice mixture. The flask is vented through Tygon tubing into a jar of water so any rapid evolution of gases can be monitored. The apparatus was later modified by incorporating fittings for a second 3/8" OD stainless steel tube so the vessel can be flushed with inert gas during the run.

The vessel was placed on a 4-1/2" diameter resistance heater which was mounted on a heat sink. Temperature instrumentation was spot-welded on the container to monitor the temperature through the sample / container assembly. The entire assembly was surrounded by a cylindrical furnace with the interspace filled with expanded vermiculite to minimize temperature gradients.

Figures 1 and 2 are respectively pictures showing the vessel surrounded by the heaters and the modified vessel connected to two lengths of 3/8" OD stainless steel tubing in the oven with the upper heating element removed. The results of the compatibility tests are summarized in Table I.

The results indicate the following:

The chemical reaction between the Therminol-66 and Thermkeep at temperatures up to 320°C (close to the boiling point of the Therminol-66) are mild and produce no visible evolution of gases. Such reactions as do occur (darkening and thickening of the Therminol) should not have a detrimental effect of the Thermal Energy Storage (TES) system.

A-7

When a dry inert gas (helium) is circulated above the Thermkeep, it sweeps out any Therminol-66 present by the time the temperature of the Thermkeep has reached 326°C.

Section 4

FURTHER ANALYSIS OF THE THERMINOL-66 AND THERMINOL-66 RESIDUES

4.1 Gas Chromatography

After 9-1/4 hours a very sharp peak for Therminol-66 was obtained in the first run using our Gow Mac 69-750 Gas Chromatograph with a 6' long 1/8" stainless steel column packed with 3% OV-101 silicone oil on chromosorb W obtained from Applied Science Laboratories State College, PA. The column was heated to 290°C. We were unable to obtain a peak on subsequent runs and concluded that either the column had been inactivated by long exposure at 290°C or that the peak observed was due to "noise" of some kind.

A second column was obtained only 2' long packed with Tenax 6-C on 60/80 Chromosorb W. This column is claimed to be capable of prolonged heating up to 350°C. However, we obtained no Therminol peak during 14 hours operating at 300°C with maximum nitrogen flow. 300°C is the maximum temperature available with our Gow Mac 39-750 apparatus. We concluded that our gas chromotagraph is not capable of analyzing Therminol-66 for breakdown because of its low vapor pressure at 300°C.

4.2 Viscosity Changes

A qualitative assay of the viscosity of Therminol-66 and Therminol-66 from runs 21745 and 21746 summarized in Table I was made by putting a drop of each in three flat dishes, simultaneously tipping the dishes and observing the comparative rate of flow of the drops. From this, we estimate the viscosities to be as follows:

	cps
Therminol-66 as received	150*
Therminol-66 heated to 320°C in contact with Thermkeep	225
Therminol-66 heated to 320°C for 16 hours in contact with Thermkeep	300

* Monsanto data

4.3 IR Spectra

Figures 3, 4, 5, and 6 are respectively IR spectra of:

Figure	
3	Heptane
4	10% Therminol-66 in Heptane
5	10% Therminol-66 taken from Experiment 21745 (Table I) in Heptane
6	10% Therminol-66 taken from Experiment 21746 (Table I) in Heptane

All non heptane peaks observed in Figures 4, 5, and 6 are typical of aromatic hydrocarbons. There are no peaks indicating any take up of oxygen.

4.4 Conclusions from Analytical Data

The changes that take place in Therminol-66 when placed in contact with Thermkeep at 320°C in contact with air appear to be slow darkening and a slow increase in viscosity. Any oxidation of the Therminol is too low to show up in the IR spectra.

Section 5

CONCLUSIONS

We conclude from our study that accidental contact between Therminol-66 and Thermkeep in the TES will not result in a reaction which will be detrimental.

Section 6

RECOMMENDATIONS

Provide a means for sweeping the top of the Thermkeep with a dry inert gas. This will sweep out any water present in the Thermkeep and also any Therminol-66 which may accidentally leak into the Thermkeep in the TES unit. The end of the vent should be lower than the exit point and cool enough so that any Therminol-66 will condense and collect in a vessel positioned below the end of the vent.

Our experiment demonstrating the above was made with dry helium. Dry air or nitrogen should work equally well but if they are to be used tests should be made similar to the one using helium to confirm this assumption.

Table I

SUMMARY OF THERMINOL 66 - THERMKEEP COMPATIBILITY TESTS (1)

Run No.	Weight of Thermkeep g	Weight of Therminol g	Max. Temp. °C	Time at Max. Temp. Hours	Inert Gas Blanket	Volatiles in Trap	Comments
27142 (2)	100	10	275	>1	No	None	A sample of Therminol obtained from the vessel using a hypodermic needle after the run appeared similar to the original material except for a slight increase in viscosity.
21743 (2)	"	"	258	>1	No	None	No sample could be obtained. Thermkeep too solid to permit sampling fluid.
21744 (2)	"	"	310	>1	No	None	The Thermkeep had apparently melted and solidified.
21745 (2)	"	"	320	>1	No	None	After cooling the apparatus was disassembled. The Thermkeep had solidified with a semi-solid brown mush of Therminol and Thermkeep on the surface. There was a small amount of viscous liquid condensate in the lower end of the stainless steel tube. Samples were taken for further analysis and the vessel cleaned out by immersing in hot water.
21746	"	20	320	16	No	None	The vessel was cooled and examined as above. The results were similar except that the mush was darker brown in color. Samples were taken for further analysis.
27150	"	"	320	>1	Yes (3)	Yes (4)	After cooling the vessel was opened. The Thermkeep had solidified to a solid blue mass with no evidence of any Therminol remaining.

NOTES: (1) See text for description of apparatus used.

(2) The vessel was not opened after these runs.

(3) Modified apparatus used with a flow of helium passing over contents and through condenser and into water so flow rate could be monitored.

(4) The condensate was the color and viscosity of Therminol 66. There was a few drops of water suspended in the condensate.

Figure 1

Core of Heating Apparatus Showing Therminol 66-Thermkeep Compatibility Test Fixture in Place

Figure 2

Therminol 66-Thermkeep Compatibility Test Fixture Modified to Permit An Inert Gas Sweep. Lower Part of Heating Apparatus Shown Also.

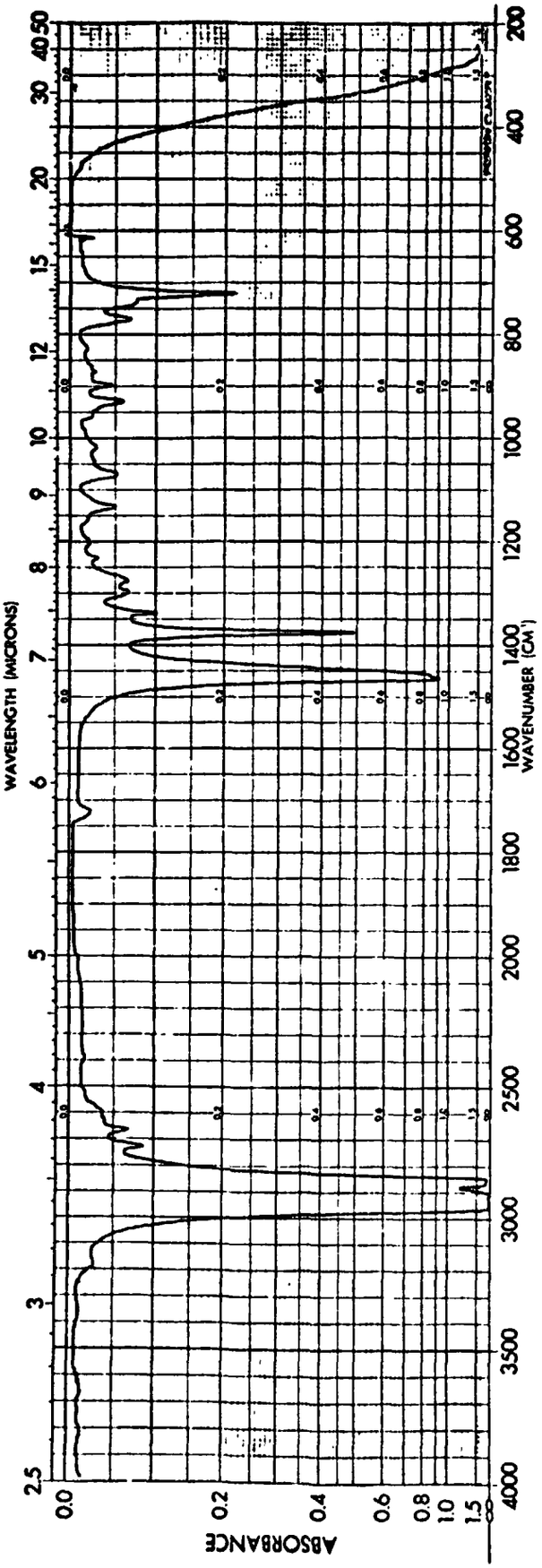

Figure 3 n Heptane Control

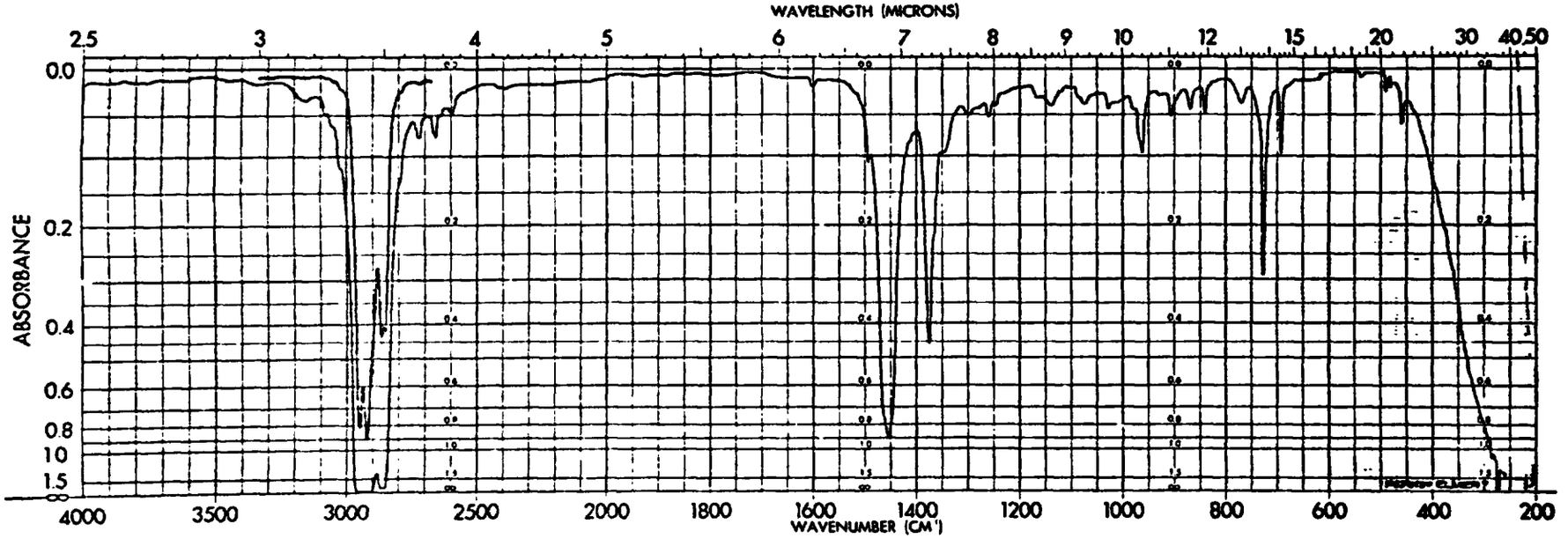

Figure 4 10% Therminol 66 in n-Heptane

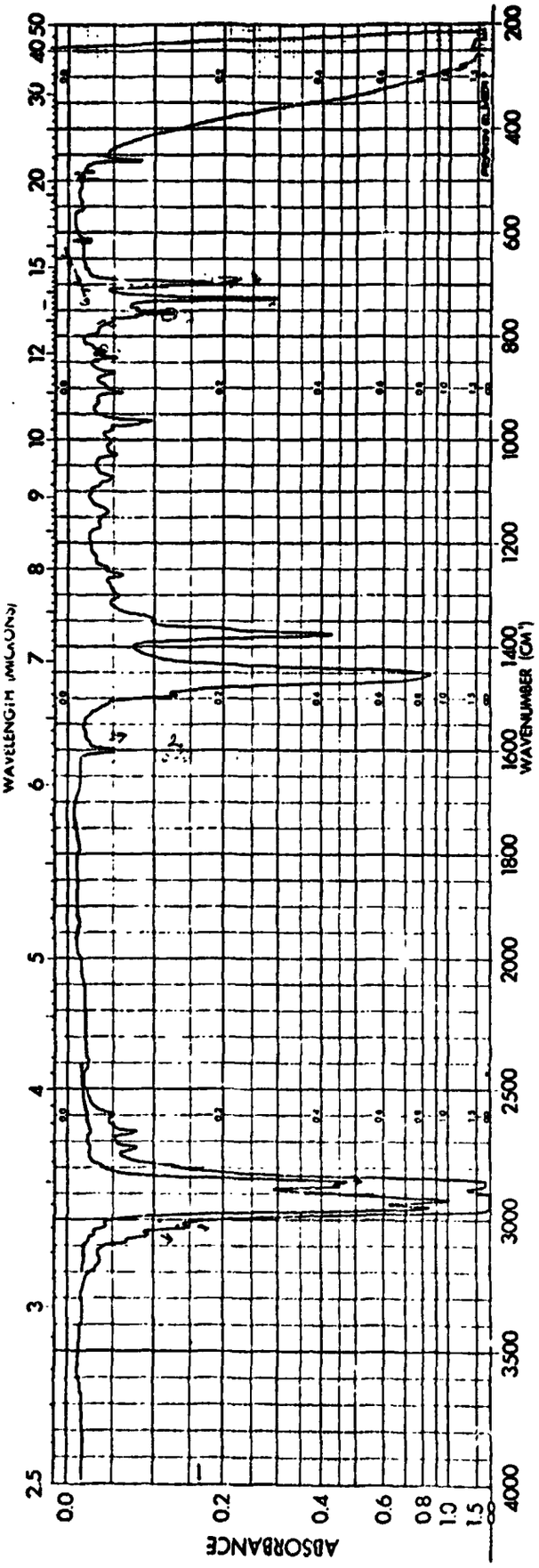

Figure 5 10% Therminol 66 in n-Heptane (Therminol 66 from run 21745 heated to 320°C)

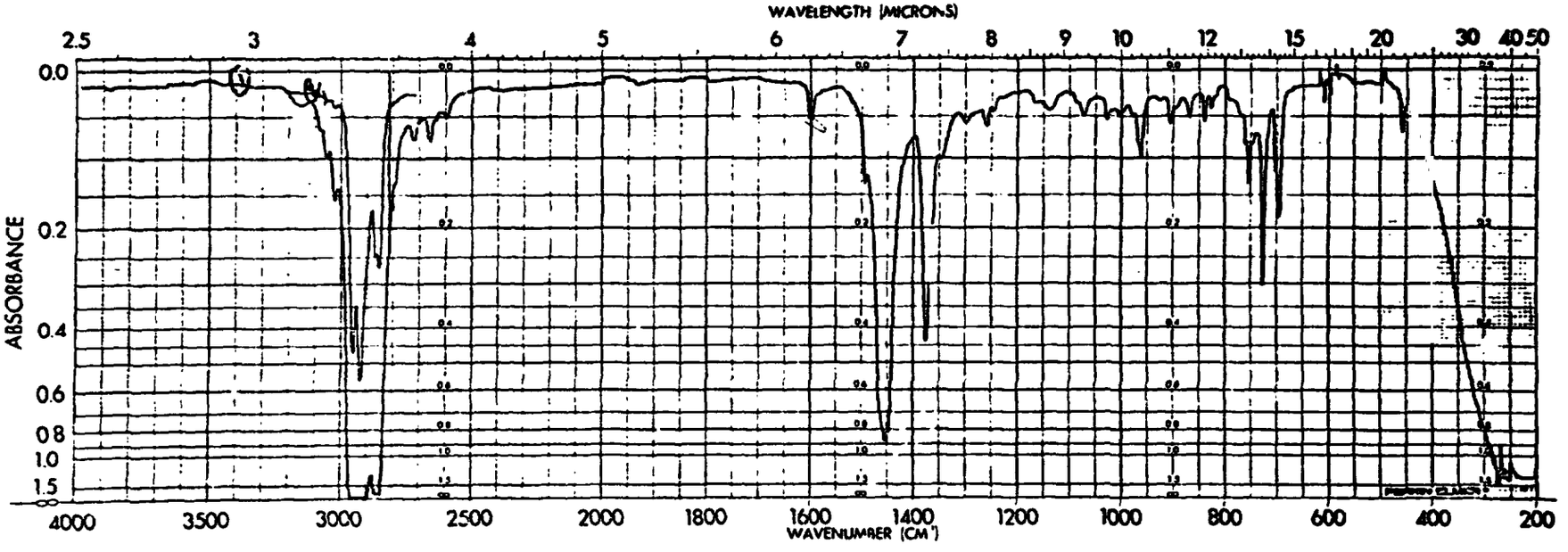

Figure 6 10% Therminol 66 in n-Heptane (Therminol 66 from run 21746 heated 16 hours at 320°C)

Task 2

Section 7

PROPOSED PROGRAM

Dynatech proposed the following techniques for the measurement of the required thermophysical properties:

a. The measurement of differential thermal analysis utilizing a Netzsch DTA with a Netzsch Temperature Programmer was undertaken on three replicate samples of the material with each sample being heated and cooled at an agreed heating and cooling rate.

b. The measurement of thermal conductivity in the solid and molten phases by the Comparative Flat Slab Technique as modified for the requirements of the material using a Dynatech Model TCFCM-N8 Thermal Conductivity Instrument.

c. The measurement of density and coefficient of thermal expansion in the solid phase by dilatometry utilizing a Netzsch Electronic Automatic Recording Dilatometer and the measurement of density in the molten phase by standard buoyancy techniques.

d. The measurement of specific heat and heats of transformation in the solid and molten phases using a Dynatech Model QTA-N7 Quantitative Adiabatic Calorimeter.

e. The measurement of viscosity utilizing a Brookfield Viscometer (with an extended spindle).

Section 8

EXPERIMENTAL PROCEDURES

8.1 Differential Thermal Analysis

A small amount of the crystalline material was placed in a specially shaped nickel DDK measuring cup centered around a protected thermocouple. A similar amount of powdered Kaolin as a reference material was similarly placed in a comparison measuring cup. The outputs of the two thermocouples were connected differentially. A separate temperature measurement protected thermocouple was placed centrally between the two cups. The cups were placed at the center of a resistance heated temperature enclosure which could be heated or cooled at constant temperature rates. After allowing the system to come to equilibrium it was heated automatically at a constant rate of 5C/min up to 230C (450F). The heating rate was then decreased to 0.1 C/min up to 350C (660F). The heating rate was then increased to 5C/min to 480C (900F). The system was then allowed to cool to 350C at 5C/min and to 230C at 0.1C/min.

The melting point and temperatures of transformation were determined from the intersection of lines drawn through the portions of the temperature time curve immediately below and above the peak.

The system had been pre-calibrated with standard reference materials $KClO_4$, SiO_2, and K_2CrO_4 obtained from National Bureau of Standards. The measured melting points were within $\pm$ 0.5C of the reference melting points.

8.2 Thermal Conductivity

8.2.1 Solid Phase

The basic method is shown schematically in Figure 7. For the measurements Pyroceram 9606, an inert ceramic glass, was chosen as the most suitable available reference material to cover all of the materials over the total temperature range. The thermal conductivity of Pyroceram 9606 is in the range 4 to 3 W/mK over the temperature range of interest and the salts were expected to be in a similar thermal conductivity range.

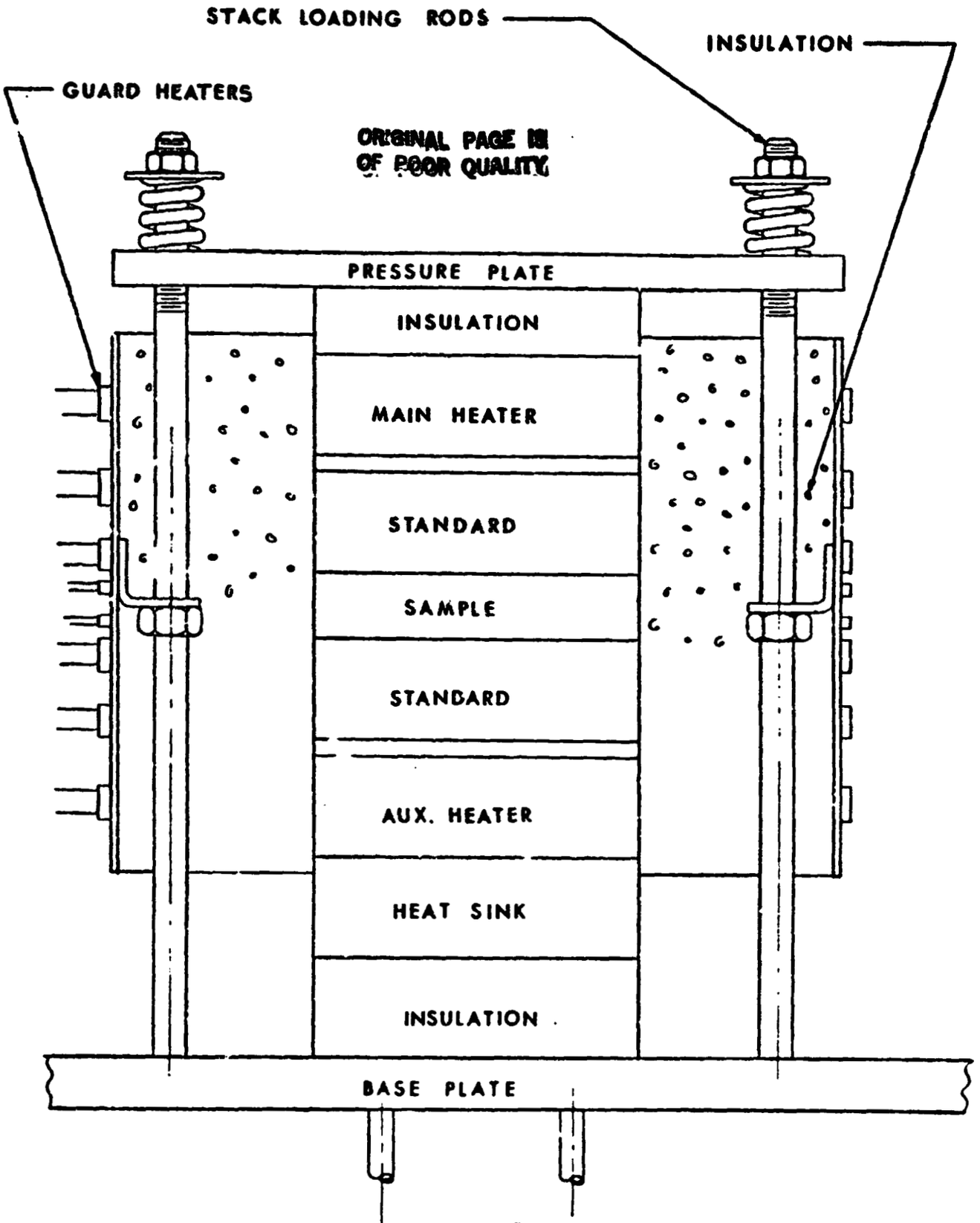

Figure 7

Comparative Method - Schematic Assembly

A- 1

For the purpose of test, fine gauge chromel/alumel thermocouples in a high nickel alloy protective sheath having overall dimensions of 0.25 mm were fitted tightly into the fine grooves cut across the surfaces of the sample. The instrumented sample was sandwiched between two similar instrumented samples of the reference material and of similar dimensions.

The composite sample was placed between two similar sized heater units and mounted on a fluid cooled heat sink under a uniform load applied at the top of the composite stack. A metal and ceramic heater guard tube some 75 mm diameter and 100 mm long which could be heated at various positions alongs its length and cooled at the bottom end was placed around the composite test stack such that the sample stack was positioned centrally with the guard tube. A further large metal fluid cooled shroud was placed around this stack and the interspaces around the sample and between the metal tubes filled with a thermal insulating powder which had been pre-dried under vacuum at elevated temperatures. A lid was fitted over the metal shroud and a large glass bell jar was placed around the whole assembly. The system was then evacuated and backfilled with pure dry argon.

A steady temperature equilibrium was established in the system by means of adjustment of the power to the heaters in the sample stack and the rate of flow of cooling water through the heat sink. The temperature gradient along the length of the guard tube was matched approximately to that on the composite test stack by automatic control of the heater along the length of the guard tube.

At equilibrium the temperatures in different sections of the stack were obtained from the various thermocouples in different locations in the system. The thermal conductivity was derived from a knowledge of the heat flow as determined from the mean value calculated in the top and bottom reference materials, the temperature difference across the sample and the known dimensions as follows:

$$\lambda = \frac{1}{2}\left(\frac{\Delta\chi}{\Delta T}\right)_{\text{sample}}\left[\left(\frac{k\lambda T}{\Delta\chi}\right)_{\text{top reference}} + \left(\frac{k\Delta T}{\Delta\chi}\right)_{\text{bottom reference}}\right]$$

where λ = thermal conductivity

$\Delta\chi$ = thickness

ΔT = temperature difference

k = thermal conductivities of the reference at respective mean temperatures

Measurements were made at regular temperature intervals up to as close to the melting point as could be obtained without any part of the test sample being at a temperature above the measured melting point. Following these measurements a repeat determination was made at a lower temperature to check whether the sample had changed during the heating or for possible contamination of the thermocouples.

8.2.2 Molten Phase

The method chosen was based on the comparative technique modified for the molten state. It is shown schematically in Figure 8.

Essentially the test sample is contained within a thin walled cavity in a larger piece of a reference material. The bottom solid section of the material acts as the lower portion of the comparative stack while an upper section of the same reference material fits tightly into the sample cavity to seal the test sample within the cavity. The upper reference material contained a vent hole to allow for expansion of the test sample on melting and subsequent increase in temperature. Sheathed protected fine gauge thermocouples were placed in the wall of the cavity, in the surfaces of the references touching the molten material, in holes along the length of the reference materials and in the sample itself. In all other respects the experimental techniques were the same as for the solid phase.

In deriving the thermal conductivity of the molten sample the same principle was used as that for the solid material. However allowances had to be made for the heat flow through the walls of the sample container. This was found to be in the order of 20 to 25% of the total heat flow measured in terms

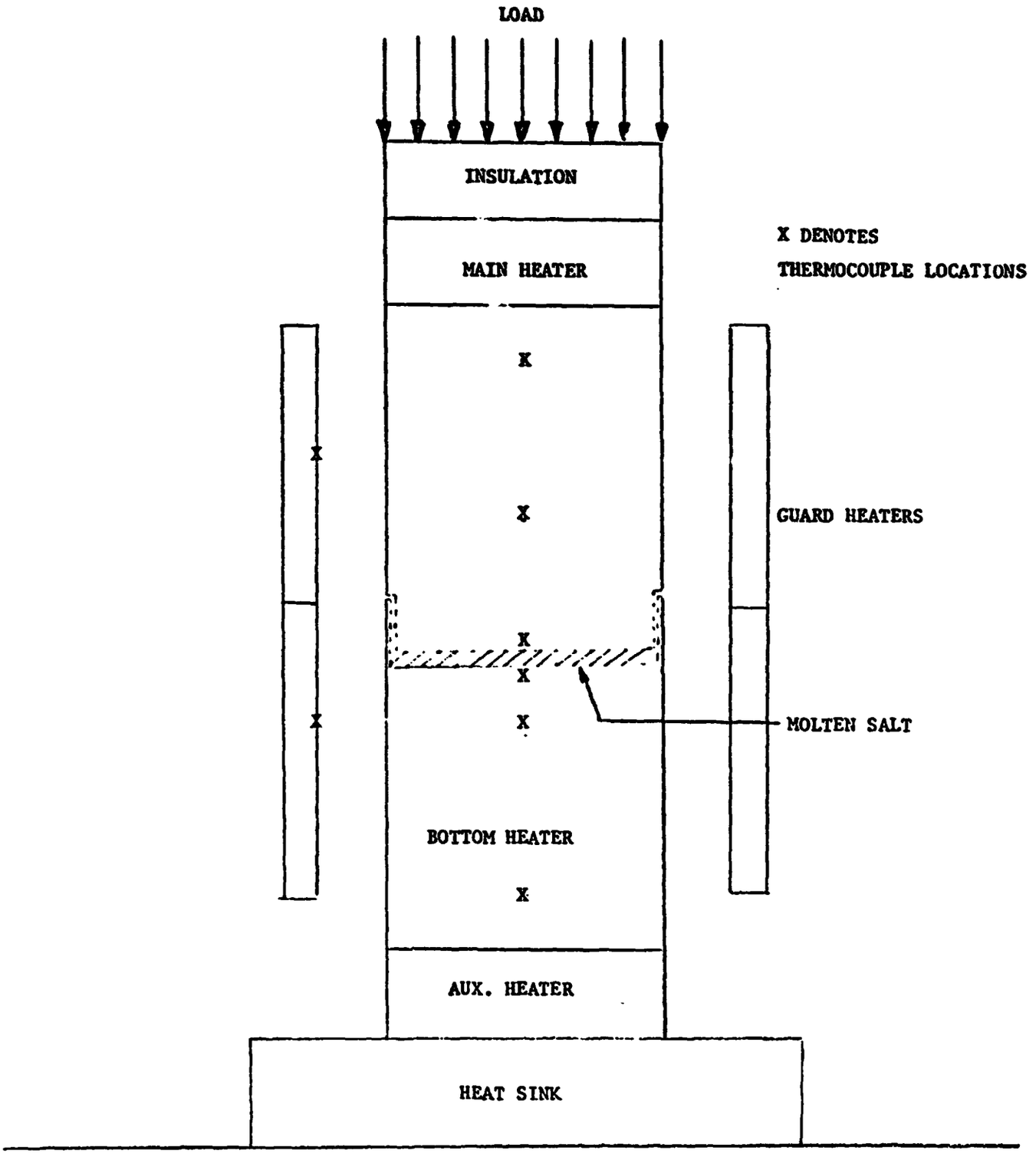

Figure 8

Molten Thermal Conductivity Test Stack Schematic Assembly

of that in the upper and lower reference materials.

The test cell was fabricated out of Inconel 600. The Inconel 600 has a much higher conductivity (10 to 20 $WM^{-1}K^{-1}$) than the salt, but this factor was compensated for by using a thin wall section and therefore decreasing the area ratio betwen the containment vessel and the specimen. The specimen was cast directly in the Inconel 600 container by melting the specimen externally and pouring it into the cavity.

8.3 Linear Expansion and Density

8.3.1 Solid Phase

For the measurement of linear expansion the initial length of a sample was measured accurately with a micrometer. The sample together with a temperature measurement thermoucouple was placed in a calibrated fused quartz push rod measuring system of a Netzsch Electronic Automatic Recording Dilatometer. The system was placed at the center of a resistance heater environmental chamber and allowed to equilibrate. Power was then supplied to the heater in a regular manner such that the sample temperature increased at a constant slow rate of 1 C / min up to as close to the melting point of the material as could be obtained before softening of the sample was noted. During the whole length of the experiment the continuous length and temperature changes of the sample were recorded.

The linear thermal expansion of the sample was obtained as follows:

$$\alpha = \frac{L}{Lo\ T}$$

where α = the coefficient of linear expansion

Lo = the initial length at 20C

L = the change in length for a particular temperature interval obtained from a curve of ΔL versus temperature, allowance being made for the length change of the quartz system calibrated previously

A-25

The volume coefficient was obtained as the sum of the three respective linear coefficients and the density calculated from knowledge of the volume coefficient and the mass of the specimen.

8.3.2 Molten Phase

The basic buoyancy method was used to determine this property. A solid cylindrical piece of nickel some 6 mm diameter and 18 mm long weighing approximately 40g at 20C was used as the suspended bob for the measurements. The expansion of a separate rod of the same nickel was measured in the Netzsch dilatometer in order to determine the change in volume of the metal bob at any particular temperature within the desired temperature range.

A sample of the material was melted into a large steel container which could be maintained at any desired temperature level. The nickel bob was suspended from the arm of a balance into the molten salt. Shields and insulation were placed around the wire and between the furnace and balance to minimize radiation, convection and updraft effects. The mass of the bob was evaluated once the system had attained equilibrium.

Measurements were made in this manner at successive increasing temperatures some 200C (360F) above the melting point.

The density of the salt was determined as follows;

$$\rho_s = \frac{\rho_{Ni}(m_{20} - m_T)}{m_{20}}$$

where ρ_s = density of salt

ρ_{Ni} = density of nickel bob at test temperature (T)

m_{20} = mass of nickel bob at 20C

m_T = mass of nickel bob at test temperature (T)

8.4 Viscosity

600 grams of Thermkeep were melted in the vessel described in Task 1 after modifying the vessel by opening up the center port and welding a 4" length of 1 inch IPS iron pipe in place. A slow stream of a dry nitrogen gas was used to blanket the salt while heating. The gas was turned off during the actual viscosity measurements.

The viscosity was measured using a LUT Brookfield Viscometer with a # 1 spindle at 60 RrM. Two spindle extensions were required to have enough length to permit the spindle to be immersed in the molten Thermkeep to the notch on the shaft and still have the instrument clear the top of the 1" pipe

The Brookfield Viscometer was calibrated using glycerine the viscosity of which was measured using a calibrated Cannonubbeholde Viscometer #400 A 35 at 35°C.

Section 9

TEST RESULTS

9.1 Differential Thermal Analysis

Table 2

The Differential Thermal Analysis of 3 "Thermkeep" Materials in Air

Test 1		Test 2		Test 3	
Heating 0.1 C min^{-1}	Cooling 0.05 C min^{-1}	Heating 0.1 C min^{-1}	Cooling 0.05 C min^{-1}	Heating 0.1 C min^{-1}	Cooling 0.05 C min^{-1}
Endotherm	Exotherm	Endotherm	Exotherm	Endotherm	Exotherm
260 C	277 C	276 C	280 C	277 C	280 C
500 F	531 F	529 F	536 F	531 F	536 F
Endotherm	Exotherm	Endotherm	Exotherm	Endotherm	Exotherm
306 C	----	290 C	223 C	287 C	228 C
583 F		554 F	432 F	549 F	442 F

9.2 Thermal Conductivity

9.2.1 Solid Phase

Table 3

The Thermal Conductivity of "Thermkeep" in the Solid Phase

Temperature		Thermal Conductivity, λ	
C	F	$Wm^{-1}K^{-1}$	Btu-in $hr^{-1}ft^{-2}F^{-1}$
50	122	1.30	9.0
150	302	1.10	7.6
250	482	1.08	7.5
150*	302	1.15	8.0

*on cooling

9.2.2 Molten Phase

Table 4

The Thermal Conductivity of "Thermkeep"
in the Molten Phase

Temperature		Thermal Conductivity, λ	
C	F	$Wm^{-1}K^{-1}$	Btu-in $hr^{-1}ft^{-2}F^{-1}$
350	662	0.90	6.2
400	752	0.92	6.4
450	842	0.935	6.5

9.3 Linear Thermal Expansion

Table 5

The Linear Thermal Expansion of "Thermkeep" in Three Mutually Perpendicular Directions

Specimen	Thermal Expansion, $(\Delta L/L_o) \times 10^4$ @					
	20	50	100	150	200	250 C
$\parallel$ to Laminations	0	6.0	19.2	37.0	60.0	90.0
$\perp$ to Laminations	0	8.5	25.2	45.5	69.5	98.8
$\parallel$ to Laminations	0	6.0	19.0	36.6	59.2	89.0

9.3.1 The Density of "Thermkeep" in the Solid and Molten Phases

Table 6

Temperature		Density (Test Specimen)		Density (Theoretical)	
C	F	kg m^{-3}	lbs ft^{-3}	kg m^{-3}	lbs ft^{-3}
20	68	1883	117.5	2140	133.5
50	122	1879	117.2	2136	133.3
100	212	1871	116.8	2127	132.7
150	302	1861	116.1	2115	132.0
200	392	1848	115.3	2100	131.0
250	482	1832	114.3	2082	129.9
300	572	1808	112.8	1808	112.8
350	662	1782	111.2	1782	111.2
400	752	1756	109.6	1756	109.6
450	842	1731	108.0	1731	108.0
500	932	1705	106.9	1705	106.4

$$\left(\frac{\rho_{solid}}{\rho_{molten}}\right)_{melting\ point} = 1.08$$

A-32

9.4 Viscosity

Table 8

The Viscosity of "Thermkeep"

Temperature		Viscosity, Centipoises
C	F	
328	622	7.9 ± 0.3
398	748	6.7 ± 0.3
480	896	5.2 ± 0.1

A P P E N D I X B

COMPUTER MODEL USED FOR REFERENCE DESIGN STUDY AND PRELIMINARY DESIGN

Main Program

The main program determines the fluid condition which is transferred to subroutine ELANAL, an element by element analysis of the heat transfer within the unit. The nature of the analysis is such that it assumes that the temperature within the unit stays constant over a very small time. The size of the time step is determined also in the main program.

The time step is computed as follows. w_f is the computed fluid flow rate at the time of the calculation. Then:

$$\Delta_t = \frac{z}{w_f}$$

where

$$z = 0.06 \frac{M_{TK}\ c_{TK}}{N_E\ \ c_f}$$

so that the time step is determined by the ratio of the thermal capacity of the Thermkeep in an element to the thermal capacity of the T-66 passing through it. The ratio M_{TK}/N_E is simply the Thermkeep mass per element.

c_{TK} varies throughout the unit as a function of temperature so that a c_{TK} is selected to be as small as will be experienced (liquid phase). Since the object is to compute a sufficiently small time step to satisfy the assumption of negligible temperature change in the Thermkeep, the time step will then be satisfactorily small for regions where c_{TK} is larger and larger time steps could be tolerated. The factor of 0.06 was selected so that in the worst case, the error in heat transfer by this assumption will be no more than 2%. Smaller time steps would reduce this error.

A table of solar collector output is read into this section of the program. It is based upon key times within the twenty-four hour day, plus other tabulated points to fully describe the shape of the output. The key times are determined in such a way that the beginning of the

cycle occurs at the beginning of discharge of the unit, T6, i.e., the time when the solar collector output has dropped to exactly the boiler demand (late afternoon). (See Fig. 1.)

From there to T1, the collectors and storage combine to produce the desired flow to the boiler. w_{min}, the desired flow rate to the boiler, is computed by

$$w_{min} = \frac{q_B}{c_f(T_H - T_L)} ,$$

where q_B is the heating rate required by the boiler.

The flow which can be provided by the collectors is:

$$w_{coll} = \frac{q_c}{c_f(T_H - T_L)} ,$$

where q_c is the heat output from the collectors, and the net flow from the storage unit during this period is:

$$w_f = w_{min} - w_{coll}$$

At T1, the collector output has dropped to zero, and all the flow required passes through the storage unit. Therefore, from T1 to T2:

$$w_f = w_{min}$$

At T2, the boiler demand goes to zero and a nighttime idle period (12 hours) occurs. At T3, the boiler demand begins again (early morning). From T2 to T3, the only calculations performed on the unit are those which are not flow related, i.e., loss to the environment and axial heat conduction.

From T3 to T4, the collectors produce no output and all the boiler flow originates in the storage unit. For this period, as from T1 to T2, $w_f \equiv w_{min}$. From T4 to T5, the collector output is less than the boiler demand and the flow, as between T0 and T1, comes from both storage and the collectors, the amount from storage again being determined by:

$$w_f = w_{min} - w_{coll}.$$

At T5, the collectors begin to put out excess heating over that demanded by the boiler. The excess heating is computed by:

$$q_{ex} = q_c - q_B$$

The flow to the storage unit during this period is calculated by:

$$w_f = \frac{q_{ex}}{c_f(T_H - T_o)}$$

and is limited to some predetermined maximum value.

A key, called K7, is recorded to be transferred to ELANAL which tells it what the flow condition is so that the calculation process is directed to the correct part of ELANAL. If K7 = 2, then the flow enters the top or hot end of the unit and charging is occurring. If K7 = 3, then the flow enters the bottom or cold end of the unit and discharging is occurring. If K7 = 1, the flow is zero and no flow related calculations occur in ELANAL. This applies to the overnight idle and the points in the cycle where the collector output exactly equals the boiler demand.

After determination of w_f, Δt and K7, the computation enters ELANAL and computes the internal heat transfer during the time step. Upon completing the computations in ELANAL, the calculation returns to the main program where it adds incremental [illegible] flows to the cumulative heat balances for the b[illegible] heating, heat absorbed, etc. Upon

completion of a daily cycle, the total cumulative heat balances are output, reset to zero, and the daily cycle begins anew with the state of the storage unit being as it was at the end of the previous cycle.

Other information is produced such as peak flow rate, peak ideal pump power, peak pressure drop, and total elapsed operating time. The computation tests the number of cycles against a preset number of daily cycles and either stops or begins analysis of a new design after the desired number of cycles has been completed.

The heat balances are computed for each time step and summed to produce cumulative heat balances over the daily cycle. Q_c, the daily total solar collector output, is dependent upon how the time increments are determined since q_c is calculated by linear interpolation of a table of q_c vs. time and is assumed constant over a time step. Thus,

$$Q_c = \sum_{i}^{\text{cycle}} q_c(t)_i \ \Delta t_i$$

Q_{abs}, the amount of heat absorbed by the TES unit for the cycle, is computed by summing the enthalpy changes of the T-66 during each time increment of the charging phase.

$$Q_{abs} = \sum_{i}^{\substack{\text{charge}\\ \text{cycle}}} w_{f,i} \ c_f(T_H - T_{o,i}) \ \Delta t_i$$

Q_{loss}, the amount of heat which is wasted, i.e., which is available from the solar collectors but not absorbable by the unit, due to reaching maximum pump flow, is the difference between these.

$$Q_{loss} = \sum_{i}^{\substack{\text{charge}\\ \text{cycle}}} \left[q_c(t)_i - w_{f,i} \ c_f(T_H - T_{o,i}) \ \Delta t_i \right]$$

Q_{del}, the amount of heat delivered by the storage unit over a cycle is also computed by summing the enthalpy changes of the T-66 during each time increment during the discharge phase:

$$Q_{del} = \sum_{i}^{\text{discharge cycle}} w_{t,i}\, c_f (T_{e,i} - T_L)\, \Delta t_i$$

Q_{burn}, the compensatory or boost heating to be applied to bring the T-66, which exits at T_e, up to T_H for delivery to the boiler is the sum of the incremental deficiencies in each time step during discharge:

$$Q_{burn} = \sum_{i}^{\text{discharge cycle}} w_{f,i}\, c_f (T_H - T_{e,i})\, \Delta t_i$$

Q_{env}, the total heat lost to the environment, is equal to the difference between Q_{abs} and Q_{del}, once steady state is established and no net change of state is experienced within the unit over a cycle:

$$Q_{env} = Q_{abs} - Q_{del} \text{ at steady state}$$

Subroutine ELANAL

This subroutine is called by the main program each time step and performs the heat transfer calculations between the T-66 and the Thermkeep. However, one section of it is utilized only once for each design, the first time into ELANAL, and bypassed thereafter. This section performs initialization of certain groups of values which are unchanged throughout the analysis, reads most of the input to the program (geometry, cost factors, fluid properties,

etc.), and computes the estimated unit cost. It indirectly sets up a table of Thermkeep properties by calling subroutine TKPROP which is used at this point to read in values and set up tables of element total enthalpies vs. temperature and solid fraction of Thermkeep vs. temperature. These tables are referred to when properties are sought within the rest of ELANAL.

Initialization Section

The following calculations are performed to determine the geometry of the unit from input values.

Displaced tube volume,

$$V_{tubes} = \frac{\pi}{4} L_T N_T d_o^2$$

where L_T is the tube length, N_T is the number of tubes, and d_o is the tube o.d.

Thermkeep volume,

$$V_{TK} = M_{TK}/\rho_{TK}$$

Total internal volume, tubes plus Thermkeep,

$$V_{Total} = V_{tubes} + V_{TK}.$$

An aspect ratio, the vessel internal height divided by the internal diameter is specified so that, from knowledge of the total volume, the height and diameter of the vessel may be computed,

$$d_{shell} = \sqrt[3]{\frac{\frac{4}{\pi} V_{total}}{R_{aspect}}}$$

$$h_{shell} = d_{shell} R_{aspect}$$

If the height of the vessel happens, by poor selection, to be less than the total tube length, L_T, then it is set exactly equal to L_T and the diameter is determined by the volume,

$$d_{shell} = 2\sqrt{\frac{V_{total}}{\pi L_T}}$$

The inner diameter of the shroud containing the insulation is determined from the insulation thickness, t_{ins}, and the vessel wall thickness, t_{shell},

$$d_{shroud} = d_{shell} + 2\, t_{ins} + 2\, t_{shell}.$$

The total shroud inner height is determined from the insulation thickness and the vessel and plate thicknesses, t_{end},

$$h_{shroud} = h_{shell} + 2\, t_{ins} + 2\, t_{end}.$$

The weights of the vessel, shroud, heat exchanger, and insulation are determined from the density of steel (heat exchanger, vessel, and shrouds), ρ_{steel}, the density of the insulation, ρ_{ins}, and the shroud thicknesses, $t_{shroud,bottom}$, $t_{shroud,\,top}$, and $t_{shroud,\,side}$,

$$W_{vessel} = \pi \rho_{st} \left(\frac{d_{shell}^2}{2}\, t_{end} + d_{shell}\, t_{shell}\, h_{shell} \right),$$

$$W_{heat\ exchanger} = \frac{\pi}{4} \rho_{steel} L_T N_T \left(d_o^2 - d_i^2 \right),$$

$$W_{ins} = \frac{\pi}{4} \rho_{ins} \left\{ \left(d^2_{shroud} - \left(d_{shell} + 2t_{end} \right)^2 \right) h_{shell} + 2d^2_{shroud}\, t_{ins} \right\},$$

$$W_{shroud} = \pi \rho_{steel} \left\{ d_{shroud}\, h_{shroud}\, t_{shroud,side} + \frac{d^2_{shroud}}{4} \left(t_{shroud,\,top} + t_{shroud,\,bottom} \right) \right\}.$$

The cost of the unit (without going into each equation used) is determined in two ways. Cost of materials is based upon the material weight and a cost per unit weight. Costs of fabrication are determined by a well accepted approximation known as the "six-tenths factor" rule. This says that, based upon some parameter, weight, volume, surface area, etc., the cost of a particular part will vary as the 0.6 power of the ratio of values of this parameter where the cost for one value is known:

$$C_{unknown} = C_{known} \left(\frac{P_{unknown}}{P_{known}} \right)^{0.6}$$

where C_{known} is the known cost for a unit of value, P_{known} for the parameter used, and $P_{unknown}$ is the value of that parameter for the unit to be estimated. For example, a heat exchanger of twice the surface area of another may increase only as $(2)^{0.6}$ or 1.5 in cost. In most cases, the calculation uses both weight and surface area as the

scaling parameters and averages the two values which were calculated.

In this section certain groups of numbers which contribute to heat transfer calculations and do not change each time increment are computed to save repetitious calculations.

The total capacitive effect of the storage unit is based upon the Thermkeep, the tubes, and the vessel. The insulation and the T-66 are ignored. Although the insulation may have a large capacitive effect, its thermal diffusivity is so low that during daily cycling, it should be unimportant.

The unit is divided into a number of numerical elements which are horizontal slices through the total unit. Each element, except for the first and last, have an equal weight distribution due to Thermkeep, tubes, and vessel sides. The weight of Thermkeep in each element, ΔM_{TK}, is the total weight divided by the number of numerical elements. The weight of steel in all but the end element, $\Delta M_{st,m}$, is the total tube weight plus the total vessel weight less the ends divided by the number of numerical elements. The weight of steel in the end elements, $\Delta M_{st,e}$, is $\Delta M_{st,m}$ plus the weight of an end plate for each.

During the course of the analysis, the calculation works with the total enthalpies or energies of each element where

$$E_m(T) = \Delta M_{TK} h_{TK}(T) + \Delta M_{st,m} c_{steel} T$$

$$E_e(T) = \Delta M_{TK} h_{TK}(T) + \Delta M_{st,e} c_{steel} T$$

These two tables of element enthalpies are established during the first pass through subroutine TKPROP when the enthalpy table for Thermkeep is read. In the initialization section of ELANAL, the starting temperature is known and the energies are computed. Thereafter, new energies are determined from element heat balances and TKPROP determines the updated temperature of the elements.

Heat Transfer Section

The unit is modeled as a vertical cylinder with the numerical elements being horizontal slices each assumed to be at uniform temperature. In this way, a step-wise temperature gradient is calculated which approaches a smooth curve as the number of elements increases. The computed temperature of each element is taken to be the midpoint temperature for purposes of axial conduction calculations and plotting of the output.

A heat balance is made around each element consisting of three components:

... the axial conduction from one element to the next consisting of conduction through the Thermkeep, through the tubes, and through the vessel wall;

... the conduction to the environment which is primarily conduction loss through the thermal insulation; and

... the heat transfer between the T-66 and the Thermkeep.

The last component is, of course, set equal to zero when no T-66 is flowing. The rates of heat flow by these modes are multiplied by the time step and summed, a net energy change per element is computed, and the new temperature is found from subroutine TKPROP.

The key, K7, selects which part of ELANAL is used for these computations, depending upon the direction of flow. The computations within each part are identical but the direction of movement through the numerical elements is reversed causing a reversal of the indexing, and a change in the defirition of which T-66 condition is specified and which is sought. Consequently, the computational method will be described only once with differences between the parts being specified where necessary.

The numerical elements are numbered from 1 to N_E, with 1 being at the cold or bottom end and N_E being at the hot or top end. Fluid temperatures are numbered from 1 to $N_E + 1$. One is the lower manifold temperature which is the inlet during discharge when it is fixed at T_L and

is the outlet during charging and has been called T_o. $1 + N_E$ is the upper manifold temperature which is the inlet during charging when it is fixed at T_H and in the outlet during discharge and has been called T_e. 2 through N_E are the T-66 temperatures between the elements. Thus, for each element, T-66 inlet and outlet temperatures are defined, the outlet temperature from one element being the inlet temperature to the next element in the flow direction.

T-66 thermophysical properties, viz., specific heat, viscosity, density, and thermal conductivity, are assumed constant and are taken to be the value at the nominal arithmetic mean temperature. The properties do vary with temperature but these variations are small over the temperature range of operation of the unit and accounting for this variation would add unnecessary complexity to the analysis.

The calculations on the T-66 side are as follows. The fluid Reynolds number is defined as

$$N_{RE} = w_f \frac{d_i}{A_{fl}\mu_f}$$

where the flow area is

$$A_{fl} = \frac{\pi}{4} d_i^2 N_T.$$

The T-66 side heat transfer coefficient is calculated as

$$h_f = 0.022 N_{RE}^{0.8} N_{PR}^{0.4} \frac{k_f}{d_i}$$

(Ref. 2)

Where N_{PR}, the Prandtl number is

$$N_{PR} = \frac{\mu_f c_f}{k_f}$$

In the laminar flow region, $N_{RE} < 2000$, the heat transfer coefficient is described by

$$h_f = 3.66 \frac{k_f}{d_i} *$$

The object is to compute an overall heat transfer resistance between the T-66 and the Thermkeep. One component of this is the resistance between the T-66 and the inside wall of the tube which is

$$R_f = \frac{1}{h_f A_i}$$

where the total inside surface area, A_i, of the tubes in a numerical element is

$$A_i = \pi d_i L_T \frac{N_T}{N_E}$$

The fluid side pressure drop through the heat exchanger is:

$$\Delta P = 0.102 f(N_{RE}) \frac{L_T}{d_i} \frac{\left(w_f/A_{fl}\right)^2}{2 \rho_f}$$

---

* In the final form of the analysis, this has been modified to account for the effect of helically coiled tubes. See pages 72 and 74 of this report.

where $f(N_{Re})$ is the friction factor and is a user supplied function of the Reynolds number, and the coefficient, 0.102, represents conversion factors to arrive at ΔP in units of kg/m^2. The ideal pumping power is

$$P_p = \frac{w_f \Delta P}{102 \rho_f}$$

in kilowatts. The peak values of ΔP and P_p are output at the end of each cycle. The total cyclic pump work is

$$W_p = \frac{1}{3600} \sum_{i}^{\text{cycle}} P_{p,i} \Delta t_i$$

in kilowatt hours.

All calculations are performed in the mks system of units which is essentially the SI designation. Mass is expressed in kilograms, length in meters, temperature in Kelvin degrees, time in seconds, energy in kilojoules, power in kilowatts, etc.

The other components of heat transfer resistance between the T-66 and the Thermkeep are the "lateral" resistance through the tube and the resistance between the tube outside surface and the Thermkeep. The tube has an "axial" component also which is associated with axial heat conduction. The "lateral" tube resistance is computed by the usual cylindrical conduction equation:

$$R_{T,\ell} = \frac{\ell n \frac{d_o}{d_i}}{2\pi k_{steel} \left(\frac{L_T}{N_E} \right) N_T}$$

The only resistance calculated on the Thermkeep side is the resistance of the solid layer built up on the tube surfaces. The amount of solid in a numerical element is taken to be a function of the temperature of the Thermkeep and is input to the program together with the temperature variation of the enthalpy in tabular form. From knowledge of the solid fraction, ϕ, the total solid layer size may be estimated. The volume of the solid layer around each tube in an element is

$$V_{solid} = \frac{\phi \ \Delta M_{TK}}{\rho_{TK} \ N_T} \quad ,$$

from which the diameter of the solid layer is determined,

$$d_{solid} = \sqrt{\frac{\frac{4}{\pi} V_{solid}}{\frac{L_T}{N_E}} + d_o^2}$$

The heat transfer resistance through this solid layer is also computed by the cylindrical conduction equation,

$$R_{solid} = \frac{\ell n \ \frac{d_{solid}}{d_o}}{2\pi k_{solid} \left(\frac{L_T}{N_E} \right) N_T}$$

The three resistances are summed to determine the total resistance between the T-66 and the Thermkeep:

$$R_{total} = R_f + R_{T,\ell} + R_{solid}$$

The number of transfer units, NTU, of the elemental heat exchanger is

$$NTU = \frac{1}{w_f \, c_f \, R_{total}}$$

where the T-66 side capacity is taken to be the minimum capacity. This is in agreement with the assumption that the temperature change of the storage medium is negligible over a time step. With this assumption and the assumption of uniform Thermkeep temperature within an element, the effectiveness of the heat transfer process, ε, is calculated by

$$\varepsilon = 1 - e^{-NTU}$$

For a fluid with constant specific heat, the effectiveness represents the degree of approach of the fluid temperature to the Thermkeep temperature. Where T_{in} is the temperature of the fluid into the element, T_{out} is the temperature out of the element, and T_E is the temperature of the storage material in the element,

$$T_{out} = T_{in} + \varepsilon(T_E - T_{in}).$$

The rate of heat transfer between the T-66 and the storage material in the element is

$$q_f = w_f c_f \, (T_{out} - T_{in}).$$

Excluding the end elements, the "lateral" insulation resistance to heat transfer is determined also by the cylindrical conduction equation,

C-3

$$R_{ins,\ell} = \frac{\ell n \left(\frac{d_{shroud}}{d_{shell}} \right)}{2\pi\, k_{ins} \left(\frac{h_{shell}}{N_E} \right)} \quad ,$$

and the rate of heat loss from an element at T_E through the insulation in the lateral direction to ambient temperature, T_{amb}, which is an approximation to the shroud surface temperature is

$$q_{ins,\ell} = \frac{T_{amb} - T_E}{R_{ins,\ell}}$$

The axial conduction term for all except the end elements, i.e., between the N_E storage temperatures of which there are $(N_E - 1)$ conduction calculations, consists of conduction through the heat exchanger tubes, the shell, and the Thermkeep. The resistances for each mode are computed separately and summed as parallel resistance paths. The tube axial conduction resistance is

$$R_{T,a} = \frac{\frac{L_T}{N_E}}{\frac{\pi}{4} k_{steel} (d_o^2 - d_i^2) N_T}$$

while the shell axial conduction term is

$$R_{shell} = \frac{\frac{h_{shell}}{N_E}}{\pi\, k_{steel}\, t_{shell}\, d_{shell}}$$

Both of these terms are the same for every conduction path and for all times and are not changed after being set initially.

The conduction through the Thermkeep is rather complex due to the geometry of the buildup of solid on the tubes. The conductivity in the solid is slightly higher than that in the liquid phase but not enough to warrant consideration of the above-mentioned geometry. Rather, an average resistance within an element is calculated assuming a net thermal conductivity which is the average of that in the solid and liquid weighted by the fraction of each,

$$\bar{k}_{TK} = \phi\, k_{solid} + (1 - \phi)\, k_{liquid},$$

and these conductivities are available as temperature dependent functions within the program.

The axial conduction resistance within a uniform element is calculated from the average cross-sectional area of the Thermkeep itself and the conduction length as:

$$R_{TK,a} = \frac{\frac{h_{shell}}{N_E}}{\frac{\pi}{4}\,\bar{k}_{TK}\left(d_{shell}^2 - N_T d_o^{\,2}\right)}$$

and is different for each element. Since the element temperature is considered to occur at the axial midpoint of each element for purposes of conduction, the actual conduction resistance through the Thermkeep between elements is the series sum of the half values of resistance of adjacent elements. Between element j and element j + 1, e.g.,

$$\bar{R}_{TK,a}(j,j+1) + \frac{R_{TK,a}(j) + R_{TK,a}(j+1)}{2}$$

The total axial conduction resistance between these elements would now be

$$R_{TOT,a}(j,j+1) = \frac{1}{\frac{1}{R_{shell}} + \frac{1}{R_{T,A}} + \frac{1}{\bar{R}_{TK,a}(j,j+1)}}$$

and the rate of heat flow in the axial direction is calculated by

$$q_{ax}(j,j+1) = \frac{T_E(j+1) - T_E(j)}{R_{TOT,a}(j,j+1)}$$

The total rate of heat flow associated with these elements is therefore

$$q_{TOT}(j) = -q_f(j) + q_{ins}(j) + q_{ax}(j,j+1) - q_{ax}(j-1,j)$$

For each of the end elements, one axial conduction term must be modified. Both of these elements are assumed to conduct in one direction to ambient through a series of two resistances. One is the half resistance of the element and the other is the net resistance between the end plate and the shroud which consists of contributions from the insulating material and the pipes and supports which penetrate the insulation. The other axial conduction term for the end elements is the normal conduction to the adjacent element.

The result of all of this is a net $q_{TOT}(j)$ for each of the N_E elements. The total heat flow associated with an element over a time step is the net energy change of the whole element and is

$$\Delta E(j) = q_{TOT}(j)\ \Delta t$$

These energy changes are applied to the total energies of each element to arrive at a new energy for each.

These values of energy are used, by calling subroutine TKPROP, to determine the updated temperature array, $T_E(j)$ and solid fraction array, $\phi(j)$, for the storage unit. This updated state then becomes the starting state for the next time step. The state of the storage unit is printed at key times as a table of Thermkeep temperature, solid fraction, and T-66 temperature for all the elements.

After solving for the new updated state of the storage unit and the exit temperature of the fluid, the calculation returns to the main program for determination of the new fluid condition to be delivered to the unit.

Secondary Subroutines and Functions

In addition to the two major sections of the computer analysis there are three functions and one subroutine which are auxiliary in nature. These are used in subroutine ELANAL for the purposes already described.

Subroutine TKPROP is a routine used to determine the updated temperature and fraction of solid in a numerical element after the energy change over a time step has been applied. During the initialization section of ELANAL, TKPROP is called for the purpose of reading in a table of Thermkeep enthalpy and solid fraction as a tabular function of temperature, setting up tables of total element energy for internal and end elements as a function of temperature, and determining the starting value of energy for each element from the starting temperature by linear interpolation between the table values. Thereafter, the subroutine is used in the reverse mode to determine, as mentioned above, the updated temperature and solid fraction in each element as a function of the updated element energy arrived at in the elemental heat balances in ELANAL. This also is done by linear interpolation within the tabulated values.

Function THCS is used to determine the thermal conductivity of solid phase Thermkeep from the element temperature. Function THCL is used to determine the thermal conductivity of liquid phase Thermkeep from the element temperature.

At the time of the preliminary reference design analysis the temperature dependence was not known and these values were assumed constant.

Function FF is used to determine the friction factor in the heat exchange tubing as a function of Reynolds number. It is a curve fit approximating the friction factors on the well-known Moody chart for an estimated relative roughness of 0.00012.

A P P E N D I X C

ORIGINAL COMPUTER ANALYSIS

Introduction

Prior to the start of the current project, a detailed computer analysis was formulated. This analysis is similar to the one generally used in the project. It does, however, attempt to account for additional effects not considered in the analysis described in the main text.

It was not used for a number of reasons:

... It is considerably more costly to use.

... It is less flexible.

... It would not as easily lend itself to the incorporation of empirical modification.

... It is based upon a published phase diagram for the binary system $NaOH-NaNO_3$ which may not be characteristic of Thermkeep.

Being made from commercial grade chemicals, Thermkeep contains impurities which probably alter its phase diagram.

This analysis does compute for each element during each time step an overall heat transfer coefficient accounting for the temperature dependence of all properties. It uses the phase diagram to include the effect of solubility of the two components in each other. It accounts for redistribution of mass as the density changes due to the solid-liquid phase change. The major purpose of this appendix is to describe the parts of this analysis which differ from the simplified version used in the report.

This analysis consists of a larger number of functions and subroutines for the purpose of describing the temperature dependence of fluid properties and Thermkeep properties, and the characteristics of the phase diagram, and of handling the different conditions of Thermkeep distribution which occur in the numerical elements. However, the basic program structure, method and order of calculations, etc., are the same in both analyses.

Description

The TES unit is assumed to be a vertical, cylindrical, insulated vessel containing Thermkeep into which is immersed a heat exchanger consisting of coiled parallel tubes manifolded at the top and bottom. The analytical approach is to divide the unit into a number of numerical elements which represent horizontal slices taken out of the cylinder. In the simplified analysis, density change is not considered. Consequently, elements contain both fixed mass and fixed volume. Here, the volume of each element is considered fixed but mass is allowed to redistribute itself.

Figure C1 describes the way the important part of the NaOH-$NaNO_3$ phase diagram was approximated. Thermkeep is roughly 8% sodium nitrate. It is assumed that the unit never operates at or above the melting point of pure sodium hydroxide. This can be changed but was not necessary for this project since NaOH melts at about 592 K (319 C) and the specified charging temperature is 584 K (311 C). Thus, the only process for liquefying NaOH is that of dissolving into the melt.

The first eutectic point for this system occurs at about 33% $NaNO_3$. Consequently, the concentration of $NaNO_3$ will never exceed this. Once enough NaOH precipitates out of solution, the eutectic behaves like a pure substance and freezes isothermally with no change in concentration.

The numerical elements within the unit are assumed to be at uniform, constant temperature during a time increment. This was also done in the simplified analysis. The condition of the liquid Thermkeep is determined by the equilibrium concentration at the element temperature and any excess NaOH precipitates out as a solid. Determination of the new equilibrium condition, however, requires an iterative procedure.

The cool-down process can be described in the following way. Assume one starts with every element in the liquid phase and occupying the full volume of the element. In fact, the size of the numerical elements is determined by the liquid phase volume. The net heat transfer by convection, axial conduction, and loss to the environment is computed generally as it is in the simplified program with an exception to be described later. The program generally works with element energies also as in the simplified program.

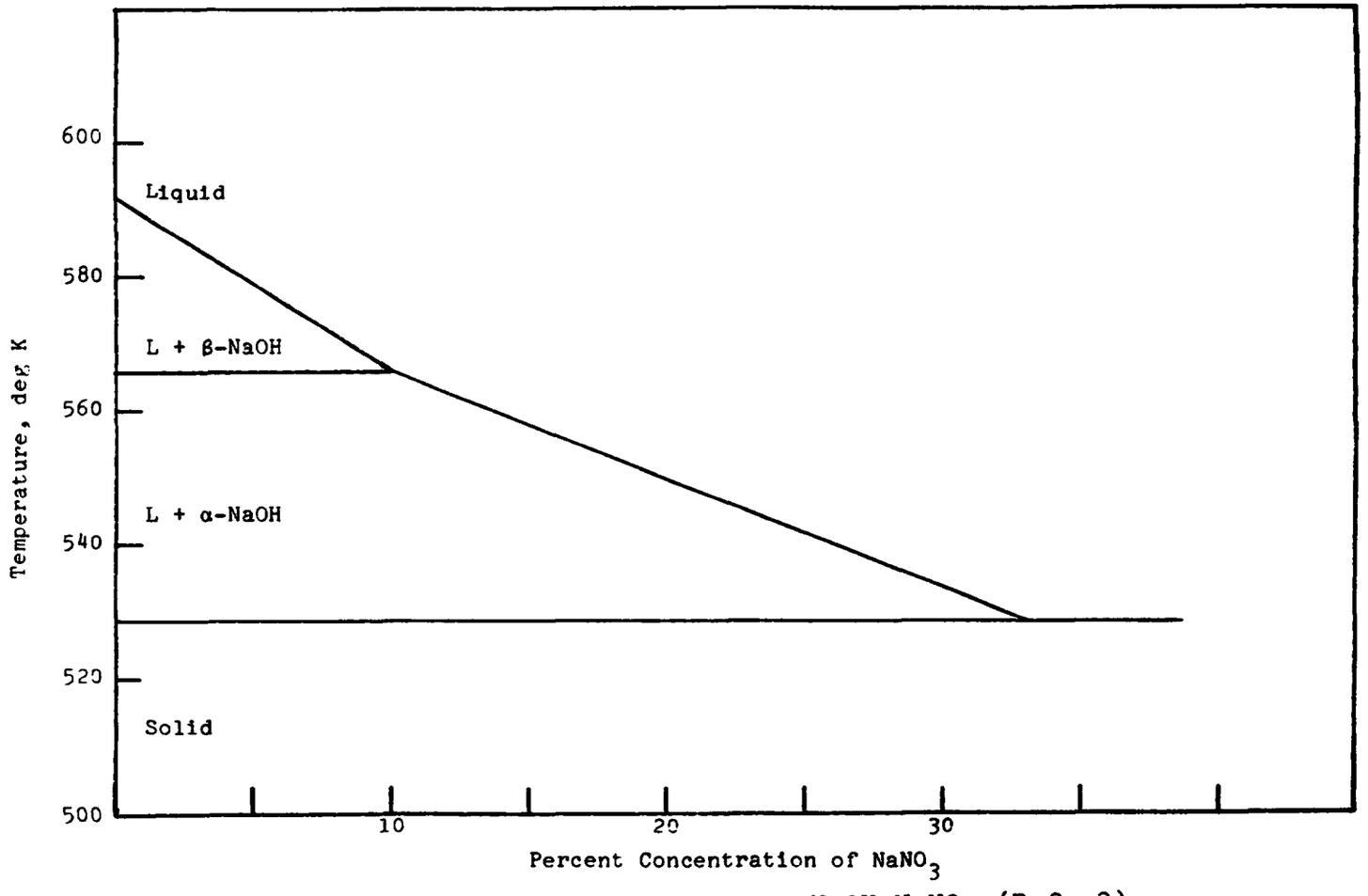

Figure 31. Assumed phase diagram $NaOH-NaNO_3$ (Ref. 3)

An energy loss is computed yielding a net energy at the end of a time step. The total mass of material in an element is not adjusted until the end of a time step. The program keeps track of the amount of mass of each component (NaOH, $NaNO_3$) in an element. The Liquidus line of the phase diagram defines the solubility of NaOH in the melt of NaOH-$NaNO_3$. However, the amount of solid NaOH is dependent upon the way mass has been transferred and the solid, of course, stays in its element since it is assumed to be frozen to a tube wall. The liquid phase is distributed to fill in any void space caused by solidification with consequent higher density.

Ignoring for the moment the way in which liquid is redistributed, the analysis takes the updated energy content, knows the amount of each component as well as the steel associated with the vessel wall and the heat exchanger and computes a new temperature. This temperature is one where the total of the energy associated with an equilibrium solution of melt plus the contributions from solid Thermkeep and steel agrees with the known element energy. Finding the proper temperature is an iterative process.

The Thermkeep changes state in the following way. Pure liquid exists down to the Liquidus line. No volume change occurs. Between the Liquidus and the α-β transition, β-NaOH precipitates out as a solid assumed to adhere to the cool tube walls. Again, putting redistribution of liquid aside for the moment, the cooling continues to precipitate solid β-NaOH until the α-β transition temperature is reached. At this point, the melt is about 10% $NaNO_3$ from which one can deduce the amount of solid β-NaOH in the element.

The energy extraction process at the α-β temperature (566 K; 293 C) is then attributed only to the latent heat associated with the transformation of the NaOH not in solution in the melt. Once all the solid β-NaOH has transformed to α-NaOH, the cooldown continues. The solid NaOH which precipitates out below 566 K (293 C) appears in the α phase. Thus from 566 K (293 C) down to 529 K (≈56 C) (the eutectic temperature), the analysis combines energy contributions from α-NaOH and an equilibrium melt to determine the updated temperature.

At 529 K (256 C), the Thermkeep begins as a melt of eutectic concentration, 33% $NaNO_3$, and a solid of α-NaOH. The eutectic melt then freezes as if it were of a pure material, i.e., isothermally, and no energy is removed from the α-NaOH or the steel. When all the latent heat associated with freezing the eutectic has been removed, the materials then cool sensibly with a layer of eutectic composition solid over the layer of α-NaOH frozen to the heat exchanger tubes.

During heating, the reverse process is assumed to occur: sensible heating of the eutectic plus the α-NaOH solid phases; melting of the eutectic at 529 K (256 C); heating of the solid α-NaOH and the melt with NaOH dissolving into the melt; transformation of the solid α-NaOH on the tube walls to solid β-NaOH at 566 K (293 C); further heating of the melt and the solid β-NaOH with the NaOH dissolving into the melt; and, finally, sensible heating of the liquid phase Thermkeep up to 584 K (311 C).

The volume change during cooling is treated by computing resultant void spaces in the constant volume elements and filling downward so that all the void space is transferred to above the liquid level. At the end of a time step a new fraction of liquid and solid results from the new energy content and consequent new equilibrium temperature. An array of volumes of liquid is composed for the elements as well as an array of the total volumes in each element not occupied by solid. The liquid is then used to fill the dead space in each element taking liquid from sequential upper elements as needed to completely fill lower elements until all the liquid is accounted for. The reverse procedure is used during heating where excess volume is generated by melting and must be transferred up to successive volume elements.

The relative amounts of each chemical component in elements of different temperatures are different and the actual amount of each being transferred is calculated to arrive at a new concentration of each in the melt at the end of a time step together with a new total energy contained in the element. In reality, this might imply a new equilibrium concentration after mixing but it was assumed that, since the time steps are quite short and since the transfer of material should be proportionally quite small, the resultant temperature of each numerical element is unchanged and the subsequent time step uses the temperature distribution as computed at the end of heat transfer for the previous time step. Thus, the available ΔT for heat transfer is infinitesimally

inaccurate, but the energy and material contents are accurately accounted for, so that in all respects the laws of thermodynamics of the process are obeyed.

In the write-up on the simplified program, it was explained that a criterion was used for computing the time step whereby the capacitances of the fluid and the storage medium were compared. The resultant time step would be small enough to justify the assumption of negligible temperature change in the storage medium and the use of the simplified relationship,

$$\varepsilon = 1 - e^{-NTU},$$

to characterize the heat transfer process. Where no loss of mass is experienced, the use of a minimum value of c_{TK} was considered a sufficient criterion.

In this analysis, it is possible to lose enough material in a particular element to cause this assumption to be inaccurate. When this is the case, the time step is still determined as before but for the elements at the upper end of the unit where insufficient mass may exist, calculations are performed which account for the changing element temperature during the heat transfer process. The calculation is separated into sections of the phase diagram to include the knowledge of temperature arrests, etc. The general formulation for variable temperature is as follows.

The temperature of adjacent elements ought to rise or fall similarly to the one in question. Moreover, the axial transfer is assumed to be small. Therefore, the axial heat flows are based upon starting temperatures and are assumed to be constant during a time step. A heat balance around the element in question says:

$$(\Sigma M_c) \frac{dT_E}{dt} = q_2 - q_1 - w_f c_f \varepsilon (T_E - T_{f,in}) - \frac{T_E - T_{amb}}{R_{ins}}$$

where q_2 and q_1 are the axial heat flows computed in advance, the next term is transfer to the fluid, and the last term is insulation loss. The calculation of ε may be unchanged as long as the time variation of T_E, the

element temperature, is considered. The solution to this first order differential equation is simply

$$T_E = \frac{\beta}{\alpha} + \left(T_{E,o} - \frac{\beta}{\alpha}\right) e^{-\frac{\Delta t}{\tau}}$$

where

$$\alpha = w_f c_f \tau + \frac{1}{R_{ins}}$$

$$\beta = q_2 - q_1 + \frac{T_{amb}}{R_{ins}} + w_f c_f \varepsilon \, T_{f,in}$$

$$\tau = \frac{\Sigma M_c}{\alpha}$$

and (ΣM_c) represents the total heat capacity of the storage materials in the element.

The computer analysis uses two subroutines for this process, one for heating and one for cooling, in order to properly move along the phase diagram. Comparing the value of $\frac{\beta}{\alpha}$ with $T_{E,o}$, the initial element temperature, determines which of these to use.

If use of this relationship over the whole time step, Δt, passes a transition temperature, such as α-β transition, then a reduced Δt is computed to get to the transition temperature and the element is assumed isothermal at the transition temperature. The computations proceed this way until the whole time step, Δt, is traversed. Some simplifications are made in the way the capacitance term is handled but in the end the thermodynamic balances are always preserved and no serious errors arise.

As one will now realize, the computations are considerably more involved than those in the simplified program which is why it is so costly to run and so hard to modify empirically. The following sections will try to describe each of the subroutines and functions used. At this

point, the program works reasonably well; but since it was never used in detail for design or test analysis, it is possible that there are areas requiring modification which would be discovered through extensive use.

Main Program

The main program is, in essence, identical to the main program of the simplified analysis already described. It does refer to a subroutine, COLL, to determine the solar collector characteristic but this is an unimportant difference.

It is, as before, in this section where the time step, the fluid flow rate, and direction are computed. The cyclic heat balances are performed. All the data are printed.

HTCALC

This subroutine performs all of the heat balances except for the case where the element temperature is assumed to change during the time step. In that case, basic heat transfer information is still computed here but the calculation is transferred to either VRTHS or VRTCS to determine the energy change in the element. In certain cases where sufficient material exists to justify it, the program uses a sequence of up to three calculations assuming constant temperature but with the time step divided and an updated temperature computed between each reduced time step.

The calculation method is essentially identical to that used in ELANAL in the simplified program. The difference is that the program keeps track of the masses and volumes of solid and liquid in each element and the masses and volumes of the chemical components, so that accurate accounting is made of the process of transfer of mass from one element to another.

At the end of the energy balances, regardless of which method was used to accomplish them, the analysis has arrays of variables describing the material content of the elements. These are listed below with both algebraic and computer notation:

$A_{\ell,i}$ = AL(I) = mass of liquid in element i(I)

$A_{s,i}$ = AS(I) = mass of solid in element i(I)

$A_{n\ell,i}$ = ANL(I) = mass of $NaNO_3$ (liquid) in element i(I)

$A_{ns,i}$ = ANS(I) = mass of $NaNO_3$ (solid) in element i(I)

$E_{\ell,i}$ = EL(I) = energy of liquid in element i(I)

These values together with knowledge of the liquid and solid densities (one value only is used for each, and the total fixed element volume can be used to compute the material transfer. The computations are as follows:

The volume of solid in element i is

$$V_{s,i} = A_{s,i}/\rho_s$$

the volume of liquid is

$$V_{\ell,i} = A_{\ell,i}/\rho_\ell$$

The volume available for liquid is the difference between the element volume, V_E, and the solid volume.

$$V_{v,i} = V_E - V_{s,i}$$

From this information is created a K-long array of available liquid volumes and associated enthalpy and $NaNO_3$ concentration

$$V_j = V_{\ell,i}$$

$$C_j = A_{n\ell,i}/A_{\ell,i}$$

$$h_j = E_{\ell,i}/A_{\ell,i}$$

where j = 1 is the first of the i array of elements with available void space, and the total available liquid volume is

$$V_{TOT,\ell} = \sum_{j=1}^{K} V_{\ell,j}.$$

The total available void space (not solid space) is

$$V_{TOT,V} = \sum V_{v,i}$$

and the volume remaining at the top of the unit which is empty becomes

$$V_{void,unit\ top} = V_{TOT,V} - V_{TOT,\ell}$$

The liquid is then redistributed in the following way. The values of void and liquid are compared sequentially. If the void is larger than the liquid, all the liquid is assigned to that void and the next liquid volume is examined, etc. until the value of liquid is larger than

the remaining void. Then the void is filled, the volume of liquid from which it was taken is reduced by that amount, and the next void is examined and compared with this next available liquid volume.

The arrays AL(I), EL(I), and ANL(I) are then reevaluated as the sums of the contributions from each of the amounts of liquid deposited into the particular element. In this way, all the mass, energy, and chemical components are accounted for. The calculation, on the assumption that the transfer of material is small, does not readjust the element temperature to allow for the new mixed temperature since it would involve new considerations of solution equilibrium, etc., and new fractions of liquid and solid, requiring a repetition of the above procedure. This did not seem necessary.

FULLEL

This subroutine is used to determine the updated states of the elements when the normal calculation of heat balances can be used in HTCAAC. It takes the newly computed energy of the element together with the total mass of material and the knowledge of the amount of $NaNO_3$ in the element and computes the new equilibrium temperature and relative amounts of solid and liquid phase.

The computation determines where the total energy of the element lies with reference to key identifiable points in the phase diagram. These points are: the Liquidus line temperature at the concentration of $NaNO_3$ which is input, the α-β transition temperature, with all β and all α points of the NaOH component; the eutectic temperature both all liquid and all solid eutectic component. Above the Liquidus line, between all α and all β-NaOH at the transition temperature, between the all liquid and all solid eutectic points, and below the eutectic temperature, the calculations are straightforward since they involve either pure sensible or pure latent heat effects.

Between the Liquidus temperature and the α-β transition temperature or between α-β transition temperature and the eutectic temperature, an iterative approach is used. This is a standard method known as "the method of regula falsi" and is described in mathematics textbooks (Ref. 5). The calculation begins by assuming a straight line between

reference points and iterates with successive straight line approximations until the error is small.

VRTCS, VRTHS

These two subroutines compute the element energy change when the amount of material in the capacitance of the element is small enough to require considerations of the variation in temperature during the time step. It assumes that only solid phase remains and consequently considers only pure sensible or pure latent heat transfer.

In the case where some liquid resides in the element, it will underestimate the heat transfer but it is assumed that the error is not significant. Energy and material balances are maintained at all times. It should be noted that at any time there would be only one element containing solid plus some liquid and it is only here, and only when the liquid is quite deficient in terms of filling the available space, when the error would occur.

VRTCS is used during cooling and VRTHS is used during heating. The method of calculation has already been described. As discussed, the variable temperature analysis is used when sensible heating occurs. When a crossover into a latent heat region occurs, the time step is divided and the calculation for variable temperature is used when needed. Two subroutines were written for control purposes to allow selection of moving either up or down in temperature in the phase diagram.

These routines compute the energy change in the material directly, and secondarily compute the energy change of the fluid to determine the nominal fluid temperature out of an element.

Most calculations are done in the reverse order where the fluid energy change is computed first and then assigned to the element.

COLL

This subroutine reads in the solar collector characteristic and is used to determine collector output in the main program. The simplified computer program does this directly in the main program.

RLCALC

This subroutine was to be used to describe an additional heat transfer resistance between the T-66 and the Therm-keep which is associated with the liquid phase transferring heat to the solid on the tubes. At present it is assumed to be zero and the subroutine is not used.

FF

This function is used to calculate the flowing T-66 friction factor as a function of Reynolds number. It is used for pressure drop calculations.

FLTEMP

The temperature variation of the specific heat of the T-66 is considered in this analysis. During HTCALC, the specific heat at inlet temperature to an element is used to compute the heat transfer. Subsequently, the computed enthalpy change of the T-66 is applied to the inlet enthalpy and a corrected outlet temperature is computed. This function computes the temperature of T-66 as a function of that enthalpy.

CPF, VISF, ENTHF

These functions compute the specific heat, viscosity, and enthalpy of the T-66 as a function of temperature.

CPA, HA, HB

These functions compute the specific heat of α-NaOH, the enthalpy of α-NaOH, and the enthalpy of β-NaOH as functions of temperature. The specific heat of β-NaOH is relatively constant so that the enthalpy is a linear function of temperature. The α-NaOH appears to have a temperature dependence but within the temperature range of interest here it is not significant, so that for now this has been assumed constant and the enthalpy is a linear function of temperature.

THCA, THCB, THCE

These functions compute the thermal conductivities of α-NaOH, β-NaOH, and eutectic solid phase as functions of temperature primarily for purposes of solid resistance to heat transfer between the T-66 and the liquid phase Thermkeep. At the present time these are assumed to be equal and constant.

CLIQ, TLIQ, HLIQ, CPT

The first two functions are the inverse of each other. CLIQ computes the concentration of $NaNO_3$ in the melt as a function of temperature along the Liquidus line. TLIQ computes the temperature of the melt as a function of concentration of $NaNO_3$ along the Liquidus line. The line is assumed to be strai- , at present, as shown on Figure B1, since the accurate locus was not required at this point.

Energies derived from the phase diagram are estimated based upon the appearance of the phase program and all compositions are assumed to have the same total enthalpy change distributed according to the phase diagram. HLIQ computes the enthalpy of the melt as a function of temperature for the Liquidus line. No solution effects are accounted for. Eventually, good h(T) data should be obtained for a range of concentrations so that a good map of h(T,C) could be produced.

CPT computes the specific heat of the liquid phase as a function of concentration of $NaNO_3$. This implies that no temperature dependence is expected. At this point the function does not provide even the concentration dependence since data are not available.

Conclusion

At the completion of the work on this computer analysis, Comstock & Wescott submitted an interim report, "Computer Program Development," dated December 7, 1976, to Sandia Laboratories (their P.O. No. 87-5030).

This report discusses the general program philosophy and the way by which data are fed into the program. Sample output was presented. Decks of computer cards were delivered for both the FORTRAN and the binary programs along with listings of the routines in both FORTRAN and machine language. Following this discussion are listings of the FORTRAN code for all the routines.

FORTRAN CODE


```
C          HEAT-OF-FUSION THERMAL STORAGE ANALYSIS
C
C     THIS PROGRAM ANALYZES THE DYNAMIC RESPONSE OF A TWO-COMPONENT,
C     HEAT-OF-FUSION, COUNTERFLOW HEAT STORAGE DEVICE
C     INPUT HEATING IS DETERMINED BY A SOLAR COLLECTOR CHARACTERISTIC
C     OUTPUT IS TO A CONSTANT DEMAND BOILER FOR A RANKINE CYCLE TURBINE
C
  100 FORMAT(3F10.5,F10.3,F10.2,F4.0,/F10.3,F10.7,I3,F10.3,3F10.6)
  101 FORMAT(4F10.4,I3,F10.4)
  102 FORMAT(F10.5,F10.7,2F10.3)
  103 FORMAT(7F10.3/3F10.5,F10.7)
  201 FORMAT(1H1,5X,' HEAT-OF-FUSION THERMAL STORAGE ANALYSIS',///)
  202 FORMAT(18X,' DATA',//)
  203 FORMAT(5X,' NO. PARALLEL TUBES              ',F10.0)
  204 FORMAT(5X,' TUBE I.D., M.                  ',F10.4)
  205 FORMAT(5X,' TUBE O.D., M.                  ',F10.4)
  206 FORMAT(5X,' TUBE LENGTH, M.                ',F10.2)
  207 FORMAT(5X,' TUBE MATL DENSITY, KG/CU.M.    ',F10.3)
  208 FORMAT(5X,' TUBE THERMAL K, KW/M.-K        ',F10.5)
  209 FORMAT(5X,' AMT STORAGE MATL, KG.          ',F10.2)
  210 FORMAT(5X,' VESSEL DIAMETER, M.            ',F10.3)
  211 FORMAT(//,5X,' NO. ELEMENTS                  ',F10.0)
  212 FORMAT(5X,' MAX. TIME INCR., SEC.          ',F10.2)
  213 FORMAT(5X,' BOILER INLET TEMP., K          ',F10.2)
  214 FORMAT(5X,' BOILER OUTLET TEMP., K         ',F10.2)
  215 FORMAT(5X,' MAX.PUMP FLOW, KG/SEC          ',F10.3)
  216 FORMAT(5X,' SOLAR COLLECTOR OUTPUT NO.     ',6X,I4)
  217 FORMAT(5X,' BOILER DEMAND, KW              ',F10.3)
  218 FORMAT(5X,' TOTAL WEIGHT, KG(APPROX)       ',F10.1)
  219 FORMAT(5X,' VESSEL HEIGHT, M.              ',F10.1)
  220 FORMAT(1H1, 9X,' ELAPSED TIME, HR            ',F10.2)
  221 FORMAT(10X,' CYCLE TIME, SEC           ',F10.1)
  222 FORMAT(10X,' LOST COLLECTOR HEAT, KJ   ',E10.4)
  223 FORMAT(10X,' COLLECTOR OUTPUT, KJ      ',E10.4)
  224 FORMAT(10X,' STORAGE OUTPUT, KJ        ',E10.4)
  225 FORMAT(10X,' STORAGE INPUT, KJ         ',E10.4)
  226 FORMAT(10X,' AUXILIARY INPUT, KJ       ',E10.4)
  227 FORMAT(10X,' BOILER REQUIREMENT, KJ    ',E10.4)
  228 FORMAT(///,'                                SYSTEM MAP',//)
  229 FORMAT(' (I)     TE(I)        TF(I)        VS(I)        VL(I)        AN
     1S(I)       ANL(I)    ',//)
  230 FORMAT(1X,I3,1X,F9.2,3X,F9.2,3X,F9.5,3X,F9.5,3X,F9.5,3X,F9.5)
  231 FORMAT(1X,I3,13X,F9.2)
  232 FORMAT(5X,' ESTIM. MATL COST, DOLLARS      ',F10.2)
  233 FORMAT(5X,' OVERALL HEIGHT, M.             ',F10.1)
  234 FORMAT(5X,' OVERALL DIAMETER, M.           ',F10.2)
  235 FORMAT(5X,' AMOUNT OF INSULATION, KG       ',F10.2)
  236 FORMAT(5X,' AMBIENT TEMPERATURE, K         ',F10.1)
  237 FORMAT(////,' VS,VL,ANS,AND ANL SHOULD BE MULTIPLIED BY THE NUMBER
     1 OF TUBES WHICH IS    ',F10.1)
  238 FORMAT(5X,' SHROUD THICKNESS, M.           ',F10.6)
  239 FORMAT(10X,' PEAK PUMP POWER, KW       ',E10.4)
  240 FORMAT(10X,' TOTAL PUMP WORK, KW-HR    ',E10.4)
  241 FORMAT(10X,' PEAK PRESS DROP, KGF/SM   ',E10.4)
  242 FORMAT(10X,' PEAK STORAGE FLOW, KG/S   ',F10.4)
  245 FORMAT(5X,' VESSEL WALL TH., M.            ',F10.6)
```

```
  246 FORMAT(5X,' VESSEL BASE TH., M.              ',F10.6)
  247 FORMAT(5X,' INSULATION THICKNESS, M.         ',F10.4)
  248 FORMAT(5X,' TH. COND. INSUL., KW/M-K         ',F10.5)
  250 FORMAT(5X,' LIQU. PHASE DENS, KG/CU.M.       ',F10.2)
  251 FORMAT(5X,' SOLID PHASE DENS, KG/CU.M.       ',F10.2)
  252 FORMAT(5X,' INSULATION DENS., KG/CU.M.       ',F10.2)
  253 FORMAT(5X,' H.T. FLUID DENS, KG/CU.M.        ',F10.2)
      COMMON TE(101),TF(101),VS(101),VL(101),ANS(101),ANL(101)
      COMMON/DATA/RHOL,RHOS,TTR,TEU,HWO,HEUT,HABT,CPEU,CPB,CW,TKL
      COMMON/VCON/RWAX,RINS,RINEN,TAMB,HIT
C     COMPUTE THE UNIT GEOMETRIC CONFIGURATION
      READ(5,100) DO,DI,DV,XLT,ASTOR,XN,RHOW,TKW,M,DTMAX,TWV,TBV,TSH
      READ(5,102) TINS,THCIN,RHOF,RHOI
      READ(5,103) RHOL,RHOS,TTR,TEU,HWO,HEUT,HABT,CPEU,CPB,CW,TKL
C     BASIC UNIT GEOMETRY AND FIXED HEAT FLOW RESISTANCES
      XM=M
      VSTOR=ASTOR/RHOL
      VTUB=0.7854*XN*XLT*DO**2
      HIT=(VSTOR+VTUB)/(0.7854*DV**2)
      XLTE=XLT/XN
      AIET=3.14159*DI*XLTE
      VEL=VSTOR/(XM*XN)
      AW=0.7854*(DO**2-DI**2)*XLTE*RHOW
      RW=ALOG(DO/DI)/(6.2832*TKW*XLTE)
      RVW=HIT*XN/(3.14159*DV*TWV*TKW*XM)
      RTUB=XLTE/(0.7854*(DO**2-DI**2)*TKW)
      RWAX=1./(1./RVW+1./RTUB)
      RINS=TINS*XM*XN/(3.14159*THCIN*DV*HIT)
      REND=TINS*XN/(0.7854*THCIN*DV**2)
      RPEN=TINS/(0.7854*TKW*(DO**2-DI**2))
      RINEN=1./(1./RINS+1./REND+1./RPEN)
      AFLT=0.7854*DI**2
      AVW=3.14159*RHOW*DV*TWV*HIT
      AVEL=AVW/(XN*XM)
      AW=AW+AVEL
      AVB=0.7854*RHOW*TBV*DV**2
      WB=AVB/XN
      HSH=HIT+2.*TINS
      DSH=DV+2.*TINS
      WINS=0.7854*RHOI*((DSH**2-DV**2)*HIT+2.*TINS*DSH**2)
      WSH=0.7854*RHOW*TSH*DSH*(4.*HSH+DSH)
      WTF=AFLT*XLT*XN*RHOF
      WEIT=AW*XN*XM+2.*AVB+ASTOR+WINS+WSH+WTF
      COST=1.1*(AW*XN*XM+2.*AVB+WSH)+0.44*ASTOR+0.22*WINS
      READ(5,101) TU,TL,WMAX,CLIQR,ND,TAMB
      HU=ENTHF(TU)
      HL=ENTHF(TL)
      DHMAX=HU-HL
C     COEFFICIENT FOR DETERMINATION OF TIME STEP
      Z=0.1*VEL*CLIQR*RHOL/CPF(TU)
      J1=99
      CALL COLL(CT,QC,T1,T2,T3,T4,QB,J1)
      WMIN=QB/DHMAX
      WRITE(6,201)
      WRITE(6,202)
      WRITE(6,209) ASTOR
      WRITE(6,203) XN
      WRITE(6,204) DI
```

```
      WRITE(6,205) DO
      WRITE(6,206) XLT
      WRITE(6,207) RHOW
      WRITE(6,252) RHOI
      WRITE(6,253) RHOF
      WRITE(6,250) RHOL
      WRITE(6,251) RHOS
      WRITE(6,245) TWV
      WRITE(6,246) TBV
      WRITE(6,208) TKW
      WRITE(6,238) TSH
      WRITE(6,248) THCIN
      WRITE(6,219) HIT
      WRITE(6,210) DV
      WRITE(6,247) TINS
      WRITE(6,233) HSH
      WRITE(6,234) DSH
      WRITE(6,235) WINS
      WRITE(6,218) WEIT
      WRITE(6,232) COST
      WRITE(6,211) XM
      WRITE(6,212) DTMAX
      WRITE(6,213) TU
      WRITE(6,214) TL
      WRITE(6,236) TANB
      WRITE(6,215) WMAX
      WRITE(6,216) J1
      WRITE(6,217) QB
      NC=0
      J5=1
      ET=0.
      CT=T4
      TF(1)=TL
      QBOIL=QB*T4
      GO TO 3
C     ENTER SUBROUTINE FOR INTERNAL HEAT TRANSFER ANALYSIS
   10 CALL HTCALC(WT,G,DTIME,K3,M,DI,RB,AIET,AB,DO,XLTE,VEL,J5,WB)
C     COMPUTATION OF PUMP REQUIREMENT FOR PUMP EFF=1.0
      TLM=(TF(M+1)-TF(1))/ALOG(TF(M+1)/TF(1))
      REA=G*DI/VISF(TLM)
      PD=0.102*FF(REA)*XLT*G**2/(2.*DI*RHOF)
      IF(PD.GT.PDMAX) PDMAX=PD
      POWER=W*PD/(102.*RHOF)
      IF(POWER.GT.PMAX) PMAX=POWER
      WPUMP=2.723E-6*PD*DTIME/RHOF+WPUMP
      IF(W.GT.WPEAK) WPEAK=W
      GO TO (50,51),K3
C     COMPUTATIONS ASSOCIATED WITH CHARGING PHASE
   50 QLOSS=QLOSS+(QC-QB-W*(HU-ENTHF(TF(1))))*DTIME
      QSOL=QSOL+QC*DTIME
      QCHG=QCHG+W*(HU-ENTHF(TF(1)))*DTIME
      GO TO 52
C     COMPUTATIONS ASSOCIATED WITH DISCHARGING PHASE
   51 QBURN=QBURN+W*(HU-ENTHF(TF(M+1)))*DTIME
      QDIS=QDIS+W*(ENTHF(TF(M+1))-HL)*DTIME
      QSOL=QSOL+QC*DTIME
   52 IF(CT.GE.T4) GO TO 2
   30 CALL COLL(CT,QC,T1,T2,T3,T4,QB)
```

```
      IF(CT.GE.T1) GO TO 6
C     INADEQUATE COLLECTOR OUTPUT AT END OF DAY. EVENING
      WCOLL=QC/DHMAX
      W=WMIN-WCOLL
      WT=W/XN
      G=WT/AFLT
      K3=2
      IF(CT.EQ.0.) GO TO 2
      DTIME=Z/WT
      IF(DTIME.LE.DTMAX) GO TO 11
      DTIME=DTMAX
   11 CT=CT+DTIME
      IF(CT.LE.T1) GO TO 12
      DTIME=DTIME-(CT-T1)
      CT=T1
   12 ET=ET+DTIME/3600.
      TF(1)=TL
      GO TO 10
    6 IF(CT.GE.T2) GO TO 7
C     NO HEATING AVAILABLE FROM COLLECTORS
      W=WMIN
      WT=W/XN
      G=WT/AFLT
      K3=2
      DTIME=Z/WT
      IF(DTIME.LE.DTMAX) GO TO 13
      DTIME=DTMAX
   13 CT=CT+DTIME
      IF(CT.LE.T2) GO TO 14
      DTIME=DTIME-(CT-T2)
      CT=T2
   14 ET=ET+DTIME/3600.
      TF(1)=TL
      GO TO 10
    7 IF(CT.GE.T3) GO TO 8
C     INADEQUATE COLLECTOR OUTPUT AT BEGINNING OF DAY. MORNING
      WCOLL=QC/DHMAX
      W=WMIN-WCOLL
      WT=W/XN
      G=WT/AFLT
      K3=2
      DTIME=Z/WT
      IF(DTIME.LE.DTMAX) GO TO 15
      DTIME=DTMAX
   15 CT=CT+DTIME
      IF(CT.LE.T3) GO TO 16
      DTIME=DTIME-(CT-T3)
      CT=T3
   16 ET=ET+DTIME/3600.
      TF(1)=TL
      GO TO 10
C     EXCESS SOLAR HEATING AVAILABLE FOR STORAGE
    8 QST=QC-QB
      W=QST/(HV-ENTHF(TF(1)))
      IF(CT.EQ.T3) GO TO 2
      WCOLL=W+WMIN
      IF(WCOLL.GT.WMAX) GO TO 20
      HIC=(W*ENTHF(TF(1))+WMIN*HL)/WCOLL
```

```
      TIC=FLTEMP(HIC)
      WT=W/XN
      G=WT/AFLT
      K3=1
      DTIME=Z/WT
      IF(DTIME.LE.DTMAX) GO TO 21
      DTIME=DTMAX
   21 CT=CT+DTIME
      IF(CT.LE.T4) GO TO 22
      DTIME=DTIME-(CT-T4)
      CT=T4
   22 ET=ET+DTIME/3600.
      TF(M+1)=TU
      GO TO 10
C     INSUFFICIENT PUMP FLOW CAPABILITY
   20 W=WMAX-WMIN
      WT=W/XN
      G=WT/AFLT
      K3=1
      DTIME=Z/WT
      IF(DTIME.LE.DTMAX) GO TO 26
      DTIME=DTMAX
   26 CT=CT+DTIME
      IF(CT.LE.T4) GO TO 27
      DTIME=DTIME-(CT-T4)
      CT=T4
   27 ET=ET+DTIME/3600.
      TF(M+1)=TU
      GO TO 10
C     OUTPUT DATA
    2 WRITE(6,220) ET
      WRITE(6,221) CT
      WRITE(6,222) QLOSS
      WRITE(6,223) QSOL
      WRITE(6,224) QDIS
      WRITE(6,225) QCHG
      WRITE(6,226) QBURN
      WRITE(6,227) QBOIL
      WRITE(6,242) WPEAK
      WRITE(6,241) PDMAX
      WRITE(6,239) PMAX
      WRITE(6,240) WPUMP
      WRITE(6,228)
      WRITE(6,229)
      DO 60 I=1,M
   60 WRITE(6,230) I,TE(I),TF(I),VS(I),VL(I),ANS(I),ANL(I)
      K7=M+1
      WRITE(6,231) K7,TF(K7)
      WRITE(6,237) XN
    3 DTIME=DTMAX
      ET=ET+DTMAX/3600.
      IF(CT.LT.T4) GO TO 61
C     BEGIN NEW DAILY CYCLE
      CT=0.
      QLOSS=0.
      QSOL=QB*DTIME
      QDIS=0.
      QCHG=0.
```

```
      QBURN=0.
      PDMAX=0.
      PMAX=0.
      WPUMP=0.
      WPEAK=0.
      NC=NC+1
61    CT=CT+DTMAX
      IF(NC.EQ.ND) GO TO 99
      GO TO 30
99    STOP
      END
```

```
      SUBROUTINE HTCALC(NT,G,DTIME,K3,M,DI,RW,AIET,WW,DO,XLTE,VEL,J5,WB)
C     THIS SUBROUTINE PERFORMS THE HEAT TRANSFER COMPUTATIONS ON THE
C     ELEMENTS AND THE REDISTRIBUTION OF LIQUID.
C
  500 FORMAT(2F12.5)
  501 FORMAT(//,5X,' INITIAL NITRATE CONCENTRATION ',F10.5)
  502 FORMAT(5X,' INITIAL STORAGE TEMPERATURE,K ',F10.3)
      DIMENSION RS(101),EELD(101),EL(101),AS(101),AL(101),VV(101),VE(101
     1),H(101),C(101),RAX(101),RAXS(101),QC(101)
      COMMON TE(101),TF(101),VS(101),VL(101),ANS(101),ANL(101)
      COMMON/DATA/RHOL,RHOS,TTR,TEU,HWO,HEUT,HABT,CPEU,CPB,CW,TKL
      COMMON/VALS/HBTR,HLTR,HWTR,HATR,HAEU,HLEU,HWEU,CTR,CEU,CAEU,TKATR,
     1TKBTR,TKAEU,TKEEU,CATR
      COMMON/VCON/RMAX,RINS,RINEN,TAMB,HIT
      IF(J5.EQ.99) GO TO 9
C     INITIAL AND CONSTANT VALUES
      CAEU=CPA(TEU)
      CATR=CPA(TTR)
      CTR=CLIQ(TTR)
      CEU=CLIQ(TEU)
      HBTR=HB(TTR)
      HLTR=HLIQ(TTR)
      HWTR=HWO+CW*TTR
      HATR=HA(TTR)
      HAEU=HA(TEU)
      HLEU=HLIQ(TEU)
      HWEU=HWO+CW*TEU
      TKATR=THCA(TTR)
      TKBTR=THCB(TTR)
      TKAEU=THCA(TEU)
      TKEEU=THCE(TEU)
      XM=M
      ADVL=VEL*(XM/HIT)**2
      K1=M
      VVL=0.
      READ(5,500) CO,TO
      J7=1
C     INITIAL CONDITION OF STORAGE UNIT
      DO 8 I=1,M
      TE(I)=TO
      AS(I)=0.
      AL(I)=VEL*RHOL
      AW=WB
      IF(I.EQ.1) AW=WW+WB
      IF(I.EQ.M) AW=WW+WB
      RS(I)=0.
      RAXS(I)=0.
      VL(I)=VEL
      VS(I)=0.
      EELD(I)=AW*(HWO+CW*TO)
      TL=TLIQ(CO)
      EL(I)=AL(I)*(HLIQ(TL)+CPT(CO)*(TO-TL))
      ANS(I)=0.
    8 ANL(I)=CO*AL(I)
      WRITE(6,501) CO
      WRITE(6,502) TO
```

ORIGINAL PAGE IS
OF POOR QUALITY

```
      JS=99
C     COMPUTE AXIAL CONDUCTION RESISTANCES AND HEAT FLOWS
    9 IF(K1.EQ.1) GO TO 32
      K8=K1-1
      DO 30 I=1,K8
      IF(RAXS(I).EQ.0.) GO TO 34
      RTK=VEL/(AOVL*(VL(I)*TKL+XLTE**2/RAXS(I)))
      GO TO 30
   34 RTK=1./(AOVL*TKL)
   30 RAX(I)=1./(1./RTK+1./RMAX)
   32 DO 31 I=K1,M
      IF(RAXS(I).EQ.0.) GO TO 35
      RAX(I)=1./(1./RMAX+1./RAXS(I))
      GO TO 31
   35 RAX(I)=RMAX
   31 CONTINUE
      VELL=VEL-VS(K1)
      RABOV=RAX(K1)*VVL/VELL
      IF(RAXS(K1).EQ.0.) GO TO 36
      RBELO=VEL/(AOVL*(VELL*TKL+XLTE**2/RAXS(K1)))
      GO TO 37
   36 RBELO=1./(AOVL*TKL)
   37 RBELO=(VELL-VVL)/(VELL*(1./RMAX+1./RBELO))
      RAX(K1)=RABOV+RBELO
      DO 33 I=2,M
   33 QC(I)=2.*(TE(I)-TE(I-1))/(RAX(I)+RAX(I-1))
      QC(1)=0.
      QC(M+1)=0.
      GO TO(1,101),K3
C     HEATING SECTION
    1 DO 10 I=1,M
      J=M-I+1
      AW=WW
      IF(J.EQ.1) AW=WW+WB
      IF(J.EQ.M) AW=WW+WB
      RAMB=RINS
      IF(J.EQ.1) RAMB=RINEN
      IF(J.EQ.M) RAMB=RINEN
C     FILM RESISTANCE, INSIDE TUBE
      TK=THCF(TF(J+1))
      CF=CPF(TF(J+1))
      VF=VISF(TF(J+1))
      REY=G*DI/VF
      IF(REY.LT.2000.) GO TO 2
      HI=0.022*(REY**0.8)*((VF*CF/TK)**0.3)*TK/DI
      GO TO 11
    2 HI=3.66*TK/DI
   11 RF=1./(HI*AIET)
      IF(J-K1) 21,22,23
C     FULL ELEMENT, ASSUMED ISOTHERMAL
   21 CALL RLCALC(RL)
      ROV=RW+RS(J)+RF+RL
      EFF=1.-EXP(-1./(ROV*WT*CF))
      TF(J)=TF(J+1)+EFF*(TE(J)-TF(J+1))
      DQF=WT*(ENTHF(TF(J))-ENTHF(TF(J+1)))*DTIME
      DQAMB=(TE(J)-TAMB)/RAMB
      ETOT=EL(J)+EELD(J)-DQF-(DQAMB+QC(J)-QC(J+1))*DTIME
      ATOT=AS(J)+AL(J)
```

```
      CALL FULLEL(ATOT,ETOT,DQ,AW,XLTE,AL(J),AS(J),RS(J),TE(J),EL(J),K3,
     1EELD(J),ANL(J),ANS(J),RAXS(J))
      GO TO 29
C     COMPLETELY SOLID. VARIABLE REFERENCE TEMPERATURE USED
   23 ROV=RW+RS(J)+RF
      EFF=1.-EXP(-1./(ROV*WT*CF))
      ALPH=WT*CF*EFF+1./RAMB
      BETA=QC(J+1)-QC(J)+TAMB/RAMB+WT*CF*EFF*TF(J+1)
      GAMMA=BETA/ALPH
      IF(GAMMA.GE.TE(J)) GO TO 45
      CALL VRTCS(TE(J),EELD(J),AS(J),AW,WT,CF,EFF,TF(J+1),XLTE,DTIME,ANS
     1(J),DQ,TF(J),RS(J),RAXS(J),QC(J),QC(J+1),RAMB,TAMB)
      GO TO 29
   45 CALL VRTMS(ANS(J),AS(J),TE(J),EELD(J),AW,TF(J+1),EFF,CF,WT,DQ,XLTE
     1,DTIME,ANL(J),AL(J),TF(J),EL(J),RS(J),RAXS(J),QC(J),QC(J+1),RAMB,T
     2AMB)
      GO TO 29
C     THE ELEMENT INCLUDING THE SURFACE, PARTIALLY FULL
   22 CALL RLCALC(RL)
      ROV=RW+RS(J)+RF+RL
      EFF=1.-EXP(-1./(ROV*WT*CF))
C     CHECK FILLING RATIO.  IF .GT. 0.25, USE REDUCED TIME INTERVALS
C     IF .LT. 0.25, NEGLECT LIQUID AND USE V.R.T.
      VRATIO=1.-VVL/VEL
      IF(VRATIO.LT.0.6) GO TO 70
      DTMOD=DTIME/2.
      NI=2
      GO TO 50
   70 IF(VRATIO.LT.0.333) GO TO 71
      DTMOD=DTIME/3.
      NI=3
      GO TO 50
   71 IF(VRATIO.LT.0.25) GO TO 72
      DTMOD=DTIME/4.
      NI=4
   50 DQFT=0.
      DO 55 ISUB=1,NI
      TFO=TF(J+1)+EFF*(TE(J)-TF(J+1))
      DQF=WT*(ENTHF(TFO)-ENTHF(TF(J+1)))*DTMOD
      DQFT=DQFT+DQF
      DQAMB=(TE(J)-TAMB)/RAMB
      ETOT=EL(J)+EELD(J)-DQF-(DQAMB+QC(J)-QC(J+1))*DTMOD
      ATOT=AS(J)+AL(J)
      CALL FULLEL(ATOT,ETOT,DQ,AW,XLTE,AL(J),AS(J),RS(J),TE(J),EL(J),K3,
     1EELD(J),ANL(J),ANS(J),RAXS(J))
   55 CONTINUE
      HFO=ENTHF(TF(J+1))+DQFT/(WT*DTIME)
      TF(J)=FLTEMP(HFO)
      GO TO 29
   72 ALPH=WT*CF*EFF+1./RAMB
      BETA=QC(J+1)-QC(J)+TAMB/RAMB+WT*CF*EFF*TF(J+1)
      GAMMA=BETA/ALPH
      IF(GAMMA.GE.TE(J)) GO TO 75
      CALL VRTCS(TE(J),EELD(J),AS(J),AW,WT,CF,EFF,TF(J+1),XLTE,DTIME,ANS
     1(J),DQ,TF(J),RS(J),RAXS(J),QC(J),QC(J+1),RAMB,TAMB)
      GO TO 29
   75 ELR=0.
      ALR=0.
```

```
      ANLR=0.
      CALL VRTHS(ANS(J),AS(J),TE(J),EELD(J),AW,TF(J+1),EFF,CF,WT,DO,XLTE
     1,DTIME,ANLR,ALR,TF(J),ELR,RS(J),RAXS(J),QC(J),QC(J+1),RAMB,TAMB)
      ANL(J)=ANL(J)+ANLR
      AL(J)=AL(J)+ALR
      EL(J)=EL(J)+ELR
   29 VS(J)=AS(J)/RHOS
      VL(J)=AL(J)/RHOL
      VV(J)=VEL-VS(J)
   10 CONTINUE
      GO TO 200
C     COOLING SECTION
  101 DO 110 I=1,M
      AW=WW
      IF(I.EQ.1) AW=WW+WB
      IF(I.EQ.M) AW=WW+WB
      RAMB=RINS
      IF(J.EQ.1) RAMB=RINEN
      IF(J.EQ.M) RAMB=RINEN
C     FILM RESISTANCE, INSIDE TUBE
      TK=THCF(TF(I))
      CF=CPF(TF(I))
      VF=VISF(TF(I))
      REY=G*DI/VF
      IF(REY.LT.2000) GO TO 102
      HI=0.022*(REY**0.8)*((VF*CF/TK)**0.3)*TK/DI
      GO TO 111
  102 HI=3.66*TK/DI
  111 RF=1./(HI*AIET)
      IF(I-K1) 121,122,123
C     FULL ELEMENT, ASSUMED ISOTHERMAL
  121 CALL RLCALC(RL)
      ROV=RW+RS(I)+RF+RL
      EFF=1.-EXP(-1./(ROV*WT*CF))
      TF(I+1)=TF(I)+EFF*(TE(I)-TF(I))
      DQF=WT*(ENTHF(TF(I+1))-ENTHF(TF(I)))*DTIME
      DQAMB=(TE(I)-TAMB)/RAMB
      ETOT=EL(I)+EELD(I)-DQF-(DQAMB+QC(I)-QC(I+1))*DTIME
      ATOT=AS(I)+AL(I)
      CALL FULLEL(ATOT,ETOT,DO,AW,XLTE,AL(I),AS(I),RS(I),TE(I),EL(I),K3,
     1EELD(I),ANL(I),ANS(I),RAXS(I))
      GO TO 129
C     COMPLETELY SOLID, VARIABLE REFERENCE TEMPERATURE USED
  123 ROV=RW+RS(I)+RF
      EFF=1.-EXP(-1./(ROV*WT*CF))
      ALPH=WT*CF*EFF+1./RAMB
      BETA=QC(I+1)-QC(I)+TAMB/RAMB+WT*CF*EFF*TF(I)
      GAMMA=BETA/ALPH
      IF(GAMMA.LE.TE(I)) GO TO 130
      CALL VRTHS(ANS(I),AS(I),TE(I),EELD(I),AW,TF(I),EFF,CF,WT,DO,XLTE,D
     1TIME,ANL(I),AL(I),TF(I+1),EL(I),RS(I),RAXS(I),QC(I),QC(I+1),RAMB,T
     2AMB)
      GO TO 129
  130 CALL VRTCS(TE(I),EELD(I),AS(I),AW,WT,CF,EFF,TF(I),XLTE,DTIME,ANS(I
     1),DO,TF(I+1),RS(I),RAXS(I),QC(I),QC(I+1),RAMB,TAMB)
      GO TO 129
C     THE ELEMENT INCLUDING THE SURFACE, PARTIALLY FULL
  122 CALL RLCALC(RL)
```

```
      ROV=RW+RS(I)+RF+RL
      EFF=1.-EXP(-1./(ROV*WT*CF))
C     CHECK FILLING RATIO.  IF .GT. 0.25, USE REDUCED TIME INTERVALS
C     IF .LT. 0.25, NEGLECT LIQUID AND USE V.R.T.
      VRATIO=1.-VVL/VEL
      IF(VRATIO.LT.0.5) GO TO 170
      DTMOD=DTIME/2.
      NI=2
      GO TO 150
  170 IF(VRATIO.LT.0.333) GO TO 171
      DTMOD=DTIME/3.
      NI=3
      GO TO 150
  171 IF(VRATIO.LT.0.25) GO TO 172
      DTMOD=DTIME/4.
      NI=4
  150 DQFT=0.
      DO 155 ISUB=1,NI
      TFO=TF(I)+EFF*(TE(I)-TF(I))
      DQF=WT*(ENTHF(TFO)-ENTHF(TF(I)))*DTMOD
      DQFT=DQFT+DQF
      DQAMB=(TE(I)-TAMB)/RAMB
      ETOT=EL(I)+EELD(I)-DQF-(DQAMB+QC(I)-QC(I+1))*DTMOD
      ATOT=AS(I)+AL(I)
      CALL FULLEL(ATOT,ETOT,DO,AW,XLTE,AL(I),AS(I),RS(I),TE(I),EL(I),K3,
     1EELD(I),ANL(I),ANS(I),RAXS(I))
  155 CONTINUE
      HFO=ENTHF(TF(I))+DQFT/(WT*DTIME)
      TF(I+1)=FLTEMP(HFO)
      GO TO 129
  172 ALPH=WT*CF*EFF+1./RAMB
      BETA=QC(I+1)-QC(I)+TAMB/RAMB+WT*CF*EFF*TF(I)
      GAMMA=BETA/ALPH
      IF(GAMMA.LE.TE(I)) GO TO 175
      ELR=0.
      ALR=0.
      ANLR=0.
      CALL VRTHS(ANS(I),AS(I),TE(I),EELD(I),AW,TF(I),EFF,CF,WT,DO,XLTE,D
     1TIME,ANLR,ALR,TF(J+1),ELR,RS(I),RAXS(I),QC(I),QC(I+1),RAMB,TAMB)
      ANL(I)=ANL(I)+ANLR
      AL(I)=AL(I)+ALR
      EL(I)=EL(I)+ELR
      GO TO 129
  175 CALL VRTCS(TE(I),EELD(I),AS(I),AW,WT,CF,EFF,TF(I),XLTE,DTIME,ANS(I
     1),DO,TF(I+1),RS(I),RAXS(I),QC(I),QC(I+1),RAMB,TAMB)
  129 VS(I)=AS(I)/RHOS
      VL(I)=AL(I)/RHOL
      VV(I)=VEL-VS(I)
  110 CONTINUE
C     LET LIQUID REDISTRIBUTE DUE TO GRAVITY ASSOCIATED WITH CHANGING
C     VOID SPACE AS SOLID MELTS OR LIQUID SOLIDIFIES
  200 VTOTL=0.
      J=1
      DO 210 I=1,M
      IF(VL(I).EQ.0.) GO TO 210
      VE(J)=VL(I)
      C(J)=ANL(I)/AL(I)
      H(J)=EL(I)/AL(I)
```

```
      VTOTL=VTOTL+VE(J)
      J=J+1
  210 CONTINUE
C     HAVE A  K-LONG ARRAY OF LIQUID VOLUMES AND ASSOCIATED C AND H
      K=J-1
      IF(K.EQ.0) GO TO 231
      VTOTV=0.
      DO 211 I=1,M
      VTOTV=VTOTV+VV(I)
      IF(VTOTV-VTOTL) 211,213,213
  213 K1=I
      VVL=VTOTV-VTOTL
      GO TO 214
  211 CONTINUE
C     HAVE A K1-LONG ARRAY OF VOIDS THAT IS JUST LARGER THAN LIQUID VOLUME
C     REDISTRIBUTE THE LIQUID TO FILL SUCCESSIVE VOIDS
  214 J=1
      DO 219 I=1,K1
      AL(I)=0.
      EL(I)=0.
      ANL(I)=0.
  218 IF(VV(I)-VE(J)) 216,216,217
  216 VE(J)=VE(J)-VV(I)
      AL(I)=AL(I)+VV(I)*RHOL
      EL(I)=EL(I)+VV(I)*RHOL*H(J)
      ANL(I)=ANL(I)+VV(I)*RHOL*C(J)
      L1=1
      GO TO 219
  217 AL(I)=AL(I)+VE(J)*RHOL
      EL(I)=EL(I)+VE(J)*RHOL*H(J)
      ANL(I)=ANL(I)+VE(J)*RHOL*C(J)
      VV(I)=VV(I)-VE(J)
      L1=2
      IF(J.EQ.K) GO TO 219
      J=J+1
      GO TO 218
  219 VL(I)=AL(I)/RHOL
  220 K5=K1+1
      IF(K5-M) 221,240,232
  221 DO 225 I=K5,M
      AL(I)=0.
      EL(I)=0.
      ANL(I)=0.
  225 VL(I)=0.
  232 CONTINUE
      RETURN
  231 K1=1
      K5=1
      VVL=VEL-VS(1)
      GO TO 221
  240 AL(K5)=0.
      EL(K5)=0.
      ANL(K5)=0.
      VL(K5)=0.
      VV(K5)=VEL-VS(K5)
      RETURN
      END
```

```
      SUBROUTINE FULLEL(ATOT,ETOT,DD,AW,XLTE,AL,AS,RS,T,EL,K3,EELD,ANL,A
     1NS,RAXS)
C     THIS SUBROUTINE COMPUTES THE FINAL CONDITION OF AN INITIALLY FULL
C     ELEMENT INCLUDING TOTAL MASS, MASS OF NITRATE, AND ENERGY LEVEL OF
C     BOTH THE LIQUID AND SOLID PHASE, AS WELL AS THE FINAL TEMPERATURE,
C     AND THE SOLID H.T. RESISTANCE
C
      COMMON/DATA/RHOL,RHOS,TTR,TEU,HWO,HEUT,HABT,CPEU,CPB,CW,TKL
      COMMON/VALS/HBTR,HLTR,HWTR,HATR,HAEU,HLEU,HWEU,CTR,CEU,CAEU,TKATR,
     1TKBTR,TKAEU,TKEEU,CATR
      C1=(ANL+ANS)/ATOT
      T1L=TLIQ(C1)
      ETEST1=ATOT*HLIQ(T1L)+AW*(HWO+CW*T1L)
      IF(ETOT.LT.ETEST1) GO TO 1
C     PURE LIQUID
      T=T1L+(ETOT-ETEST1)/(CW*AW+ATOT*CPT(C1))
      AS=0.
      RS=0.
      RAXS=0.
      ANL=ANL+ANS
      ANS=0.
      AL=ATOT
      EELD=AW*(HWO+CW*T)
      EL=ETOT-EELD
      RETURN
C     CHECK SOLID TRANSITION AT ALL BETA
    1 C2=CTR
      AL2=(ANL+ANS)/C2
      AS2=ATOT-AL2
      ETEST2=AS2*HBTR+AL2*HLTR+AW*HWTR
      IF(ETOT.LT.ETEST2) GO TO 2
C     REGULA FALSI BETWEEN LIQUIDUS AND TRANSITION
      E1=ETEST1-ETOT
      E2=ETEST2-ETOT
      C0=C2-E2*(C1-C2)/(E1-E2)
      T0=TLIQ(C0)
      AL0=(ANL+ANS)/C0
      AS0=ATOT-AL0
      ETEST0=AS0*HB(T0)+AL0*HLIQ(T0)+AW*(HWO+CW*T0)
      E0=ETEST0-ETOT
      IF(E0) 20,21,22
   21 T=T0
      AL=AL0
      AS=AS0
      ANL=ANL+ANS
      ANS=0
      EELD=AW*(HWO+CW*T)+AS*HB(T)
      EL=ETOT-EELD
      GO TO 25
   20 DO 26 J=1,3
      C0=C0-E0*(C1-C0)/(E1-E0)
      T0=TLIQ(C0)
      AL0=(ANL+ANS)/C0
      AS0=ATOT-AL0
      ETEST0=AS0*HB(T0)+AL0*HLIQ(T0)+AW*(HWO+CW*T0)
   26 E0=ETEST0-ETOT
```

```
      GO TO 21
   22 C1=C2
      E1=E2
      GO TO 20
C     SOLID RESISTANCE
   25 VS=AS/RHOS
      DS=SQRT(DO**2+1.2732*VS/XLTE)
      RS=ALOG(DS/DO)/(6.2832*THCB(T)*XLTE)
      RAXS=XLTE**2/(VS*THCB(T))
      RETURN
C     CHECK SOLID TRANSITION AT ALL ALPHA
    2 ETEST3=ETEST2-AS2*HABT
      IF(ETOT.LT.ETEST3) GO TO 3
      AB=(ETOT-ETEST3)/HABT
      AA=AS2-AB
      AS=AS2
      AL=AL2
      T=TTR
      ANL=ANL+ANS
      ANS=0
      EELD=AW*HWTR+AS*HATR+AB*HABT
      EL=ETOT-EELD
      GO TO(28,29),K3
C     SOLID RESISTANCE. COOLING AT TRANSITION
   29 VA=AA/RHOS
      DA=SQRT(DO**2+1.2732*VA/XLTE)
      RA=ALOG(DA/DO)/(6.2832*TKATR*XLTE)
      VB=AB/RHOS
      DS=SQRT(DA**2+1.2732*VB/XLTE)
      RS=ALOG(DS/DA)/(6.2832*TKBTR*XLTE)+RA
      RAXS=XLTE**2/(VA*TKATR+VB*TKBTR)
      RETURN
C     SOLID RESISTANCE. HEATING AT TRANSITION
   28 VB=AB/RHOS
      DB=SQRT(DO**2+1.2732*VB/XLTE)
      RB=ALOG(DB/DO)/(6.2832*TKBTR*XLTE)
      VA=AA/RHOS
      DS=SQRT(DB**2+1.2732*VA/XLTE)
      RS=ALOG(DS/DB)/(6.2832*TKATR*XLTE)+RB
      RAXS=XLTE**2/(VA*TKATR+VB*TKBTR)
      RETURN
C     CHECK LIQUID EUTECTIC
    3 C4=CEU
      AL4=(ANL+ANS)/C4
      AS4=ATOT-AL4
      ETEST4=AS4*HAEU+AL4*HLEU+AW*HWEU
      IF(ETOT.LT.ETEST4) GO TO 4
C     REGULA FALSI BETWEEN TRANSITION AND EUTECTIC
      E3=ETEST3-ETOT
      E4=ETEST4-ETOT
      CO=C4-E4*(C2-C4)/(E3-E4)
      TO=TLIQ(CO)
      ALO=(ANL+ANS)/CO
      ASO=ATOT-ALO
      ETESTO=ASO*HA(TO)+ALO*HLIQ(TO)+AW*(HWO+CW*TO)
      EO=ETESTO-ETOT
      IF(EO) 30,31,32
   31 T=TO
```

```
      AL=ALO
      AS=ASO
      ANL=ANL+ANS
      ANS=0
      EELD=AW*(HWO+CW*T)+AS*HA(T)
      EL=ETOT-EELD
      GO TO 36
   30 DO 36 J=1,3
      CO=CO-EO*(C2-CO)/(E3-EO)
      TO=TLIQ(CO)
      ALO=(ANL+ANS)/CO
      ASO=ATOT-ALO
      ETESTO=ASO*HA(TO)+ALO*HLIQ(TO)+AW*(HWO+CW*TO)
   36 EO=ETESTO-ETOT
      GO TO 31
   32 C2=C4
      E3=E4
      GO TO 30
C     SOLID RESISTANCE
   35 VS=AS/RHOS
      DS=SQRT(DO**2+1.2732*VS/XLTE)
      RS=ALOG(DS/DO)/(6.2832*THCA(T)*XLTE)
      RAXS=XLTE**2/(VS*THCA(T))
      RETURN
C     CHECK SOLID EUTECTIC
    4 ETEST5=ETEST4-AL4*HEUT
      IF(ETOT.LT.ETEST5) GO TO 5
C     TWO-PHASE EUTECTIC
      AL5=(ETOT-ETEST5)/HEUT
      T=TEU
      AS=ATOT-AL5
      AL=AL5
      EL=AL*HLEU
      EELD=ETOT-EL
      ANTOT=ANL+ANS
      ANL=C4*AL
      ANS=ANTOT-ANL
C     SOLID RESISTANCE
      VA=AS4/RHOS
      DA=SQRT(DO**2+1.2732*VA/XLTE)
      RA=ALOG(DA/DO)/(6.2832*TKAEU*XLTE)
      VE=(AL4-AL5)/RHOS
      DS=SQRT(DA**2+1.2732*VE/XLTE)
      RS=ALOG(DS/DA)/(6.2832*TKEEU*XLTE)+RA
      RAXS=XLTE**2/(VA*TKAEU+VE*TKEEU)
      RETURN
C     ALL SOLID BELOW TEU
    5 T=TEU-(ETEST5-ETOT)/(CW*AW+CAEU*AS4+AL4*CPEU)
      AL=0.
      AS=ATOT
      EELD=ETOT
      EL=0.
      ANS=ANL+ANS
      ANL=0.
C     SOLID RESISTANCE
      VA=AS4/RHOS
      DA=SQRT(DO**2+1.2732*VA/XLTE)
      RA=ALOG(DA/DO)/(6.2832*THCA(T)*XLTE)
```

```
VE=AL4/RHOS
DS=SQRT(DA**2+1.2732*VE/XLTE)
RS=ALOG(DS/DA)/(6.2832*THCE(T)*XLTE)+RA
RAXS=XLTE**2/(VA*THCA(T)+VE*THCE(T))
RETURN
END
```

```
      SUBROUTINE VRTCS(TE,EELD,AS,AW,WT,CF,EFF,TFI,XLTE,DTIME,ANS,DO,TFO
     1,RS,RAXS,Q1,Q2,RAMB,TAMB)
C     THIS SUBROUTINE USES VARIABLE REFERENCE TEMPERATURE TO DETERMINE
C     THE COOLING PROCESS IN A PURE SOLID ELEMENT
C
      COMMON/DATA/RHOL,RHOS,TTR,TEU,HWO,HEUT,HABT,CPEU,CPB,CW,TKL
      COMMON/VALS/HBTR,HLTR,HWTR,HATR,HAEU,HLEU,HWEU,CTR,CEU,CAEU,TKATR,
     1TKBTR,TKAEU,TKEEU,CATR
      A=WT*CF*EFF+1./RAMB
      B=Q2-Q1+TAMB/RAMB+WT*CF*EFF*TFI
      C=B/A
      IF(AS.EQ.0.) GO TO 10
      IF(TE-TTR) 1,2,3
C     SOLID ABOVE TRANSITION AT START, ALL BETA
    3 SMC=AS*CPB+AW*CW
      TAU=SMC/A
      TDT=C+(TE-C)*EXP(-DTIME/TAU)
      IF(TDT-TTR) 41,42,42
   10 SMC=AW*CW
      TAU=SMC/A
      TDT=C+(TE-C)*EXP(-DTIME/TAU)
      Q=AW*CW*(TE-TDT)
      RAXS=0.
      GO TO 43
   42 Q=AS*(HB(TE)-HB(TDT))+AW*CW*(TE-TDT)
   43 EELD=EELD-Q
      QF=WT*CF*EFF*(DTIME*(C-TFI)+TAU*(TE-C)*(1.-EXP(-DTIME/TAU)))
      TE=TDT
      HFO=ENTHF(TFI)+QF/(WT*DTIME)
      TFO=FLTEMP(HFO)
      RETURN
   41 DTIM1=TAU*ALOG((TE-C)/(TTR-C))
      QF=WT*CF*EFF*(DTIM1*(C-TFI)+TAU*(TE-C)*(1.-EXP(-DTIM1/TAU)))
      DTIM2=DTIME-DTIM1
      TFOT=TFI+EFF*(TTR-TFI)
      Q=(WT*CF*(TFOT-TFI)+Q1-Q2+(TTR-TAMB)/RAMB)*DTIM2
      DQL=AS*HABT
      IF(Q-DQL) 52,52,53
   52 QTOT=AS*(HB(TE)-HBTR)+AW*CW*(TE-TTR)+Q
      EELD=EELD-QTOT
      QF=WT*CF*(TFOT-TFI)*DTIM2+QF
      TE=TTR
      HFO=ENTHF(TFI)+QF/(WT*DTIME)
      TFO=FLTEMP(HFO)
      AA=Q/HABT
      AB=AS-AA
      VA=AA/RHOS
      DA=SQRT(DO**2+1.2732*VA/XLTE)
      RA=ALOG(DA/DO)/(6.2832*TKATR*XLTE)
      VB=AB/RHOS
      DS=SQRT(DA**2+1.2732*VB/XLTE)
      RS=ALOG(DS/DA)/(6.2832*TKBTR*XLTE)+RA
      RAXS=XLTE**2/(VA*TKATR+VB*TKBTR)
      RETURN
   53 DTIM3=AS*HABT/(WT*CF*(TFOT-TFI)+Q1-Q2+(TTR-TAMB)/RAMB)
      DTIM4=DTIM2-DTIM3
```

```
      QF=WT*CF*(TFOT-TFI)*DTIM3+QF
      SMC=AS*CATR+AW*CW
      TAU=SMC/A
      TDT=C+(TTR-C)*EXP(-DTIM4/TAU)
      Q=AS*(HB(TE)-HA(TDT))+AW*CW*(TE-TDT)
      EELD=EELD-Q
      QF=WT*CF*EFF*(DTIM4*(C-TFI)+TAU*(TTR-C)*(1.-EXP(-DTIM4/TAU)))+QF
      FACT=THCB(TE)/THCA(TDT)
      RS=RS*FACT
      RAXS=RAXS*FACT
      TE=TDT
      HFO=ENTHF(TFI)+QF/(WT*DTIME)
      TFO=FLTEMP(HFO)
      RETURN
C     SOLID AT TRANSITION AT START. ALPHA + BETA
    2 TFOT=TFI+EFF*(TE-TFI)
      Q=(WT*CF*(TFOT-TFI)+Q1-Q2+(TTR-TAMB)/RAMB)*DTIME
      Q=WT*CF*(TFOT-TFI)*DTIME
      DEA=ETOT-AW*HBTR-AS*HATR
      IF(Q-DEA) 54,54,55
   54 TFO=TFOT
      EELD=EELD-Q
      TE=TTR
      RETURN
   55 DTIM1=DEA/(WT*CF*(TFOT-TFI)+Q1-Q2+(TTR-TAMB)/RAMB)
      QF=WT*CF*(TFOT-TFI)*DTIM1
      DTIM2=DTIME-DTIM1
      SMC=AS*CATR+AW*CW
      TAU=SMC/A
      TDT=C+(TTR-C)*EXP(-DTIM2/TAU)
      Q=AS*(HATR-HA(TDT))+AW*CW*(TTR-TDT)+DEA
      EELD=EELD-Q
      QF=WT*CF*EFF*(DTIM2*(C-TFI)+TAU*(TTR-C)*(1.-EXP(-DTIM2/TAU)))+QF
      TE=TDT
      HFO=ENTHF(TFI)+QF/(WT*DTIME)
      TFO=FLTEMP(HFO)
      RETURN
C     SOLID BELOW TRANSITION AT START
    1 IF(ANS) 61,61,62
C     PURE ALPHA
   61 SMC=AS*CPA(TE)+AW*CW
      TAU=SMC/A
      TDT=C+(TE-C)*EXP(-DTIME/TAU)
      Q=AS*(HA(TE)-HA(TDT))+AW*CW*(TE-TDT)
      EELD=EELD-Q
      QF=WT*CF*EFF*(DTIME*(C-TFI)+TAU*(TE-C)*(1.-EXP(-DTIME/TAU)))
      TE=TDT
      HFO=ENTHF(TFI)+QF/(WT*DTIME)
      TFO=FLTEMP(HFO)
      RETURN
C     ALPHA PLUS EUTECTIC
   62 AE=ANS/CEU
      AA=AS-AE
      SMC=AA*CAEU+AE*CPEU+AW*CW
      TAU=SMC/A
      TDT=C+(TE-C)*EXP(-DTIME/TAU)
      Q=AA*(HA(TE)-HA(TDT))+(AE*CPEU+AW*CW)*(TE-TDT)
      EELD=EELD-Q



      QF=WT*CF*EFF*(DTIME*(C-TFI)+TAU*(TE-C)*(1.-EXP(-DTIME/TAU)))
      TE=TDT
      HFO=ENTHF(TFI)+QF/(WT*DTIME)
      TFO=FLTEMP(HFO)
      RETURN
      END
```

```
      SUBROUTINE VRTHS(ANS,AS,TE,EELD,AW,TFI,EFF,CF,WT,DO,XLTE,DTIME,ANL
     1,AL,TFO,EL,RS,RAXS,Q1,Q2,RAMB,TANB)
C     THIS SUBROUTINE USES VARIABLE REFERENCE TEMPERATURE TO DETERMINE
C     THE HEATING PROCESS IN AN INITIALLY PURE SOLID ELEMENT
C
      COMMON/DATA/RHOL,RHOS,TTR,TEU,HWO,HEUT,HABT,CPEU,CPB,CW,TKL
      COMMON/VALS/HBTR,HLTR,HWTR,HATR,HAEU,HLEU,HWEU,CTR,CEU,CAEU,TKATR,
     1TKBTR,TKAEU,TKEEU,CATR
      A=WT*CF*EFF+1./RAMB
      B=Q2-Q1+TANB/RAMB+WT*CF*EFF*TFI
      C=B/A
      IF(AS.EQ.0.) GO TO 30
      IF(ANS) 1,2,1
C     PURE HYDROXIDE, NO NITRATE
    2 IF(TE-TTR) 4,6,6
    6 SMC=AS*CPB+AW*CW
      TAU=SMC/A
      TDT=C+(TE-C)*EXP(-DTIME/TAU)
      Q=AS*(HB(TDT)-HB(TE))+AW*CW*(TDT-TE)
      EELD=EELD+Q
      QF=WT*CF*EFF*((C-TFI)*DTIME+TAU*(TE-C)*(1.-EXP(-DTIME/TAU)))
      TE=TDT
      HFO=ENTHF(TFI)+QF/(WT*DTIME)
      TFO=FLTEMP(HFO)
      RETURN
    5 TFOT=TFI+EFF*(TE-TFI)
      Q=(WT*CF*(TFI-TFOT)+Q2-Q1-(TE-TANB)/RAMB)*DTIME
      DEA=AW*HWTR+AS*HBTR-EELD
      IF(Q-DEA) 10,10,11
   10 EELD=EELD+Q
      QF=WT*CF*(TFOT-TFI)*DTIME
      TE=TTR
      HFO=ENTHF(TFI)+QF/(WT*DTIME)
      TFO=FLTEMP(HFO)
      RETURN
   11 DTIM1=DEA/(WT*CF*(TFI-TFOT)+Q2-Q1-(TE-TANB)/RAMB)
      QF=WT*CF*(TFOT-TFI)*DTIM1
      DTIM2=DTIME-DTIM1
      SMC=AS*CPB+AW*CW
      TAU=SMC/A
      TDT=C+(TTR-C)*EXP(-DTIM2/TAU)
      Q=AS*HB(TDT)+AW*(HWO+CW*TDT)-EELD
      EELD=EELD+Q
      QF=WT*CF*EFF*(DTIM2*(C-TFI)+TAU*(TE-C)*(1.-EXP(-DTIM2/TAU)))+QF
      TE=TDT
      HFO=ENTHF(TFI)+QF/(WT*DTIME)
      TFO=FLTEMP(HFO)
      RETURN
    4 SMC=AS*CPA(TE)+AW*CW
      TAU=SMC/A
      TDT=C+(TE-C)*EXP(-DTIME/TAU)
      IF(TDT-TTR) 14,14,15
   14 Q=AS*HA(TDT)+AW*(HWO+CW*TDT)-EELD
      EELD=EELD+Q
      QF=WT*CF*EFF*((C-TFI)*DTIME+TAU*(TE-C)*(1.-EXP(-DTIME/TAU)))
      TE=TDT
```

```
      HFO=ENTHF(TFI)+QF/(WT*DTIME)
      TFO=FLTEMP(HFO)
      RETURN
   15 DTIM1=TAU*ALOG((TE-C)/(TTR-C))
      QF=WT*CF*EFF*((C-TFI)*DTIM1+TAU*(TE-C)*(1.-EXP(-DTIM1/TAU)))
      DTIM2=DTIME-DTIM1
      TFOT=TFI+EFF*(TTR-TFI)
      Q=(WT*CF*(TFI-TFOT)+Q2-Q1-(TTR-TAMB)/RAMB)*DTIM2
      DEA=AS*HABT
      IF(Q-DEA) 17,17,18
   17 Q=Q+AS*(HATR-HA(TE))+AW*CW*(TTR-TE)
      EELD=EELD+Q
      QF=WT*CF*(TFOT-TFI)*DTIM2+QF
      TE=TTR
      HFO=ENTHF(TFI)+QF/(WT*DTIME)
      TFO=FLTEMP(HFO)
      RETURN
   18 DTIM3=DEA/(WT*CF*(TFI-TFOT)+Q2-Q1-(TTR-TA)/RAMB)
      QF=WT*CF*(TFOT-TFI)*DTIM3+QF
      DTIM4=DTIM2-DTIM3
      SMC=AS*CPB+AW*CW
      TAU=SMC/A
      TDT=C+(TTR-C)*EXP(-DTIM4/TAU)
      Q=AS*HB(TDT)+AW*(HWO+CW*TDT)-EELD
      EELD=EELD+Q
      QF=WT*CF*EFF*(DTIM4*(C-TFI)+TAU*(TTR-C)*(1.-EXP(-DTIM4/TAU)))+QF
      TE=TDT
      HFO=ENTHF(TFI)+QF/(WT*DTIME)
      TFO=FLTEMP(HFO)
      RETURN
C     SOLID WITH NITRATE(EUTECTIC). MUST BE BELOW TEU
    1 C1=CEU
      AE=ANS/C1
      AA=AS-AE
      SMC=AA*CAEU+AE*CPEU+AW*CW
      TAU=SMC/A
      TDT=C+(TE-C)*EXP(-DTIME/TAU)
      IF(TDT-TEU) 20,20,21
   20 Q=AA*(HA(TDT)-HA(TE))+(AE*CPEU+AW*CW)*(TDT-TE)
      EELD=EELD+Q
      QF=WT*CF*EFF*((C-TFI)*DTIME+TAU*(TE-C)*(1.-EXP(-DTIME/TAU)))
      TE=TDT
      HFO=ENTHF(TFI)+QF/(WT*DTIME)
      TFO=FLTEMP(HFO)
      RETURN
   21 DTIM1=TAU*ALOG((TE-C)/(TEU-C))
      QF=WT*CF*EFF*((C-TFI)*DTIM1+TAU*(TE-C)*(1.-EXP(-DTIM1/TAU)))
      DTIM2=DTIME-DTIM1
      TFOT=TFI+EFF*(TEU-TFI)
      Q=(WT*CF*(TFI-TFOT)+Q2-Q1-(TEU-TAMB)/RAMB)*DTIM2
      DEA=AE*HEUT
      IF(Q-DEA) 23,23,24
   23 AL=Q/HEUT
      Q=AA*(HAEU-HA(TE))+AE*CPEU*(TEU-TE)+AL*HEUT+AW*CW*(TEU-TE)
      EL=AL*HLEU
      EELD=EELD+Q-EL
      QF=WT*CF*(TFOT-TFI)*DTIM2+QF
      TE=TEU
```

```
      HFO=ENTHF(TFI)+QF/(WT*DTIME)
      TFO=FLTEMP(HFO)
      AS=AS-AL
      ANL=C1*AL
      ANS=ANS-ANL
C     SOLID RESISTANCE
      VA=AA/RHOS
      DA=SQRT(DO**2+1.2732*VA/XLTE)
      RA=ALOG(DA/DO)/(6.2832*TKAEU*XLTE)
      VE=(AE-AL)/RHOS
      DS=SQRT(DA**2+1.2732*VE/XLTE)
      RS=ALOG(DS/DO)/(6.2832*TKEEU*XLTE)+RA
      IF(VA.EQ.0..AND.VE.EQ.0.) GO TO 25
      RAXS=XLTE**2/(VA*TKAEU+VE*TKEEU)
      RETURN
   25 RAXS=0.
      RETURN
C     BEYOND LIQUID EUTECTIC. LESS ACCURATE AND LESS LIKELY
   24 DTIM3=DEA/(WT*CF*(TFI-TFOT)+Q2-Q1-(TEU-TA)/RAMB)
      QF=WT*CF*(TFOT-TFI)*DTIM3+QF
      DTIM4=DTIM2-DTIM3
      SMC=AA*CAEU+AE*CPT(C1)+AW*CW
      TAU=SMC/A
      Q=-SMC*(TEU-C)*(1.-EXP(-DTIM4/TAU))
      Q=Q+AA*(HAEU-HA(TE))+AE*HEUT+(AW*CW+AE*CPEU)*(TEU-TE)
      QF=WT*CF*EFF*(DTIM4*(C-TFI)+TAU*(TEU-C)*(1.-EXP(-DTIM4/TAU)))+QF
      HFO=ENTHF(TFI)+QF/(WT*DTIME)
      TFO=FLTEMP(HFO)
      ETOT=EELD+Q
      K3=1
      CALL FULLEL(AS,ETOT,DO,AW,XLTE,AL,AS,RS,TE,EL,K3,EELD,ANL,ANS,RAXS
     1)
      RETURN
   30 SMC=AW*CW
      TAU=SMC/A
      TDT=C+(TE-C)*EXP(-DTIME/TAU)
      Q=AW*CW*(TDT-TE)
      EELD=EELD+Q
      QF=WT*CF*EFF*((C-TFI)*DTIME+TAU*(TE-C)*(1.-EXP(-DTIME/TAU)))
      TE=TDT
      HFO=ENTHF(TFI)+QF/(WT*DTIME)
      TFO=FLTEMP(HFO)
      RETURN
      END
```

```
      SUBROUTINE COLL(CT,QC,T1,T2,T3,T4,QB,J)
C     THIS SUBROUTINE READS A TABLE OF COLLECTOR OUTPUT VS. CYCLE TIME.
C     AND COMPUTES THIS OUTPUT AT A GIVEN CYCLE TIME
C
  100 FORMAT(I3,4F12.0,F10.4,I2)
  101 FORMAT(F10.4,F12.0)
      DIMENSION Q(20),T(20)
      IF(J.NE.99) GO TO 10
      READ(5,100) K,T1,T2,T3,T4,QB,J
      DO 1 I=1,K
    1 READ(5,101) Q(I),T(I)
      RETURN
   10 DO 2 I=2,K
      IF(CT.GE.T(I)) GO TO 2
      QC=Q(I-1)+(Q(I)-Q(I-1))*(CT-T(I-1))/(T(I)-T(I-1))
      GO TO 3
    2 CONTINUE
    3 RETURN
      END
```

```
      SUBROUTINE RLCALC(RL)
C     THIS SUBROUTINE COMPUTES A LIQUID PHASE HEAT TRANSFER RESISTANCE
C     IN THERMKEEP.
C     FOR NOW IT IS A DUMMY ROUTINE. SETTING RL=0
C
      RL=0.
      RETURN
      END
```

```
      FUNCTION FF(R)
C     THIS FUNCTION COMPUTES THE CIRCULAR TUBE FRICTION FACTOR FOR
C     ROUGHNESS RATIO OF 0.0002
C
      IF(R.GT.2000.) GO TO 1
      FF=64./R
      RETURN
    1 IF(R.GT.100000.) GO TO 2
      FF=0.1923*R**(-0.1772)
      RETURN
    2 FF=0.025
      RETURN
      END
```

```
      FUNCTION FLTEMP(H)
C     THIS FUNCTION COMPUTES FLUID TEMPERATURE IN K FROM ENTHALPY
C     IN KJ/KG USING H=0 AT 400K
C
      FLTEMP=-111.1+SQRT(0.2612E+06+530.5*H)
      RETURN
      END
```

```
      FUNCTION THCF(T)
C     THIS FUNCTION GIVES FLUID THERMAL CONDUCTIVITY IN KJ/M-SEC-K
C     FROM TEMPERATURE IN K
C
      THCF=0.1379E-3-0.520E-7*T
      RETURN
      END
```

ORIGINAL PAGE IS
OF POOR QUALITY

```
      FUNCTION CPF(T)
C     THIS FUNCTION COMPUTES FLUID SPECIFIC HEAT IN KJ/KG-K FROM
C     TEMPERATURE IN K
C
      CPF=0.4189+0.377E-02*T
      RETURN
      END
```

```
      FUNCTION VISF(T)
C     THIS FUNCTION COMPUTES ABSOLUTE VISCOSITY IN KG/M-SEC FROM
C     TEMPERATURE IN K
C     FOR T-66 IT IS A FAIR APPROIMATION FROM 367K TO 589K
C
      X=1079./T-5.34
      VISF=10.**X
      RETURN
      END
```

```
      FUNCTION ENTHF(T)
C     THIS FUNCTION   COMPUTES FLUID ENTHALPY IN KJ/KG FROM TEMPERATURE
C     IN K USING H=0 AT 400K
C
      ENTHF=(1.173+0.1885E-02*T)*(T-400.)
      RETURN
      END
```

```
      FUNCTION CPA(T)
C     THIS FUNCTION COMPUTES THE SPECIFIC HEAT OF ALPHA-NAOH IN KJ/KG-K
C     FROM TEMPERATURE IN K. IT IS ASSUMED CONSTANT.
C
      CPA=2.018
      RETURN
      END
```

```
      FUNCTION HA(T)
C     THIS FUNCTION COMPUTES THE ENTHALPY OF ALPHA-NAOH IN KJ/KG FROM
C     TEMPERATURE IN K. IT WILL BE ASSUMED THAT H(ALPHA)=0 AT 500K AND
C     ALL ENTHALPIES WILL BE RELATIVE TO THIS. CP IS ASSUMED CONSTANT
C
      HA=2.018*(T-500.)
      RETURN
      END
```

```
      FUNCTION HB(T)
C     THIS FUNCTION COMPUTES THE ENTHALPY OF BETA-NAOH IN KJ/KG FROM
C     TEMPERATURE IN K. CP OF BETA IS ASSUMED CONSTANT.
C
      HB=292.08+2.15*(T-566.)
      RETURN
      END
```

```
      FUNCTION THCA(T)
C     THIS FUNCTION COMPUTES THE THERMAL CONDUCTIVITY OF ALPHA-NAOH.
C     SOLID. IN KJ/SEC-M-K FROM TEMPERATURE IN K.
C
      THCA=0.001471
      RETURN
      END
```

```
      FUNCTION THCB(T)
C     THIS FUNCTION COMPUTES THE THERMAL CONDUCTIVITY OF BETA-NAOH.
C     SOLID. IN KJ/SEC-M-K FROM TEMPERATURE IN K.
C
      THCB=0.001471
      RETURN
      END
```

ORIGINAL PAGE IS
OF POOR QUALITY

```
      FUNCTION THCE(T)
C     THIS FUNCTION COMPUTES THE THERMAL CONDUCTIVITY OF EUTECTIC NA-OH.
C     NANO3. SOLID. IN KJ/SEC-M-K FROM TEMPERATURE IN K.
C
      THCE=0.001471
      RETURN
      END
```

```
      FUNCTION CLIQ(T)
C     THIS FUNCTION FINDS THE CONCENTRATION OF NANO3 ON THE LIQUIDUS
C     LINE VS. TEMPERATURE IN K. C=MASS(NANO3)/TOTAL MASS.THERMKEEP.
C     THIS IS A SIMPLE VERSION UNTIL PHASE DIAGRAM IS FOUND.
C
      IF(T.LT.566.) GO TO 1
      CLIQ=2.2769-0.003646*T
      RETURN
    1 CLIQ=3.6184-0.006216*T
      RETURN
      END
```

```
      FUNCTION TLIQ(C)
C     THIS FUNCTION COMPUTES TEMPERATURE IN K ON THE LIQUIDUS LINE VS.
C     CONCENTRATION OF NANO3. C=MASS(NANO3)/TOTAL MASS.THERMKEEP.
C     THIS IS A SIMPLE VERSION UNTIL PHASE DIAGRAM IS FOUND.
C
      IF(C.GT.0.10) GO TO 1
      TLIQ=592.-260.*C
      RETURN
    1 TLIQ=582.09-160.87*C
      RETURN
      END
```

```
      FUNCTION CPT(C)
C     THIS FUNCTION COMPUTES THE LIQUID THERMKEEP SPECIFIC HEAT AS A
C     FUNCTION OF CONCENTRATION(KJ/KG-K)
C     IT IS ASSUMED TO BE A FUNCTION OF CONCENTRATION ONLY
C     IT IS NOW A DUMMY FUNCTION WITH A CONSTANT VALUE
C
      CPT=2.14
      RETURN
      END
```

```
      FUNCTION HLIQ(T)
C     THIS FUNCTION COMPUTES THE ENTHALPY OF SATURATED SOLUTION( ON THE
C     LIQUIDUS LINE) AS A FUNCTION OF SOLUTION TEMPERATURE.
C     IT IS NOW A SIMPLIFIED FUNCTION NEGLECTING PRIMARILY HEAT OF
C     SOLUTION AS WELL AS ABSOLUTE VARIATION FROM NO3 TO OH.
C
      HLIQ=2.14*T-760.
      RETURN
      END
```

A P P E N D I X D

LIST OF SYMBOLS FOR COMPUTER ANALYSIS

A_{fl}	total T-66 flow area (m^2)
A_i	tube inside surface area per element (m^2)
c_f	specific heat of heat transfer fluid (kJ/kg-K)
c_{steel}	specific heat of steel (kJ/kg-K)
c_{TK}	Thermkeep minimum specific heat (kJ/kg-K)
d_i	inside diameter of tubes (m)
d_o	outside diameter of tubes (m)
d_{shell}	inside diameter of vessel (m)
d_{shroud}	inside diameter of shroud (m)
d_{solid}	solid layer diameter around a tube (m)
E_e	energy content of an end element (kJ)
E_m	energy content of an interior element (kJ)
f	T-66 friction factor
h_f	T-66 side heat transfer coefficient (kW/m^2-k)
h_{shell}	inside height of vessel (m)
h_{shroud}	inside height of shroud (m)
h_{TK}	enthalpy of Thermkeep (kJ/kg)
k_f	T-66 thermal conductivity (kW/m-K)
k_{ins}	thermal conductivity of insulation (kW/m-K)
k_{liquid}	thermal conductivity of Thermkeep, liquid (kW/m-K)
k_{solid}	thermal conductivity of Thermkeep, solid (kW/m-K)
k_{steel}	thermal conductivity of steel (kW/m-K)
$\bar{k}_{TK}$	average axial thermal conductivity of Thermkeep in an element (kW/m-K)

L_T	length of each tube (m)
M_{TK}	total mass of Thermkeep (kg)
N_E	number of spatial elements
N_{PR}	T-66 Prandtl number
N_{RE}	T-66 Reynolds number
N_T	total number of heat exchanger tubes
NTU	number of transfer units in an element
P_p	ideal pumping power (kW)
q_{ax}	axial heat transfer rate between elements (kW)
q_B	heat rate required for boiler (kW)
q_c	collector output (kW)
q_{ex}	excess heating provided by collectors (kW)
q_f	heat transfer rate to fluid per element (kW)
$q_{ins,e}$	heat transfer rate to environment per element (kW)
q_{TOT}	total heat transfer rate to an element (kW)
Q_{abs}	total daily heat absorption by storage (kJ)
Q_{burn}	total daily make-up heating required (kJ)
Q_c	total daily output of collectors (kJ)
Q_{del}	total daily heat delivered from storage (kJ)
Q_{env}	total daily heat lost to environment (kJ)
Q_{loss}	total daily collector heat not used (kJ)
R_{aspect}	aspect ratio, vessel height/vessel diameter
R_f	resistance to heat transfer, fluid side (K/kW)
$R_{ins,\ell}$	lateral resistance to heat transfer of insulation per element (K/kW)

R_{shell}	vessel axial heat transfer resistance per element (K/kW)
R_{solid}	resistance of solid to radial heat transfer (K/kW)
$R_{T,a}$	tube axial heat transfer resistance per element (K/kW)
$R_{TK,a}$	Thermkeep axial heat transfer resistance per element (K/kW)
$\bar{R}_{TK,a}$	average Thermkeep axial resistance between elements (K/kW)
$R_{T,\ell}$	tube lateral heat transfer resistance per element (K/kW)
$R_{TOT,a}$	total axial resistance between elements (K/kW)
R_{TOTAL}	total elemental heat transfer resistance (T-66 and Thermkeep) (K/kW)
t_{end}	vessel end plate thickness (m)
t_{ins}	insulation thickness (m)
t_{shell}	vessel side wall thickness (m)
$t_{shroud, bottom}$	shroud bottom thickness (m)
$t_{shroud, side}$	shroud side wall thickness (m)
$t_{shroud, top}$	shroud top thickness (m)
T_{amb}	ambient temperature (K)
Te	storage outlet temperature-upper (K)
T_H	collector outlet temperature (K)
T_{in}	fluid temperature into an element (K)
T_L	boiler outlet temperature of T-66 (K)
T_o	storage outlet temperature-lower (K)
T_{out}	fluid temperature out of an element (K)
T, T_E	element temperature (K)

V_{solid}	solid layer volume per tube per element (m^3)
V_{TK}	total Thermkeep volume (m^3)
V_{TOTAL}	total internal volume of vessel (m^3)
V_{tubes}	total volume occupied by heat exchanger (m^3)
w_{coll}	T-66 mass flow rate from collectors (kg/sec)
w_f	fluid (T-66) mass flow rate to TES unit (kg/sec)
w_{min}	T-66 mass flow rate to boiler (kg/sec)
$W_{heat\ exchanger}$	heat exchanger weight, tubes only (kg)
W_{ins}	insulation weight (kg)
W_p	total pump work (ideal) per daily cycle (kW-hr)
W_{shroud}	shroud weight (kg)
W_{vessel}	total vessel weight (kg)
z	factor for time step calculation (kg)
ΔE	energy change in an element per time step (kJ)
$\Delta M_{st,e}$	mass of steel per end element (kg)
$\Delta M_{st,m}$	mass of steel per interior element (kg)
ΔM_{TK}	mass of Thermkeep per element (kg)
ΔP	heat exchanger pressure drop (kg/m^2)
Δt	time step (sec)
ξ	effectiveness of heat transfer in an element
μ_f	T-66 viscosity (kg/m-sec)
ϕ	fraction of Thermkeep in solid phase in an element
ρf	T-66 density (kg/m^3)
ρ_{ins}	density of insulation (kg/m^3)
ρ_{steel}	density of steel (kg/m^3)
ρ_{TK}	Thermkeep density, liquid phase (kg/m^3)

A P P E N D I X E

LIST OF SYMBOLS FOR SCALING PROCEDURE

A	heat exchange surface area
A_L	heat exchange surface area per unit length
a	cross sectional area of storage medium
a_t	tube cross-sectional area
c	fluid specific heat
c_s	storage medium specific heat
d_{sh}	diameter of shroud
d_v	diameter of vessel
h_v	height of vessel
k	thermal conductivity of storage medium
k_i	thermal conductivity of insulation
k_t	thermal conductivity of tube
L_t	tube length
M	Storage medium total mass
M_L	storage medium mass per unit length
m	fluid mass flow rate
P	reference time period
s	distance along tube
t	storage medium temperature
t_f	fluid temperature

t_L	reference temperature
t_s	shroud surface temperature
U	overall heat transfer coefficient
V	fluid volume
V_L	fluid volume per unit length
x	distance along flow direction in storage unit
θ	dimensionless storage medium temperature, t/t_L
μ	dimensionless time, τ/P
ν	dimensionless distance, x/h_v
ρ	fluid density
τ	time

A P P E N D I X F

REFERENCES

1. Report No. 1503, "Thermal Energy Storage Material Thermophysical Property Measurement and Heat Transfer Impact" - August 11, 1976
   Dynatech R/D Company
   99 Erie Street
   Cambridge, MA 02139

2. Bulletin No. 1c/FF-64
   Monsanto Industrial Chemicals Co.
   800 N. Lindbergh Blvd.
   St. Louis, MO 63166

3. Mellor's Comprehensive Treatise on Inorganic and Theoretical Chemistry: Vol II, Supplement II; John Wiley and Sons, Inc., New York, N.Y. 1961; p. 1250

4. Hopwood, P.F.: Pressure Drop, Heat Transfer, and Flow Phenomena for Forced Convection Boiling in Helical Coils -- A Literature Review. United Kingdom Atomic Energy Authority, 1972.

5. Kreyszig, E.: Advanced Engineering Mathematics. John Wiley and Sons, Inc., New York, N.Y. 1962; p. 31.